

**A SEISMOTECTONIC ANALYSIS OF THE SEISMIC AND VOLCANIC
HAZARDS IN THE PRIBILOF ISLANDS - EASTERN ALEUTIAN
ISLANDS REGION OF THE BERING SEA**

by

Dr. Klaus H. Jacob and Dr. Egill Hauksson

**Lament-Doherty Geological Observatory
Columbia University in the City of New York**

**Final Report
Outer Continental Shelf Environmental Assessment Program
Research Unit 16**

1983

135

TABLE OF CONTENTS

List of Figures 139

List of Tables 145

Acknowledgments 147

1. ABSTRACT AND SUMMARY OF MOST IMPORTANT RESULTS 148

2. INTRODUCTION . * ** 150

3. DATA ANALYSIS ** * 154

 3.1 Seismicity Recorded by the Shumagin Network 1973-1982 154

 3.2 Teleseismic Data 1973-1982 . * * 171

 3.3 Strong-Motion Data 177

 3.4 Historic and Instrumental Large Earthquakes, 1788 to Present 190

 3.5 Historical Eruptive Activity of Pavlof, Akutan, and Makushin Volcanoes 237

 3.6 Geology and Geodetic Surveys 247

 3.7 Seismicity Recorded by the Unalaska Array 1980-1982 252

 3.8 Tsunami Data * 256

4. RESULTS 259

 4.1 Seismic Hazards 259

 4.2 Volcanic Hazards * * * 264

5. CONCLUSIONS 279

6. UNRESOLVED PROBLEMS 281

7. APPENDICES * 282

 7.1 Earthquake Data Processing Methods 282

 7.2 Magnitude Determinations . . * 291

 7.3 Annual Plots of **Shumagin** Network Seismicity 1973-1982 300

 7.4 **Shumagin** Network Status 1973-1982 315

 7.5 Seismic and Eruptive Activity of **Pavlof** Volcano, 1973-1982 . . . 325

 7.6 Preliminary Risk Assessment in the St. George Basin 335

 7.7 List of Publications Supported by Contract NOAA-03-5-022-70 . . 357

8. REFERENCES * 359

LIST OF FIGURES

Figure 2.1 - Approximate regions (boxes) in which **L-DGO** collected data by operating seismic stations or networks in St. Paul (**SNP**), Dutch Harbor (**DUT**) on **Unalaska** Island, and in the **Shumagin** Islands with central recording at Sand Point (**SAN**)

Figure 3.1.1 - Map of epicenters showing all the **seismicity** located by the **Shumagin** network eastern Aleutians, Alaska, from 1973-1981

Figure 3.1.2 - Map of epicenters showing all the shallow **seismicity** (depth less than 30 km) located by the **Shumagin** network, eastern Aleutians, Alaska, from 1973-1981

Figure 3.1.3 - Map of epicenters showing all the intermediate depth and very deep **seismicity** (depth greater than 40 km) located by the **Shumagin** network, eastern Aleutians, Alaska from 1973-1981

Figure 3.1.4 - Histogram of number of earthquakes located by the **Shumagin** seismic network, eastern Aleutians, **Alaska**

Figure 3.1.5 - Cumulative number of all local earthquakes located by the **Shumagin** network from 1978 to 1982

Figure 3.1.6 - Both cumulative number and number of earthquakes as a function of magnitude for the whole data set recorded by the **Shumagin** network from 1977 to 1981

Figure 3.1.7 - Both cumulative number and number of earthquakes as a function of magnitude for all shallow earthquakes (depth less than 30 km) recorded by the **Shumagin** network from 1977 to 1981

Figure 3.1.8 - Map of epicenters where seismicity **lineaments** are emphasized by drawing straight lines by eye **through** clusters that appear to form linear alignments

Figure 3.1.9 - Cumulative number of seismicity **lineaments** from Figure 3.8 versus length of **seismicity lineament**

Figure 3.1.10 - Magnitude versus source dimension relationship

Figure 3.1.11 - Recurrence relation for the Gulf of Alaska random sources

Figure 3.2.1 - Map of epicenters showing **teleseismically** located earthquakes from the PDE bulletin from 1973-1981

Figure 3.2.2 - The vertical bars indicate the occurrence and the magnitude of **teleseismically** located earthquakes from the PDE bulletin

Figure 3.2.3 - Cumulative number of earthquakes located by the PDE from 1973 to 1982 in the **Shumagin** Islands region

Figure 3.2.4 -. Both cumulative number and number of earthquakes as a function of magnitude for the PDE data from 1973 to 1981 located in the **Shumagin** Islands region

Figure 3.3.1 - Comparison of peak horizontal accelerations for Alaska with empirical attenuation laws obtained by Joyner and **Boore** (1981) by regression of mostly western U.S. strong motion data

Figure 3.3.2 - Comparison of Alaska peak horizontal accelerations with type-A attenuation relations proposed by **Woodward-Clyde** (1982) for shallow, **non-Benioff** zone earthquakes

Figure 3.3.3 - Comparison of Alaska peak horizontal accelerations with B-type attenuation relations proposed by **Woodward-Clyde** (1982) for Benioff-zone earthquakes

Figure 3.4.1 - Location map of presently existing seismic gaps and of rupture zones of the most recent sequence of major earthquakes since 1938

Figure 3.4.2 - Major earthquakes in the Alaska-Aleutian region for the instrumental period 1898 to 1982

Figure 3.4.3 - **Seismicity** of the Aleutian arc versus time for the instrumental period 1898 to 1982

Figure 3.4.4 - Histogram of all major earthquakes for which magnitudes were available, plotted in $M_w = 0.1$ -intervals

Figure 3.4.5 - Logarithmic frequency plots for the instrumental **seismicity** 1898 to 1982 for the Alaska-Aleutian arc

Figure 3.4.6 - Same as Figure 3.4.5 with number of events n as solid line and cumulative number of events N as broken line

Figure 3.4.7 - Arc-wide seismic moment release for the Aleutian arc during the period 1898 to 1982

Figure 3.4.8 - Space-time plot of instrumental (1898 to 1982) and historical (1788 to 1897) **seismicity** of the Aleutian arc considering great earthquakes only

Figure 3.4.9 - Statistical properties of recurrence periods

Figure 3.4.10 - Same as Figure 3.4.9 except that a normal (rather than a log-normal) distribution is fitted to observed recurrence times distribution which **consists** of a reduced number of samples

Figure 3.5.1 - The number of reported eruptions per decade vs. time

Figure 3.6.1 - Maps showing level lines and tide gauges in the Shumagin Islands

Figure 3.6.2 - Data from those level lines in the Shumagins that have been **levelled** at least twice

Figure 3.7.1 - Dutch Harbor Array, Eastern Aleutians, operated by Lament-Doherty Geological Observatory

Figure 3.7.2 - Number of earthquakes recorded per day by the Dutch Harbor Array in 1980 and 1981

Figure 3.7.3 - Number of earthquakes recorded per day by the Dutch Harbor Array in 1982

Figure 3.8.1 - Diagram showing tsunami run-up heights and inferred earthquake source region of the 1788 event(s)

Figure 4.1.1 - Map view of arc with instrumental seismicity since 1898

Figure 4.2.1 - Volcano hazards map for the Western Alaska Peninsula

Figure 4.2.2 - Volcano hazards map for the Eastern Aleutian Islands

Figure 4.2.3 - Distribution of volcanic ash layers in North Pacific deep-sea cores

Figures 4.2.4a,b - Sample locality maps in **Shumagin** Islands and adjacent peninsula

Figures 4.2.5a,b - Examples of volcanic ash layers in cores taken on marine terraces in summer 1979

Figure 4.2.6 - \log_{10} of the cumulative number of eruptions of a given size per hundred years per volcano vs. the \log_{10} of the volume of eruptive products

Figure 4.2.7 - Maximum ash thickness in **cm** vs. distance from the vent

Figure 7.1.1 - A block diagram showing how the routine velocorder data processing was carried out for the Shumagin seismic network

Figure 7.1.2 - A block diagram showing how the routine digital data processing is carried out for the **Shumagin** seismic network

Figure 7.1.3 - A summary display of seismic traces from the program ping

Figure 7.1.4 - A sample seismogram from station CNBZ

Figure 7.1.5 - A sample output from **HYPOINVERSE**

Figure 7.1.6 - A sample output from the program **dplt2**

Figure 7.2.1 - Sensor responses and recorder responses shown as a function of frequency for seismic stations in the **Shumagin** network

Figure 7.2.2 - Magnification curves for a typical high gain **short-period** station (NGI at 48 db **Amp/VCO** gain)

Figure 7.2.3 - Comparison between magnitude values determined by the Shumagin network and values published by NEIS

Figure 7.3.1 - **Seismicity** located by the Shumagin network during 1973

Figure 7.3.2 - Seismicity located by the **Shumagin** network during 1974

Figure 7.3.3 - **Seismicity** located by the **Shumagin** network during 1975

Figure 7.3.4 - Seismicity located by the **Shumagin** network during 1976

Figure 7.3.5 - **Seismicity** located by the **Shumagin** network during 1977

Figure 7.3.6 - Seismicity located by the **Shumagin** network during 1978

Figure 7.3.7 - **Seismicity** located by the Shumagin network during 1979

Figure 7.3.8 - **Seismicity** located by the Shumagin network during 1980

Figure 7.3.9 - Seismicity located by the **Shumagin** network during 1981

Figure 7.3.10 - Seismicity located by the Shumagin network from January-June 1982

Figure 7.3.11 - **Seismicity** located by the Shumagin network from 1973-1981

Figure 7.4.1 - The **Shumagin** seismic **network**, Alaska

Figure 7.4.2 - Operational status of the Shumagin network in 1973 and 1974

Figure 7.4.3 - Operational status of the **Shumagin** network in 1975 and 1976

Figure 7.4.4 - Operational status of the Shumagin network in 1977 and 1978

Figure 7.4.5 - Operational status of the "Shumagin network in 1979 and 1980

Figure 7.4.6 - Operational status of the Shumagin network in 1981 and 1982

- Figure 7.5.1 - Map showing stations of the **Pavlof** seismic array
- Figure 7.5.2 - Types of seismic signals recorded on **helicorder** from station **PVV**
- Figure 7.5.3 - Number of B-type earthquakes and explosions per day
- Figure 7.5.4 - Number of B-type earthquakes and explosions per day .
- Figure 7.5.5 - Number of B-type earthquakes **and** explosions per day
- Figure 7.5.6 - Number of B-type earthquakes and explosions per day
- Figure 7.5.7 - Number of B-type earthquakes and explosions per day
- Figure 7.6.1 - Earthquake, epicenters, greater St. George Basin area, 1925 through 1978
- Figure 7.6.2 - Epicenters of shallow earthquakes, limited St. George Basin area, 1957 through 1978
- Figure 7.6.3 - Earthquakes per year for the greater and the limited St. George Basin region
- Figure 7.6.4** - Logarithm cumulative number of earthquakes vs. magnitude for the limited St. George Basin region during the period 1957 through 1978
- Figure 7.6.5 - Peak acceleration vs. distance for some western U.S. earthquakes and eastern Aleutian earthquakes
- Figure 7.6.6 - Detection threshold for St. Paul Seismic station (**SNP**)

LIST OF TABLES

Table 3.3.1 - Alaska-Aleutian Strong Motion Data

Table 3.4.1 - List of 116 Large Earthquakes in the Alaska-Aleutian Arc

Table 3.4.2 - Estimates of Minimum-, Average-, and Maximum Recurrence Times Derived from the b-Value Plot for the Entire Arc

Table 3.4.3 - Comparison of A and b Values and Recurrence Times T_R for $m = 5.0$ Events Using Different Data Sources

Table 3.4.4 - Parameters for Plate-Kinematic Model of Seismic Moment Release

Table 3.4.5 - Recharge Status of Rupture Zones or Gaps Since Last Significant Event

Table 3.4.6 - List of Great Historic Events and Inferred Source Parameters Based on the 'Time Predictable' Model

Table 3.4.7 - Moment Balance (expressed in equivalent M_w) Since 1760

Table 3.4.8 - Observed or Computed Recurrence Times for Rupture Zones Which Broke During the Historic and Instrumental Period 1788 to 1965

Table 3.4.9 - Probabilities P(%) for Recurrence Periods $T_R(\text{years})$

Table 3.4.10 - Cumulative, Conditional, and Annual Probabilities for Great Earthquakes in 1983, 1993 and 2003

Table 3.4.11 - Cumulative, Conditional, and Annual Probabilities for Great Earthquakes in 1983, 1993 and 2003, for Major Aleutian Rupture Zones Assuming Normally Distributed Recurrence Periods

Table 3.5.1 - Pavlof Sister

Table 3.5.2 - Pavlof

Table 3.5.3 - Akutan

Table 3.5.4 - Makushin

Table 3.5.5 - Data on Eruptive Activity of Alaska and Aleutian Volcanoes

Table 4.2.1 - Carbon 14 Dates and Number of Volcanic Ash Layers for Marine Terrace Cores

Table 7.2.1 - Earthquakes Located by Both the Shumagin Network & PDE

Table 7.3.1 - Number of Earthquakes Located by the Shumagin Network and NEIS/PDEE Bulletin Per Year in the Region 52° - 57° N and 156° - 165° W. 161

LIST OF TABLES (con' t.)

Table 7.3.2 - Flat-Layered P-Velocity Model for the Shumagin Islands Array Region

Table **7.4.1** - Eastern Aleutian Regional Networks Operated by **Lamont-Doherty** Geological Observatory, 1973-1982

Table 7.5.1 - Preliminary List of **Pavlof** Volcano Eruptions, 1973-1983, Deduced from **Seismicity**

Table 7.6.1 - All Events in the Greater St. George Basin Region for the Period 1925 Through 1978

Table 7.6.2 - Shallow Events in the Limited St. George Basin Region for the Period 1957 Through 1978

Table 7.6.3 - Frequency of Occurrence by Magnitude

Table 7.6.4 - Reports of Volcanic Activity in the Eastern Aleutian Arc from Okmok Volcano, Umnak Island to **Pavlof** Volcano, Alaska Penn

Table 7.6.5 - Probability for Acceleration to Exceed 0.2 or 0.5 g in 40 Years for a Site Within the St. George Basin Region

Table 7.6.6 - Events Detected at SNP in a Distance Range Such That Origin in St. George Basin is Possible

ACKNOWLEDGMENTS

This study was funded in part by the Bureau of Land Management through interagency agreement with the National Oceanic and Atmospheric Administration, (contract NOAA-03-5-022-70) as part of the Outer Continental Shelf Environmental Assessment Program in the eastern Aleutians, Alaska. The broad **seismotectonic** aspects of this work were also supported by the U.S. Department of Energy (contract DE-AS02-76ERO-3134) .

Dr. John N. Davies, Alaska State Seismologist, who installed the **Shumagin** Network in 1973 was in charge of this project until July 1981. John's enthusiasm and unceasing efforts are the basis of the results presented in this report.

Thanks to Margaret Eubank for running the seismic recording station in Sand Point and to Bill Eubank for providing logistics support and accommodation at Sand Point. Also, thanks to Beverly Wiggers and William **Tcheripanoff**, Jr., for running the seismic recording stations in Dutch Harbor and on St. Paul Island, respectively.

Technical work was performed by **Laszlo** Skinta, Douglas Johnson, David Lentricchia, Fred England, Robert Steuer, Warren Leonard, Larry **Shengold**, George Gunther, and Tom Ray.

Data reduction and analysis were done by Mary Ann Luckman, Stephan Rosen, John Armbruster, Jim Mori, John Peterson, Jeff Hauptman, Mike Hamburger, Steve Hickman, Leigh House, Janet Krause, and Phil **Lelyveld**.

We would like to thank our contract monitors at NOAA in Juneau, Rodney A. **Combellick** and Laurie **Jarvela**, for their excellent cooperation. George LaPiene and Mike Albertson of NOAA organized the helicopter schedule every year and thanks to the generous help of the NOAA helicopter crews we managed to keep the seismic networks operating through the years.

We owe special thanks to **Elvonne Wellmon**, who carried out the administration of the contract and proofread this report. Lynn Niebour typed the manuscript and Kazuko **Nagao** and Mary Ann **Luckman** drafted the figures.

1. ABSTRACT AND SUMMARY OF MOST IMPORTANT RESULTS

This report presents and summarizes seismic and volcanic data collected by Lamont-Doherty in the eastern Aleutian arc and adjacent Bering Sea between 1973 and 1982. The data were collected with support by the **NOAA-OCSEA** Program during the period 1975-1982. Seismic networks were operated by Lamont-Doherty in the Shumagin Islands, **Unalaska** Island, and **Pribilofs**. The network data are analyzed in combination with **teleseismic** and historic (preinstrumental) data to: 1) obtain a tectonic model of the subduction process; 2) give a comprehensive definition of seismic and volcanic sources; and 3) determine the probabilities for the occurrence of earthquakes and of volcanic eruptions where the data allow such determinations.

Most of the newly collected data originate from earthquakes in sections of the eastern Aleutian arc and directly adjacent Bering Sea regions close to the following three lease sale planning regions: 'St. George Basin', 'North Aleutian Basin' and '**Shumagin** Basin'. Some results regarding great earthquakes concern hazards in the more distant 'Kodiak', 'Lower Cook Inlet' and 'Eastern Gulf of Alaska' lease sale planning regions. The main results are:

1) Mean recurrence times for great earthquakes ($M_w \geq 7.8$) at any given segment in the Aleutian arc are approximately 70 years but have very large uncertainties.

2) Probabilities for the occurrence of great earthquakes ($M_w \geq 7.8$) especially near the Shumagin Islands, **Unalaska** Island and perhaps near the 1938-rupture zone SW of Kodiak Island are high during the next 20 years and virtually approach certainty (in the first two segments only) for a 40 year planning period (1983-2023). Therefore, future **off-** or near-shore installations near the **seismogenic** regions need to be designed for the effects of great earthquakes.

3) Tsunami heights on shorelines with south-facing Pacific Ocean exposures have in the past reached local run up heights of up to about 30 meters (90 feet). Future events can be expected to behave similarly. The Bering Sea side is less prone to tsunami effects.

4) **Volcanic hazards** are generally of lesser importance than seismic hazards except within close range of volcanoes.

5) Presently there is a general scarcity of strong motion data from Alaska-Aleutian subduction zone earthquakes and a complete global absence of strong motion data from any great ($M_w \geq 7.8$) earthquake. Until such data are collected and analyzed for incorporation into seismic exposure mapping, the latter can only produce tenuous results that may or may not correctly predict future groundmotions from great earthquakes at or near the lease sale regions of interest.

6) The single most important recommendation for future action resulting from this study **is** to maintain or upgrade a **strong motion** recording capability in seismic gaps of the Alaska-Aleutian arc and subduction zone so as to collect the urgently required strong motion data at the earliest possible time.

2. INTRODUCTION

This report summarizes the seismic and volcanic data collected from local seismic networks (Figure 2.1) that were operated by Lamont-Doherty in the **Shumagin** Islands, on **Unalaska** Island and St. George Island (**Pribilofs**). We assess the significance of these newly collected data for **seismicity** and **volcanicity** in the context of a tectonic model and integrate these results together with globally collected data of instrumental and historic (i.e., preinstrumental) periods from the eastern Aleutian arc and the adjacent Bering Sea to arrive at quantitative probabilistic descriptions of **seismicity** and **volcanicity**. Therefore, this report is primarily concerned with a quantitative description of the sources for seismic and volcanic hazards rather than their final effects on hazards exposure.

To complete the assessment of seismic and volcanic hazards exposure, at least two additional steps would therefore be required that are not covered under this project. For instance, from seismology one needs to obtain some empirical attenuation laws that prescribe the **groundmotions** as a function of distance from, and as a function of the magnitude of, the seismic source. Reliable empirical laws for groundmotions for moderate-sized Alaskan earthquakes do not exist at present in sufficient numbers, and do not exist at all, even on a global scale, for earthquakes with magnitudes ($M_w \geq 7.8$). We discuss extensively the problems caused by this paucity of empirical groundmotion data. We conclude that without the necessary **groundmotion** data and related attenuation laws, the third and final step, i.e., the computation and mapping of parameters at certain prescribed probability levels of non-exceedence for given periods of interest, cannot be meaningfully completed.

Various attempts in the past have nevertheless been made to compute and map seismic exposure for Alaska offshore regions. One of the first important and comprehensive studies in this category was the so-called 'OASES' Project (**Woodward-Clyde** Consultants, 1978) that was commissioned by the Oil Industry with interests in Alaska. That study provided a first complete overview but suffered from a number of deficiencies some of which are related to: 1) an inadequate

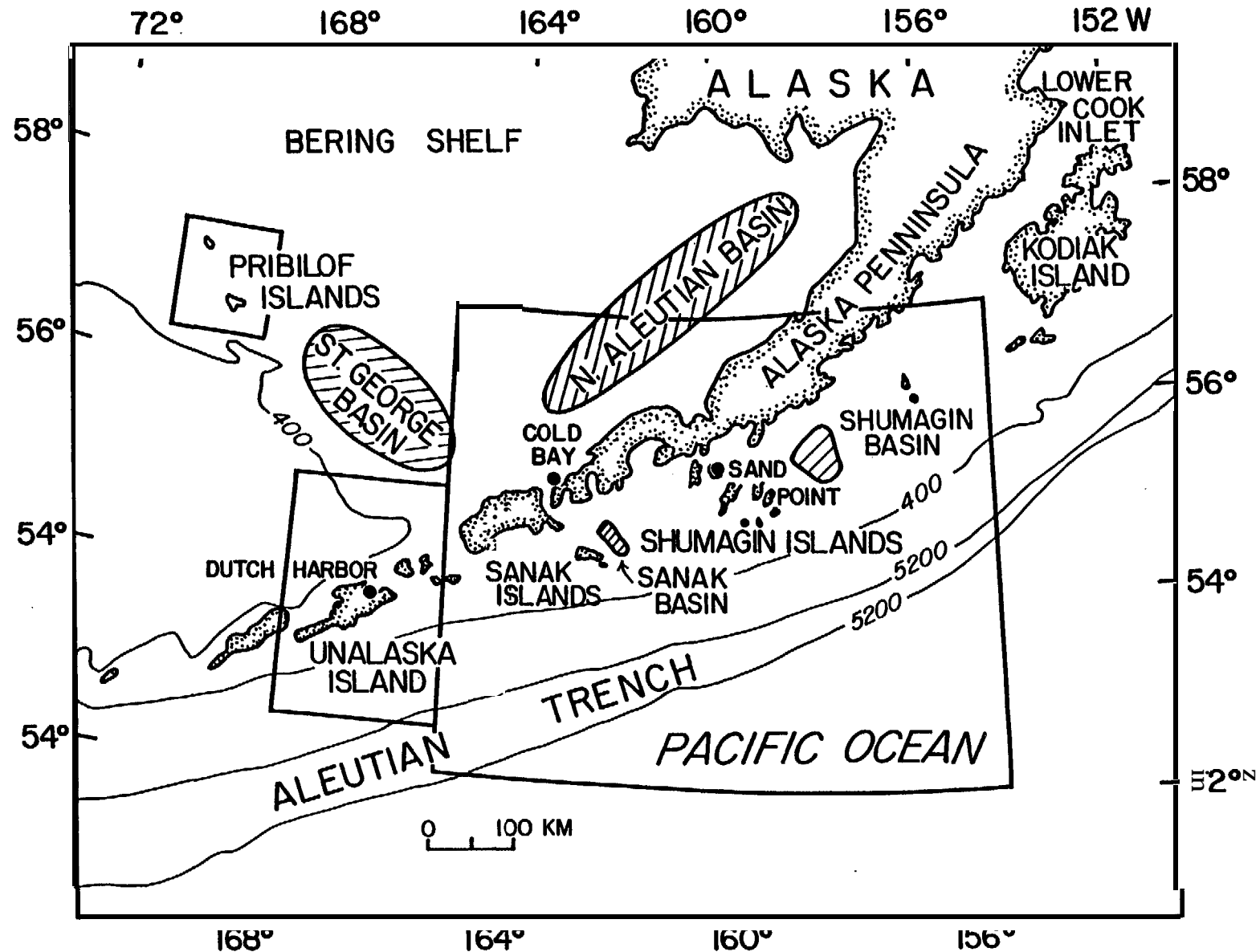


Figure 2.1. Approximate regions (boxes) in which L-DGO collected data by operating seismic stations or networks in St. Paul (SNP), Dutch Harbor (DUT) on Unalaska Island, and in the Shumagin Islands with central recording at Sand Point (SAN). Also labeled are the Lease Sale Planning regions 'St. George Basin', 'North Aleutian Basin', 'Shumagin Isl.' and 'Lower Cook Inlet'.

assessment of the occurrence of great subduction zone events ($M_w \gg 7.8$) which may have the most destructive potential in some regions; 2) poorly constrained strong **groundmotion** attenuation laws for the Alaska tectonic setting, especially those applicable to great earthquakes.

Therefore as part of the **OCSEA** Program a revision of the analysis applied in the OASES-project was solicited, to specifically incorporate:

- 1) A provision for the concept of seismic gaps that recognizes that the probability for the occurrence of a great earthquake in any arc segment is time-dependent and somehow is related to the time since the last great event that occurred in the segment;

- 2) A revised source definition with arc segmentation related to the historic record of great earthquakes; and

- 3) Usage of updated or modified **groundmotion** attenuation laws suitable for the Alaska-Aleutian subduction zone setting.

Results of these revisions and software development are summarized in the Final Report to NOAA-OCSEAP prepared by **Woodward-Clyde** Consultants (1982, and herein referred to as WCC).

In our opinion the following additional improvements should be incorporated in future efforts or at least need further consideration:

- 1) " Integration of the historic **seismicity** record for great earthquakes ($M_w \geq 7.8$) presented in this report (chapter 3.4) for the purpose of specifying the initial "state" of arc segments in the model of the **Markov-process** for great earthquakes as defined in Section 4.1 of Volume I of WCC (1982), provided the **Markov-model** is to be used.

- 2) A critical assessment of whether the **Markov-model** yields similar results for conditional probabilities for great earthquakes as those presented in chapter 4.1 (Figure 4.1.1) of the present report.

- 3) A test of the transition-probabilities p_{ij} and of holding times h_{ij} (defined in Wcc, 1982) using the data set of Table 3.4.8 of the present study.

- 4) A westward extension of the "**thrust-and-Benioff** seismic source" beyond those sources shown in Figure 2, Volume 2 of WCC (1982) to incorporate the entire 1946-rupture zone, **Unalaska** Gap, and the 1957 rupture zone. These source regions will contribute to

seismic exposure particularly in the southern portions of the St. George Basin. They will clearly affect adjacent regions of potential future interest (i.e., **Umnak-Plateau, Unalaska** Island).

5) A redefinition of the presently ill-defined '**Yakutat** Gap' and '**Yakataga** Gap' thrust zone sources (Figure 2, Volume 2 of WCC, 1982).

6) Comparison of "Random Source 1" and "Deformed Source 1" outlined in Figure 2, Volume 2 of WCC (1982) with regard to level and spatial distribution discussed in chapters 3.1 and 3.2 of the present study (i.e., see Figure 3.1.4). Clearly these sources must be extended to **the** S-W in order to avoid a fictitious southwesternly decrease of expected **groundmotion** levels as produced by preliminary maps based on WCC (1982).

7) Probably the single most important future improvement for seismic hazards assessment in the eastern Aleutian arc may come from a new strong motion data set to be collected in the Alaska-Aleutian subduction zone environment. The problems arising from the virtual absence of such a data set are discussed throughout this report but are specifically addressed in chapter 3.3 of this study.

In summary: previous studies have made important contributions to improve the methods of quantitative hazards assessment. The present report provides the data base, that can now be used as input into existing programs for computing and mapping of hazards. Furthermore, we show where the data base needs to be improved before reliable hazards assessments can be made. We also point to incomplete or erroneous data that have been used **in** the past.

3. DATA ANALYSIS

3.1 Seismicity Recorded by the Shumagin Network 1973-1981

Introduction. Since 1973 **L-DGO** has operated a short-period, high gain seismic network in the Shumagin Islands region, eastern Aleutians, Alaska. The purpose of operating the network is to collect data that can be applied for analysis of seismic and volcanic hazards as well as for basic seismotectonic studies. The specific tasks related to the analysis of hazards consist of: 1) to determine the hypocenter and magnitude of all locatable earthquakes; 2) to develop frequency of occurrence versus magnitude relationships; and 3) to correlate the shallow seismicity with possible geologic faults.

The details of how the earthquake data were processed are described in Appendix 7.1. The **hypocenter** locations are determined by the computer program **HYPOINVERSE** (Klein, 1978). Using **P-** and S-wave arrivals from more than three stations the program calculates geographical coordinates and depth of the hypocenter as well as uncertainties in arrival times and spatial coordinates. These uncertainties are relative to the flat-layered velocity model and hence, do not include possible systematic biases in the earthquake locations.

For most of the earthquakes recorded since 1977 either coda length or amplitude magnitudes were determined. Prior to 1977 neither amplitudes nor coda lengths had been read. Moreover, since not all the instrument constants and gains are known for this earlier period, it is not possible to determine with any certainty magnitudes for the old data before 1977. A further description of the computations of magnitudes of the earthquakes is included in Appendix 7.2.

As an initial step toward analysis of seismic hazard in the region we evaluate below: 1) the spatial distribution of **seismicity**; 2) the rate of **seismicity**; and 3) the linear alignments in the seismicity. The objective of this analysis is to identify the main features in the data that can play a crucial role in identifying the seismic sources for the construction of a seismic exposure map for the eastern Aleutians.

Seismicity distribution and tectonics. In the **Shumagin** Islands-Cold Bay region the rate of occurrence of small to moderate size earthquakes ranges from 350 to 800 earthquakes per year. This seismicity is associated with the subduction of **the** Pacific Plate underneath the North American Plate, which takes place at an average convergence rate of about 7.5 **cm/yr** (Minster and Jordan, 1978).

In Figure 3.1.1 we have plotted all the earthquakes located by the Shumagin network from 1973 to the end of 1981. The symbol type indicates within which depth range the earthquake is located and the actual symbol size is proportional to magnitude. If no magnitude is available for a particular earthquake a symbol size equivalent to magnitude one **is** plotted. Data from the seismic stations that are shown as triangles were used to calculate both the hypocenters and magnitudes. (See also Appendix 7.4 regarding station status during 1973-1982.)

The axis of the Aleutian Trench is defined by the 5000 m bathymetric contours in Figure 3.1.1 and its orientation is almost perpendicular to the direction of plate convergence, north 30° west. The region that extends from the axis of the Aleutian Trench approximately 100 to 150 km to the north north-east and constitutes the expected rupture zone of great plate-boundary earthquakes, is presently almost **aseismic**. The bulk of the shallow seismicity in Figure 3.1.1 is located close to the down-dip end of the main thrust zone and is associated with deformation of the upper plate.

Figure 3.1.2 shows only the shallow seismicity where we have plotted high quality solutions as open circles and low quality solutions as **y's**. The general pattern consists of high-quality solutions (open circles) within the network and low-quality solutions (y's) outside the network extending across the trench. The largest clusters of shallow activity are located on the Shelf between the inner wall of the trench and the Alaska Peninsula. These clusters cut across both the Shumagin Islands and the **Sanak** Basin forming an approximate east-west trend that coincides with the down dip edge of the main thrust zone. In addition, several significant **lineaments** of shallow seismicity are found throughout the region.

The seismicity at depths ranging from 40 to 250 km is shown in Figure 3.1.3 where we have excluded the seismicity that is shallower

than 40 km. **This seismicity** defines the Benioff zone, which outlines the subducted part of the Pacific Plate. A striking feature of the deep seismicity is the fairly **uniform** spatial distribution of activity extending from the **CNB-station** toward north north-west beyond the volcanic axis. Both toward west and east of the network the locatable activity tapers off because **small** earthquakes are no longer being detected. In Appendix 7.4 we have included annual maps and cross sections of **Shumagin seismicity** from 1973 to 1982, which give a detailed picture of temporal and spatial variations in the seismicity.

Rates of seismicity. An important step in establishing recurrence relations for moderate size earthquakes **is** to evaluate whether the available seismic data are complete and cover a long enough time period. To ensure that all recorded moderate size or large earthquakes are included we cross checked the Shumagin **catalogue** of earthquakes with the **PDE-bulletin**. The next step consisted of checking how continuous the data are through time and if the rate of seismicity is anomalously low or high during the period on which the calculation of the recurrence relation is based.

The continuity of data recorded by the **Shumagin** network varies considerably through time as is shown in Figure 3.1.4. **Hence**, it is difficult to make meaningful statements about the rate of seismic activity from 1973 to 1978, based on the Shumagin network data alone.

During the first half of 1974 and second half of 1975 the level of seismic activity, however, appears to be somewhat higher than the average level observed until the end of 1977 (see Figure 3.1.4). The increase in activity in **April** 1974 consist in part of an aftershock sequence following a pair of large earthquakes of magnitude 5.8 and 6.0 that occurred near the Nagai Island.

Since early 1978 to present the data recording has been almost continuous (Figure 3.1.4). The temporal distribution of the seismicity since 1978 is illustrated in Figure 3.1.5 where we have plotted the cumulative number of earthquakes located by the Shumagin network since 1978 to present. The data shown in Figure 3.1.5 demonstrate that the seismicity rate in the **Shumagin** region was higher during 1978 and 1979 than it has been during 1980 to 1982. Anomalously high levels of both shallow and deep seismicity contributed to the burst in activity during 1978 and 1979.

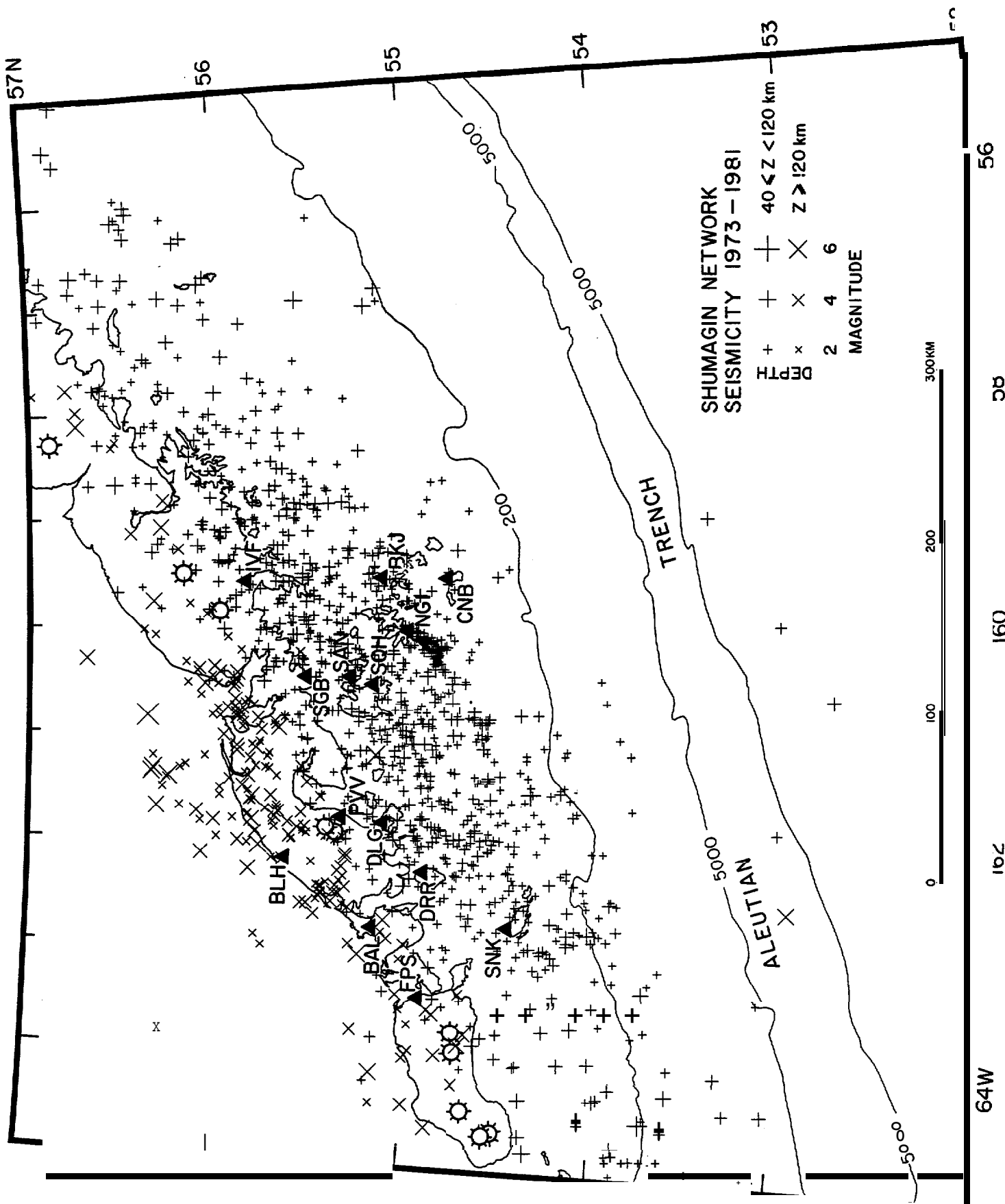


Figure 3.1.3. Map of epicenters showing all the intermediate depth and very deep seismicity (depth greater than 40 km) located by the Shumagin network, eastern Aleutians, Alaska, from 1973-1981. (See also the caption of Figure 3.1.1).

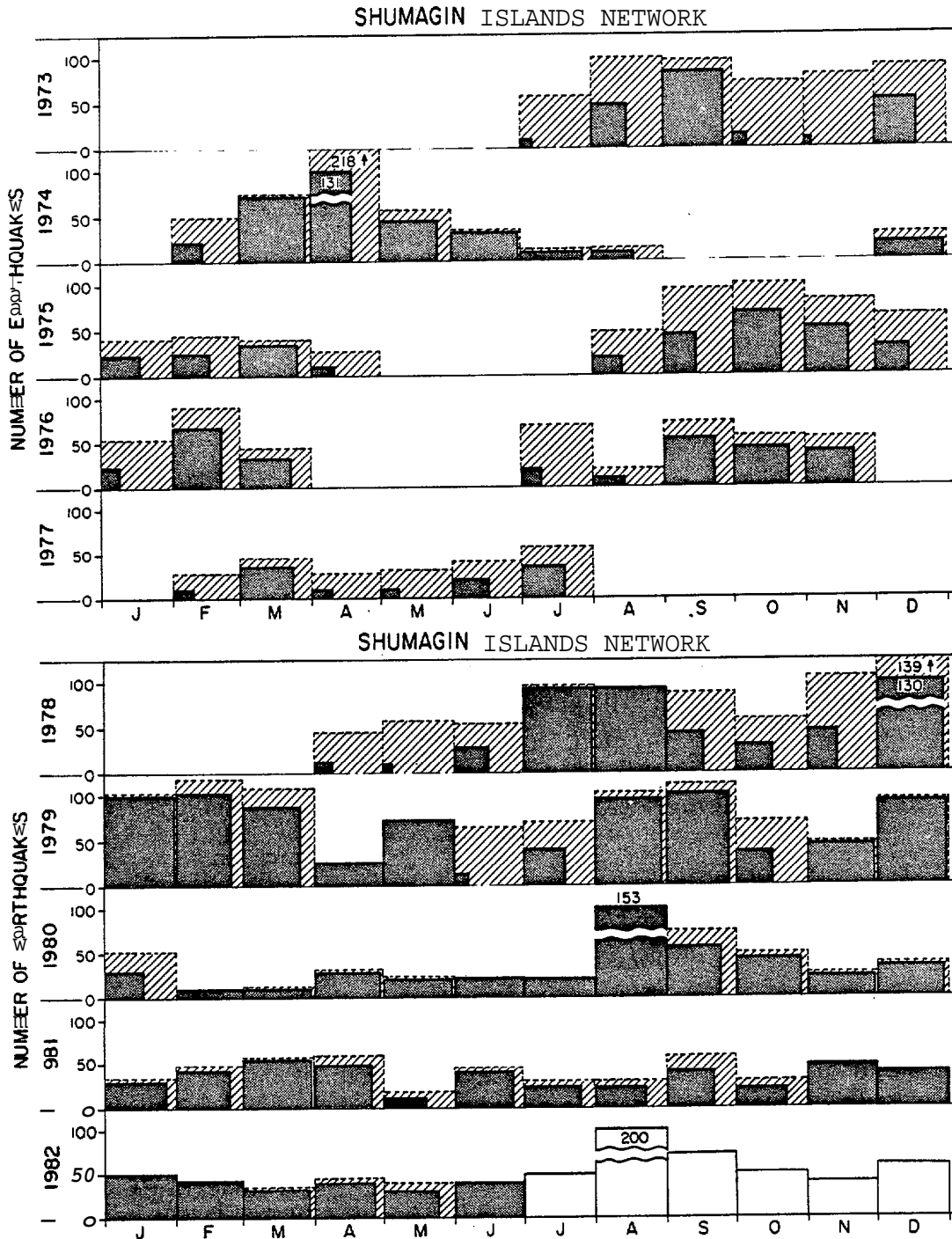


Figure 3.1.4. Histogram of number of earthquakes located by the Shumagin seismic network, eastern Aleutians, Alaska. The dark, stippled rectangles represent total number of events versus number of days in a month during which data was recorded. The hatched rectangles represent the monthly number of events, which is estimated from the stippled rectangles.

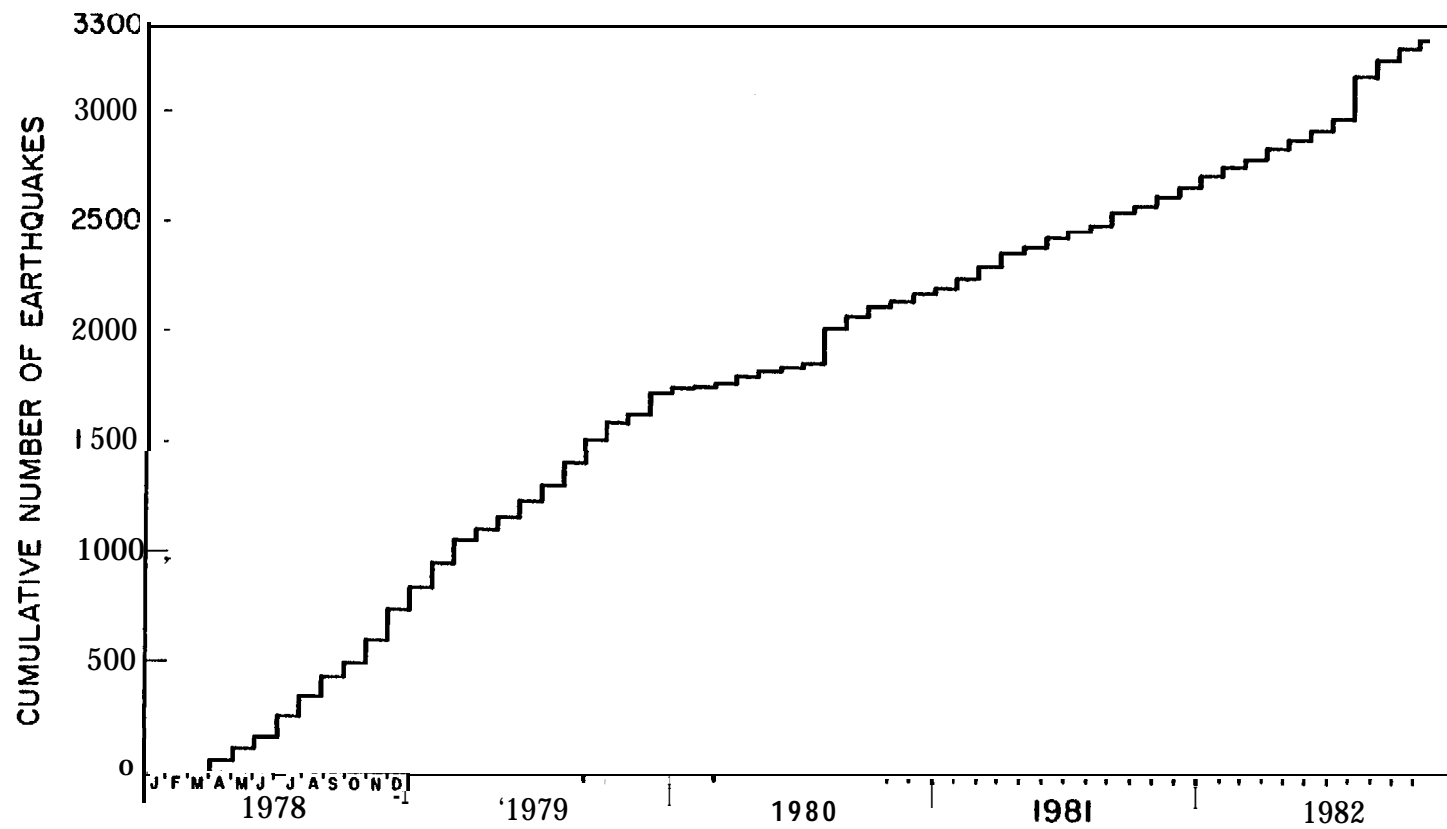


Figure 3.1.5. cumulative number of all local earthquakes located by the Shumagin network from 1978 to 1982.

We conclude that the time period from 1977 to end of 1981 is probably representative of the long-term **seismicity** rates of background activity in the eastern Aleutians. Especially, since this time period contains a burst in activity and a following period of average activity it is unlikely that we are underestimating the rate of earthquake occurrence.

b-values. A fundamental part of evaluating **seismic** hazard consists of determining repeat **times** for large and possibly damaging earthquakes. Calculations of repeat times for a region that is not located exactly along a plate boundary but rather adjacent to it, such as the **Shumagin Shelf**, often are based on the Gutenberg-Richter relation,

$$\log N = a - bM$$

where N is the number of earthquakes with magnitude greater than or equal to M, a and b are **empirical** constants. If representative values of a and b are known for a region, one can calculate N per **unit time** and **unit** area for a **given** maximum magnitude **using** the equation above.

We have applied the **Shumagin** data from 1977 to 1981 to determine values of a and b using the method of maximum likelihood as described by Page (1968) (see Figures 3.1.6 and 3.1.7). It is worth pointing out that the cumulative number of earthquakes in Figures 3.1.6 and 3.1.7 levels off at smaller magnitudes because distant smaller earthquakes are not recorded or included in the analysis. In a similar way the cumulative curve may drop off more rapidly at larger magnitudes, if the period of observation is too short compared to the repeat time of the larger earthquakes.

In Figure 3.1.6 we have included in the b-value calculation all the earthquakes since 1977 for which magnitude values are available. The a and b-values were calculated for the magnitude intervals 2.5-6.0 and 3.0-5.5 to test for a possible absence of smaller earthquakes. The two b-values of 0.75 ± 0.06 and 0.85 ± 0.09 fall within the approximate 95 percent confidence limits of each other. These b-values are in the same range (0.8 to 0.9) as determined by Page (1968) for aftershocks following the Great Alaskan 1964 earthquake.

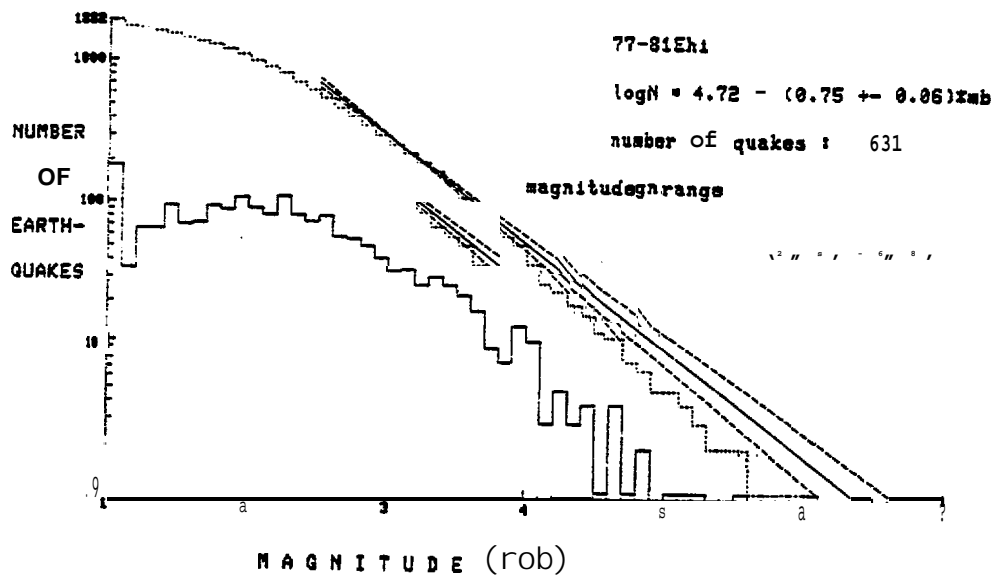
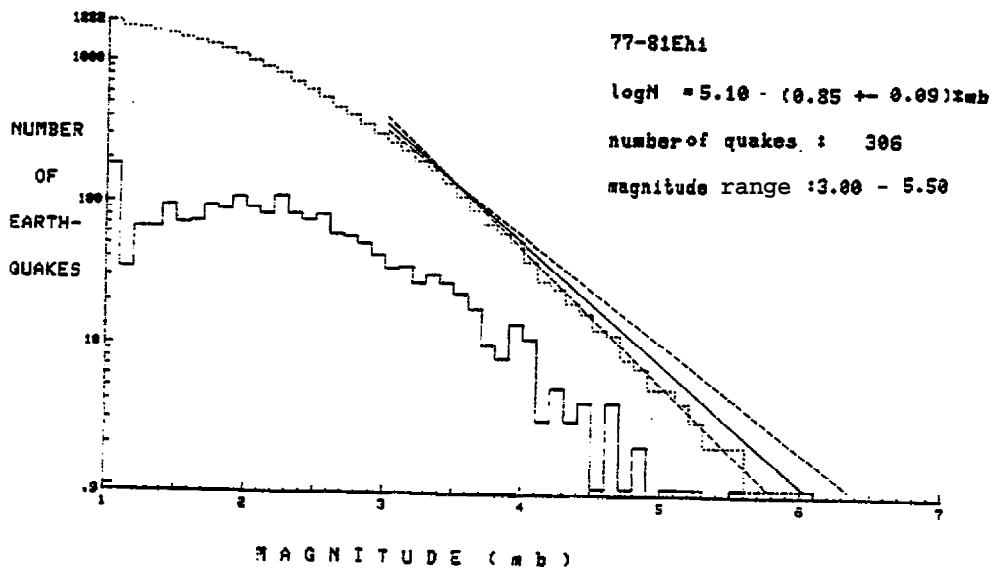


Figure 3.1.6. Both cumulative number and number of earthquakes as a function of magnitude for the whole data set recorded by the Shumagin network from 1977 to 1981. (above) magnitude range is 2.5-6.0; (below) magnitude range is 3.0-5.5. Note that maximum, minimum and average b-value slopes are plotted.



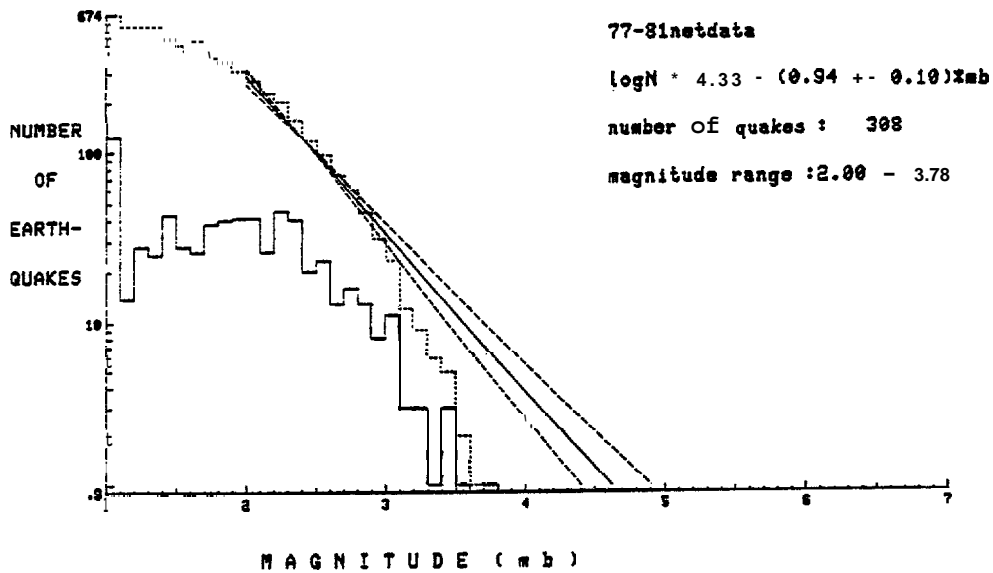
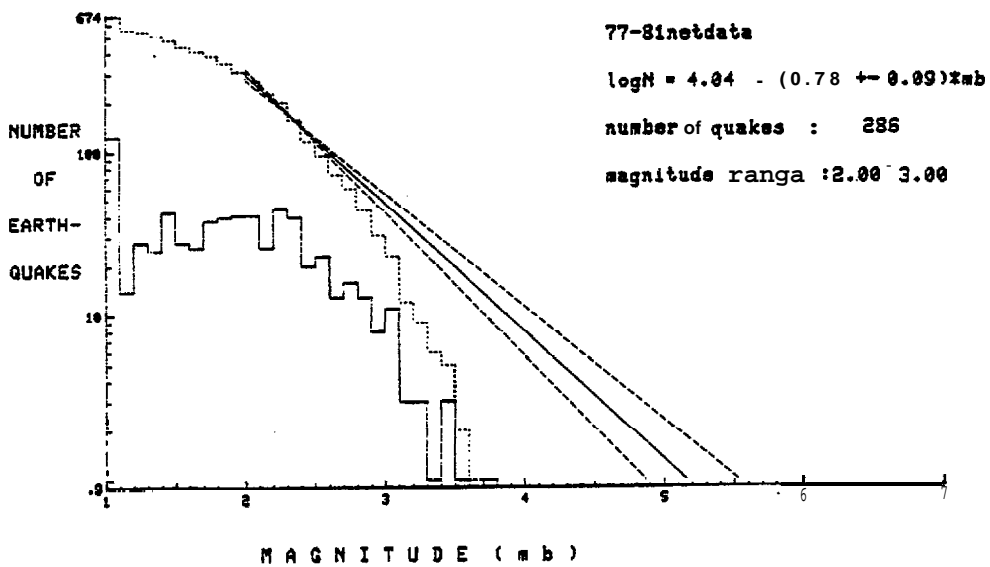


Figure 3.1.7. Both cumulative number and number of earthquakes as a function of magnitude for all shallow earthquakes (depth less than 30 km) recorded by the Shumagin network from 1977 to 1981. (above) magnitude range is 2.0-3.7; (below) magnitude range is 2.0-3.0.



To investigate, if the seismicity shallower than 30 km has a- and b-values that differ from the values calculated for the whole data set, we have determined separately **a-** and b-values for the shallow **seismicity** (see Figure 3.1.7). (The shallow **seismicity** also is plotted separately in Figure 3.1.2.) We note that the number of earthquakes of magnitude greater than 3.1.5 is much smaller than in Figure 3.1.6. The b-values estimated from the data in Figure 3.1.7 fall within the same range as the values estimated from the whole data set. The a-values in Figure 3.1.7 are somewhat smaller since the data set of only shallow earthquakes is smaller than the whole data set. The smaller a-values and the lack of moderate size earthquakes suggest that a longer monitoring period might provide more reliable a- and b-values for the eastern Aleutians.

In conclusion, the a- and b-values that result from this study are inherently more reliable than previously published values, since those were usually based on much smaller data sets (e.g., Page, 1968; **Utsu, 1962**).

Lineaments of seismicity. To estimate the size of the maximum expected earthquake in a given region some knowledge of the distribution of possible geological fault lengths is needed. On land such information is gained through geologic mapping, but in submarine areas expensive seismic reflection studies are needed to map the fault structure. In both cases seismicity data can be used to identify presently active faults.

Although seismic reflection data were collected in the Shumagin region in October 1982, no results are available yet. Hence, we have attempted to use **seismicity lineaments** to evaluate the approximate distribution of fault lengths in the region. In Figure 3.1.8 **seismicity lineaments** are identified by visual inspection of the shallow (less than 30 km) **seismicity**. In all the cases where dense, linear clustering of seismicity occurs we have drawn a line that represents the observed linear alignment of epicenters. The results of this method, which only yield an approximate **estimate** of the distribution faults, can be improved in the future by **applying** relative master-event location techniques and by constructing fault plane solutions for the shallow seismicity.

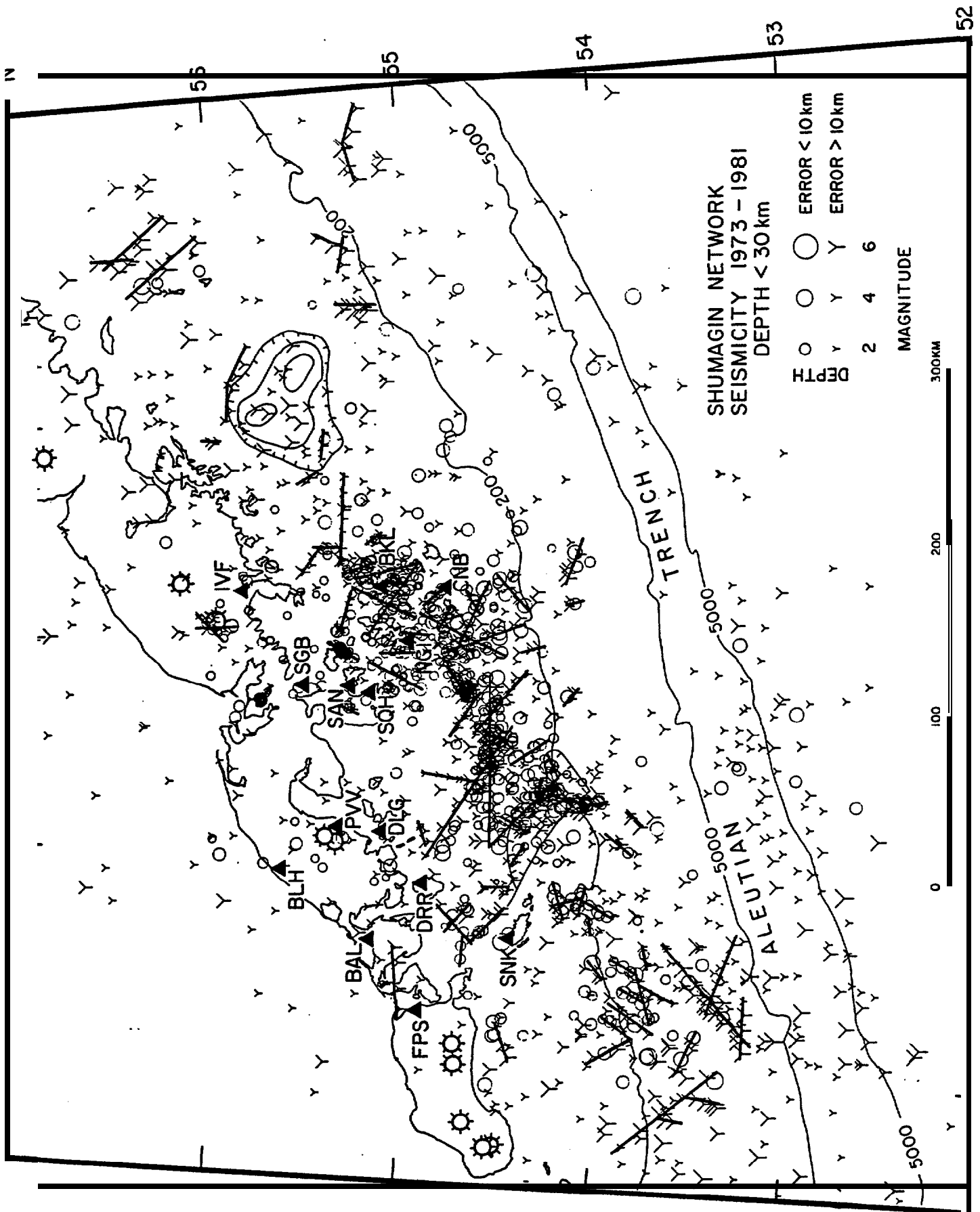


Figure 3.1.8. Map of epicenters (same as Figure 3.1.2) where seismicity lineaments are emphasized by drawing straight lines by eye through clusters that appear to form linear alignments.

A histogram of number of **lineament** lengths is presented in Figure 3.1.9. **Lineament** lengths of 10 to 30 km appear to be most common. The **lineaments** shorter than 10 km are probably under-represented because the **scale** of the Figure 3.1.8 makes it difficult to resolve those. It is a somewhat surprising result that only a very few **lineament** lengths from 30 to 100 km length are identified.

Presuming that the most commonly occurring source dimension is 30 km or less, we can apply known source dimension versus magnitude relationships to estimate the maximum magnitude of the earthquake that corresponds to the particular source" size (see Figure 3.1.10). The particular relationships that are shown in Figure 3.1.10 are based on: 1) data from California (**Wyss and Brune, 1968**); 2) data from Japan (**Wesnousky et al., 1982**); and 3) a general relationship established by Wyss (1979). Furthermore, we have also plotted data from two source parameter studies in the **Shumagins** by House and **Boatwright** (1980) and **Hauksson** (1982). The relationships in Figure 3.1.10 indicate that a source dimension of 30 km can be associated with an earthquake magnitude of 5.6-7.1. Hence, a prudent approach would be to assume that the maximum size of a random source within the **Shumagin** Shelf can be associated with a magnitude 7.0 earthquake.

A general recurrence relation for the Gulf of Alaska, which was established during the early stages of the **OCSEA** program is plotted in Figure 3.1.11. This general relation is based on a maximum earthquake source of 7.0 which is in agreement with our studies of the length of seismicity lineaments. The relative rate of recurrence of the maximum random source, however, may be underestimated by as much as a factor of 6 for shallow sources or a factor of 30 when all possible random sources are included.

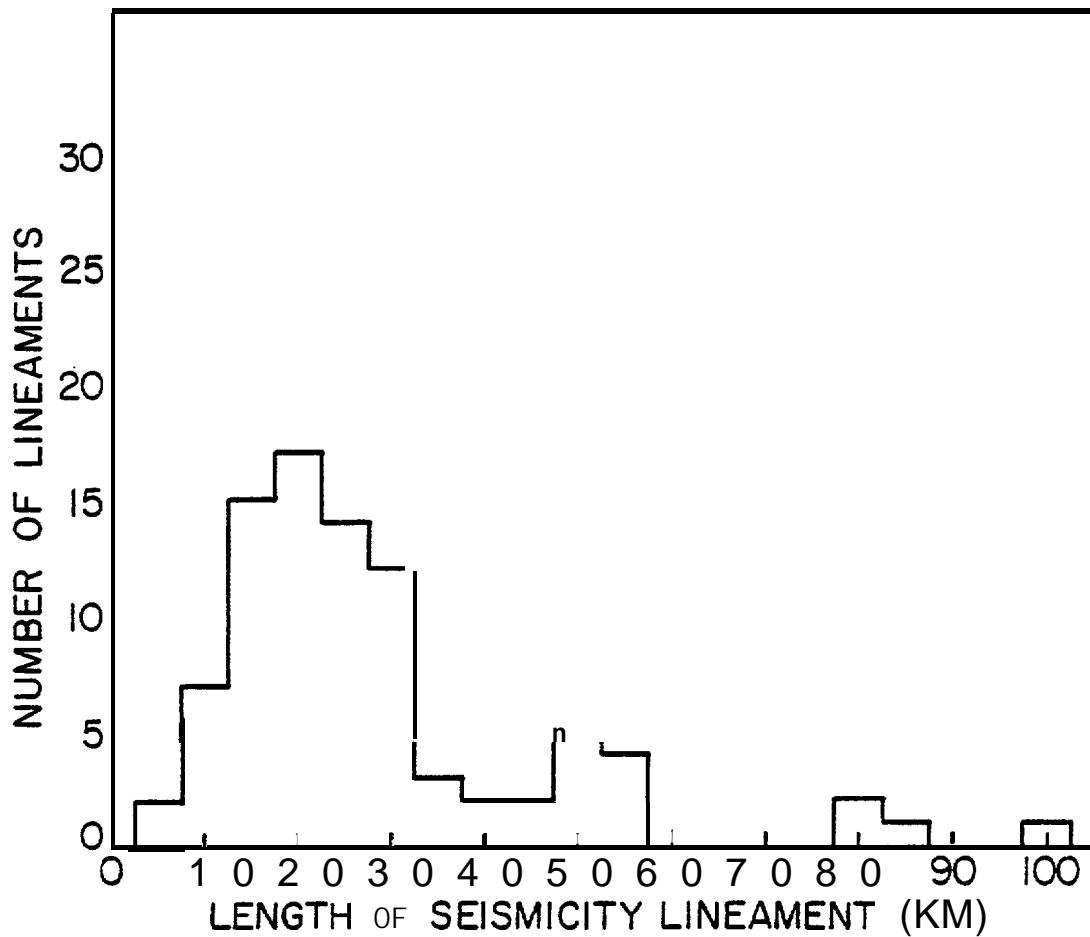


Figure 3.1.9. Cumulative number of- **seismicity lineaments** from Figure 3.1.8 **versus**, length of seismicity **lineament**. Note the lack of **lineaments** in the **rang** from 30 to 100 km.

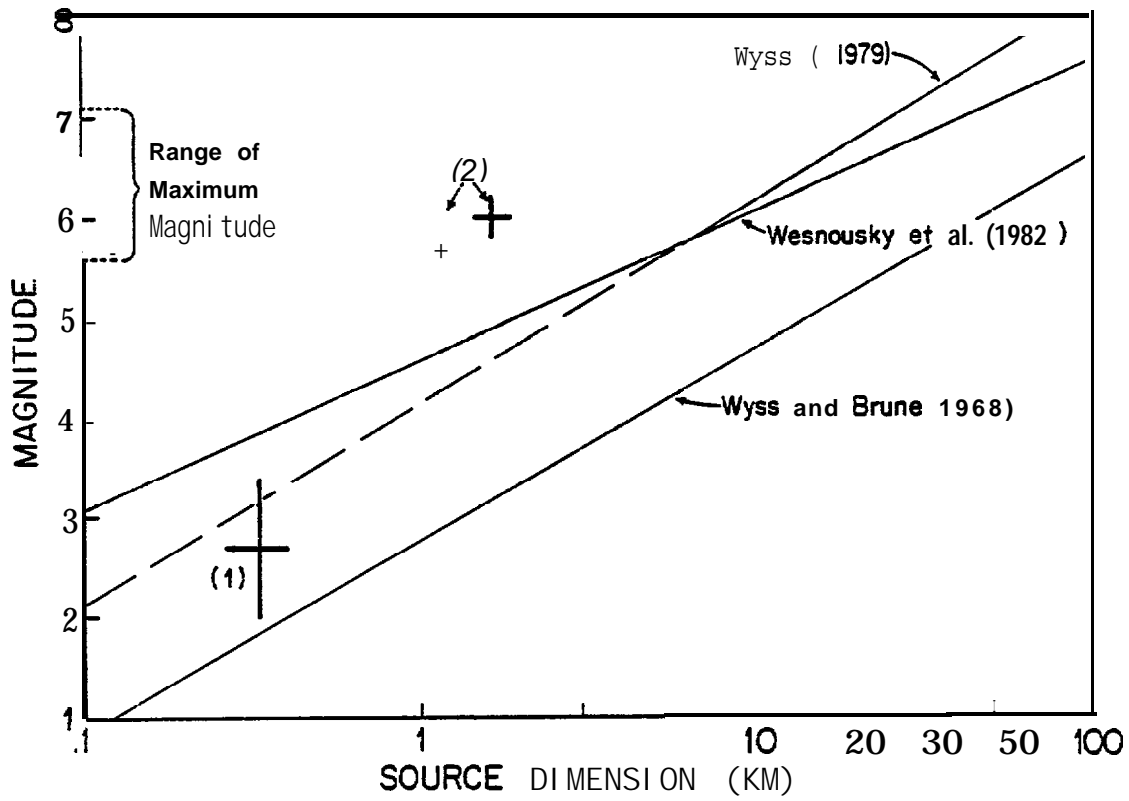


Figure 3.1.10. Magnitude versus source dimension relationships. The data points: 1) is from Hauksson (1982); and 2) is from House and Boatwright (1980); see also the text. The probable range of maximum magnitude is indicated on the left.

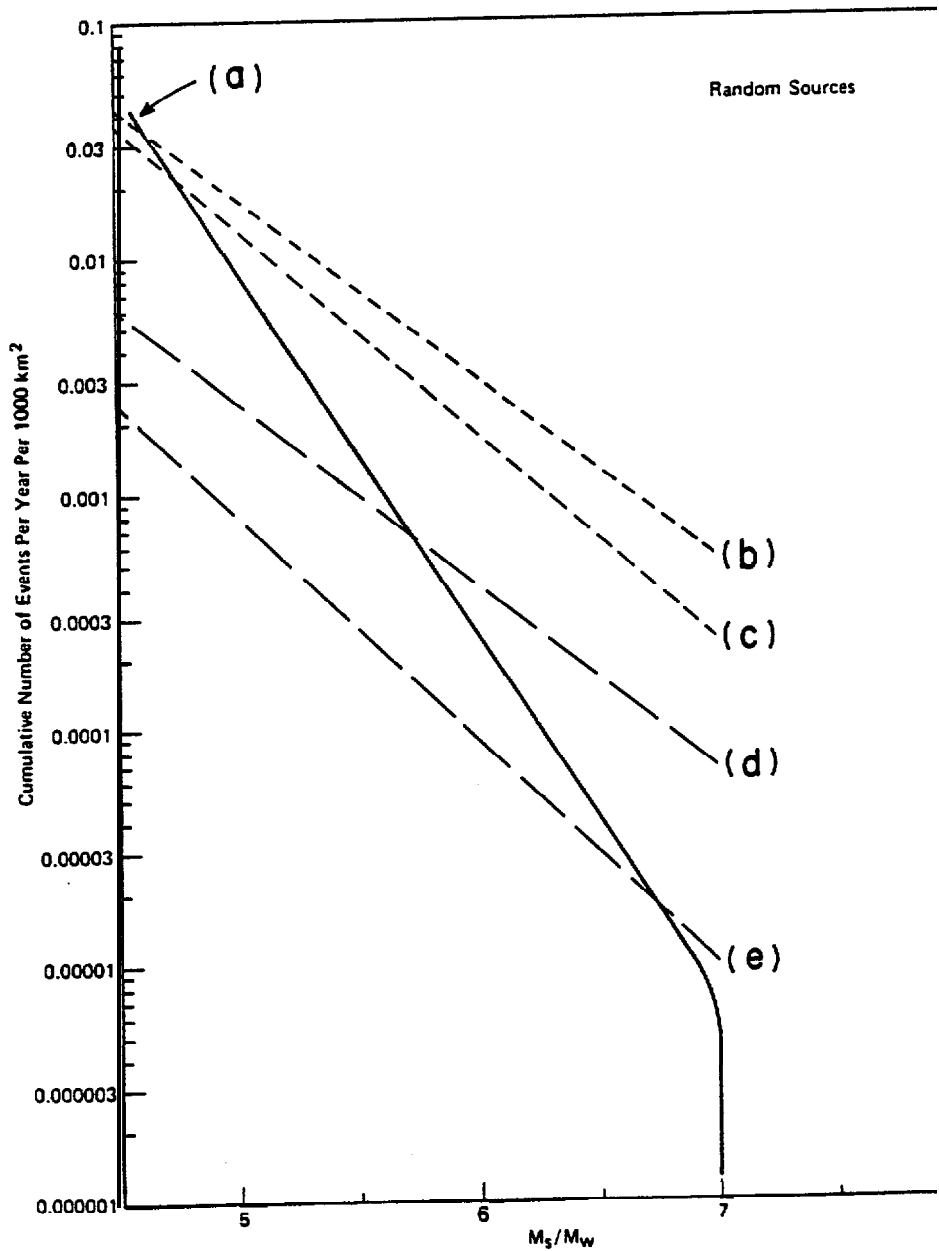


Figure 3.1.11. Recurrence Relation for the Gulf of Alaska Random Sources. a) the initial curve; b) curve based on b-value for all sources in Figure 3.6 (above); c) curve based on b-value for all sources in Figure 3.6 (below); d) curve based on b-value for only shallow sources in Figure 3.7 (above); and e) curve based on b-value for only shallow sources in Figure 3.7 (below).

3.2 Teleseismic Data 1973-1982

As an independent means of **verifying** the results of the data from the **Shumagin** network, we have analyzed **seismic** data from the **Shumagin region** recorded by the National Earthquake Information Service (**NEIS**) at **teleseismic** distances. These **teleseismic** data are published in the Preliminary Determination of Epicenters (**PDE**) Bulletin.

The PDE data are considered to be continuous **in time** and **in** most cases PDE magnitudes for larger earthquakes ($M > 4.0$) are more homogeneous than magnitudes from local networks. The major drawbacks with PDE data are that they have a rather high minimum magnitude threshold of detection ($M \approx 4.5$ in **the Shumagins**) and **epicentral** locations may be systematically biased in island arc regions by **as** much as 20-40 km away from the trench.

Figure 3.2.1 is an **epicentral** map of the **teleseismic** data located **within** the **Shumagin region** from 1973 to 1981. When comparing Figures 3.1.1 and 3.2.1 we see that there **is** a substantial difference **in** the level of activity and many of the patterns seen in the **Shumagin** network data are almost absent. The **region of high activity** west of the station, SNK (**Sanak** Island) coincides **with** the aftershock zone of a major earthquake **in** 1946 as described by Sykes (1971). Another cluster **is** observed south of the **Shumagin Basin** (latitude 55.5°N and longitude 157°W) and consist of a 6.5 magnitude main shock-aftershock sequence in 1979. As also demonstrated by the **Shumagin** network, shallow earthquakes appear to be more common on the Shelf than between the Shelf and the trench axis.

The temporal rate of occurrence of earthquakes located **using teleseismic** data **is** illustrated in Figure 3.2.2. We have plotted a bar **with** a length proportional to magnitude for each earthquake and next **to** it we show the depth of the earthquake in kilometers. It is worth noting that the rate of occurrence of **teleseismically** located earthquakes is fairly uniform in time, except for the burst in activity during 1978 and 1979. In the last 10 years six earthquakes of magnitude 6.0 or greater have occurred in the **Shumagin** region. The cumulative number of **teleseismically** located earthquakes within the **Shumagin** region show a similar trend as the seismicity located by the

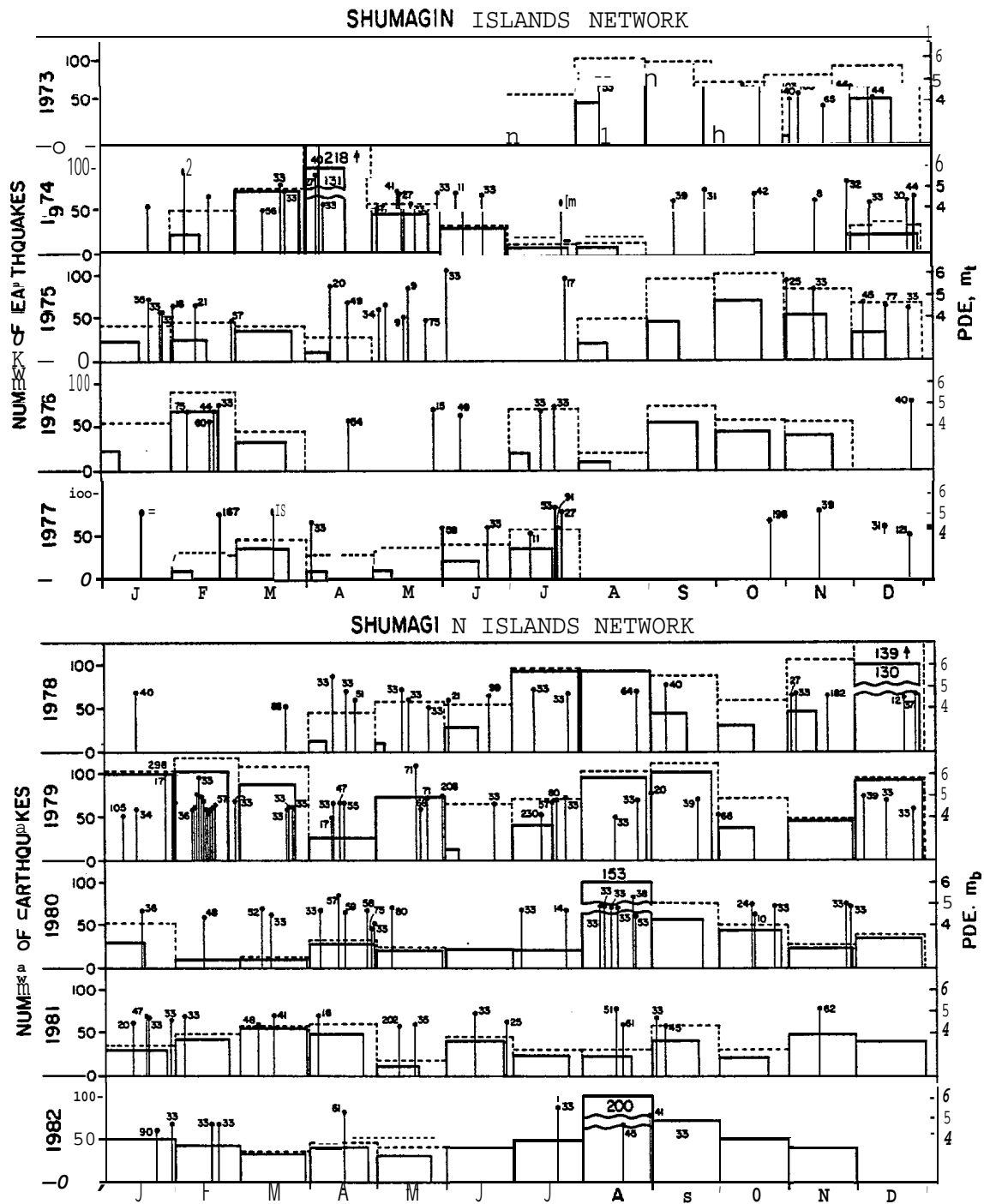


Figure 3.2.2. The vertical bars indicate the occurrence and the magnitude of teleseismically located earthquakes from the PDE bulletin. The solid line and dashed line rectangles indicate the number of earthquakes located by the Shumagin network (see also Figure 3.1.4).

Shumagin network, with a burst **in activity during** the latter half of 1978 and 1979 (see **Figure 3.2.3**).

The more **subtle** or smaller changes **in** the rate **during** 1973-1975 compared to **during** 1975-1979, however, are considered to be changes **in** the **teleseismic** detection threshold (**Habermann, 1983**).

The b-value ($b = 0.92 \pm 0.10$, see **Figure 3.2 .4**) for the **teleseismic** data **is** similar to what was observed for the **Shumagin** network data (compare **Figures 3.1.6, 3.1.7 and 3.2.4**). Although the **Shumagin** network data are somewhat discontinuous in time, the similar b-values indicate that both the **teleseismic** and the network data sets are **fairly** homogeneous,

In conclusion, when comparing **teleseismic** and **Shumagin** data we have found: 1) a **fairly** steady rate of occurrence of earthquakes **in** the magnitude range 4.5 to 6.0 during the last 10 years; 2) the temporal increase **in** the rate of occurrence of earthquakes appears **in** both data sets; and 3) both data sets show **similar** b-values although the network b-value **is** based on the magnitude range 2.0-6.0 and the b-value of **teleseismic** data **is** based on the magnitude range 4.4-6.3.

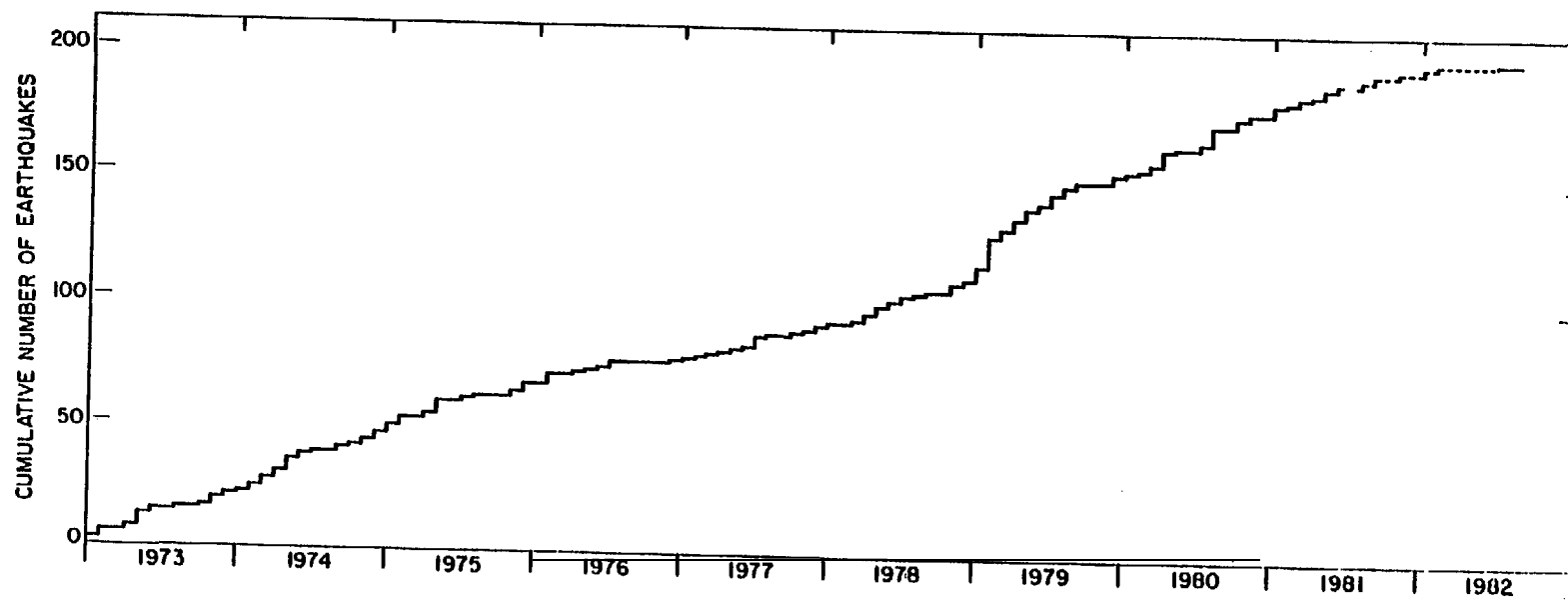


Figure 3.2.3. Cumulative number of earthquakes located by the PDE from 1973 to 1982 in the Shumagin Islands region. (The region chosen is 52°N to 57°N and 156°W to 165°W).

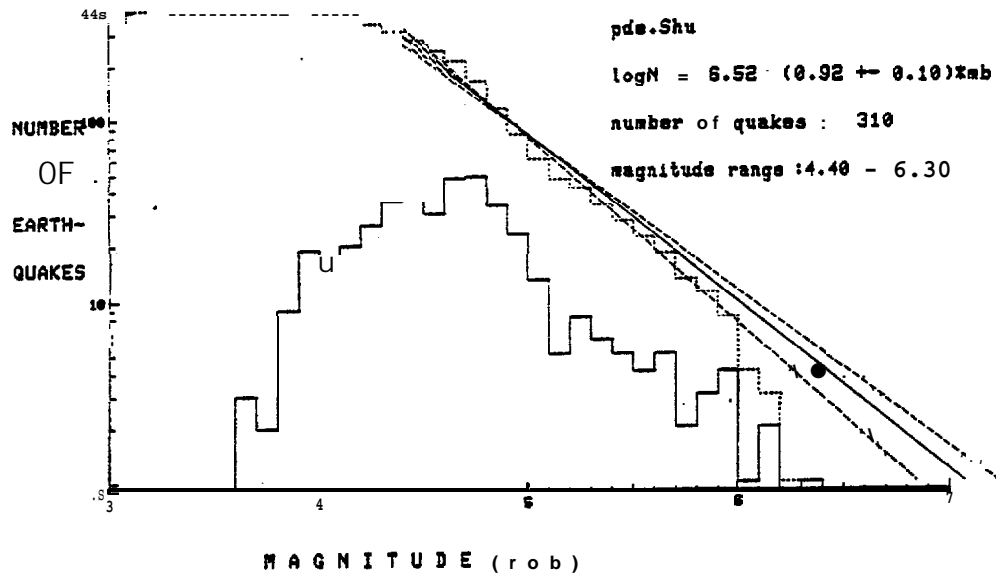
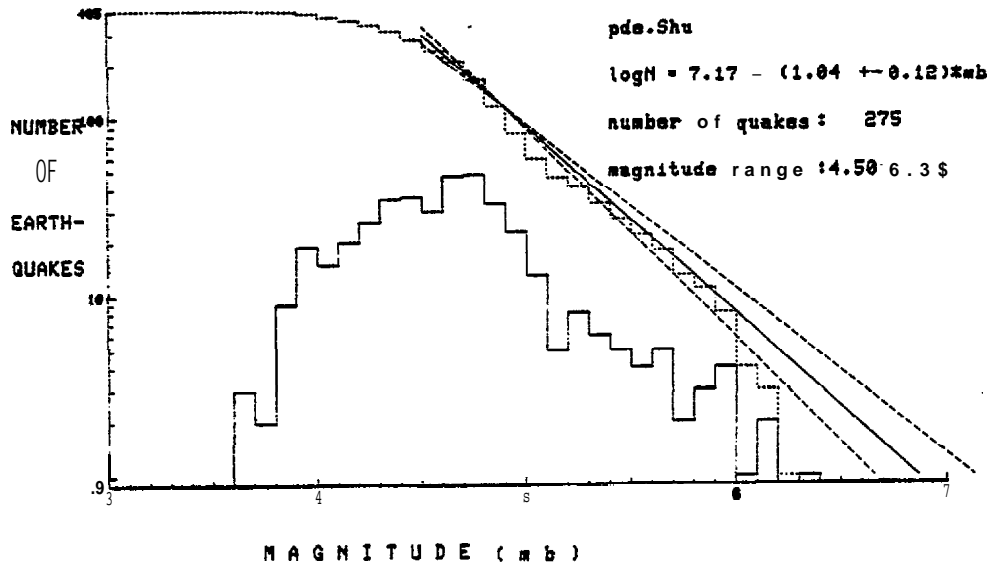


Figure 3.2.4. Both cumulative number and number of earthquakes as a function of magnitude for the PDE data from 1973 to 1981 located in the Shumagin Islands region. (above) magnitude range is 4.4-6.3; (below) magnitude range is 4.5-6.3. Maximum, minimum and average b-value slopes are plotted.



3.3 Strong Motion Data

3.3.1 Historic overview: a subject of neglect. The near-absence of a sufficient strong-motion data base in Alaska is probably the weakest element in any seismic hazards assessment for Alaskan OCS regions. Historic, and still persisting factors have contributed to this severe deficiency. Remedies are urgently needed. Some of the contributing factors are:

1) Large portions of Alaska have lacked until recently in major civil engineering projects such as major highways, bridges, dams, (nuclear) power plants, etc. The Alaska Pipeline, several airports and a few military installations and communication links are but some notable exceptions. The deployment of strong motion **accelerographs (SMA-s)** has been traditionally linked to major existing engineering projects, rather than being guided by seismological priorities or long-term land-use considerations, planning ahead of actual developments. Because of the few structures of principal engineering interest, the **U.S.G.S.** (or its cognizant predecessor agencies, i.e., U.S.C.G.S.) operated only one or at most two dozen strong motion instruments distributed throughout the 4000 km long seismic belt stretching from Shemya to **Ketchikan**, not counting interior Alaska. No state program is (as yet) in existence. Most strong motion instruments were installed after(!) the great Prince William Sound earthquake ($M_w = 9.2$) of 1964, mostly in buildings in Anchorage and a few other municipalities or communication centers. (In comparison, over a smaller and less seismic, but more populated region along the California West Coast, more than a thousand instruments are operated by federal, state and local agencies and/or the private sector.) With an average spacing of several hundred miles between instruments - as is the case in most of Alaska - one can hardly collect strong motion data that can be analyzed in a sensible way.

2) Alaska's subduction-zone tectonic setting is unique in the U.S. in that it exposes any structures to earthquakes (with magnitude M_w up to 9.2) that are among the largest on earth. Their ruptures extend in length up to many hundreds of kilometers and result in rupture durations of one to three minutes and severe shaking that can

easily last twice as long. Nowhere on earth has such an earthquake been recorded by strong motion **accelerographs**, not in Alaska, not (yet) in Japan, nor anywhere else. The likelihood that future or existing structures near the **Shumagin** (i.e., St. George and North Aleutian Basins) and **Yakataga** gaps will be exposed to shaking from such giant earthquakes is very high during the next few decades (chapter 3.4). And so is the chance to monitor such motions. Large or tall structures such as off-shore drilling rigs or production platforms, or **oil** storage tanks at ship or pipe-line terminals with their often low (f. ≈ 1 Hz) natural **eigenfrequencies** must be designed to safely survive the long periods and long durations of strong ground motions that are particular to these giant earthquakes. Since no strong motion record from any earthquake larger than $M_w = 7.8$ to 8 is presently available from anywhere on earth, the design of such structures is based on expert **judgement** and not on hard strong motion data in existence.

3) At an early stage of the OCSEA Program this deficiency of a local **SMA** data base became clear, and two of the research units (RU 210 in the **Yakataga** gap, and this project, RU 16, in the **Shumagin** gap) installed each about a dozen strong motion instruments (mostly with USGS funding for instruments) in both high-probability regions. Both SMA networks became fully operational only until the final 1 or 2 years of the **OCSEA** Program--much too late to collect a significant number of SMA recordings. Since termination of the **OCSEA** Program in both regions, **SMA** operation is jeopardized (e.g., requests to NSF and USGS for continued support of the Shumagin SMA network have been declined to date). Under **this** circumstance SMA operation at least **in** the **Shumagin** seismic gap could cease **in** summer 1983 despite the potential for a great earthquake **in** that gap. We urge that federal, state, scientific, and engineering institutions work together to reverse this historic trend of neglect and ensure that the proper strong motion data base will be established. Without this data base, engineers will not be able to cost-efficiently safeguard in their designs against excessive losses from great subduction earthquakes.

The remainder of this section summarizes the strong motion data that presently exist and some of their characteristics.

3.3.2 Peak horizontal accelerations - the Alaska data set.

We have systematically searched through the U. S. G. S. data files and original-record archives collecting both unpublished original data and derivative information accessible from the U.S.G.S. strong motion computer data banks (SMIRS). We were able to compile a list of recorded peak accelerations that include those from our own processed Shumagin records, for which the associated earthquakes and their magnitudes, epicenters and depths are well known. The list of compiled peak accelerations and pertinent parameters are shown in Table 3.3.1. In compiling the earthquake source parameters we have attempted to use the most reliable sources. For example, for earthquakes in the Shumagin Islands region we chose the local-network location parameters rather than PDE (N.E.I.S.-U.S.G.S.) teleseismic determinations. For magnitudes we attempted to use what we perceive the closest approximation to a uniform moment-magnitude scale (i.e., M_w). For this purpose we used $M_w = M_s$ if $m_b \geq 6.0$ and M_w known (usually for $5 \leq M_s \leq 7.5$); $M_w = M_L$ if M_L known ($3 \leq M_L \leq 7$); $M_w = M_s = 1.8 m_b - 4.3$ if no M_s or M_L available (usually for $m_b \leq 6.0$); and $M_w = 2/3 \log M_0 - 10.7$ if moment M (dyn cm) is known.

The formulations for a computed M_s from m_b (PDE) are based on empirical regression curves by Wyss and Haberman (1982) valid for the period 1963-1980. In some instances where several readings of one magnitude type (i.e., M_s (PAS), M_s (BRK), M_s (NEIS)), or where different magnitude types (i. e., M_s , M_L , m_b) gave vastly differing M_w values, we either averaged or had to subjectively decide which value of M_w would best describe the source process as we understand it. Therefore, in some instances the M_w values quoted in Table 3.3.1 may differ in minor aspects from some other author's assessments.

Peak-accelerations are only of limited value in hazards assessment--particularly for giant earthquakes where much of the damage is often related to long durations of severe shaking at low frequencies, rather than peak values. Since information other than peak acceleration is presently rarely available for Alaskan strong

TABLE 3.3.1. Alaska-Aleutian Strong Motion Data.

Record Number	Date	Epicenter	Depth (km)	Magnitude	Station	Distance (km)		Peak Acceleration (g)
						At Surface	Inclined	
1	4/03/64 22:33	61 .62N 147. 39W	41	6.0	2718 Anchorage	136	142	.049
6	6/05/64 22:06	58.14N 152.18W	13	4.7	2710 Kodiak	47	49	.026
7	5/11/65 17:37	61.33N 149.52W	61	5.6	2702 Anchorage	21	65	.050
8	5/11/65 17:37	61.33N 149.52W	61	5.6	2704 Anchorage	23	65	.033
11	9/04/65 14:32	58.29N 152. 50w	30	6.8	2710 Kodiak	60	67	.017
12	12/22/65 19:41	58.35N 153.13W	38	7.0	2710 Kodiak	72	86	.046
13	12/22/65 19:41	58 .35N 153.13W	38	7.0	2719 Seldovia	146	151	.016
14	12/29/65 02:06	54.09N 164.28W	19	6.0	2705 Cold Bay	161	162	.009
17	8/30/66 20:20	61 .34N 147 .44W	45	6.1	2704 Anchorage	132	139	.018
18	8/30/66 20:20	61.34N 147 .44W	45	6.1	2702 Anchorage	132	139	.031
20	6/21/67 18:04	64.91N 147.59W	15	5.4	2721 Fairbanks	13	20	.055
22	10/29/68 22:16	65.46N 150.07W	†	6.7	2707 Fairbanks	125	125	.120
24	12/17/68 12:02	60.15N 152 .82W	82	6.3	2719 Seldovia	101	130	.042
27	3/11/70 22:38	57 .39N 153.97W	16	6.3	2710 Kodiak	97	98	.050
28	4/18/70 08:50	59.82N 152.79W	89	6.0	2713 Seward	190	210	.020
29	4/18/70 08:50	59.82N 152.79W	89	6.0	2719 Seldovia	74	116	.010
30	6/12/70 02:59	61.54N 151 .79W	80	5.6	2703 Anchorage	113	138	.020
32	8/18/70 17:52	60.70N 145 .38w	30	5.8	2706 Cordova	27	40	.020
36	5/02/71 06:08	51 .42N 177.21W	38	6.8	2701 Adak	67	77	.190
38	7/30/72 21:45	56.77N 135.91W	29	7.5	2714 Sitka	45	53	.110
39	7/30/72 21:45	56.77N 135.91W	29	7.5	2708 Juneau	145	148	.010
41	8/03/72 04:40	51.20N 178.13W	24	6.2	2701 Adak	131	133	.010
42	8/15/72 21:39	65 .05N 148.70W	20	4.2	2707 Fairbanks	46	50	.030
a	4/06/74 01:53	54.87N 160.29W	37	5.6	2744 Sand Point	54	65	.100
b	4/06/74 03:55	54.90N 160. 29W	40	5.8	2744 Sand Point	51	65	.120
43	8/13/74 03:46	51.49N 178.11W	47	6.1	2701 Mak	114	123	.040
44	11/11/74 05:17	51.59N 178 .08w	69	6.1	2701 Adak	108	12s	.050
45	12/29/74 18:24	61.57N 150 .60w	65	5.8	2704 Anchorage	54	84	.010
46	12/29/74 18:24	61.57N 150.60W	65	5.8	2703 Anchorage	54	84	.030
47	12/29/74 18:24	61.57N 150. 60W	65	5.8	2702 Anchorage	60	88	.030
48	12/29/74 18:24	61 .57N 150. 60W	65	5.8	2716 Anchorage	54	84	.010
50	1/13/75 00:31	61.40N 150. 58w	68	4.4	2704 Anchorage	42	80	.010
51	1/13/75 00:31	61 .40N 150.58W	68	4.4	2716 Anchorage	42	80	.010
53	5/18/75 15:42	63.17N 150.25W	108	5.4	2727 Talkeetna	97	145	.020
54	7/25/75 10:40	55.04N 160.41W	1	5.6	2705 Cold Bay	148	148	.010

TASLE 3.3.1 (con't.)

Record Number	Date	Epicenter	Depth (km)	Magnitude	Station	Distance (km)		Peak Acceleration (g)
						At Surface	Inclined	
c	7/25/75 10:40	55.04N 160.41W	1	5.6	2744 Sand Point	33	33	.018
55	2/05/75 09:36	59.98N 149.27W	2 8	4.9	2713 Seward	17	3 3	.030
56	1/01/75 03:55	61.92N 149.72W	5 8	6.0	2727 Talkeetna	47	15	.090
57	1/01/75 03:55	61.92N 149.72W	5 8	6.0	2716 Anchorage	79	98	.080
58	1/01/75 03:55	61.92N 149.72W	5 8	6.0	2716 Anch. (roof)	79	98	.140
59	1/01/75 03:55	61.92N 149.72W	5 8	6.0	2702 Anchorage	81	100	.090
60	1/01/75 03:55	61.92N 149.72W	5 8	6.0	2703 Anchorage	81	100	.070
61	1/01/75 03:55	61.92N 149.72W	5 8	6.0	2704 Anchorage	79	98	.050
63	2/22/76 07:21	51.57N 176.81W	6 1	4.7	2701 Adak	38	72	.050
68	9/17/77 21:25	64.81N 147.60W	2 0	4.0	2707 Fairbanks	12	23	.030
69	9/22/77 10:25	51.72N 175.93W	6 5	3.6	2701 Adak	48	81	.010
d	1/27/79 18:57	54.79N 160.64W	5 3	6.2	2744 Sand Point	62	82	.018
e	2/13/79 05:34	55.17N 156.94W	4 7	6.5	2744 Sand Point	227	232	.030
70	2/28/79 21:27	60.64N 141.59W	1 3	7.3	2728 Yakutat	92	93	.090
71	2/28/79 21:27	60.64N 141.59W	1 3	7.3	2723 Icy Bay	25	28	.160
f	2/28/79 21:27	60.64N 141.59W	1 3	7.3	Shell, Monday Creek	33	35	.064

motion records we, nevertheless, use this set of peak accelerations for a brief comparison. Note that most (but not all) of the reported peak **values** are raw readings from the unprocessed records without instrument corrections applied. Also, a few values may be contaminated by building response.

A common practice in strong motion seismology is to plot the respective strong motion parameter versus distance to determine its empirical "attenuation" properties, further parameterized by magnitude of the generating earthquake. Such a plot of the Alaskan peak acceleration data versus distance is shown in Figure 3.3.1 and is superimposed on peak acceleration curves derived by Joyner and Boore (1981) from a **multivariate** regression of a large data set dominated by observations in the western U.S. strike-slip tectonic regime. The Joyner and Boore regression yielded

$$\log A = -1.02 + 0.249M - \log r - 0.00255 r + 0.26P$$

$$\text{with } r = (d^2 + 7.3^2)^{1/2} \text{ for } 5.0 \leq M \leq 7.7$$

where A is peak horizontal acceleration in g, M is moment magnitude, d is the closest distance to the surface projection of the fault rupture in km, and P is zero for 50-percentile values and unity for the 84-percentile values. The curves drawn in Figure 3.3.1 are those for P = 0 (i.e., **50%-iles**) and must be uniformly raised by the amount indicated by the bar (upper right corner of figure) to **yield 85%-ile** curves.

Several aspects become immediately apparent from this comparison of the Alaskan data set **with** the attenuation relationship derived by Joyner and Boore (1981):

- 1) There may be both a DC **shift in** the Alaska data set compared to the Joyner-Boore curves as well as a much larger scatter **in** the Alaska data. For instance the Joyner-Boore **50%-ile** curve for $M = 6.5$ exceeds only 19% of the Alaska data **in** the magnitude range $6 \leq M < 6.9$, and the **84%-ile** curve (not plotted) **still** exceeds only 38% of the Alaska data for the same magnitude bracket. Thus, at a **given** distance from an earthquake of **given** magnitude, the range of **likely** peak

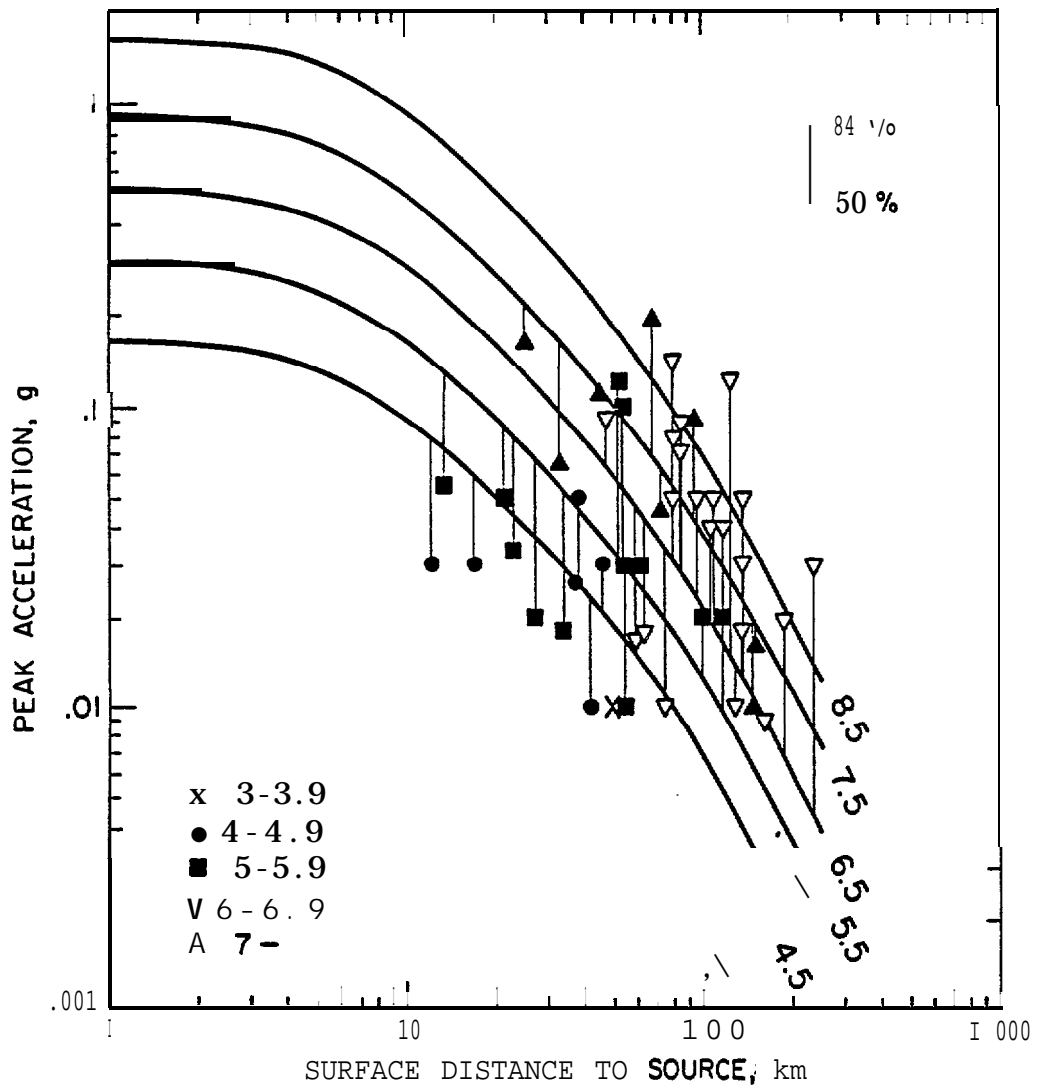


Figure 3.3.1. Comparison of peak horizontal accelerations for Alaska with empirical attenuation laws obtained by Joyner and Boore (1981) by regression of mostly western U.S. strong motion data. The continuous curves correspond to the 50-percentile level of non-exceedence; 84%-ile curves would be offset to a higher level by a constant amount shown in the upper right corner. Symbols represent magnitude ranges M_w as indicated in lower left corner.

accelerations appears much larger for Alaska than that for the western Us.

2) The slopes of the Joyner-Boore curves appear to be steeper than the Alaskan data would suggest: i.e., at surface distances larger than about 50 km most of the Alaska data seem to **yield** higher peak values while at shorter distances they tend **to** yield smaller values. This would suggest that attenuation is stronger in the western U.S. tectonic setting than it is in the Alaska subduction zone environments.

Both features, scatter and slope, may, however, only be **an** artifact that largely stems from plotting the data versus horizontal surface distance from the source, rather than inclined distance between source and receiver. Since Joyner and **Boore** used mostly data from shallow earthquakes whose depths rarely exceeds 10 or 15 km, they may have well been justified to carry out their analysis assuming a constant fault depth of 7.3 km, as they did. A quick inspection of Table 3.3.1 shows, however, that in the subduction zone environment where Benioff-zone **subcrustal** events are common, this approach is not **valid** since horizontal distance may occasionally be only a fraction of the depth. In these instances, plotting the acceleration at the horizontal rather than the inclined (**≈hypocenter**) distance will be totally misleading. Data points to which this applies are for instance those of record numbers 7, 8, 53, 63, 69, and **d** (see Table 3.3.1).

Another, physically important difference may lie in the variability of stress drops, which we suspect is much larger in subduction zones than it is in strike-slip tectonic settings. House and Boatwright (1980) have determined stress drops of more than one half kbar for two Shumagin Islands earthquakes of magnitudes $M_w = 5.6$ and 5.8 , respectively (events associated with strong motion records **a** and **b** of Table 3.3.1). The associated peak accelerations at Sand Point exceed those of the 50%-curve of Joyner and **Boore** for a $M_w = 7.5$ earthquake at the same surface distance. Since stress drop is theoretically expected to scale linearly with peak-acceleration we **suggest** that the **Joyner-Boore** (1981) regression for peak-acceleration versus distance, parameterized by magnitude and percentile of

non-exceedence, do not apply in the subduction zone tectonic setting, not only for geometrical reasons, but also because of inherent differences in stress drop variations and related source properties.

We, therefore, test the Alaska data set of Table 3.3.1 against attenuation laws that were specifically designed to suit the needs of Alaska OCS seismic hazards assessment. **Woodward-Clyde** (1982) proposed in its contribution to the NOAA-OCSEA Program two different attenuation laws for peak-accelerations. Their type-A (non **Benioff-zone** earthquakes depth < 20 km and for stiff rock sites) is:

$$A_{\max} \text{ (median value)} = 191 (e^{0.823M_w}) \times (r + c)^{-1.56}$$

where A_{\max} is the **median** value of the maximum acceleration in **cm/sec²**, r is the closest distance in km to the rupture plane, c is a magnitude-dependent distance-normalizing parameter with

$$c = 0.864 e^{0.463M_w}$$

Note that for normally or other symmetrically distributed acceleration data ensembles, the median value corresponds to the **50%-ile** value of non-exceedence.

Their type-B attenuation relationship (**Benioff zone**, all source depth >6 km, stiff rock sites), that is somewhat modified from their former OASES-study to account now for sites as close as 6 km (instead of 20 km) proximity to the source, is as follows:

$$A_{\max} \text{ (median value)} = 210 (e^{0.5M_w}) \times (r + c)^{-0.85}$$

In Figures 3.3.2 and 3.3.3 we compare the Alaska peak-acceleration data with these A- and B-type attenuation curves, respectively. Note that the abscissa now represents the inclined distance (r) to **the** nearest portion of the rupture plane, rather than distance at the surface. We find that 16 out of 23 data points (i.e., 70%) in the magnitude bracket $6 < M_w < 6.9$ exceed the $M_w = 6.5$ type A curve (Figure 3.3.2), while 11 out of 23 (i.e., 48%) exceed that for the

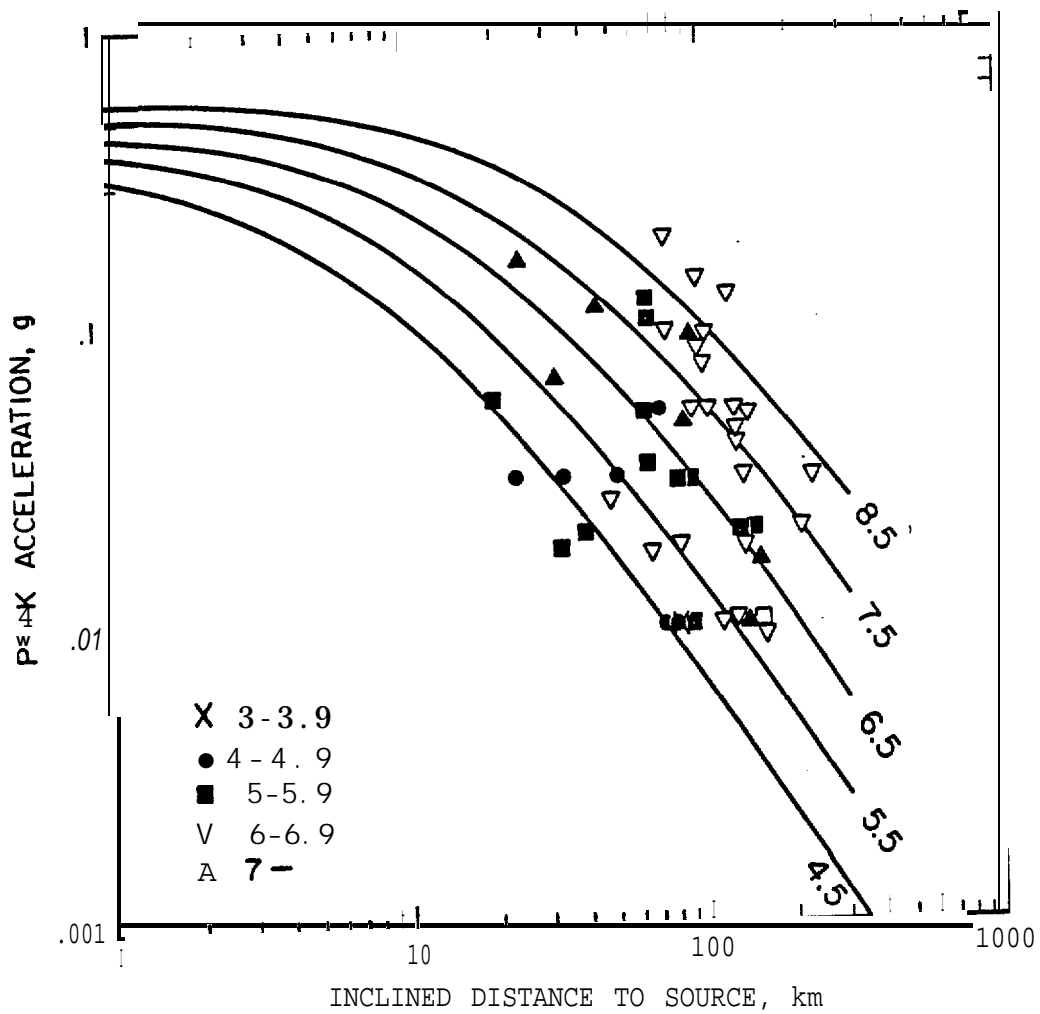


Figure 3.3.2. Comparison of Alaska **peak** horizontal accelerations with type-A attenuation relations proposed by Woodward Clyde (1982) for shallow, **non-Benioff** zone earthquakes. The curves apply to stiff rock sites and represent the median in a statistical distribution. The discrete data for Alaska apply to any type of site and in a few instances may be contaminated with effects of building response.

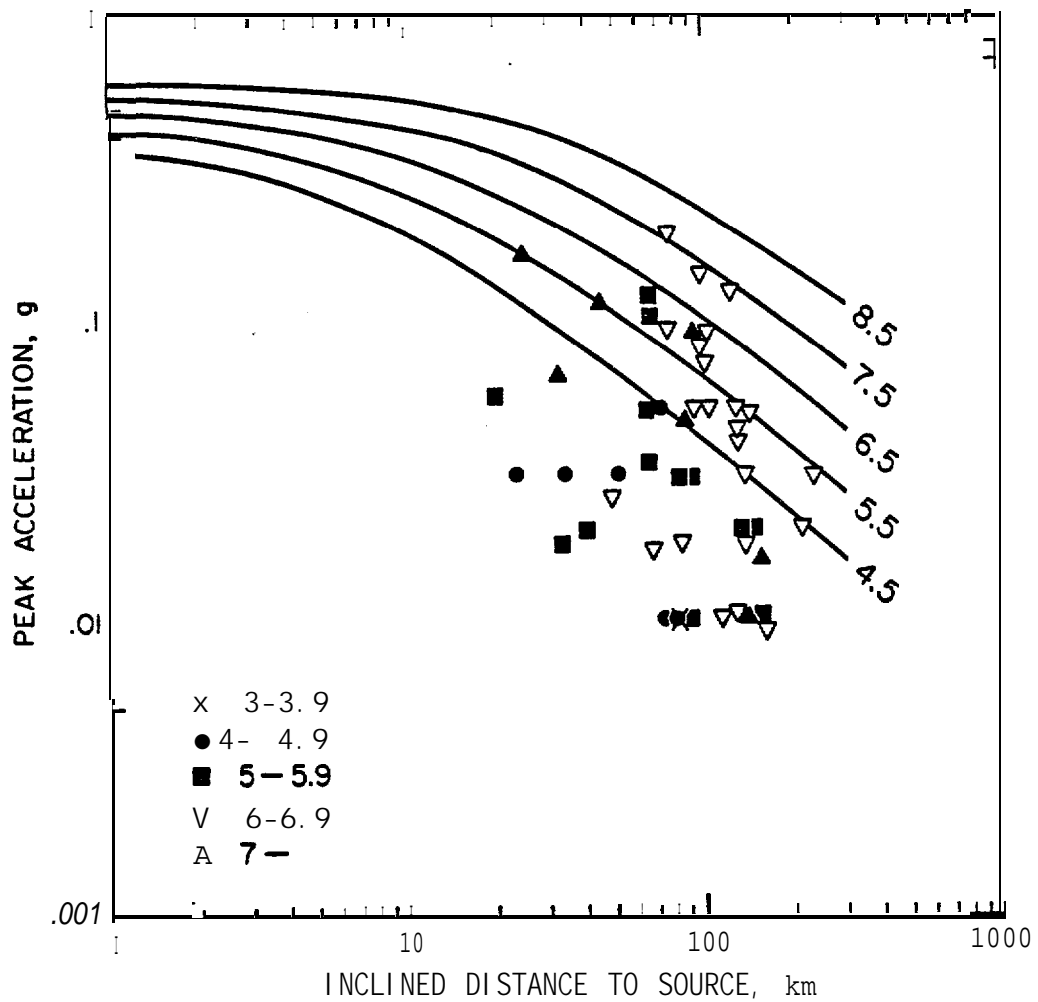


Figure 3.3.3. Comparison of Alaska peak horizontal accelerations with B-type attenuation relations proposed by Woodward Clyde (1982) for Benioff-zone earthquakes. Curves are for stiff sites and represent the median. For other details compare legends of Figures 3.3.1 and 3.3.2.

$M_w = 7.5$ type-A curve that applies to shallow, **non-Benioff** zone events.

For comparison (Figure 3.3.3), only 3 out of 23 points (i. e., 13%) in the same magnitude bracket ($6 \leq M_w \leq 6.9$) exceed the $M_w = 6.5$ type B-curve (proposed for **Benioff** zone events) and only one ($\approx 4\%$) exceeds the $M_w = 7.5$ curve.

Thus, we conclude: despite the fact that Alaska peak accelerations may have a wide scatter (high variance probably due to large variations in stress drops), the B-type curves are sufficiently conservative to correctly account for the Alaskan strong motions, and may satisfy the data probably even at a higher percent level of non-exceedence than median value ($\approx 50\%$ -ile if symmetrically distributed).

Ideally we would have liked to carry out a regression analysis on the Alaskan data set similarly to that done by Joyner and **Boore** (1981) for the western U.S. data. This **is** not justified, however, for two reasons: 1) the data set **is** rather small (a total of 51 points, see Table 3.3.1), and 2) there **are** few earthquakes with more than one recording per event (because of insufficiently dense spacing of **SMA's**). In **cases where** multiple recordings exist there are usually not more than two or three recordings and at similar distances. Hence, during regression analysis we would not be able to decouple magnitude (or other source effects) from distance effects as was the main point of the **Joyner-Boore** analysis.

This conclusion points again toward the urgent need to operate a sufficiently dense SMA network at least in a few selected regions, where the necessary data can be obtained as soon as possible, especially for large events ($M_w > 7.8$) for which a single strong motion record has yet to be collected.

The above data set (Table 3.3.1 and Figures 3.3.1 to 3.3.3) included observations from events in both, subduction zone and strike-slip **regimes** in Alaska. A data set better suited to the southern Bering Sea and Gulf of Alaska-Aleutian OCS regions could be obtained by selecting only the subduction zone events and combining them with those collected by **EXXON** Production Research Company (Wildenstein-Mori and **Crouse**, 1981) which they obtained by processing

original Japanese strong motion records, many of them subduction zone events. Such an improved and enlarged data set for subduction zone strong motions may also permit the magnitude-distance decoupling procedure introduced by **Joyner** and **Boore** (1981). Results from such a proposed analysis could serve as a temporary substitute until empirical attenuation laws based on locally recorded Alaskan strong motions become available. However, even the suggested substitute data set **is** still limited to events with only moderately large events since the Japanese data also do not yet contain recordings from any great subduction earthquakes ($M_w > 7.8$). The strong motion network in the **Shumagin** seismic gap may provide at present an almost **unique** opportunity to obtain these urgently needed records of a truly great or giant earthquake.

3.4 Historic and Instrumental Large Earthquakes, 1788 to Present

3.4.1 Overview. Because the destructive potential is greatest for large ($M \geq 7$) and great ($M \geq 7.8$) earthquakes, we need to know the probability of their future occurrence. Two kinds of data are available to assess the occurrence of **large** events in the past: a) instrumentally recorded data since about 1898, and b) historically reported events for the pre-instrumental period 1788 to 1898. Prior to 1788 no events are known for the Aleutians since no written records were kept prior to establishing the first Russian settlements at **Iliuliuk** on **Unalaska** Island at latest by 1776 and on Kodiak Island in 1784. Some indirect evidence for earlier significant earthquakes is of course preserved in the geologic record, e.g., by uplifted marine terraces. But this record is **still** poorly known for most portions of the Aleutians and many parts of southern Alaska.

The instrumental record of **large** earthquakes in the Alaska-Aleutian arc has been previously discussed by Sykes (1971), **Kelleher** (1970) and was later combined with information from the historic record (Sykes et al., 1980 and 1981) to yield a first qualitative assessment of the seismic potential of the eastern Aleutian arc with special emphasis of the Shumagin Islands seismic gap (Davies et al., 1981). The conclusions of these combined studies can be summarized as follows:

1) The entire Alaska-Aleutian plate boundary is capable of producing great earthquakes. Virtually each arc segment has been broken by large or great earthquakes at least once during historic times.

2) The slip released during the **large and** great events accounts for a large portion of the relative plate motion between the Pacific and North American plates. Hence, if **aseismic** slip occurs at the plate interface it is less significant than the portion of plate motion that **is** released seismically.

3) Typical recurrence time between great earthquakes (at the same arc segment) **varies** along the arc primarily because of variations (a) **in** the width of the plate contact and (b) **in** rates of relative plate motions. A typical recurrence time for great events in the

Alaska-Aleutian arc is of the order of 100 years but may vary between about 50 and 200 years or--in few instances--perhaps more.

4) Arc segments with a lack of great earthquakes during the last 30 years or more are identified as 'seismic gaps'. They **are very** likely to break in a great earthquake much sooner than those that have participated in a great inter-plate earthquake since 30 years or less. In the U.S. portion of the Alaska-Aleutian arc (for the purpose of this study limited between **169°E** and **140°W**) three seismic gaps have been identified (Figure 3.4.1): the **Shumagin** gap (Davies et al., 1981); the **Yakataga** gap (McCann et al., 1980; Lahr et al., 1980; Perez and Jacob, 1980); and the probable **Unalaska** gap (House et al., 1981).

To further assess the seismic potential for future great events in these three seismic gaps, and of the arc segments in between, we combine these earlier evaluations with one that is based on the history of seismic moment release. Since **it** is difficult to estimate seismic moments for events during the pre-instrumental period we begin with the instrumental period 1898 to present. We proceed by testing the instrumental seismic moment release against one based on plate kinematic arguments, and then attempt some limited inferences on possible moments that were associated with events during the period of historically documented events, 1788 to 1898. Finally we address some of the problems associated with the difficult questions of where and when great earthquakes may occur next, and the consequences for hazards assessment in the OCS region under study.

3.4.2 Instrumental seismic record. To document thoroughly the large $(M \geq 7)$ and great $(M \geq 7.8)$ earthquakes along the Alaska-Aleutian arc since world-wide commencement of seismic instrumentation at about 1898, we examined a large number of existing **catalogues**. The sources we consulted are: Gutenberg and Richter (1949), Duda (1965), **Rothé** (1969), Tobin and Sykes (1968), Richter (1958), Sykes (1971), Kanamori and Abe (1979), Abe (1981), Abe (1979), Meyers (1976), Meyers et al. (1976), **Glover** and Meyers (1981), Meyers and Hake (1976), **Glover** (1980), **Glover** and Meyers (1982), Davis and **Echols** (1961), **BCIS**, 1SS, the chronological and regional files of the **ISC catalogues**, PDE and EDR files of the USGS and predecessors, the

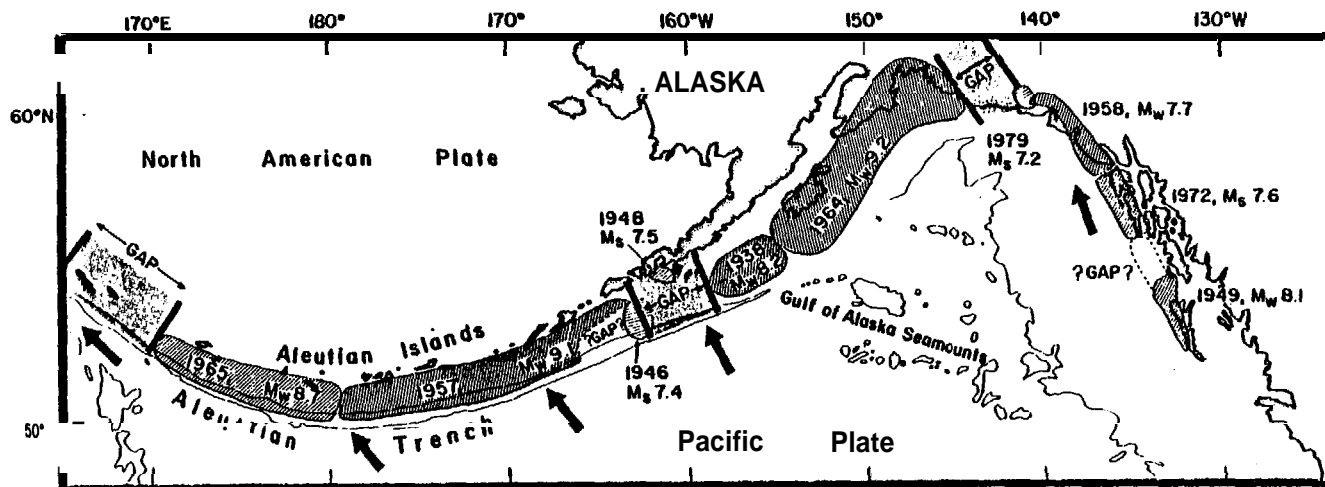


Figure 3.4.1. Location map of presently existing seismic gaps and of rupture zones of the most recent sequence of major earthquakes since 1938. Only the subduction segments of the plate boundary west of 140°W are analyzed in the remainder of this study. The seismic gaps along that portion of the plate boundary are, from east to west: Yakataga gap (near 143°W), Shumagin gap (~160°W), the possible Unalaska gap (queries near 165°W), and the Kommandorski gap (~170°E). The magnitudes indicated are those used by Sykes et al. (1981), House et al. (1981), and Davies et al. (1981) some of which will be modified in the course of this study (see Figure 3.4.8). Solid arrows indicate directions of motion of the Pacific relative to the North American plate (after Sykes et al., 1981).

NEIS-NOAA event-tape-file, and the "Seismological Notes" published in the Bulletin of the Seismological Society of America. For each event a filing card was established and all parallel entries of source parameters noted to detect inconsistencies, printing errors, or systematic variations in determination of source parameters. After careful consideration of all sources we chose a set of parameters. The resulting list of 116 large events along the arc is shown in Table 3.4.1. These and some additional events outside the arc segment studied (**169°E to 140°W**) are plotted in Figure 3.4.2.

For locations and origin times we adopt the parameters from the first source available when progressing in the following sequence of priority: Sykes (1971), Tobin and Sykes (1968), **ISC catalogue**, Gutenberg and Richter (1956) and any others. Many of the earliest events (1898-1903) are based on locations determined by Gutenberg or **Milne**, and are derived from only a few global station readings (see **Kanamori** and Abe, 1979). After 1904, the world-wide number of stations is generally sufficient to yield reasonably good locations (errors $\lesssim 1^\circ$) for most events. However, uncertainties in locations for several crucial events remain unresolved. Following McCann et al. (1980), Perez and Jacob (1980), Sykes et al. (1981) and Davies et al. (1981), we place the October 10, 1900 ($M = 8.1$) event somewhere (**58°N, 150°W**) between Kodiak and Seward based on intensity and aftershock reports, although Richter (1958, p. 710) after Gutenberg (1956), and practically every secondary source thereafter, have placed it probably erroneously at **60°N, 142°W**.

The location of the $M = 7.7$ event of July 14, 1899, is noted as 'Arctic near Alaska' in several sources probably after **Milne** as reported by Gutenberg (1956, Table 3) and as commented on by **Kanamori** and Abe (1979, Table 4, p. 6136), but the coordinates given (**60°N, 150°W**) by all these sources suggest a location at the **Kenai Peninsula**. Sykes et al. (1981) and Davies et al. (1981) note that Tarr and Martin (1912) list felt reports from **Unalaska** and Unga Islands at the time of this poorly located event of 1899 and thus argue that it may have been located in or near the **Unalaska** or

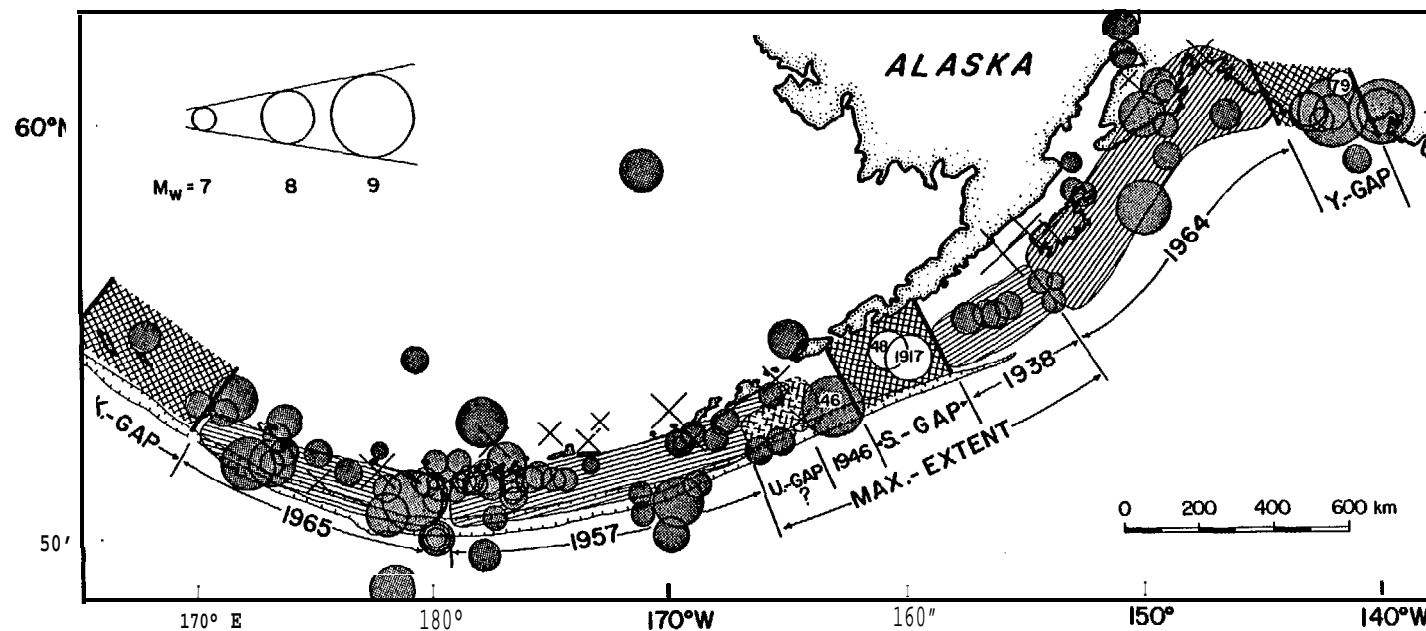


Figure 3.4.2. Major earthquakes ($M_w \geq 7$ and larger) in the Alaska-Aleutian region for the instrumental period 1898 to 1982. All shallow earthquakes ($h < 60$ km) are plotted as circles, except those of the four great earthquakes of 1964, 1938, 1957 and 1965 with magnitudes $M_w = 9.2, 8.4, 9.0$ and 8.7 , respectively, for which rupture zones are indicated by arc-parallel hatching. The Yakataga (Y), Shumagin (S), Kommandorski (K) and possible Unalaska (U?) seismic gaps are indicated by cross hatching. Intermediate depth earthquakes ($h > 60$ km) are shown as crosses. Symbol size indicates magnitude M_w (upper left insert). The 6000-m bathymetric contour outlines the Aleutian trench.

Shumagin seismic gaps. We have retained the 'instrumental' location near **Kenai** but emphasize how tenuous it is.

One event, that of 31 May 1917 (M = 7.8), **is** of special interest. Its only published source can be traced back to a catalog prepared by T. **Usami** printed in 1975 in the Science Almanac of the Tokyo Astronomical Observatory and was reproduced by **Glover** and Meyers (1981). Since this event had not been reported by Gutenberg and Richter (1956) or any other western source prior to 1981, it went unnoticed by Davies et al. (1981) in their assessment of the Shumagin gap despite the fact that the epicenter coordinates place **it** within the **Shumagin** gap. This new finding requires corrections to some of the statements by **Davies** et al. (1981) or **Sykes** et al. (1981) regarding the duration of quiescence for events larger than M = 7.5, and measured recurrence times of great events in the **Shumagin** gap, however, **it** only inconsequentially alters these author's assessments of the gap's seismic potential for a future large earthquake.

For magnitudes we adhere as closely as possible to a uniform scale and choose those magnitude values from different sources and methods of determinations that--within the limits of available data--appear to represent most closely the moment magnitude M_w proposed by **Kanamori** (1977). It relates moment M_0 (dyn cm) to magnitude M_w by

$$\log_{10} M_0 = 16.1 + 1.5 M_w$$

under the assumption of constant and complete stress drop (≈ 50 bar) and a ratio of $A_s/p = 10^{-4}$ (that is $\mu = 5 \times 10^{11}$ dyn/cm²) regardless of event size. The latter assumption may not be fully valid (**Kanamori**, 1977; **Purcaru** and Berckhemer, 1978; **Sykes** and Quittmeyer, 1981).

For events between 1898 and 1903 (inclusive) we use the magnitude determinations of **Kanamori** and **Abe** (1979), except for the September 4, 1899, event which is adopted from **Thatcher** and **Plafker** (1977). For most events between 1904 and 1980 we rely on the magnitude determinations by **Abe** (1981) except for those largest events where

either Abe (1979), Kanamori (1977), Purcaru and Berckhemer (1978) or Sykes and Quittmeyer (1981) have determined or discussed a moment magnitude M_w using information from either long-period seismograms, aftershock zone dimensions, or tsunami heights. Three great events need special mention: we reduce the M_w from 9.1 to 9.0 for the March 9, 1957, event because of a possible reduction of aftershock dimension in the Unalaska region (House et al., 1981). We adopt (after Purcaru and Berckhemer, 1978), a $M_w = 8.3$ for the highly tsunamigenic (MT = 9.3) 1946 earthquake near Unimak (Abe, 1979). We are forced to use $M_w = 7.8$ (Glover and Meyers, 1981) for the 1917 Shumagin gap earthquake without knowing the method of its magnitude determination. At least these three events need further analysis of original instrumental records.

Where several of the magnitude sources give different values (i.e., mb, M_s , ML, MT, Mw, ME, M_{100}) we often (but not always) tend to choose a value towards the upper limit, to represent M_w , while systematically avoiding the upward revised surface-wave magnitudes M of Gutenberg cited by Richter (1958) and quoted as M_s by Sykes (1971), Sykes et al. (1981), and Davies et al. (1981). A more detailed justification and documentation is in preparation (Jacob et al., 1983).

Note that we first adopt the "magnitude M_w and then calculate (or recalculate) the moment M. (Table 3.4.1) using

$$\log_{10} M_0 = 16.1 + 1.5 M_w$$

Thus, the moments listed in Table 3.4.1 may be in error by as much as 20 to 30% compared to those moments given in the original sources. This is largely due to the fact that round-off to the nearest 0.1- M_w -value can result in this large an error. (Since the difference of a $M_w = 9.20$ and a $M_w = 9.25$ corresponds to a moment increase that in itself is equivalent to a magnitude $M_w = 8.72$, these rounding errors are not trivial for the largest events. For magnitudes $M_w > 7.9$, and for certain purposes, it may therefore be in order to carry a second decimal position through all M_w calculations.)

TABLE 3.4.1. List of 116 Large Earthquakes in the Alaska-Aleutian Arc (169°E to 140°W) for the Period 1898-1982 for which at Least One Source Reported a Magnitude $M \geq 7$

Columns indicate Date (Y, M, D), Origin Time (E, M, S), Latitude and Longitude (°), Depth (km), Magnitude (??.), and Equivalent Moment (Dyne cm).

Date	Time	Lat	Lon	D	M_w	M_0	Date	Time	Lat	Lon	D	M_w	M_0
980629	1s36 .	52.00	172.00	s	8.00	S. 12 59e+29	440727	4 23.00	54.00	-155.50	7a	7.10	0.5623e+27
981111	I 1637 30.00	50.00	-180.00	.9	7.40	a. 1585e+28	441212	417 10.00	51.50	179.50	a	7.19	0.5623e+27
990714	1332 .	50.00	-150.00	0	7.70	a. 4467e+28	460112	2025 4a. 2a	59.11	-148.97	56	7.2a	0.7943e+27
990904	904 .	6s. ss-142. ss	0	8.50	a. 7079e+29		460401	1220 56.00	S3.32	-163.19	a	8.30	0.3548e+29
990904	440 17. .	6s. ss-142. ss	0	7.40	a. 1585e+28		461101	1114 24.00	51.50	-171.50	0	7.50	0.3981e+27
990910	1794 9. .	6s. ss-140. ss	0	7.30	0.5310e+28		480514	2231 43.4a	54.71	-150.00	a	7.50	0.2239e+28
990910	2141 e.	6s. ss-140. ss	0	8.40	a. 5012e+29		49a2a2	1741 29.00	53.00	-173.00	220	5.00	0.1995e+27
990923	1194 .	5s. ss-143. ss	0	7.4s	a. 1585e+28		490927	1530 45.00	59.75	-149.00	50	7.00	0.3981e+27
990923	1250 9.	5s. ss-143. ss	0	7.50	a. 2239.2a		510213	2212 53.00	SS. S3-186.3S	a	7.1a	0.5623e+27	
991009	1220 .	50.00	-150.00	s	8.10	0.1770e+29	S21129	2346 27. as	56.30	-153. as	s	6.75	a. 1679e+27
991121	952 367.00	52.00	-177.00	0	7.5s	0.2239e+28	530105	74a 21.6S	S3.32	171.00	0	7.10	0.5623e+27
991101	520 30.00	55.00	-165.00	a	7.50	0.2239e+28	540417	2010 37.00	51.50	-179.00	a	6.75	a. 1679e+27
991117	1605 .	50.00	-170.00	0	7.4s	0.1585e+28	541003	1110 as. 00	50.71	-150.52	73	6.75	s. 1679e+27
991117	1317 .	57.00	-150.00	0	8.30	0.3548e+29	550314	1312 a.	52.50	-173.50	75	7.00	0.3981e+27
991214	046 36.08	53.00	-170.00	0	7.90	0.0912e+28	550620	1297 25.00	51.50	-180.00	0	6.00	0.1995e+27
990322	33a E.	50.00	-180.00	a	7.20	0.0912e+28	570102	312 52.00	52.51	-150.00	0	7.00	0.3981e+27
991210	1236 .	51.00	-180.00	0	7.5s	0.3981e+27	570102	348 47.00	52.50	-150.00	0	7.00	0.3981e+27
a617817	10 42. ss	51.00	179.00	0	8.20	0.2512e+29	570309	1422 27.00	51.53	-175.41	a	9.30	0.3981e+30
990902	1601 30.00	52.00	173.00	a	7.00	0.6310e+28	570309	2039 16.50	52.43	-159.50	a	7.10	0.5623e+27
990515	031 36.00	59.00	-141.00	s	7.1s	0.5623e+27	570311	312 42.6a	51.00	-177.13	a	6.80	9.199 e8.27
990908	1649 40.00	52.50	-169.00	0	7.00	0.3981e+27	570311	950 44.40	52.66	-169.00	0	7.00	0.3981e+27
990909	2000 .9.	50.60	-149.30	0	7.40	0.1520e+28	570311	1405 19.50	51.54	-178.55	J	7.10	0.5623e+27
100909	113 18.00	51.50	-176.00	a	7.1s	0.5623e+27	570312	720 40.30	51.89	-173.42	a	6.75	0.1679e+27
110917	326 .	51.00	-180.00	a	7.00	0.3981e+27	570312	1144 53.30	51.1a	-176.73	J	7.10	0.5623e+27
110922	501 .	50.50	-149.00	0	6.9a	0.2010e+27	570314	1447 44.6a	51.32	-176.70	a	7.10	0.0623e+27
111113	1613 12.00	52.00	173.00	x	7.00	0.3981e+27	S70316	234 17.00	51.47	-170.70	a	7.00	0.3981e+27
120104	1546 54.00	52.00	-179.00	2s	7.00	0.3981e+27	570322	1421 5.50	53.61	-155.76	0	7.00	0.3981e+27
120121	2011 40.00	61.00	-147.50	0	7.00	0.3981e+27	570410	1129 50.20	50.00	-153.00	a	7.00	0.3981e+27
120610	1600 5.00	59.00	-153.00	2s	6.90	0.2010e+27	570419	2219 30.00	52.20	-155.10	50	7.10	0.5623e+27
121018	1140 .	54.60	179.20	0	7.10	S. 5623e-27	570613	1000 3a. as	51.50	-175.00	0	7.00	0.3981e+27
121107	740 24.00	57.50	-155.00	0	7.3s	0.1122e+28	600703	2020 50.00	50.50	-177.50	0	7.00	0.3981e+27
121208	1227 36. ss	87. ss-15.4. ss	9a	6.9a	0.2010e+27		601113	920 30.00	51.23	-160.00	32	7.10	0.5623e+27
130331	340 48.00	49.50	-170.00	a	7.3s	0.1122e+28	611200	39 27. 1a	52.30	177.60	56	6.80	a. 1995e+27
130622	1349 .	4a. 00	-170. as	a	7.20	0.0912e+28	640205	1307 21.10	50.75	-155.70	a	7.10	0.5623e+27
160206	2151 .	40.50	170.50	a	7.7a	0.4457e+28	640329	336 13.00	61.10	-147.50	2a	9.20	0.7943e+30
160410	401 40.00	53.25	-170.00	0	7.40	0.1585e+28	640404	1740 9.00	56.30	-154.40	24	7.00	0.3981e+27
170531	047 .	54.50	-160.00	0	7.80	0.6310e+29	650204	501 21.00	51.30	170.60	0	6.7a	0.1413e+30
200504	1636 39.30	55.55	-156.75	a	7.10	0.5623e+27	650204	040 42. as	51.40	179.6a	40	7.00	0.3981e+27
201013	1000 10.30	51.60	-175.50	a	7.10	0.5623e+27	650310	227 7.2a	50.60	177.90	51	7.00	0.3162e+28
200621	1627 13.00	60.00	-146.50	a	7.3s	0.1122e+28	650702	2050 10.00	53.00	-167.50	0	7.00	0.3981e+27
200907	134 37.9s	50.00	-169.00	0	7.9a	0.0912e+28	650709	029 22.00	51.10	-171.30	10	7.00	0.3981e+27
200705	1419 1.90	51.42	-170.30	a	7.00	0.3981e+27	650904	1432 50.00	50.30	-152.50	0	7.00	0.3981e+27
200707	2123 10.20	51.60	-177.00	6	7.40	0.1585e+28	651222	1941 23.00	50.40	-152.00	0	7.00	0.3981e+27
201217	1050 36.90	53.67	171.46	a	7.90	0.6310e+29	650704	1033 30.00	51.99	179.57	16	7.9a	0.3501e+27
200325	2350 .	52.50	-152.50	25	6.9a	0.2010e+27	660907	213 4.10	50.50	-171.30	29	7.00	0.3981e+27
200427	236 7.00	51.25	-150.75	a	7.10	0.5623e+27	670120	352 50.00	52.40	-159.54	42	6.70	0.1413e+30
200504	420 7.00	51.25	-147.50	0	7.10	0.5623e+27	670514	1900 55.00	51.20	-179.35	22	7.00	0.3981e+27
200222	1705 54.00	52.20	175.00	0	7.10	0.5623e+27	690912	057 5.00	51.27	-179.17	3a	7.00	0.3981e+27
200903	1848 12.00	52.50	-177.50	0	7.20	0.7943e+27	700220	1042 31.20	52.70	-175.10	152	7.00	0.23a*2.20
201110	2010 11.2s	55.40	-150.30	a	8.40	0.6310e+29	700415	533 10.20	50.00	-142.43	7	7.00	0.3981e+27
201117	354 34.00	55.45	-157.55	a	7.30	0.1122e+28	710207	229 29.10	51.47	-170.00	0	7.00	0.3981e+27
200207	1716 27.00	51.50	175.00	0	7.10	0.3981e+27	710502	500 25.00	51.42	-177.21	3a	7.10	0.5623e+27
200415	007 47.00	52.30	173.50	0	7.10	0.5623e+27	750202	a43 39.00	53. da	173.00	10	7.10	0.1585e+29
200416	543 2.4s	52.60	173.20	0	7.10	0.5623e+27	770219	2214 5.40	S3. S4	169.96	44	7.10	0.5623e+27
400714	552 53. as	51.75	177.50	0	7.40	0.1585e+28	770904	1724 46.60	51.31	177.01	24	7.10	0.5623e+27
400820	320 14.00	52.41	-160.30	0	7.2s	0.7943e+27	790220	2127 6.00	60.60	-141.50	10	7.10	0.3981e+27
420900	120 26.00	53.00	-154.50	es	6.9a	0.2010e+27	800324	3a9 51.30	S2. S7	-167.67	33	7.00	0.5623e+27
431103	1432 17.50	51.90	-150.00	s	7.40	a. 1585e+28	810110	052 44.10	S1. 74	176.27	33	7.1a	0.5623e+27

3.4.3 Magnitude-time distribution for entire arc, and mean occurrence. Before analyzing the data for their time-space distribution and its consequences for seismic potential in seismic gaps, it is of interest to analyze the overall-properties of the data ensemble disregarding any systematic spatial patterns.

Figure 3.4.3 (A through E) displays the major seismicity of the arc (**169°E to 140°W**) as a function of time. All events ($M_w \geq 7$) within 300 km lateral distance of the arc are included, regardless of depth or focal mechanism. Several features can be discerned from these graphs: Whenever one or more great ($M_w \geq 7.8$) earthquakes occur in any given year (curve B), the number of large events ($M_w \geq 7$) generally is also higher for the same year (see curves A and D). This is consistent with the notion that some great earthquakes trigger large aftershocks, (notably the 1899, 1957, and 1965 sequences). Two kinds of exceptions *exist*: a) there *are* times of increased seismicity ($M \geq 7$) without great events (1912 \pm 1 y, 1940), and b) there are great events with few reported large aftershocks (1964, 1938, 1917, 1907, 1906). The 1912 'swarm' may represent some volcanically induced seismicity culminating in the 1912 **Katmai** eruption; interestingly much of it is associated with intermediate-depth earthquakes (60-250 km) that occur probably *in* the descending Pacific slab beneath the volcanic axis. This volcano-seismic sequence may have started with the great ($M_w = 8.3$) event of 1903 which reportedly (Gutenberg and Richter, 1956) occurred at a depth of ≈ 100 km [The magnitude 8.3 quoted is one of the few events in **Table 3.4.1** for which only a revised magnitude **M** is available (after Gutenberg, 1956) (see also Richter, 1958, p. 714)].

A second feature in Figure 3.4.3 is that the rate of significant seismicity is high around the turn of the century (1898-1908) and around 1960 \pm 5 y, and low in between. This trend is apparent in both large ($M_w \geq 7$, curves A and D) and great earthquake ($M \geq 7.8$, curve B) activity. To emphasize the energy release dominated by the larger and greatest events we have plotted cumulative excess magnitude above $M_w = 7$ as a function of time in curve C. Excluding the high release before 1901, one can draw *an* upper and lower envelope to the data in this plot. The envelopes contain a span of about 5 excess units above

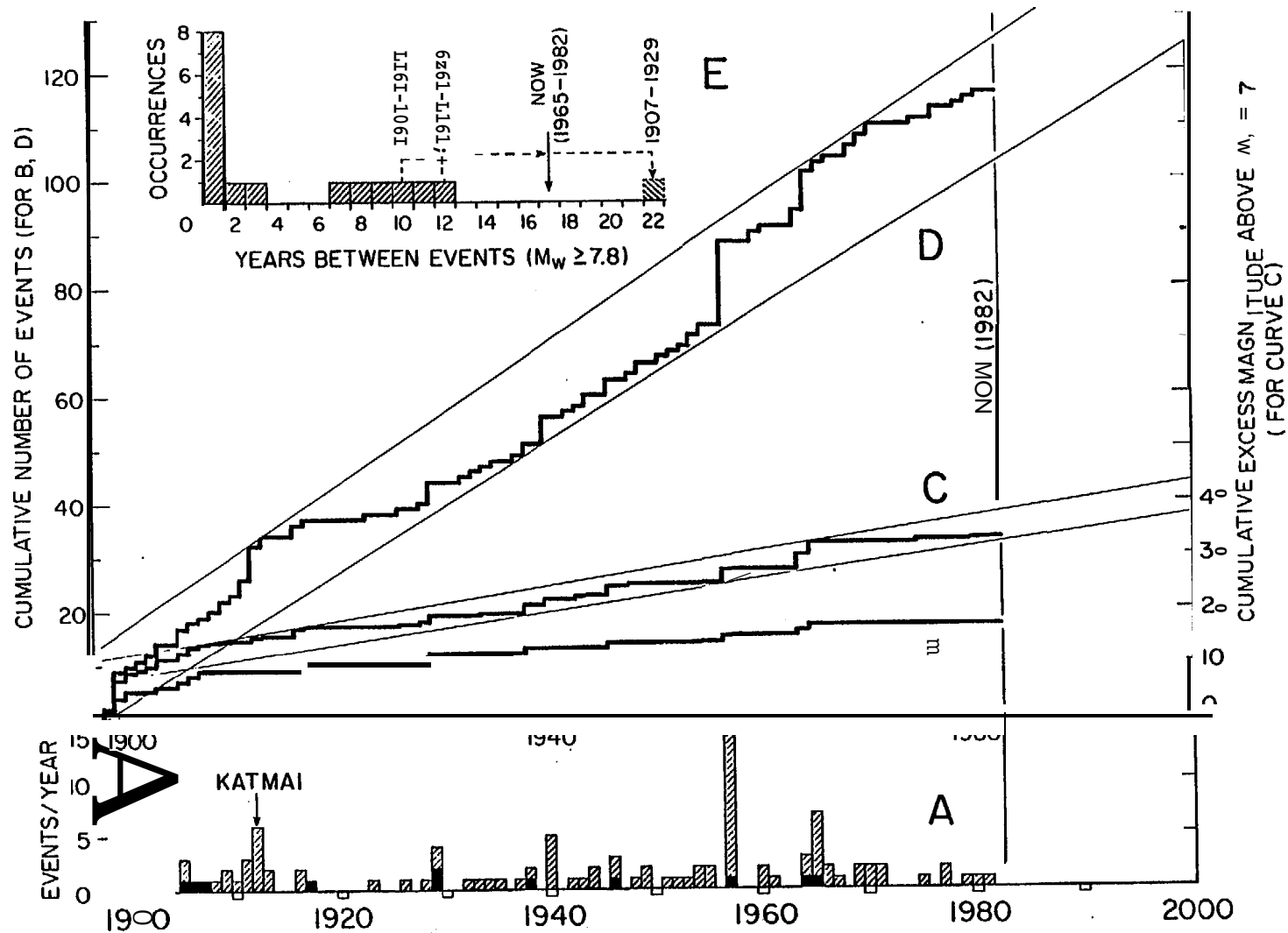


Figure 3.4.3. Seismicity ($M_w \geq 7$) of the Aleutian arc (140°W to 169°E) versus time for the instrumental period 1898 to 1982. The occurrence of events per year (curve A) is differentiated for great ($M_w \geq 7.8$) and large ($M_w < 7.8$) events by solid and hatched symbols, respectively. Cumulative number of events for all major events (curve D) and for great events ($M_w \geq 7.8$) only (curve B) use left-hand scale, cumulative excess-magnitude above $M_w = 7$ (curve C) uses right-hand scale of abscissa. Inset E shows the histogram for the periods (years) between subsequent great earthquakes ($M_w \geq 7.8$) along the arc. Note the long recent period of quiescence of 17 years.

magnitude $M_w = 7$ (i. e., two $M_w = 9$ plus one $M_w = 8$, or five $M_w = 8$ events, etc.). Since 1965 no great earthquake has occurred and from the graph follows that some major activity is due in the Alaska-Aleutian arc by at latest 1985 provided such a representation has any physical significance. Of course no statement can be made from such a presentation where the seismicity would take place within the arc.

Another way to present the same temporal aspect of seismicity is shown in Figure 3.4.3, insert E. There we have plotted for only great events ($M_w \geq 7.8$) the frequency distribution for time intervals between consecutive events (anywhere between 169°E and 140°W). An outstanding feature of this distribution is the strong peak of occurrences of **mutliplet** events in the same or two consecutive years (i.e., $\Delta t < 2$ years). The 1900 ± 1 y sequence contributes half of the occurrences in this spike, the 1905-07, 1929, and 1964/65 bursts contribute the other half. Note that we have excluded from this study the SE-Alaska strike-slip boundary. Otherwise the 1958 Lituya Bay-FairWeather event would have added another occurrence in 1957/58 to this strong clustering of great events. This clustering occurs mostly in time (1964/65), but sometimes also in time and space (1899). The occurrence of great events in the arc gives the appearance that stress release is communicated over large distances. A physically plausible explanation may be that episodic large-scale plate motions may be the common cause to events that can be large distances apart, rather than one event 'triggering' the other.

Apart from this 'burst'-like clustering in insert E at $\Delta t < 2$ years, another aspect needs to be reiterated that we commented on earlier. In the past 85 years there is no occurrence of a time period longer than 12 years (represented by events in 1917 and 1929) in which no great event has occurred **between 169°E and 140°W** , except for the ongoing period 1965 to present (i.e., $\Delta t \geq 17$ years). This is to say that the last 17 years have been unusually quiescent and represent a statistically possible but unlikely situation. Even if we remove the questionable event of 1917 whose magnitude $M_w = 7.8$ may in fact not have been as high as reported, than the longest quiescent interval in the last 85 years may have measured 22 years (1907 to 1929), and the

recent quiescence of 17 years is still remarkable. In either interpretation, one can expect soon an arc-wide increase of major **seismicity**, if the distribution of Figure 3.4.3-E is representative of long-term seismicity. Again, no consideration of depth, location, or nature of faulting (thrusting **on** the subduction zone, normal faulting at the trench, and some strike-slip in the Near Islands) has been given in this examination of the likelihood of future increased activity.

One can make some simple estimates of average occurrence for significant earthquakes from the presentations A-E of Figure 3.4.3. Of the total of 116 considered events, 102 events had magnitudes $M_w \geq 7$. They occurred during the last 85 years over a 3600 km long arc distance. From these figures we obtain **an** average occurrence of one large event ($M \geq 7$) about every 10 years within a 300 km long arc segment. The total of 17 great events yields an average occurrence of one great earthquake ($M_w \geq 7.8$) about every 60 years within any 300-km distance along the arc. Because of clustering associated with the seismic cycle, and because of systematic variations in the rates of plate motion and of boundary width (see later sections), the actual values may deviate substantially from these mean values of 10 and 60 years, respectively, in any given 300-km arc segment. We will compare these estimates with those derived by other methods and find some important systematic discrepancies that will be discussed later.

3.4.4 Recurrence estimates from b-values for the entire arc.

The distribution of occurrences of large events per **0.1- M_w -intervals** for the entire Alaska-Aleutian arc (**169°E to 140°W**) is shown in Figure 3.4.4. A more commonly used method in seismology is to plot the logarithm of the cumulative number $N(M_w)$ of events at and above a magnitude M_w as a function of this variable lower boundary M_w , and then find some function

$$\log_{10} N = A - bM_w$$

that in a specifically defined way (**say** maximum likelihood or least-squares sense) approximates the observed distribution over a limited magnitude range. Figure 3.4.5 (bottom) shows the data set of

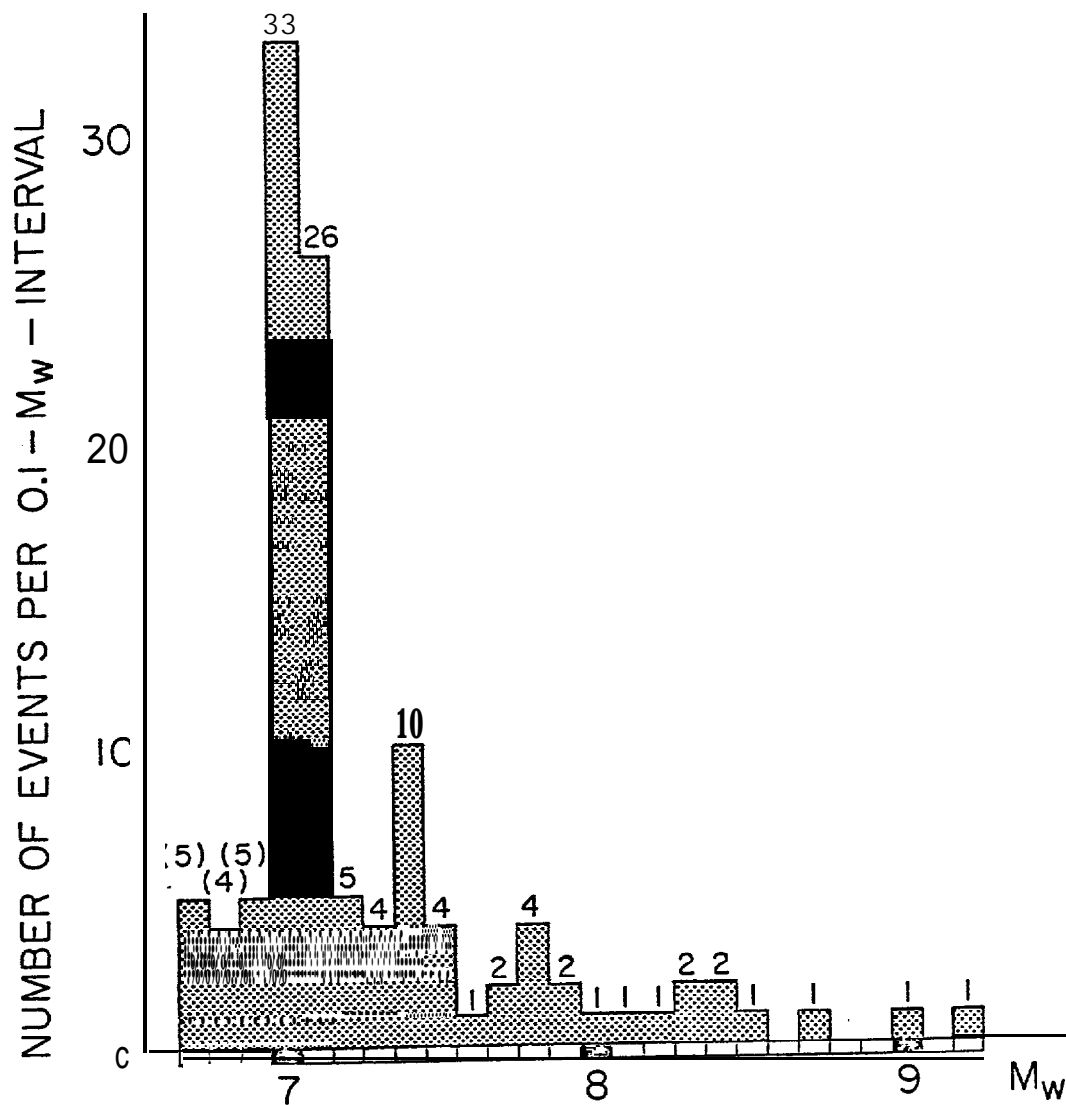


Figure 3.4.4. Histogram of all major earthquakes for which magnitudes were available, plotted in $M_w = 0.1$ -intervals. Note that several earthquakes (a total of 14 events) for which at least one source reported a magnitude 7 or larger, were reassigned to magnitudes $M_w < 7$.

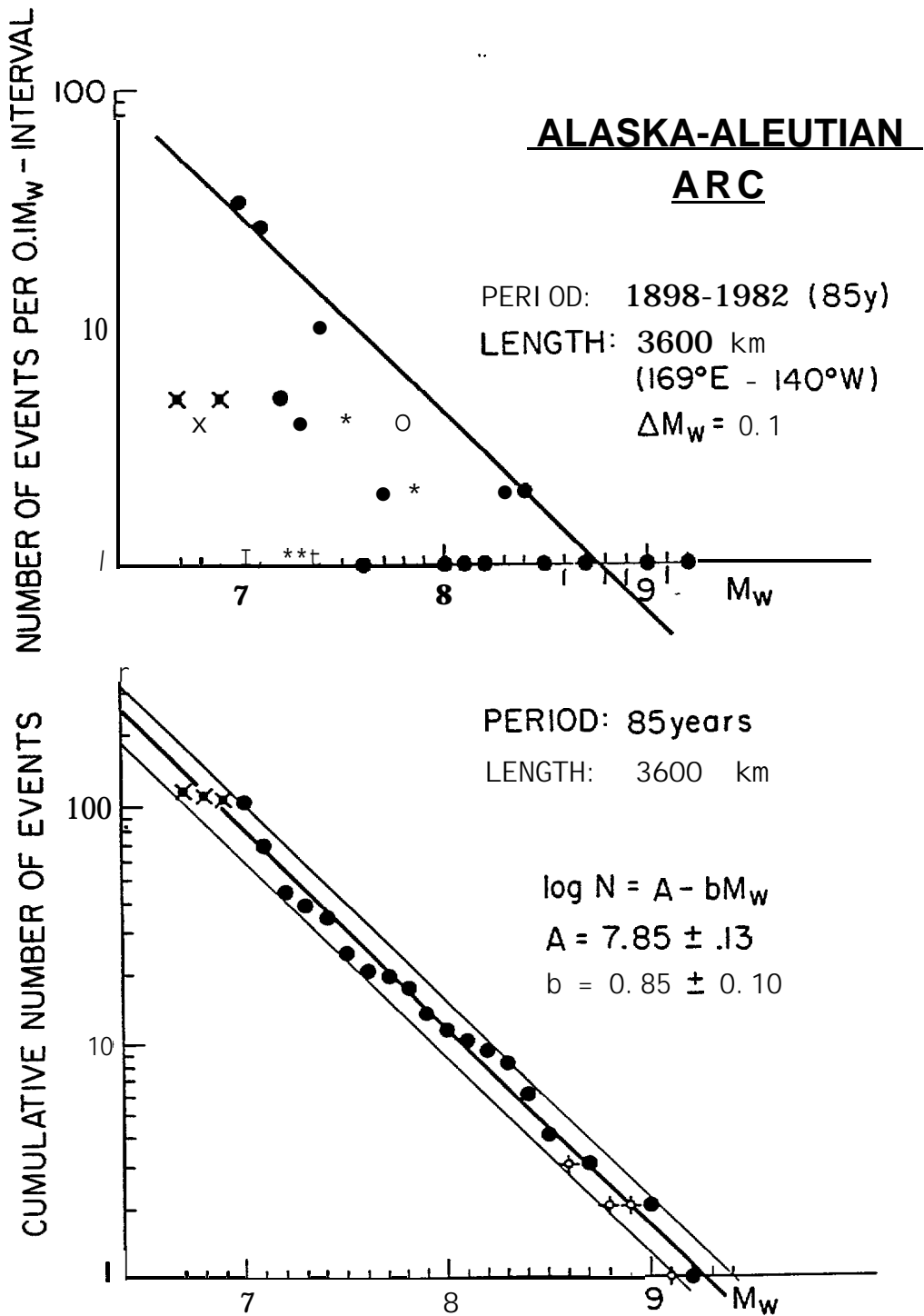


Figure 3.4.5 . Logarithmic frequency plots for the instrumental seismicity 1893 to 1982 (85 years) for the Alaska-Aleutian arc (total arc length 3600 km). Top: number of events n (on logarithmic scale) per 0.1- M_w -interval vs. magnitude M_w . Bottom: cumulative number N of events (on log-scale) with magnitudes M_w and larger M_w . Heavy line represents the relation $\log N = A - bM_w$ with $A = 7.85$ and $b = 0.85$; light lines represent error $\Delta A = \pm 0.13$.

Table 3.4.1 represented in this form. Depending on the method of curve-fitting one obtains different **A** and **b** values and associated errors with them. Maximum likelihood methods (Figure 3.4.6) emphasize the slope and absolute number of events close to the average magnitude which is very close to the lower bound of considered magnitudes in the data sample. Because of the importance of the great events (in terms of strain energy **or** moment release) we have (against common practice) given here more weight towards a regular straight-line least-squares regression and/or 'eye-ball fit' with assigning errors (**AA** and **Δb**) for the constants such that not a single observation **in** the range $6.7 \leq \mu \leq 9.2$ falls outside the regression and assigned error range. With this approach we obtain

$$\log_{10} N = (7.85 \pm .13) - (0.85 \pm 0.10) M_w$$

shown as straight lines in Figure 3.4.5 (bottom).

Clearly, the total number in the data-sample is too small to attach great significance to any of these fits when extrapolating to magnitudes outside the observational range. Disregarding, however, this warning we nevertheless proceed to derive recurrence time estimates from this relationship. To do so, we have to keep in mind that the data comprise a time period $T_0 = 85$ years and arc-length $L_0 = 3,600$ km. To scale the number of cumulative occurrences $N(L_0, T_0, M_w)$ to another arc length L and time period T , a vertical shift of the (logarithmic) intercept from $A(L_0, T_0, M_w=0)$ to a new intercept $A(L_0, T_0, M_w=0) + \log(L \cdot T / L_0 \cdot T_0)$ must be performed. Choosing **arc** length $L = 300$ km for all magnitudes $\mu \leq 8.5$, and **larger values** of L for the greatest earthquakes ($M \geq 9.0$) because they require larger rupture zones; and setting $T = 1$ year, we calculate, first, the number (or fractional number) of occurrences per year by using T and L in

$$\log_{10} N(L, T, M_w) = A(L_0, T_0) + \log_{10} (L/L_0 \cdot T/T_0) - bM_w$$

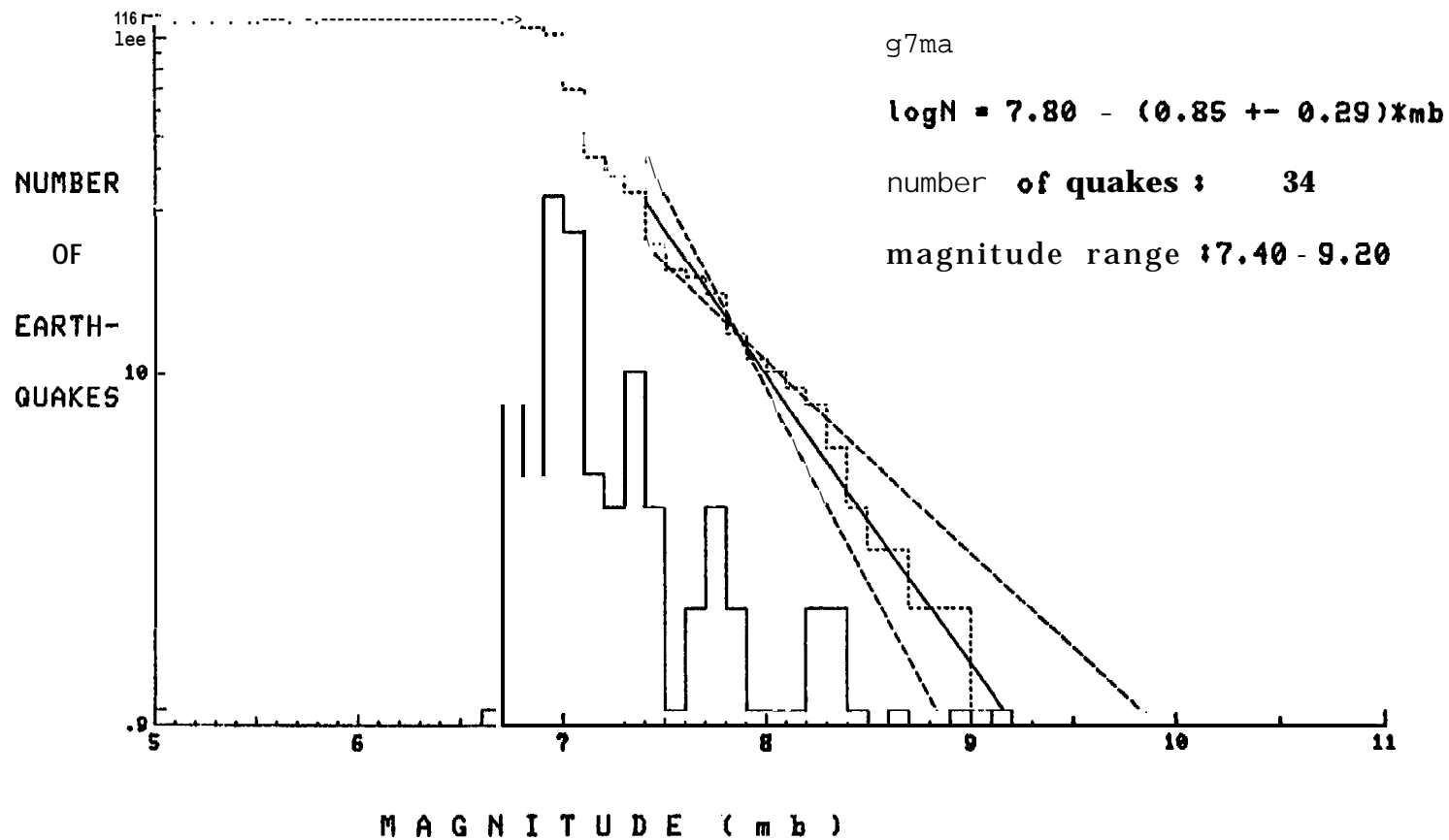


Figure 3.4.6 . Same as Figure 3.4.5 with number of events n as solid line and cumulative number of events N as broken line. Straight-line fits $\log N = A - bM_w$ are calculated by the maximum likelihood method and yield $A = 7.85$ and $b = 0.85$, virtually identical to that for linear regression, but the error $\Delta b = \pm 0.29$ is much larger. Only magnitudes $7.4 < M_w < 9.2$ were used in the calculation. Maximum likelihood straight-line fits to the data with cut-off magnitudes lower than 7.4 yield poor representation of the observations for high magnitudes.

Having calculated the number of events per year, then the inverse of this number yields recurrence times, i.e. ,

$$T_R = N^{-1} (L, T=1, M_w)$$

The results of these calculations are summarized in Table 3.4.2, where the recurrence times T_{avr} , T_{min} , T_{max} refer to the usage of $A(L_0, T_0) = 7.85$, and of the marginal values $A \pm AA$, respectively, where $AA = 0.13$.

The recurrence times derived from the exponential relation (Table 3.4.2) for magnitudes $M_w \approx 7$ and $M_w = 7.8$ agree well with those earlier determined from the mean occurrence rates (chapter 3.4.2) which measured about 10 and 60 years, respectively. The so-calculated recurrence times for the greatest events ($M_w \geq 9.0$), measure up to several hundred years.

Extrapolation to smaller magnitudes than those covered by this data set (i.e., to $M_w < 7$) yield recurrence times for events in a 300-km long arc-segment that are very close to those derived from network data (Figure 3.1.6) or those from teleseisms (Figure 3.2.4). Normalizing the different log-linear relationships derived from the different data sets to a **300-km** arc length and a 1-year period yields the values summarized in Table 3.4.3. The different relationships give recurrence times (when extrapolated, for instance, to a common magnitude $m = 5.0$) that all lie within a factor of 2 to 3.5. This variation is remarkably small considering that both the magnitude range covered ($2 \leq m \leq 9.2$) and the method of magnitude determination vary strongly among those data sets.

3.4.5 Arc-wide. instrumentally determined seismic moment release, 1898-1982. Moment M_0 (dyn cm) is related to moment magnitude M_w by the relationship

$$\log M_0 = 16.1 - 1.5 M_w$$

assuming a constant and complete stress drop ($\Delta\sigma \approx 50$ bar) and constant shear modulus ($\mu \approx 5 \times 10^{11}$ dyn cm⁻²) (Kanamori, 1977). Because moment magnitudes are known for all events listed in Table

TABLE 3.4.2. Estimates of minimum-, average-, and maximum recurrence times derived from the b-value plot for the entire arc. The times are **scaled** to represent the occurrence of one event of magnitude M_w within a sector of length L **along** the arc.

M_w	L (km)	T_{min} (years, except for m = months)	T_{av}	T_{max}
5	300	2m	3m	4m
6	300	1.3	1.8	2.4
7	300	9.5	13	17
7.8	300	45	61	82
8	300	67	91	123
8.5	300	180	240	380
9	600	240	320	430
9.2	800	260	360	480
9.5	1000	380	510	690

TABLE 3.4.3. Comparison of A and b values and recurrence times T_R for $m = 5.0$ events using different data sources.

Source	Observed Magnitude Range	Number of Events	$A(L_0, T_0)$	$\frac{L}{L_0} \times \frac{T}{T_0}$ (km/km) x (Y/Y)	$A(L=300, T=1)$	b	$T_R(m=5.0)$ (years)
Shumagin network, all depth, (1977-1981)	2.5-6.0	631	4.72	$\frac{300}{400} \times \frac{1.0}{4.5}$	3.94	0.75 ± 0.06	0.643
Shumagin network, all depth, (1977-1981)	3.0-5.5	306	5.10	$\frac{300}{400} \times \frac{1.0}{4.5}$	4.32	0.85 ± 0.09	0.848
Teleseismic, all depths (1973-1981)	4.4-6.3	310	6.52	$\frac{300}{600} \times \frac{1.0}{9.0}$	5.26	0.92 ± 0.10	0.216
Teleseismic, all depths (1973-1981)	4.5-6.3	275	7.12	$\frac{300}{600} \times \frac{1.0}{9.0}$	5.86	1.04 ± 0.12	0.216
Large equ., all depths (1898-1982)	6.7-9.2	116	7.85	$\frac{300}{3600} \times \frac{1}{85}$	4.84	0.85 ± 0.10	0.256
Average of above	(2.5-9.2)	---	----	-- --	4.847	0.882	0.366

3.4.1, we can calculate **the** cumulative moment for the Aleutian arc as a function of time from 1898 to 1982. The individual moments so calculated from M_w are listed in Table 3.4.1 and their cumulative values are plotted in Figure 3.4.7.

The features of activity, earlier discussed on the basis of seismicity rates, are amplified by this seismic moment vs. time plot: a rapid moment release lasting from 1898 to about 1907 is followed by a period of slow moment release from 1907 to about 1957, when a major " sequence of **events** commences that lasts from 1957 to 1965. Since 1965, seismic moment release has again been extremely low and has remained so for the last 17 to 18 years.

The cumulative seismic moment released during the last 85 years measures 1.75×10^{30} dyn cm (equivalent to a single $M_w = 9.43$ event). The mean-rate for the entire 85-year period amounts to $\dot{M}_0 \approx 2 \times 10^{28}$ dyn cm y^{-1} (equivalent to one $M_w = 8.14$ per year).

These numbers and Figure 3.4.7 demonstrate several seismicity features very clearly:

1) Moment release is almost completely dominated by the largest events.

2) Seismic activity throughout the Aleutian arc appears to occur periodically, with two peaks of activity during the last 85 years that are about 60 years apart.

3) During the quiescent interval (≈ 50 years) few great earthquakes occur contributing to an average rate of moment release that is only about 3×10^{27} dyn cm y^{-1} (equivalent to one $M_w = 7.6$ event per year), or one to two orders of magnitude lower than in the short intervals (≈ 15 y) of very high moment release (8.6×10^{28} dyn cm y^{-1} , equivalent to one **event** of about $M_w = 8.5$ per year).

3.4.6 Plate-kinematic strain accumulation rates. To compare the observed seismic moment release with one derived from a simple plate-kinematic model we make the following assumptions:

1) Seismicity that actually occurs spread out over a volume at and near the plate boundary, is assumed to be released on a single brittle fault contact of area $A = L \times W$ (km^2) that takes up the entire relative plate motion \dot{u} (cm/y) by periodic seismic slip events (i.e., seismic efficiency a $= u_{\text{seismic}}/u_{\text{total}} = 1$).

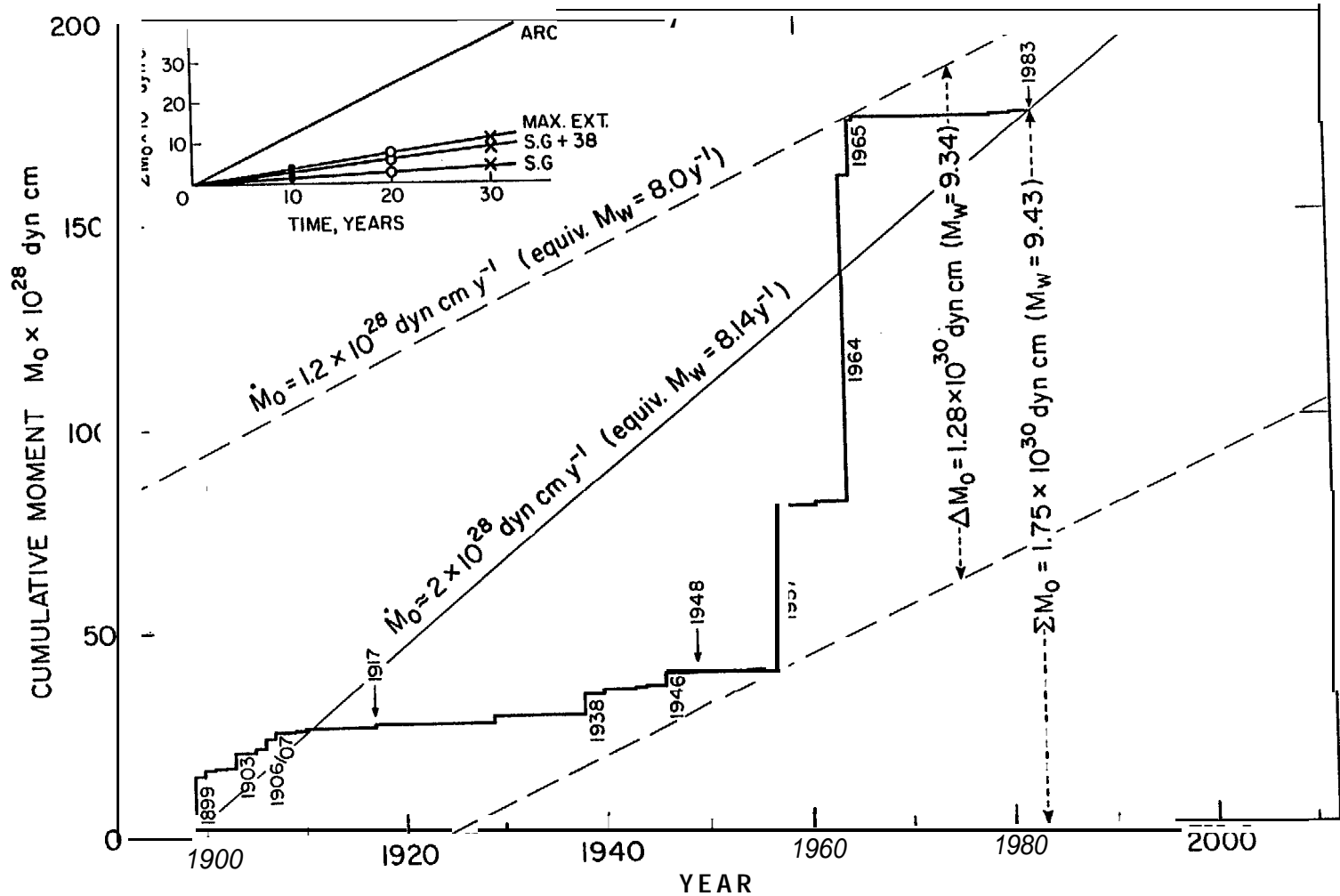


Figure 3.4.7. Arc-wide seismic moment release (heavy solid line) for the Aleutian arc during the period 1898 to 1982 (inclusive). Note periods of high moment release around the turn of century and approximately 60 years later. Fine solid line represents average moment release for 1898 to 1982 ($M_0 = 2 \times 10^{28} \text{ dyn cm y}^{-1}$). Broken lines straddling the upper and lower bounds represent the rate ($M_0 = 1.2 \times 10^{28} \text{ dyn cm y}^{-1}$) inferred from the plate-kinematic model discussed in the text. Note that this plate-kinematic rate represents only 60% of the mean rate observed during the last 85 years. Upper left insert: shows the moments that accumulate in 10, 20, and 30 years (dots, circles, crosses), respectively, for the entire arc, the maximum credible rupture extent indicated in Figure 3.4.2, for the Shumagin Gap (SG) alone, and combined with that of the 1938 rupture zone (SG + 38). Note that for some rates and moments the equivalent values in magnitude M_w are given.

2) Outside the brittle **fault** contact, slip of the plates past one another and relative to the mantle occurs entirely ductile and aseismic ($a = 0$).

3) The downdip width W (km) of the dipping fault contact that is assumed to have a full seismic efficiency of $a = 1$, is only a portion of the entire arc-trench distance. Estimates of this seismic width W_i are obtained for individual arc segments i with lengths L_i by measuring the updip distances between the '**aseismic front**', generally located at a depth of about 40 km, and the '**seismic front**', generally at a depth of about 10 km along the '**main thrust zone**' (for definition of these terms, see "House and Jacob, 1983; Davies and **House**, 1979; Yoshii, 1975).

With these assumptions, we calculate **the** plate-kinematic moment rates

$$\dot{M}_{oi} = \mu \cdot L_i \cdot W_i \cdot \dot{u}_i$$

for each arc segment of length L_i , and from their sum

$$\dot{M}_{o \text{ arc}} = \sum \dot{M}_{oi}$$

the arc-wide moment release is obtained.

We assume a constant shear modulus of $\mu = 5 \times 10^{11}$ dyn cm⁻² for the elastic properties of **the** plates near the fault contact; selecting the fault widths W_i for arc segments of length L_i , and the rates of relative motion \dot{u}_i between the North American and Pacific plates (after Minster and Jordan (1978), as indicated in Table 3.4.4), one obtains respective moment rates \dot{M}_{oi} listed in the same table, and a total moment rate for the arc. This arc-wide rate is

$$\dot{M}_{o \text{ arc}} \approx 1.2 \times 10^{28} \text{ dyn cm y}^{-1}$$

It corresponds to one event with magnitude $M_w = 8.0$ per year if it were released at such an unrealistically even mode.

The calculated rate, based on plate kinematic assumptions, yields only 60% of the seismic moment that is instrumentally observed as

TABLE 3.4.4. Parameters for plate-kinematic model of seismic moment release.

Zone	Slip Rate \dot{u} (cm y ⁻¹)	Length L (km)	Width W (km)	Area A (10 ⁴ km ²)	Moment Rate \dot{M}_0^3 (10 ²⁶ dyn cm y ⁻¹)	$\dot{M}_0/100$ km (10 ²⁶ dyn cm y ⁻¹ /100 km)	Stress Rate $\dot{\sigma}$ (bar/y)
Yakut at- Yakataga	6.0	200	100	2.0	6.0	3.00	0.30
1964-rupture	6.5	800	180 (200-150)	14.4	46.8	5.85	0.18
1938-rupture	7.0	350	120	4.2	14.7	4.20	0.29
Shumagin Gap	7.5	300	100	3.0	11.25	3.75	0.38
1946-rupture	7.5	150	80	1.2	4.5	3.00	0.47
Unalaska Gap	8.0	200	60	1.2	4.8	2.40	0.68
1957-rupture	8.0	800	50	4.0	16.0	2.00	0.80
1965-rupture	8.5	700	50	3.5	14.875	2 . 1 2 5	0.85
Entire Arc	7.1 ¹	3500 ^{2,4} 3600	95.7 ¹	33.5 ²	118.925 ²	3.398 3.303	0.37 ¹

¹Weighted average.

²Sum over arc segments.

³Assuming $\mu = 5 \times 10^{11}$ dyn cm⁻².

⁴Sum of zone lengths falls short of total arc length (3,600 km) because of minor under-lap.

⁵Stress rate $\dot{\sigma} = \mu\dot{u}/W$.

mean-rate during the last 85 years (Figure 3.4.7). Either the model underestimates fault width, plate motion, or shear modulus by that much, or their product by some combination of either. Alternatively, one may conclude that the calculated rate of $\dot{M}_0 \text{ arc} = 1.2 \times 10^{28} \text{ dyn cm y}^{-1}$ is a correct lower bound for a long-term average, but that the sequence of great events between 1957 and 1965, including **the** giant 1964 event, was unusually seismogenic and released a larger moment than the arc typically does during one of its regular seismic cycles.

Using the plate-kinematic moment rates for each individual arc segment as listed in Table 3.4.4 and the moments for the last sequence of great earthquakes, we can calculate hypothetical recharge periods, i.e., the time required to accumulate by plate motion the moment that was released during the last great event. Furthermore, we can calculate the percentage of the full recharge time that has passed between the year of that event and now (1983). That value is >100% if the recharge date has been exceeded and <100% if it will be reached in the future. The results of these calculations are summarized in Table 3.4.5. They show that the **Shumagin** gap and the 1938-rupture zone **are** 'overcharged', i.e., they have stored seismic moment far beyond that released during their last significant events. Next in that sequence rank the 1946 rupture zone and the **Yakataga** gap which have restored less than half of their moment released last. In contrast, the 1964-, 1957-, and 1965-rupture zones have recovered less than 10 to 20% of their moments released in their last great events.

Note that for the purpose of these calculations we placed the 1903 ($M_w = 8.3$) event in the **Shumagin** Gap although there is little reason to believe it ruptured (the shallow or any portion of) the **Shumagin** Gap. Hence, the **Shumagin** gap may be charged more than here indicated from the instrumentally recorded events alone. We therefore consider the next historical record to see when in fact this gap had experienced some major strain relief prior to 1898.

3.4.7 Estimates of moment release associated with historic earthquakes. The Shumagin and probably the potential **Unalaska** seismic gaps experienced very little or virtually no moment release from truly great earthquakes during the instrumental period since 1898. We therefore consider the historic seismic record of the Aleutian Arc

TABLE 3.4.5. Recharge Status of Rupture Zones or Gaps Since Last Significant Events.

Arc Segment	Year of Event	M_w	Recharge Period (years)	Time Lapsed (years)	Due Date	Years Left	Years Overdue	P Percentage of Recharge
Yakutat-Yaketaga Gap	1899	8.68¹	221	84	2120	137	--	38%
1964-zone	1964	9.2	170	19	2134	151	--	11%
1938-zone	1938	8.4	34	45	1972	---	11	132%
Shumagin Gap	1948	7.5	2	35	1950	---	33	> 1000%
Shumagin Gap	1917	7.8	6	66	1926	---	57	> 1000%
Shumagin Gap	1903²	8.3 ²	31	80	1934	---	49	258%
Shumagin Gap	1847/1788	8.78 ^{1,3}	136/195 ³	136/195 ³	1983 ³	0 ³	0 ³	100%³
1946-zone	1946	8.3	79	31	2025	42	--	47%
Unalaska Gap	1878	8.4 ³	1053	1053	1983 ³	0 ³	0 ³	100% ³
1957-zone	1957	9.0	249	26	2206	223	--	10%
1965-zone	1965	8.7	95	18	2060	77	--	19%
Kommand.-Gap	1849/59	8.69^{1,3}	129³	129 ³	1983 ³	0 ³	0 ³	100% ³

¹Composite value of several events.

²Did probably not rupture Shumagin Gap.

³Computed value if event would recur in 1983.

that (at present) dates back to about 1784 (Sykes et al. , 1980, 1981; Davies et al. , 1981). Because for historic events no instrumentally determined moments or magnitudes are directly available, and because intensity reports are spatially very incomplete due to low population density, we have essentially only a few means to assess the sizes of events. For a few events their rupture lengths can be inferred from sparse intensity reports or tsunami reports at widely spaced localities for the same day. Another and new method, which we will apply here systematically, is the concept of the 'time-predictable' model (Shimazaki and Nakata, 1980). It postulates that the time ΔT (of seismic quiescence) between two great earthquakes on the same plate boundary segment is proportional to the moment release M_0 of the first of the two events, "and they are related to the long-term plate-tectonic slip-rate \dot{u} (cm/y) by the relation

$$M_0 = \mu W L \dot{u} \Delta T$$

If we know the rupture length L for the event preceding the time interval ΔT between two great events, and use the same parameters W , \dot{u} , μ as before (see chapter 3.4.6) then we can calculate a rough moment estimate for the event that precedes the period ΔT (Table 3.4.6).

Note that the above equation can also be solved for

$$L = M_0 / (\mu W \dot{u} \Delta T)$$

We use this relation for those post-1898 events for which a moment and succeeding time-interval ΔT is known but no rupture-length is known because of poor aftershock coverage. We use this formula to estimate rupture length for seven great events ($M_w \geq 7.8$) that occurred between 1898 and 1929 and for which either no or only insufficient intensity reports exist. Applying this relation we find that between 1898 and 1929 about 60% of the 700 km long arc segment that broke in the single 1965 $M_w = 8.7$ event, had broken by a sequence of smaller events with magnitudes $7.8 \leq M_w \leq 8.2$ (Figure 3.4.8).

TABLE 3.4.6. List of great historic events and inferred source parameters based on the 'time predictable' model.

Date	M_w	M_0 (10^{28} dyn cm)	L (km)	W (km)	$\Delta\sigma_s^{1,2}$ (bar)	AT ³ (Y)	Participating Zones ⁷
7/1788	8.76	17.88	650	130(100-180)	16	56,59	64,38,SG
8/1788	8.63 to 8.77	11.09 to 18.00	150 to 300	111(100-120)	50	158,195	SG,46
1792	8.4	5.01	150	180	10	62	64
1844	8.6	10.00	150	180	21	120	64
1847	8.7 ⁶	14.13 ⁶	500	114(100-120)	226	1,70,91,136 ⁶	38,SG
1848	8.0 ⁴	1.26 ⁴	86 ⁵	86 ⁵	20 ⁵	32	38
1849	8.5 ⁶	7.08	250	50	110 ⁶	134 ⁶	KG
1854	8.6	10.00	150	180	10	110	64
1859	8.5 ⁶	7.08	250	50	110 ⁶	124 ⁶	KG
1878	8.4 ⁶	5.01	200	60	70 ⁶	105 ⁶	UG
1880	8.0 ⁴	1.26 ⁴	865	86 ⁵	205	23	38
Column Average	8.47	8.43	245	112	41 (27.43)	92	

¹Simple stress drop* $\Delta\sigma_s = M.L^{-1}W^{-2}$

²Note that 10^6 dyn cm⁻² = 1 bar

³AT are the years until the succeeding event(s) on the same rupture zone.

⁴Magnitude is estimated, not calculated from 'time-predictable model*.

⁵Source parameters inferred by assuming $A_s = 20$ bar.

⁶Minimum value which increases if succeeding event occurs later than 1983.

⁷Zones coded by year, i.e., 64 = 1964 rupture zone. SG = Shumagin Gap, KG = Kommandorski Gap, UG = Unalaska Gap.

⁸Calculated from average M_w , L, W.

We emphasize that for all these and the following calculations the same idealized assumptions apply that were used earlier: no **aseismic** slip must occur within the width W of the fault and the slip released in the quakes constitutes the entire plate motion when averaged over long periods of time (i.e., over many seismic cycles).

In many instances, we don't know the rupture length of historic events very well. To compute at least some very rough moment estimates we assume their spatial limits from whatever limited information is available. These assumptions are depicted in Figure 3.4.8 and closely agree, except for some minor details, with those of Sykes et al. (1980, 1981) and Davies et al. (1981). Where these authors left lateral extent of events undetermined we arbitrarily made ruptures terminate at the nearest boundary of a tectonic subdivision. The Figure 3.4.8 shows the moments derived for historic events based on these assumptions and on the plate kinematic and time-predictable models. The calculated moments and magnitudes should not be taken as real, but as an indication whether our models and assumptions produce magnitude values that are at least plausible. In that sense they provide a **test** of the model assumptions.

Several remarkable results emerge from this exercise. None of the magnitudes M_w calculated from the inferred moments M_0 (these magnitudes M_w are shown in parentheses **in** Figure 3.4.8) are unreasonably large for any of the historic events. The largest events considered, i.e., those in 1847 and 1788, are all smaller in magnitudes than those of the great 1957 and 1964 events, i.e., none of the calculated magnitudes are required to exceed $M_w = 8.9$. This finding may not necessarily support, but also does **not** contradict our earlier notion that the 1957-, 1964-, 1965-event sequence of truly great earthquakes may have been somewhat exceptional.

Furthermore, we have calculated hypothetical moment magnitudes M_w for unreported events that might have occurred, say, at about 1760. Using the arc-specific moment rates and the time-predictable model these hypothetical events serve to justify the long periods of apparent quiescence for which no important events are reported during both Russian and early U.S. ownership of Alaska. These hypothetical maximum-size events (assumed at 1760) are indicated near the bottom of

Figure 3.4.8 by unbracketed magnitude symbols M_w . For instance, except for the $M_w = 7.9$ event in 1905 and a normal faulting event $M_w = 7.9$ near the trench in 1929, virtually no great event has been reported in the 1957-zone since 1760, when Russian fur-trade and hunting expeditions in the arc near **Amchitka** and Attu were well underway, albeit without continuous Russian settlements. Nevertheless, the magnitude $M_w = 8.93$ that is required in order to be succeeded by such an extended quiescence - whether real or not - is still smaller than that of $M_w = 9.0$ for the 1957 event. We conclude that, while this quiescence since at least 1760 may not be real, it is permissible without requiring an unrealistically gigantic earthquake to precede it just prior to the arrival of Russian traders. Similarly, the 139-year long 'quiescence' between 1760 and 1899 in the **Yakataga** gap requires 'only' a $M_w = 8.55$ event at or prior to 1760; this magnitude is smaller than one derived from the combined moments of the 1899 Yakutat-Yakataga sequence.

As pointed out by Sykes et al. (1980, 1981) the historic record near the Shumagins and Kodiak is probably more complete than elsewhere along the **arc**. **This** applies to events since 1788 because of permanent Russian presence at **Unalaska, Unga, Sanak, and Kodiak** from at latest 1784 onward. Whether the more frequent reports of great events there reflect simply a difference in recurrence times (say 60 to 100 years) compared to more than 200 years in the 1957 zone cannot be resolved at present. The magnitudes and recurrence times permit either a true difference along the arc, a regular variance from one seismic cycle to the next, or incomplete historic records for large arc segments. If the latter is the case, the 1957 and 1964 events should be followed by above-average (quiescent) recurrence periods.

If the 1847 event with an inferred $M_w = 8.7$ ruptured only the eastern half of the Shumagin gap and not **also** the western half, and if the same applies to the July 22, 1788 event (inferred $M_w = 8.76$), then the event of August 7, 1788, **can** be calculated to have had a magnitude of at least $M_w = 8.63$ to cause the near-quiescence of the **Shumagin** gap lasting until now (1983). Should that event also have ruptured the entire 1946-zone then the inferred minimum magnitude for the August 1788 event increases to $M_w = 8.77$. Either magnitude

would be consistent with the tsunami effects at Sanak and the Alaska Peninsula described by historic reports (Sykes et al., 1980, 1981; Davies et al., 1981).

Because the hypothetical moment release for the August 1788-event may come from only a 150 to 300 km long **segment** it may have required rather high stress drops and/or stiffer elastic plates (increased μ) and thus may signify the Shumagin gap as a hard-to-break asperity. If the **Shumagin** gap constitutes such an anomaly, recurrence times for major events to break the gap could be prolonged over those of adjacent arc portions (i.e., the 1938 zone where they may measure as short **as 60 years**). Barring any misinterpretations during the instrumental period it seems that the western and eastern half portions of the Shumagin Gap were quiet for truly great events ($M_w > 8.0$) for 195 and 136 years, respectively.

On the other hand, as shown earlier (Table 3.4.5), the expected, ongoing quiescent periods (or recharge periods) in the 1957 and 1964 zones could last for 249 and 151 years, respectively, if the proposed plate-kinematic and time-predictable model is correct. Therefore the **Shumagin** gap may not be anomalous, but reflects the regular variations in the same segment of arc that may occur between different seismic cycles.

The 'time-predictable model' can be viewed as one extreme model which is contrasted by the 'slip-predictable' model (Shimazaki and **Nakata**, 1980). In the latter case the slip (and thus moment) of the earthquake succeeding the quiescent period is proportional to the duration ΔT of that period. If this model were valid we can calculate the magnitude of future great earthquakes breaking any given arc segment. For instance given the virtual quiescence (for $M_w > 8$) of 136 and 195 years of the eastern and western halves of the 300 km long **Shumagin** seismic gap we obtain a hypothetical magnitude $M_w = 8.72$ for the **year 1983** in that gap, that would increase by **small** amounts each year. We have calculated these hypothetical magnitudes for the year 1983 for each arc segment. They are indicated near the top of Figure 3.4.8 (at year 1983) by the inverted brackets). Reinterpreting these magnitudes M_w by the 'time-predictable' model implies, that wherever they are **less** than the magnitude of the

previous great earthquake in the same arc segment a great earthquake is not yet likely. Where they exceed the magnitude of the preceding event, a great event is overdue but may have a magnitude different from the one indicated by M_w . Note that the highest value among the magnitudes M_w has been determined for the **Shumagin** gap, despite its associated short arc length of only 300 km. This indicates the implied readiness of that gap for a great event, whatever its actual magnitude may be. In fact the adjacent rupture zone of the $M_w = 8.4$ event of 1938 shows a value $M_w = 8.48$ which exceeds that of 1938 and thus may break together with the **Shumagin** gap in an event that could measure as great as $M_w = 8.8$ to 8.9. Similarly the probable **Unalaska** gap shows a high value $M_w = 8.4$ for its small (200 km) arc length provided it has not or was only partially ruptured in 1957.

Finally, we can make a present-day balance between the stored cumulative moment that is generated by the plate-kinematic process from a certain year onward up to date, and the cumulative moment released by great, historically and instrumentally reported earthquakes. We choose the arbitrary limits of this period to be 1760 and 1983. The results from this balance are indicated in Table **3.4.7**. Assuming **all** underlying assumptions are correct, which most likely they are not, it shows that the 1964, 1946, and 1957 zone may have 'overspent' some of the (inferred) available moment (or slip), while the 1938, **Shumagin** and **Unalaska** Gaps, and, surprisingly, the 1965 zone would be capable of significant events at this time. In this assessment, the **Yakataga** gap would have just recently reached a moment balance. Note that the arc as a whole is nearly balanced by having to spare not more than the equivalent of a $M_w = 8.8$ to 8.9 at present. Since a balance in each arc segment depends highly on the accuracy of the instrumentally determined magnitudes and completeness of historic record as well as the choice of starting (1760) and termination (1983) of the period considered, little credibility should be attached to the moment balances for some of the arc segments with poor data quality.

3.4.8 Statistics of recurrence times and probabilities for great earthquakes. Figure 3.4.8 shows that since 1788 several of the arc

TABLE 3.4.7. Moment Balance (expressed in equivalent M_w) since 1760.

Arc Segment	Largest M_w	Moment Balance (measured in equiv. M_w)	Years Left	Years Overdue
Yakataga Gap	8.68 ¹	+7.32	.-	2
1964 zone	9.2	-8.49	15	---
1938 zone	8.4	+8.29	--	23
Shumagin Gap	8.78 ^{1,2}	+8.29	--	31
1946 zone	8.3	-7.80	14	---
Unalaska Gap	8.4 ²	+8.44	--	118
1957 zone	9.0	-8.40	31	---
1965 zone	8.7	+8.70	--	94
Kommandorski Gap	8.69 ^{1,2}	+8.60	--	95
Entire Arc		+8.86		18.8

¹Composite of several events.

²Computed from time-predictable model.

segments broke more than once in great events. For instance, the 1938 rupture zone broke in 1847 and also in 1788; similarly, various subsections of the 1965 rupture zone broke around the turn of the century. Taking **all** observations of repeated ruptures of **arc** segments, and combinations or subdivisions thereof, we can make a list of recurrence intervals between all lead and successor events that bracket the recurrence intervals. Such a listing is compiled in Table 3.4.8. There are 11 observed recurrence intervals with lead events between 1788 and 1880, during the historic period. To those 11 data, a set of five minimum recurrence **intervals can** be added assuming that a successor event would occur in 1983 or later (see Footnote 1 of Table 3.4.8). This brings the total to 16 recurrence periods following 11 historic lead events (see also Table 3.4.6). There are 8 observed recurrence periods from as many lead events during the instrumental period 1898-1982 to which 5 'observations' of minimum-periods can be added if we assume that the **Shumagin** (1917) and **Yakataga** gaps (1899) and the 1938 rupture zone will break **in** 1983 or some time soon. Note that according to the plate-kinematic calculations, these zones, except for the **Yakataga** gap (see Table 3.4.5), have recovered their moments since their last event sequences, and hence this assumption is--within the **plate** kinematic model--marginally permissible.

Furthermore, there are the four great earthquakes of 1946, 1957, 1964 and 1965 that occurred too recently to have ruptured again. For these we can estimate recurrence periods from the 'time-predictable' model (see 'recharge-periods' in Table 3.4.5). These estimates are likely maximum values compared to **most** others **since** they **are** associated with lead events with rather large moments.

In summary, Table 3.4.8 contains a total of 33 data points of which **19 are** observed, and **14** are computed values. We can rank the order of recurrence periods of Table 3.4.8 by their increasing magnitude (duration) and then assess the statistical properties of this data sample. In doing so we obtain:

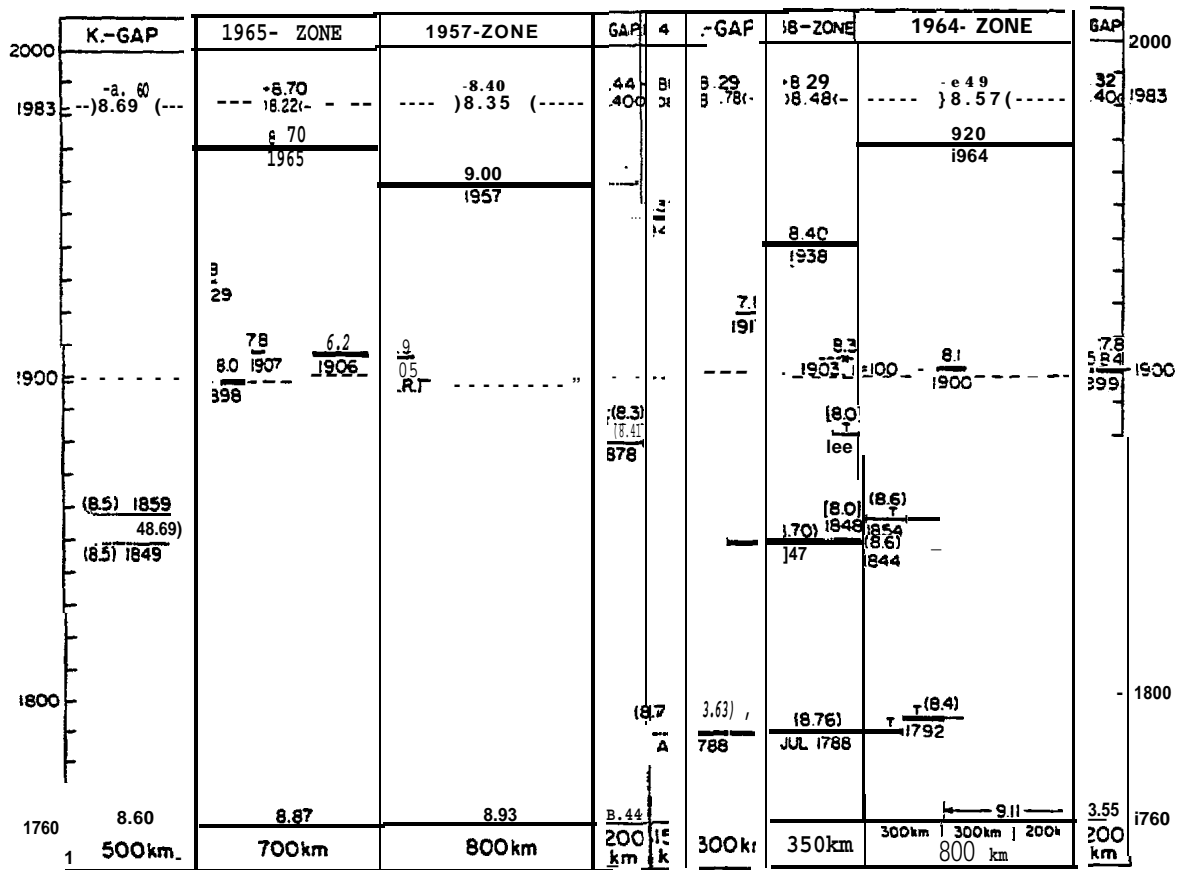


Figure 3.4.8. Space-time plot of instrumental (1898 to 1982) and historical (1788 to 1957) seismicity of the Aleutian arc considering great earthquakes ($M_w > 7.8$) only. Note that we have omitted from this plot a $M_w = 7.9$ event in 1929 that occurred presumably as normal faulting in the trench near the eastern end of the 1957 rupture zone. Each event is labeled by year, M_w , and (where applicable for historic events only) any tsunamis reported (T). Magnitudes computed for historic events from the time-predictable, plate-kinematic models are indicated in parenthesis. For hypothetical magnitudes plotted near 1760 and those indicated by M_w (at 1983, see text). The magnitudes plotted just above 1983 represent the theoretical moment balance (in equivalent M_w) for each arc segment. Positive values imply moments (measured in M_w) available for release, negative values imply that recent events have overspent the moment and require a quiescent period of plate-motion-driven moment accumulation. Uncertain rupture zones are indicated by broken lines.

TABLE 3.4.8. Observed or computed *recurrence times* for rupture zones which broke during the historic and instrumental period 1788 to 1965.

Lead Event Year	M_w	Successor Event Year	M_w	Recurrence Period (years)
1788	8.8	1844	8.6	56
1788	8.8	1847	8.7	59
1788	(8.7) ¹	(1983)	?	(195)
1788	8.7	1946	8.3	158
1792	8.4	1854	8.6	62
1844	8.6	1964	9.2	120
1847	8.7	1848	8.0	1
1847	8.7	1938	8.4	91
1847	8.7	1917	7.8	70
1847	(8.7)	(1983)	?	(136)
1848	8.0	1880	8.0	32
1849	(8.5)	(1983)	?	(134)
1854	8.6	196.4	9.2	110
1859	(8.5)	(1983)	?	(124)
1878	(8.4)	(1983)	?	(105)
1880	8.0	1903	8.3	23
1898	8.0	1965	8.7	67
1899	8.5	(1983)	?	(84)
1899	8.4	(1983)	?	(84)
1899	7.8	(1983)		(84)
1900	8.1	1964	9.2	64
1903	8.3	1938	8.4	35
1905	7.9	1957	9.0	52
1906	8.2	1965	8.7	59
1907	7.8	1965	8.7	58
1917	7.8	(1983)	?	(66)
1929	7.9	1957	9.0	28
1929	7.8	1965	8.7	36
1938	8.4	(1983)	?	(45)
1946	8.3	[2025] ²	?	[79]
1957	9.0	[2206]	?	[249 1]
1964	9.2	[2134]	?	[170 1]
1965	8.7	[2060]	?	[95]

¹The values in parentheses () are minimum values which increase if the successor event **is** not occurring in 1983 but at a later time.

²The values in brackets [] are likely to be maximum values and are calculated by the 'time-predictable' model from the magnitude M_w of the lead-event.

Number of data points: 33
 Smallest value: 1 year
 Largest value: 249 years
 Median value: 70 years
 Mean value: $\mu = 86$ years
 Standard Deviation: $\sigma = \pm 53$ years
 Mean + Standard Deviation: $\mu + \sigma = 139$ years
 Mean - Standard Deviation: $\mu - \sigma = 33$ years

The median and mean values should coincide if the sample population follows a normal distribution; the above results show, however, that this is not **the** case for these data. Therefore, we search for other distributions that provide a better approximation to the data. Eliminating the lowest value $T_R = 1$ year, we find that the remainder of the data are nearly log-normally distributed. Therefore we plot a histogram of the occurrences of the logarithm of recurrence times (i.e., $y = \log T_R$) in Figure 3.4.9 (bottom). This sample of data has the following properties:

Number of data points: 32
 Smallest value: 23 years
 Largest value: 249 years
 Median value: 74 years
 Logarithmic mean: $\mu_y = 1.88$ (i.e., $T_{\mu} = 76$ years)
 Standard Deviation: $\sigma_y = \pm 0.25$ (i.e., $T_{\mu \pm \sigma} / T_{\mu} = 1.78 \pm 1$)
 Mean + Standard Deviation: $T_{\mu + \sigma} = 135$ years
 Mean - Standard Deviation: $T_{\mu - \sigma} = 43$ years

Thus, after a double coordinate transformation

$$y = \log T_R$$

$$z = (y - \mu_y) / \sigma_y$$

we can find a normal (Gaussian) distribution for the scaled variable z that has **the** new properties (Bendat and Pierson, 1981):

Mean: $\mu_z = 0$
 Standard Deviation: $\sigma_z = 1$
 Variance: $\sigma_z^2 = 1$

The associated probability density function $p(z)$ and (cumulative) probability function $P(z)$ are:

$$p(z) = (2\pi)^{-1/2} e^{-z^2/2}$$

$$P(z) = (2\pi)^{-1/2} \int_{-\infty}^z e^{-\xi^2/2} d\xi$$

The cumulative probability $P(z)$ is plotted as the smooth curve in Figure 3.4.9 (upper frame) in comparison with the cumulative occurrence of observed recurrence periods (incremental curve), both of which have the same logarithmic mean μ , and standard deviation σ from the mean.

The distribution $P(z)$ shows that in the Aleutian arc there is a probability of only about 1% that the area of a great earthquake will rupture again in a great event after only 20 **years**, a probability of **50% that** it will rupture after about 76 years, and of 90% after about 160 years. Table 3.4.9 lists selected values of probability P and associated recurrence periods TR .

We have plotted in Figure 3.4.9 (near the upper margin) the holding times (up to 1983) for the last major earthquakes in each major arc segment. Projecting down from these values TR in Figure 3.4.9 to the probability distribution $P(z)$ yields the probability as of 1983 that each arc segment has attained for the occurrence of a great event ($M_v > 7.8$). These probabilities **P(1983)** are listed in Table 3.4.10. We note, for instance, that the two segments of the Shumagin gap that have last ruptured in 1788 and 1847, respectively, have reached respective probabilities as high as 95 and 85%, whereas the 1938 zone has reached (by 1983) a probability of only 18%.

3.4.9. Conditional probability and annual probability rate of occurrence. While it is interesting to know that the Shumagin gap has not yet broken despite such high cumulative probabilities, it is more important to ask the question: what is the probability that the Shumagin gap will rupture during the next, say 10 or 20 years, given

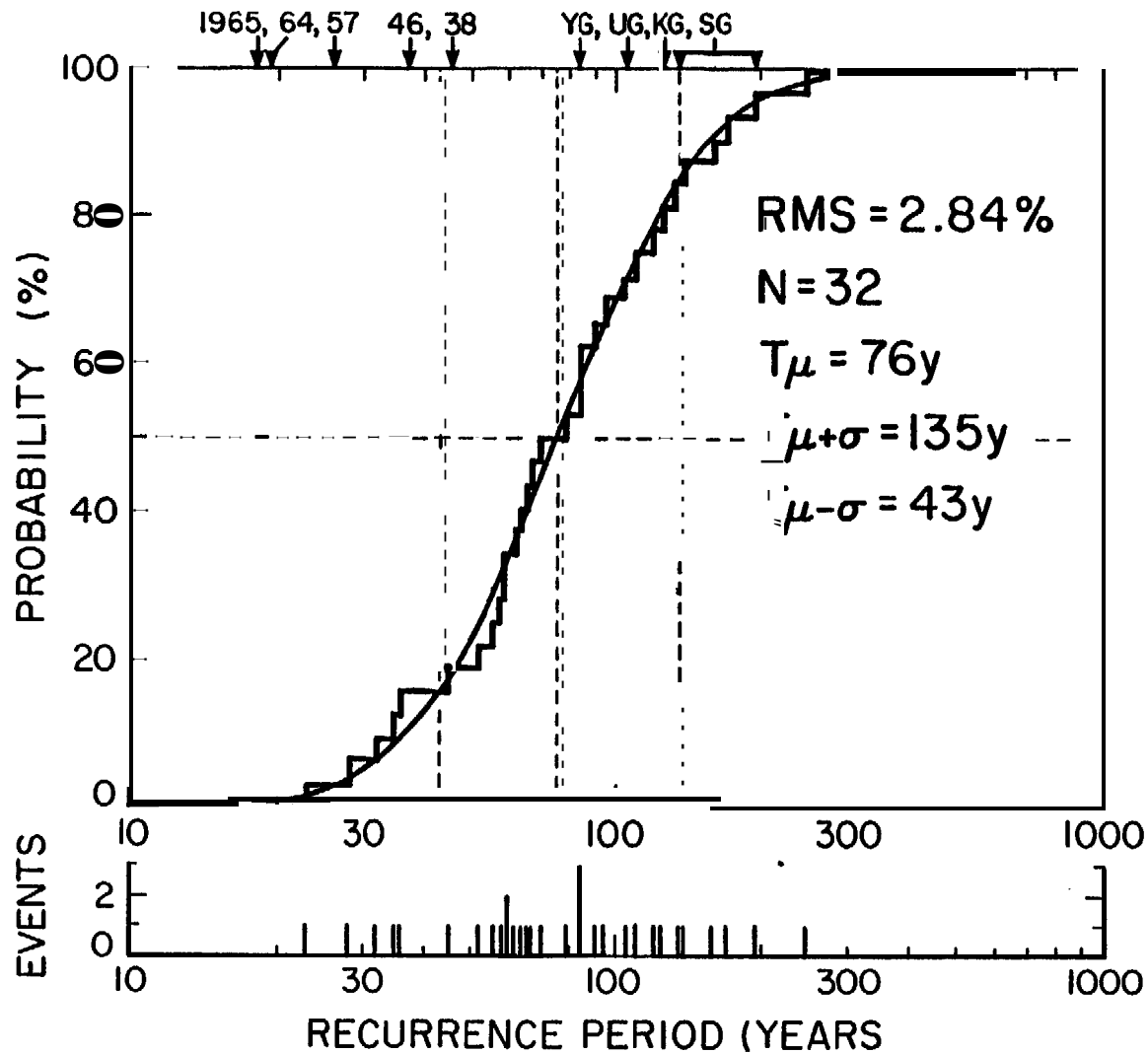


Figure 3.4.9. Statistical properties of recurrence periods. Bottom: Discrete probability density distribution of empirical recurrence periods. Top: Probability (in %) of empirical recurrence periods (incremental curve) and equivalent log-normal probability distribution (smooth curve) with the same logarithmic mean μ ($T_\mu = 76$ years) and standard deviation σ . Mean and deviation yield lower and upper values T ($\mu \pm \sigma$) of 135 and 43 years, respectively (vertical dashed lines). Labels near upper margin of figure indicate the present (1983) holding times since the last great earthquake in each zone. Projecting these times down to the probability curve permits reading of the (cumulative) probability that each zone has attained as of 1983 for a great event with any magnitude $M_w > 7.8$ to recur; e.g., for the Shumagin Gap the probability is 85 to 95%, for the 1938-zone 18%, and only about 1% for the 1964 zone. Note that these cumulative probabilities are distinct from the conditional probabilities of any zone to break in a given future period; see text and Table 3.4.10.

TABLE 3.4.9. Probabilities P(%) for Recurrence periods $T_R(\text{years})$.

P(%)	$T_R(\text{y})$
1	20
5	29
10	36
20	47
30	56
40	66
50	76
60	88
70	102
80	123 ,
85	138
90	159
95	195
98	247
99	288
100	∞

the condition that it has not ruptured during the last 136 or 195 years, respectively?

To answer this question we use the concept of the conditional probability defined as

$$P^*(T_R/T_R+\Delta T) = (P(T_R+\Delta T)-P(T_R)) / (1-P(T_R)) - 1$$

It constitutes the probability gain during the interval ΔT (during which the holding time increases from T_R to $T_R + \Delta T$), divided by the remaining probability increment $(1-P(T_R))$ which reflects the assumed certainty ($P=1$) that the gap will break sometime between T_R and $T=\infty$.

We have listed (Table 3.4.10) these conditional probabilities P^* which describe the chances (in percent) that any of the considered gaps or zones will break during **the** next one or two decades (i.e., during the periods 1983-1993 and 1983-2003, respectively). Note that these conditional probabilities P^* for the next 10 or 20 years vary much less (by a factor ≈ 5) from one region to another than do the probabilities P . Note also that the cumulative probability for the **Shumagin** gap increases by only $<2\%$ between 1983 and 2003 (from 95.0 to 96.5% for the August 1788 rupture segment), while the conditional probability $P^*_{1983/2003}$ that a great **Shumagin event** will occur between now (1983) and 2003, measures 30% (amounting to an average annual probability P^* of about 1.5% per year). Hence, to maximize **the** chance for catching a great earthquake, say, for the purpose of monitoring strong motions from a great event, the chances to do so successfully in the next decade is about 4 to 5 times higher in any of the four gaps (**Shumagin, Kommandorski, Unalaska, and Yakataga**) than, for instance, in the 1964 or 1965 rupture zones. Correspondingly the hazards ratio is similar.

When studying all the particular tectonic and physical properties of a particular gap or arc segment, its specific behavior may very well be explicable partly **deterministically**. For instance, in the present analysis we have ignored the possible underlying physical causes for some systematic variations in recurrence times T_R . We did not account for the possible systematic effect that the known

variations along the arc of plate rates \dot{u} (cm/y), contact width W and average stress drop $\Delta\sigma$, or the shear modulus μ may have.

The deterministic formulation for recurrence time T_R 's of the form (modified after Sykes and Quittmeyer, 1981):

$$T_R = (\Delta\sigma/\mu)/(W/\dot{u}) = M_0/M_0$$

We call $\Delta\sigma = M_0/LW^2$ 'simple stress' by implying that the usually associated geometrical constant C to be of uniform order 1, regardless of fault geometry. Given the dependence of T_R on $\Delta\sigma$, μ , W and \dot{u} , we could have first carried out a multivariate regression of the observed recurrence times (Table 3.4.8), then we could have removed the systematic effects of \dot{u} , W , $\Delta\sigma$, or μ if they existed, and would have obtained a new data set T_R' that presumably would have had a smaller variance σ^2 of the recurrence times from their new mean, provided a significant correlation between the original T_R and local values of \dot{u} , W , $\Delta\sigma$, and μ existed. We have abstained here from using such regression methods which will be reserved for future refinements.

3.4.10. When will the Shumagin Gap break? The key question remains: when will the **Shumagin** gap (or any of the other gaps) break? According to the deterministic models (that **use** only a single-value average behavior) the Shumagin gap should have ruptured several decades ago. When treated as part of a random process, it had a probability of about 90% to have broken by now. Given the fact it has not utilized the 90% probability, we can only estimate the probability, rather than a date itself, that it may rupture in, **say**, the next one or two decades. These conditional probabilities **are** 'only' about 16 and 30%, respectively, implying a 84 to 70% probability that this gap will not break in the next one or two decades, respectively. It remains to be seen whether the actual behavior of the gap happens to follow more closely the deterministic prediction of overdue imminence, or whether it will ride out the full range of unlikely high, but permissible cumulative probabilities that may be as high as 96% during the next 20 years while the annual probabilities are not exceeding a few percentage points. In all instances, a constant long-term preparedness for a great event is

warranted, that may have to be maintained for more than 2 decades. Shorter-term warnings can only be issued if a variety of seismic and other geophysical earthquake precursors are monitored and identified at a sufficient signal to noise ratio. These precursors can then be used to calculate temporary probability gains (Aki, 1981) that may raise the effective probability rates over and above those of the basic annual probability rates listed in Table 3.4.10 by factors of 30 or more.

Depending on when the **Shumagin** gap is ready to break, it may have a chance to rupture in a giant event, whose maximum extent (Figure 3.4.2) could include the 1938 rupture zone, the **Shumagin gap** proper, the **Unalaska** gap, and even may weakly rerupture the 1946 zone. Such an event, however unlikely, would have a maximum magnitude {calculated from a slip-predictable model) of about $M_w = 8.9$ to 9.0, depending on when it would occur.

3.4.11. Alternative probability model. In section 3.4.8 we have pointed out that a log-normal distribution yields a fit to the recurrence time data that is superior to that obtainable for a normal distribution. This conclusion may be largely due to the fact that we tried to make a statistical statement about recurrence times for the entire arc. Nishenko and Sykes (in preparation) made an analysis of recurrence times on restricted segments of the San Andreas fault and for portions of the **Chile** subduction zone. They argue that recurrence times for restricted portions of a fault that repeatedly break the name tectonic units are normally distributed. They find also that the standard deviation is only about 1/3 of the mean recurrence time T , i.e., much smaller than in the case one obtains for the variation of recurrence times along the entire fault system.

Because of a basically different behavior of probabilities in a normally and a log-normally distributed data set for times $T_R \gg T_{\mu+\sigma}$, we present here for completeness an alternative model, the results of which illustrate the great uncertainties that still **exist** in these assessments when the known seismic history covers at best only 2 to 3 mean recurrence intervals.

For this alternative model we eliminate the smallest ($T_R = 1$ year) and the four largest recurrence times ($T_r = 249, 195, 170$ and

TABLE 3.4.10. Cumulative, conditional., and annual probabilities for great earthquakes in 1983, 1993 and 2003, and intervals in between, respectively, for major Aleutian rupture zones and gaps for log-normally distributed recurrence periods (N = 32; $T_{\mu\pm\sigma} = 76 \times 1.78^{\pm 1}$ years).

Zone	Year of Last Event	Lapsed Time T_R (years) Until 1983	Cumulative Probabilities P(%) ²			Conditional Probabilities P*(%) ³		Annual Rate $\bar{P}*(\%/y)$ ⁴ (10 year avg.)
			1983	1993	2003	1983-1993 ($\Delta T_R=10y$)	1983-2003 ($\Delta T_R=20y$)	
Shumagin	1788	195	95.0	95.8	96.5	16.0	30.00	1.6
Shumagin	1847	136	84.5	87.2	89.5	17.4	32.3	1.7
Kommandorski	1854 ¹	129 ¹	82.2	85.3	88.	17.4	32.6	1.7
Unalaska	1878	105	71.4	76.5	80.7	17.8	32.6	1.8
Yakataga	1899	84	57.1	63.2	71.4	18.9	33.3	1.9
1938-rupture	1938	45	18.2	28.8	39.4	13.0	25.9	1.3
1946-rupture	1946	37	10.6	20.3	30.9	10.9	22.7	1.1
1957-rupture	1957	26	3.1	9.8	19.3	6.9	16.7	0.7
1964-rupture	1964	19	0.8	4.7	18.4	4.0	11.7	0.4
1965-rupture	1965	18	0.6	4.2	11.3	3.6	10.7	(.)4

¹Average for 1849/59.

²See curve in Figure 3.4:9.

³ $P*(1983 \text{ to year } X) = (P_X - P_{1983}) / (1 - P_{1983})$.

⁴ $\bar{P}^* = P^* / \Delta T_R$, with $\Delta T_R = \text{year } X - 1983$.

158 years) from the data set of Table 3.4.8. This yields a new restricted data set with smaller variance, to which we can marginally fit a normal (rather than a log-normal) distribution.

The new data set has the properties:

Number of data points: 28
 Smallest value: 23 years
 Largest value: 136 years
 Median value: 66.5 years
 Mean value: $\mu = 73$ years
 Standard deviation: $\sigma = \pm 32$ years
 Mean + Standard Deviation: $\mu + \sigma = 105$ years
 Mean - Standard Deviation: $\mu - \sigma = 41$ years

The histogram (probability density) of recurrence times T_R and the associated cumulative probability function $P_c(\%)$ are shown in Figure 3.4.10 and the probabilities and conditional probabilities derived for the various arc segments from this normal distribution are summarized in Table 3.4.11. The latter differ from those in Table 3.4.10 (log-normal distribution) in several important ways.

Most prominently, the cumulative probabilities increase to values very close to 100% for gaps whose holding times T_R exceed substantially $\mu + \sigma = 105$ years (i.e., the **Shumagin** and Kommandorski gaps). Moreover, the conditional probabilities for a great event to occur during the next 10- or 20-year periods increase monotonically with increasing holding time T_R and measure up to about 5 times higher than those for the log-normal distribution. The same applies of course to the annual probability rates.

The basic reason for these differences lies in the fact that the **conditional probability P^* for a fixed small time interval ΔT (into the future) is in the two cases, respectively**

normal distribution: $P^* = (p(z)/(1-P(z)))\Delta T/\sigma$

log-normal distribution: $P^* = (p(z)/(1-P(z)))\Delta T/(T\sigma)$

where

$$p(z) = (2\pi)^{-1/2} e^{-z^2/2}$$

$$P(z) = (2\pi)^{-1/2} \int_{-\infty}^z e^{-\xi^2/2} d\xi$$

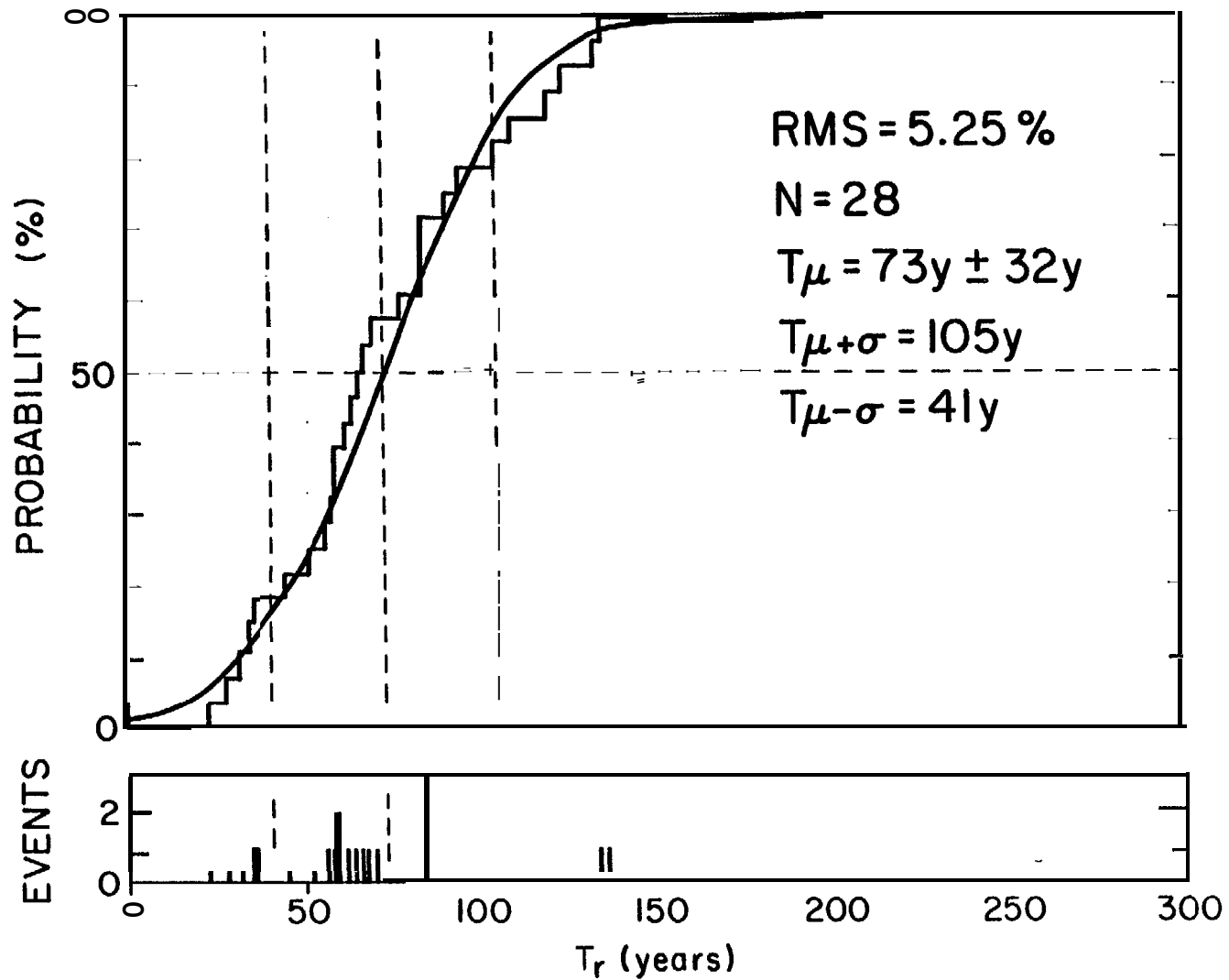


Figure 3.4.10. Same as Figure 3.4.9 except that a normal (rather than a log-normal) distribution (solid line) is fitted to observed recurrence times distribution which consists of a reduced number ($N = 28$) of samples. Note the poorer misfit (RMS = 5.25%) between fitted curve and observations compared to that (RMS = 2.85%) achieved for a log-normal distribution shown in Figure 3.4.9.

TABLE 3.4.11. Cumulative, conditional, and annual probabilities for great earthquakes in 1983, 1993 and 2003, for major Aleutian rupture zones assuming normally distributed recurrence periods ($N = 28$; $T_{\mu \pm \sigma} = 73.5 \pm 32$ years).

Zone	Year of Last Event	Lapsed Time T_R (years) Until 1983	Cumulative Probabilities P(%)			Conditional Probabilities P*(%)		Annual Rate P*(%/Y) 1983-1993
			1983	1993	2003	1983-1993 ($\Delta T_R=10y$)	1983-2003 ($\Delta T_R=20y$)	
Shumagin	1788	195	99.99	99.999	99.9999	~90 .	~99 .	9
Shumagin	1847	136	97.5	98.8	99.5	54.3	80.3	5.4
Kommandorski	1854	129	95.9	98.0	99.1	50.4	77.6	5.0
Unalaska	1878	105	83.8	91.9	94.6	49.7	66.8	5.0
Yakataga	1899	84	62.9	73.9	83.1	29.7	54.4	3.0
1938-rupture	1938	45	18.6	28.2	39.6	11.7	25.7	1.2
1946-rupture	1946	37	12.6	20.4	30.3	8.9	20.3	0.9
1957-rupture	1957	26	6.9	12.1	19.5	5.6	13.6	0.6
1964-rupture	1964	19	4.4	8.1	14.1	4.0	10.1	0.4
1965-rupture	1965	18	4.1	7.7	13.4	3.8	9.6	0.4

σ = standard deviation around mean μ , and T holding time. Note that $z = (T-\mu)/\sigma$ for normal distribution, and $z = (\log T-\mu)/\sigma$ for log-normal distribution.

Thus, with increasing T the values P^* for the log-normal case gradually decrease again, while they monotonically increase for the normal distribution.

The consequences for hazards assessment of these differences in the statistical models are summarized in the pertinent hazards assessment section (Section 4.1).

3.5 Historical Eruptive Activity of **Pavlof**, Akutan, and **Makushin** Volcanoes

In order to better understand their eruption styles, we made a detailed, systematic, and thorough search of all available literature pertaining to historic activity of the 4 volcanoes, **Pavlof**, **Pavlof** Sister, **Akutan**, and **Makushin**¹. Results of the compilation of historic records are shown in Tables 3.5.1-3.5.4. This compilation updates and completes that given in **Simkin** et al. (1981) (our Table 3.5.5). Symbols are standard symbols used in the **Bulletin of Volcanic Eruptions** (see figure caption). We find that **Pavlof** and Akutan volcanoes, with 27 and 28 reported eruptions since 1760, respectively, are two of the most active volcanoes in North America. Figures **3.5.1a,b,c** show the number of years per decade with reported eruptions for **Pavlof**, **Akutan**, and Makushin from 1760 to the present time. **Pavlof** and **Akutan** show more reported eruptions in recent years than in the past, suggesting that the more numerous reports during the past 60 **years** may represent merely better reporting, rather than a real increase in activity. **Makushin**, however, appears to be less active today than it was approximately 150 years ago (Figure **3.5.1c**).

1973-1982 eruptive activity of **Pavlof** Volcano. Based on the study of seismicity associated with volcanic activity at **Pavlof**, we have identified two main eruption styles (**McNutt, 1981a,b; McNutt and Beavan, 1981**) (see also Appendix 7.5). One is a vigorous effusion of lava lasting 1-2 days accompanied by strong volcanic tremor. Significant amounts of ash are often erupted to heights as great as 37,000' during these eruptions, and lava **commonly flows down** the flanks of the volcano to distances of **3-4 km**. The second eruption style consists of numerous small explosions, as many as 13 per hour, which occur during episodes lasting from several days to about 2 months. The explosions are accompanied by B-type earthquakes (shallow

¹**D. Shackelford** and S. **McNutt** completed the **job** of cross-referencing and verifying all reports as originally compiled by S. Hickman at Lamont-Doherty Geological Observatory in 1978-1980.

emergent events lacking a **clear S-phase**), which occur in the highest numbers a few days before the onset of explosive activity (**McNutt and Beavan, 1981**). **Examples** of the **seismicity** accompanying each of these eruption types are shown in Appendix 7.5.

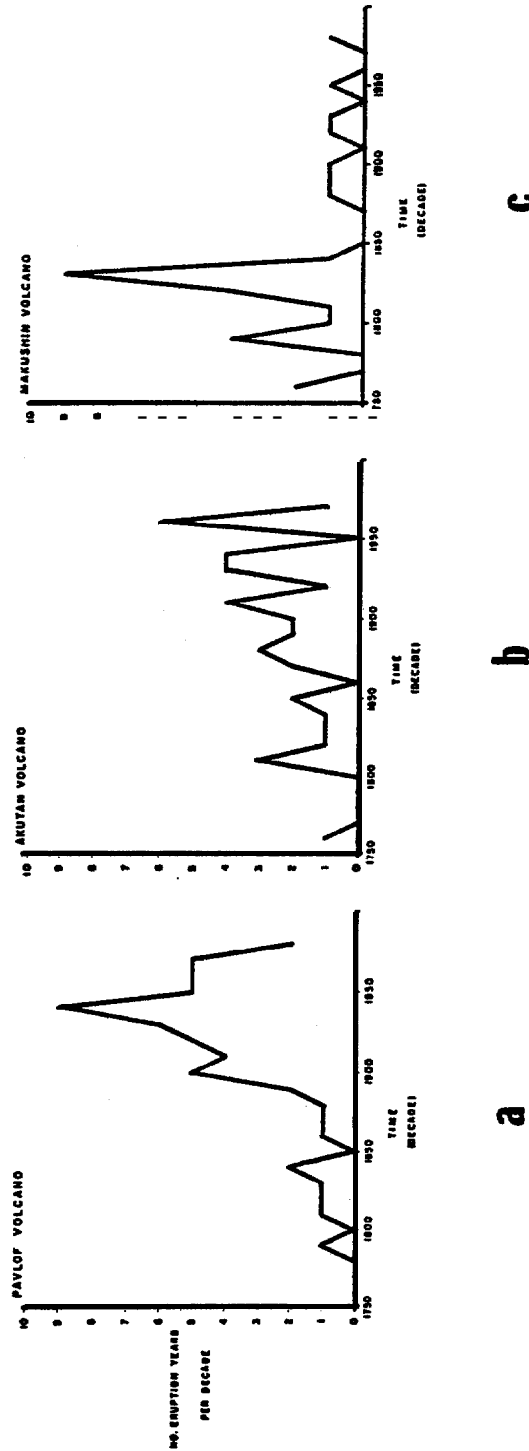


Figure 3.5.1. The number of reported eruptions per decade vs. time. a) Pavlof volcano; b) Akutan volcano; c) Makushin volcano. At Pavlof and Akutan, the apparent increase in activity after 1900 is probably caused by more complete reporting. However, Makushin seems to have had a real increase in activity around 1830.

TABLES 3.5.1-3.5.4. Data from literature search on eruptive activity at Pavlof, Pavlof Sister, Akutan, and Makushin Volcanoes. Compilation by D. Shackelford, S. Hickman, and S. McNutt, 1982, 1980, and 1983, respectively. Symbols used are standard symbols from the Catalogue of Active Volcanoes of the World and the Bulletin of Volcanic Eruptions. Symbols are shown below. (Note: all measurements are given as they appear in the original reports (for example, miles are still miles) to preserve original accuracy.)

CONVENTIONAL SYMBOLS used in the Catalogue and
the Bulletin of Volcanic Eruptions

○	Eruption in the central crater	△	extrusion of a spine
◊	eruption in a parasitic crater	‡	phreatic explosions, mud eruptions
⊙	eruption in a radial fissure	→	mud flows
=	eruption in a regional fissure	↖	subglacial eruptions
↑	normal explosions	↗	submarine eruptions
—	eruptions producing nuées ardentes*	*	islets formed by submarine eruptions
⇒	lava flows	☉	tidal waves (tsunamis)
▽	eruptions in a crater lake	‡	solfatara fields, vapours
◀	eruptions in a lava lake	☒	destruction of arable land
▲	extrusion of a lava dome	t	casualties

(* including ash flow, pumice flow etc.)

TABLE 3.5.1. Pavlof Sister (55.45°X, 161.87°W)

<u>Date</u>	<u>Activity</u>	<u>Additional Information</u>
1762-1786	[0 ?) ↑ (n?)	Eruptive period with strong eruption in 1786. The 1786 eruption accompanied by a strong earthquake (X on Rossi-Forel scale) *. It may be that only 1786 is from Pavlof Sister, the other eruptions may be from Pavlof (identity of active volcano is unclear). Observations in 1928 found fissure or breach on the cone, and there was a summit tholoid. Both features likely formed in 1786, as reports suggest violent activity ("mountain top fell in") .

*A recent investigation by Sykes et al. (1981) showed that a strong earthquake occurred on July 22, 1788, yet no mention is made of a strong quake in 1786. Since X is the highest intensity on the Rossi-Forel scale, we infer that the correct date for both the earthquake and the eruption probably should be 1788.

TABLE 3.S.2. Pavlof (55.42°N, 161.90°W)

Date	Act ivity	Additional Information
1762-1786	↑	With felt earthquake, probably Pavlof Sister (see footnote, TABLE 3.5.1).
1790	↑	
1817	↑	Lapilli falls.
1825	↑?	Eruption of unknown character.
1838	↑.E.↑	Smoking.
1845, 12 August	↑	Powerful eruption of glowing tephra.
1846, August	○ ↑ ⇒	Glowing tephra erupted from vent near summit, ash falling 55 mi. to E (Unga I.) with lava flow down E flank.
1852, early August	↑	Not an eruption, steaming from vent high on N flank.
1866, 14 March	↑	Identity of volcano uncertain. Ashfall on Kodiak I. (?) left ½" of ash during 15 minute period at ca. 0300.
1886	○	Red glares.
1892	01'	"Fire" at night, from summit.
1894	○ ↑	"Fire" at night, from summit.
1901	↑	
1906-1911	○ ○ ↑ ⇒	Continuous minor eruptions from summit from 1906-1911. The most powerful historic eruption of Pavlof took place in December of 1911, most notably 6-7 December. The N flank opened, there was lava flow- age, ejection of large blocks, roarings heard at Unga I. (55 mi. away), and felt earthquakes took place (possibly numerous, too. See 1928).
1914, 06 July	↑	Ash fell on Unge I. between 1430 and 1800. Also, eruptions may have taken place on 15-16 July, but this date is likely to be that of 6 July.
1917, October	↑	Ashfalls, felt earthquake at King Cove.
1922, 24 December-1925	○ ↑	Notable eruptions on 24 December 1922 (glow light up Belkofski vil- lage), in winter 1923, and on 17 January 1924.
1928, 28 June	↑	Observations by Jaggar found the 1911 fissure still present, with two, concentric and small cinder cones at its upper end at the s- mit, with surrounding lava field. Evidence of low-angle blast from the summit crater,
1929, March-1931, summer	○ ↑	Period of minor, continuous ash emissions with increased eruptivity in December 1929 and 30 March and 20 May 1931.
1936-1948	○ ↑ ⇒	Significant eruptions in 1936, July 1937, and 1942. Lava flow may have been extruded in May 1948. Otherwise, minor, nearly continuous ash emissions. Photo taken in 1942 shows 1911 fissure no longer present (the wound had been healed), and a single cinder cone on upper NE flank (moat between this cone and summit, but flanks of cinder cone merged with Pavlof proper elsewhere).
1950, 31 July- 1953, 25 November	of'	Period of intermittent, occasionally strong ash eruptions. Power- ful eruption on 1 August 1959, with glowing tephra rising 1 km. Strong activity in November 1951, in winter of 1951- 1952, and on 25 November 1953 (glow from eruption seen in Pribilof Is.) .
1958, 17 May-28 August	○ ↑ ⇒	Small eruptions of pumice and dust from vent shifting around the upper NNE flank. Lava flow (root less ?) or lava cascades moved down slope on 17 May,
1960, ca. -1963, ca.	○ ↑ ⇒	Mild ash eruptions, especially July 1962-June 1963.
1966, 15 March	○ ↑	Note: during the 1950's and 1960's, the active vent was never exactly located, it shifted around with each eruption high on NE or NNE flank.
1973, 12-13 November	○ ↑ (→?)	Brief, high-amp litude exp 10S ive eruption (lava flow may have occur- red) with harmonic tremor. Possible nuees ardentes down NE flank. Ash fell on Cold Bay, 35 mi. away.

1974, 02 September- 1975, 06 January	○ ↑	Moderate ash eruptions, plume rising to max. 6 km a.s.l. Reports of lava flow may be incorrect. Explosions and intermittent tremor recorded.
1974, 14-24 March -	○ ↑	Period of probable weak ash emissions. Explosion earthquakes recorded.
1975, 13 September- 1977, March	○ ↑ ≈ (≈?)	Period of generally weak ash emissions, often Likened to the chugging of a locomotive. Strong activity 18 September-6 October 1975, 6-12 October 1976, 2-22 November 1976. Both harmonic tremor and explosion earthquakes recorded. Strong explosions, some felt. Short-Lived lava flows in October 1975, in February and December 1976, and none in 1977. Sores may be lahars, or rootless, spatter-fed lava flows.
1979, July	↑ ↑ ↑	Summit venting of light steam plume.
1980, early July	↑	Steaming and possible weak ash emission in early July 1980.
1980, 8-13 November	○ ↑ ≈	Seismic activity began 8 November. Strong eruption from 11-13 November from vent on NE shoulder, lava fountaining 300 m high, plumes to 11 km a.s.l., and lava flow down N flank. Harmonic tremor recorded.
1981, 30 March-28 May	○ ↑	Period of probable weak ash emissions. Explosion earthquakes recorded.
1981, 25-27 September	○ ↑ ≈	Strong eruption, with eruptive plumes to 10.5 km a.s. l., lava flow (from vent 100 m below summit on N flank) to 600 m a.s. l. on NNW flank, and glow visible over some distance. Ce. 1 cm of ash fell at Squaw Harbor (Unga x.) as fine sand. Medium-coarse sand fell on Pavlof Bay. The lava flow may have been rootless and spatter-fed. Both B-type earthquakes and harmonic tremor recorded.

TAME 3.5.3. Akutan (54.13°N, 166.00%)

<u>Date</u>	<u>Activity</u>	<u>Additional Information</u>
1760's	r ?	
1778	Quiet	
1785	Quiet	
1790	☼ or ↑	
1828- 1830	↑ or ☼	
1838	↑ or ☼	
1845	☼ or ↑	
1848, early March	(O?) f'	In the first few days of March, with felt earthquakes.
1852, 01 September	○○↑(≈?)	Eruption from NW flank (Lava Point or Bight) , S.8 km from summit.
1862	☼ or ↑	
1865, 04-05 September	↑	Widespread glow visible.
1867	(O?)↑	
1880	☼	
1883	↑	
1887	↑ ≈	
1892, July-23 September	○ ↑	Explosions audible 30 ml. away. Plumes 1,000' high on 23 September, with felt earthquake.
1894?	○ ↑	This may be the 1892 eruption, or may be active from 1892-1894.
1896	↑	
1907	○ ↑	Year-round explosive activity from the central cone, which appeared to be much lower then present. Felt earthquake on 22 August.
1908, 22 February	↑ ≈	
1911-1912	↑	Ash fell on Akutan village in 1911.
1920's, mid or late	(○○?)↑	Imprecise date of possible eruption on NW flank (Lava Point).
1927-1928	↑	Activity stronger in 1928. Week, felt earthquakes in 1927.
1929, May-December	○ ↑ ≈ ≈	Possible lava flow in May. Lava flow in December through caldera gorge on NW, generating a mudflow. Earthquakes felt.
1931, May-11 August	○ ↑	Intermittent eruptions from the central cone. Central cone described as 600' tall and uniformly hot. Lake on S or SW floor of caldera; hot on side adjacent to cone.
Sometime between 1942 end summer 1944	none	Central cone still hot (or, perhaps, ash-covered).
1946, December-1947, January	○ ↑ ≈	Lava flow in December 1946, and another in January 1947 from SW base of central cone. The 1947 flow was 3/4 mi. x < 1/2 mi. in extent, confined to caldera, and had ended by 4 January.
1947-1953	○ ↑ (≈?)	In August 1948, central cone ca. 700' tall. Eruption plumes 1 mi. high. The August 1948 observations showed two lakes in the caldera, perhaps recent (post- 1931) lava flows had divided the original lake. Lava flow possible in May 1948.
1972, 17 September?-1973, after 22 May	○ ↑	Eruptive plumes to several km in ht.
1974, 11 February	○ or ○ ↑ (≈?)	Eruption observed at 0900Z. Original report of lava flow appears to be in error. Eruption site originally indicated as NW flank, but this is not clear at present.
1976, Fall-1977, May ?	○ ↑	Periodic Vulcanian eruptions, still erupting on 9 May 1977.
1978, Late September-6 October (or beyond)	○ ↑ ≈	Strong explosions lofted large, glowing (car-sized) blocks 100 m over crater. Probable lava flow into caldera gorge.
1980, July	○ ↑ or ↑	Small ash eruptions, plumes 0.5 to 1.0 km in ht.

TABLE 3.S.4. Makushin (53.90°N, 166.93°W)

<u>Date</u>	<u>Activity</u>	<u>Additional Information</u>
1760's	?	
1768-1769	↑	Major explosive eruption.
1778		Not active.
1790, 07 June-1792	↑	Periodic eruptione.
1795	⋈	Off SE coast, identity uncertain.
1802	↑	Major explosive eruption, with great earthquakes.
1816-1817		Quiet.
1818	↑ or ⋈	With felt earthquakes.
1826, June-1838	↑ and ⋈	Strong explosive eruption in June 1826, with two felt earthquakes, then minor activity ("smoking") into 1838.
1844	⋈	Eruption very doubtful.
1845	↑	Eruption from a fissure (site unspecified).
1865	⋈	Eruption very doubtful.
1867	⋈	Eruption doubtful.
1871-1874	⋈	
1880	⋈	
1883	↑	Minor ash eruption.
1891	⋈	
1892	○ ⋈ or ↑	In July, main vent of central cone showed incense, high-pressure steaming, with occasional subterranean explosions.
1894?	⋈	May be 1892.
1895	⋈	
1907	○ ⋈ (↑?)	Observations on 3 July found strong thermal activity on N portion of central cone, and other areas within the caldera. New crater found within caldera ("Technology crater"), apparently between central cone and N rim of caldera.
1912	⋈ or ↑	
1926, 30 December	↑	Eruption of evening of 30 December, with "fire fountains" and slight earthquake.
1931		Quiet, no steaming.
1938, October	↑ or ⋈	Minor explosive eruption.
1944, September	○ ⋈	Strong thermal activity (on N flank?) of central cone, caldera wall, and onto caldera flank.
1951, 20 December	○ ↑ or ⋈	High steam column with ash on snow.
1952	⋈ or ↑	Eruption doubtful.
1953, December	⋈ or ⋈	Steam plumes, eruption very doubtful.
1980	○ ⋈ (↑)	Observations on 8 July found thermal activity on summit of central cone. Also, just below summit on S flank, a new, small explosion crater with tephra and impact pits extending 60 m to SE from vent.

TABLE 3.5.5 Data on eruptive activity of Alaskan and Aleutian volcanoes from Volcanoes of the World, by Simkin et al. (1981). Compare with our Tables 3.5.1-3.5.4.

ERUPTIVE CHARACTERISTICS

C = Central crater eruption	CAVW
E = Excentric (parasitic) crater	⊖
R = Radial fissure eruption	
F = Regional fissure eruption	⊥ (PLACE)
S = Submarine eruption	⋈
I = Island-forming eruption	⋈
G = Subglacial eruption	⋈
C = Crater lake eruption	⋈ (WATER)
E = Explosive (normal explosions)	↑
N = Nuees ardentes, pyroclastic flows	→
P = Phreatic explosions	→
S = Solfataric activity	→
F = Lava flow(s)	→
L = Lava lake eruption	→
D = Dome extrusion	⊥
S = Spine extrusion	⊥
F = Fatalities, casualties	+
D = Destruction of land, property	⊥
M = Mud flows (lahars)	⊥
T = Tsunami (giant sea waves)	⊥ (DAMAGE)

X = recorded - = not recorded
CAVW column shows symbol used in CAVW Catalogs

VOLCANO NAME (SUBREGION)	LAT	LONG	ELEV	TYPE	NUMBER	STATUS	START		STOP		ERUPTIVE CHARACTERISTICS											
							YEAR	M-DY	P	YEAR	M-DY	CERF	SIGC	ENPS	FLDS	FDMT	VEI					
YSEVIDOF (UMNAK I)	SS.13	N 168.88 W	+2149	STRA	1101-27	HISTORIC	1784															
							1790	0830														
							1817											3	?			
							1830															
							1878									X		X	X		2	
							1880															
RECHESCHNOI (UMNAK I)	SS.15	N 168.55 W	+1940	STRA	1101-28	HOLOCENE	1957	0311	1557	0312	X		X	X			2					
							1957															
OKMOX (UMNAK I)	SS.42	M 168.13 W	+1073	STRA	1101-29	HISTORIC	1805															
							1817	0301	1820						X				3			
							1824		1829													
							1830															
							1878									K		K	X		3	
							1899															
							1931	0321	1931	0513												
							1936															
							1938															
							1943	m.										X		X		
SW CORNER OF THE CALDERA	1945	0604	1945	12							X		X	X		2						

3.6 Geology and Geodetic Surveys "

To supplement the seismic monitoring, **L-DGO** scientists have carried out some geologic mapping and geodetic leveling in the **Shumagin** Islands region since 1972. Dr. M. A. Winslow was in charge of the geologic mapping that mainly consisted of determining Holocene uplift rates **by** surveying, sampling, and dating uplifted marine terraces. Dr. J. Beavan **was** in charge of annual resurveying and expanding the geodetic leveling network up to 9 lines that are located on different islands. The purpose of maintaining the leveling lines is to determine the **pre-, co-** and postseismic deformation resulting from the forecast great earthquake.

Winslow (1982) presents the results of the geologic surveys and below we have included a summary of the main results.

Holocene uplift. The results on the ages and elevations of marine terraces indicate that the Alaska Peninsula and Inner **Shumagin** Islands have been uplifting tectonically **at an average** rate of about 7 mm/year over the past 10,000 years. The Outer **Shumagins** show a more complex history, possibly involving tectonic subsidence as well as uplift. None of the identified uplifted surfaces could be identified as being the result of one specific earthquake. The presence of large depositional or wave cut surfaces represent relatively long periods of stability near sealevel which were followed by sudden uplift of a sufficient magnitude to raise these features above the inter-tidal zone. Although we were unable to establish recurrence intervals between individual events, the presence of terrace levels **can** be explained only by sudden emergence due to major earthquakes. Thus, the 7 **mm/yr** average uplift rate is the slope of a curve which is actually episodic.

Recent faulting. A critical appraisal of aerial photography **was** done between the 1979 and 1980 field seasons. Two faults on which we suspect Holocene motion have been bracketed with benchmarks in case they are reactivated by a major earthquake. One fault intersects the Korovin level line, and the other is a high angle fault which separates Popof Head from the remainder of Popof Island. Several **other** recent faults were noted in the area including ones on northwest

Korovin and southeast **Unga**, and at Zachary Bay, Squaw Harbor (**Unga**) and Cape Aliaksin (peninsula). Holocene displacements are recognized by abrupt offsets in terrace heights, fault **scarps** intersecting till, or by development of fault **scarps** in soft sediment with **linear** trends of several kilometers. All of these faults are high angle faults striking **NNW-SSE** or NE-SW. The displacement history is presently unknown on all of these faults. Due to the ratio of water to land and the linear nature of several coasts, it is **likely** that **major faults** lie between islands. In fact, the linear segments of some coasts defined by **seacliffs** of rock and sediment and the lack of a wide shelf all suggest fault control, especially those areas where streams intersect the coast as waterfalls.

The levelling network that is described by **Beavan** et al. (1983) presently consists of nine short **level lines** which are measured, annually if possible, to first order standards. The lines vary in length between 600 and 1200 m. Their locations and azimuths are shown in Figure 3.6.1. Line **L1** at SQH was established in 1972, line **L2** at SPA in 1977 and the others since then. Figure 3.6.2 shows the results from all the lines which have been measured more than once.

The two dots plotted for each year represent the results of the forward and backward runs of **levelling**. The error bars are standard deviations ($\pm 1\sigma$) calculated from the scatter of several readings of each stadia rod from each tripod position. When the error bars from forward and backward runs overlap we can be more confident that no systematic error or blunder has occurred during the run.

The clearest feature of the SQH data is the trend between 1972 and 1978 which corresponds to tilting downwards towards the trench of $0.9 \pm 0.3 \mu\text{rad}/\text{yr}^{-1}$. It is followed by a tilt reversal of $2.2 \pm 1.0 \mu\text{rad}/\text{yr}^{-1}$ between 1978 and 1980. The agreement from 1978 to 1982 between SQH and SPA lines, which are separated by about 10 km, adds credence to the signal measured by the SQH line. Of the other lines, **SMP** has been measured most often. It shows no tilt significant at the **95%** confidence level, but does show the same general shape of tilt up towards the trench between 1978 and 1980, and tilt down towards the trench between 1980 and 1982. The differences between the SMP and SQH/SPA lines are not surprising in view of the fact that **SMP** is in a

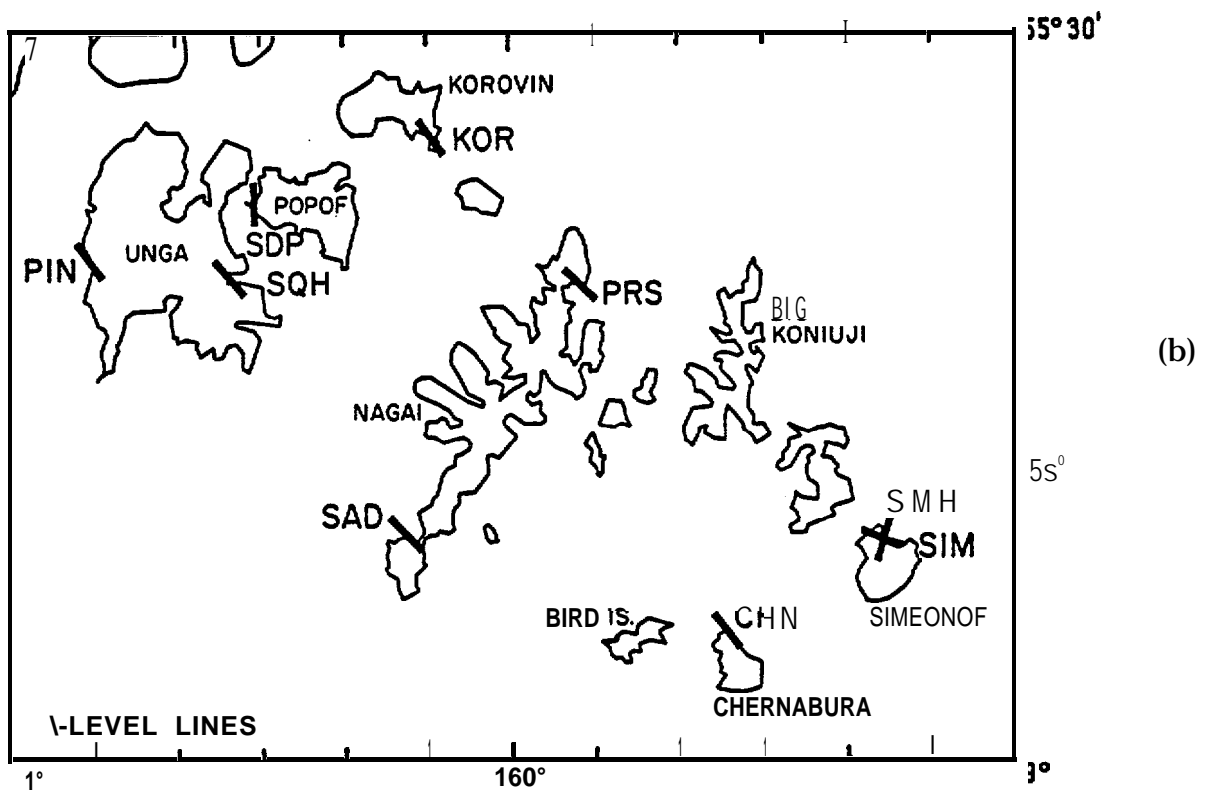
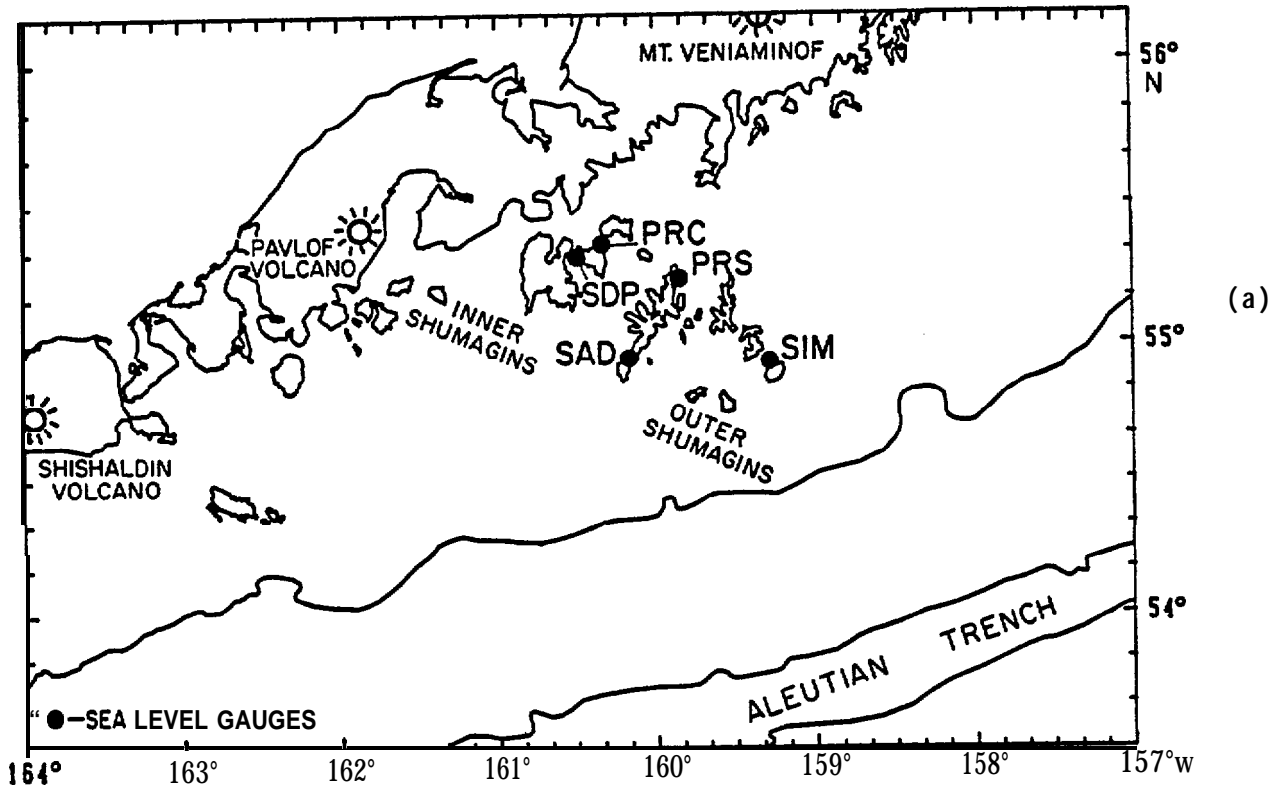


Figure 3.6.1. Maps showing level lines and tide gauges in the Shumagin Islands. The directions of the level lines are indicated by the dark lines. Their lengths vary from 600 to 1200 m.

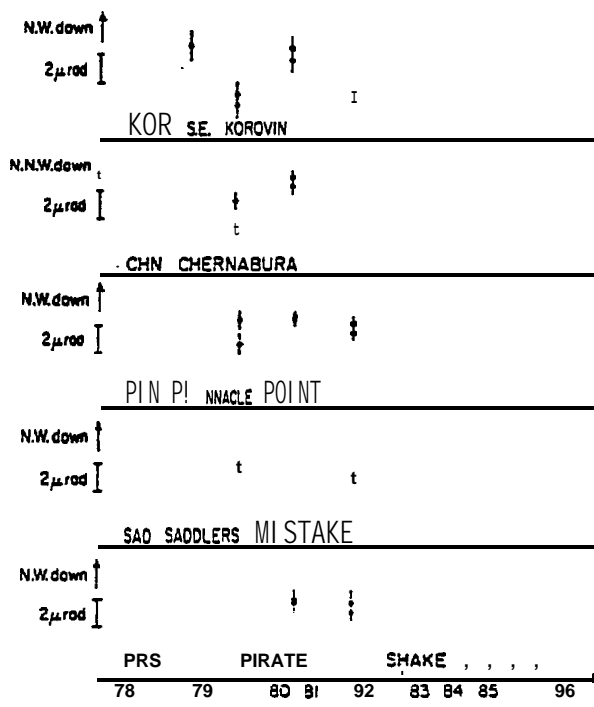
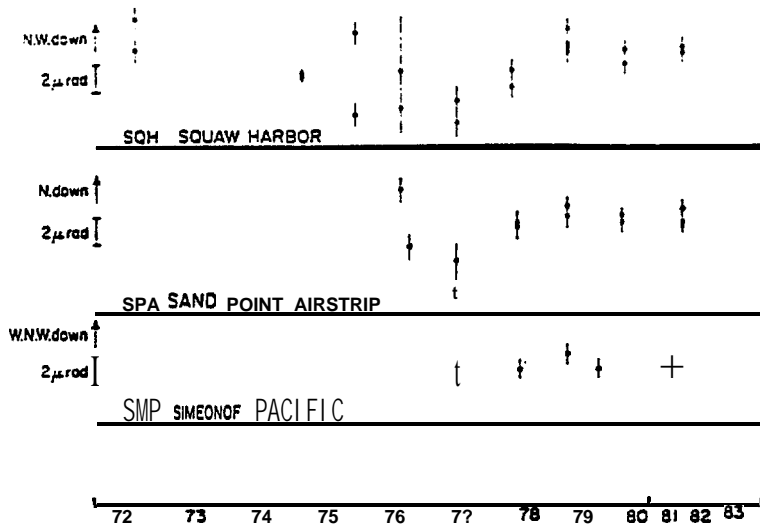


Fig. 3.6.2. Data from those level lines in the Shumagins that have been levelled at least twice. The two dots each year represent forward and backward runs of levelling. The error bars are ± 1 standard deviation based on variations in multiple readings of each station rod from each tripod position. Note particularly the $0.9 \pm 0.3 \mu\text{rad}/\text{year}$ down towards the Aleutian trench between 1972 and 1978 on line L1 (SQH). The tilt apparently reverses ($2.2 \pm 1.0 \mu\text{rad}/\text{year}$) between 1978 and 1980. The L1 data are corroborated by those from line L2 which is about 10 km away. L3, which is much closer to the trench, shows a similar pattern though with tilt rates of different magnitudes. All the other NW-SE oriented lines show a tilt down towards the trench between 1981 and 1982.

quite different part of the arc-trench gap, some 80 km distant from SQH. Winslow (1982) suspects that the two sites are on different **crustal** blocks. The remaining **lines** show less consistency of signal, but there is a general trend down towards the trench between **1981** and 1982. The 1979 KOR value is open to question because the line was not reversed. The other lines show a tendency to peak **in** 1981, as opposed **to** the **1980** peak shown by SQH, SPA and **SMP**. The two lines (**SMH** and a component of PRS) which measure tilt along the trench axis show no significant tilt between 1981, when they were installed, and 1982.

We note that the tilt down toward the trench observed between **1972** and 1978 is of the correct sense to be interpretable as due to loading of the overlying plate by subduction at depth. Conversely the tilt downwards away from the trench between 1978 and 1980 might be interpretable as due to aseismic slip relieving part of the accumulated stress on the Benioff zone beneath the islands.

3.7 Seismicity Recorded by the **Unalaska** Array 1980-1982

Since 1975 Lament-Doherty Geological Observatory has operated a small seismic array on **Unalaska** Island in the eastern Aleutian Islands, Alaska (see Figure 3.7.1). The purpose of operating this array *was to* monitor the seismic activity of **Makushin** Volcano and Akutan Volcano as well as to monitor the regional **seismicity**. Unfortunately, there were never enough funds available to analyze the data collected by this array.

Only an approximate daily event count has been carried out to compare the **level** of activity with that recorded by the **Shumagin** network (see Figures 3.7.2 and 3.7.3). These event counts are based on daily records from two **helicorders** that recorded a short period seismometer and an intermediate period seismometer located at the central recording site. The short period seismometer was usually a remote seismic station such as **MAK**, SDK or USR (see Figure 3.7.1). The event counts are somewhat discontinuous since the station operator rarely was able to repair minor equipment failures, which resulted in long gaps in the data. Nonetheless, the **event** counts indicate an average level of activity consisting of approximately 30 events per month with S-P time less than 5 seconds and approximately 60-90 events per month with S-P time between 5 and 50 seconds. This level of activity is considerably higher than the level of activity recorded by the **Shumagin** network. Although **it** is not possible to explain this difference without actually locating the earthquakes, one could speculate that some of this activity consists of aftershocks of the 1957 Andreanof-Fox Islands earthquake. It had a magnitude $M_w \approx 9.0$ and ruptured a 1200 **km** long segment of the plate boundary to the east of **Unalaska** (House et al., 1981). Some of the earthquake data were also recorded on analog magnetic tapes that will be analyzed in the near future.

In conclusion, the number of earthquakes recorded by the **Unalaska** array indicates that the level of seismicity is considerably higher in the **Unalaska** region than the level in the Shumagin seismic gap. Significant microearthquake activity with S-P time less than 5 seconds (or with **epicentral distance less than 40 km**) is observed by seismic stations located on **Unalaska** Island.

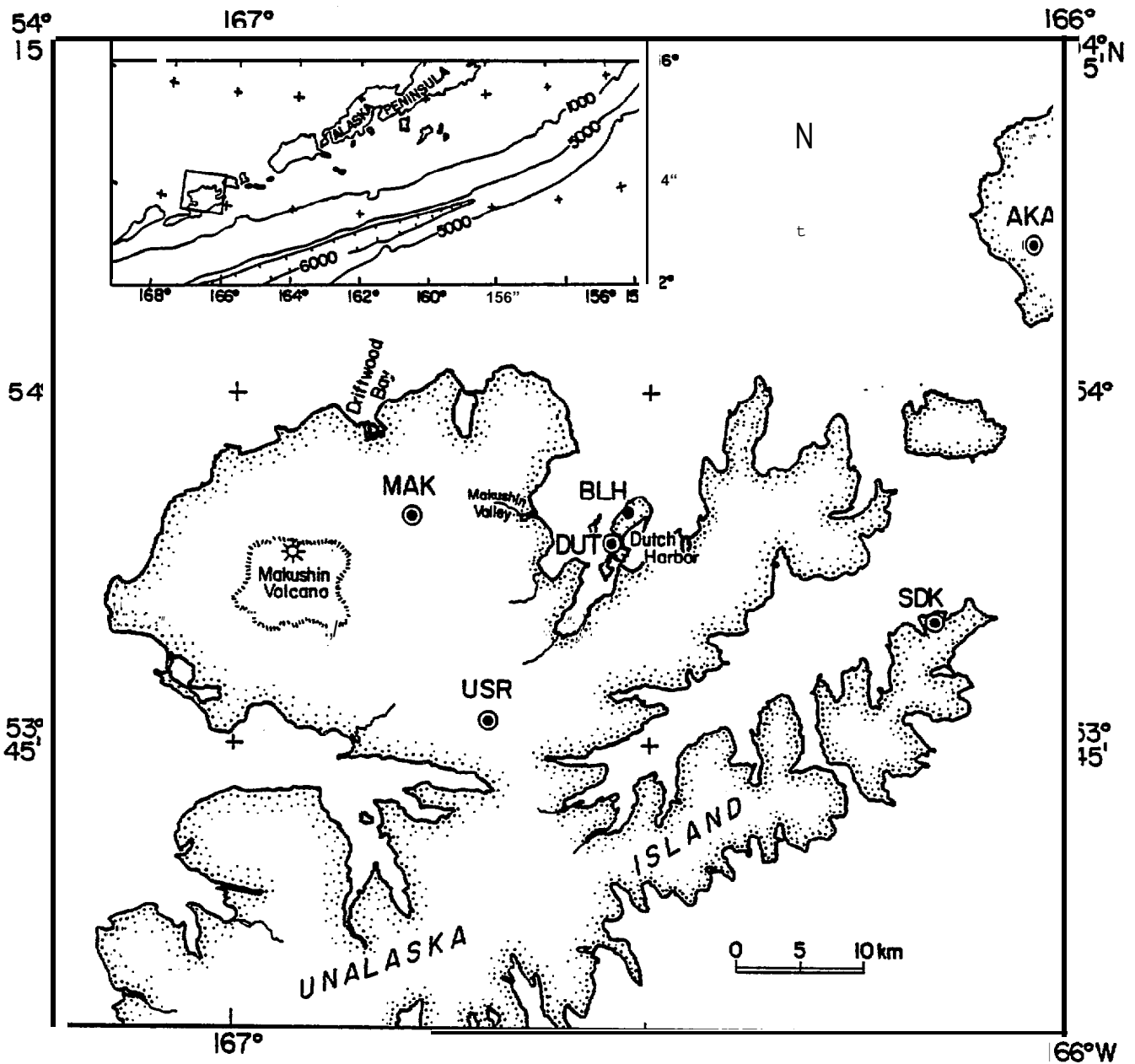


Figure 3.7.1. Dutch Harbor Array, Eastern Aleutians, operated by Lamont-Doherty Geological Observatory. -The array consist of four remote stations, MAK, USR, SDK, and AKA with short-period, vertical seismometers. At the central recording station, DUT, a set of two horizontal and one vertical seismometers are operated in addition to an independent strong motion **accelerograph (SMA-G1)**. The BLH is a repeater station for signals that are telemetered from the remote stations and recorded at the central station.

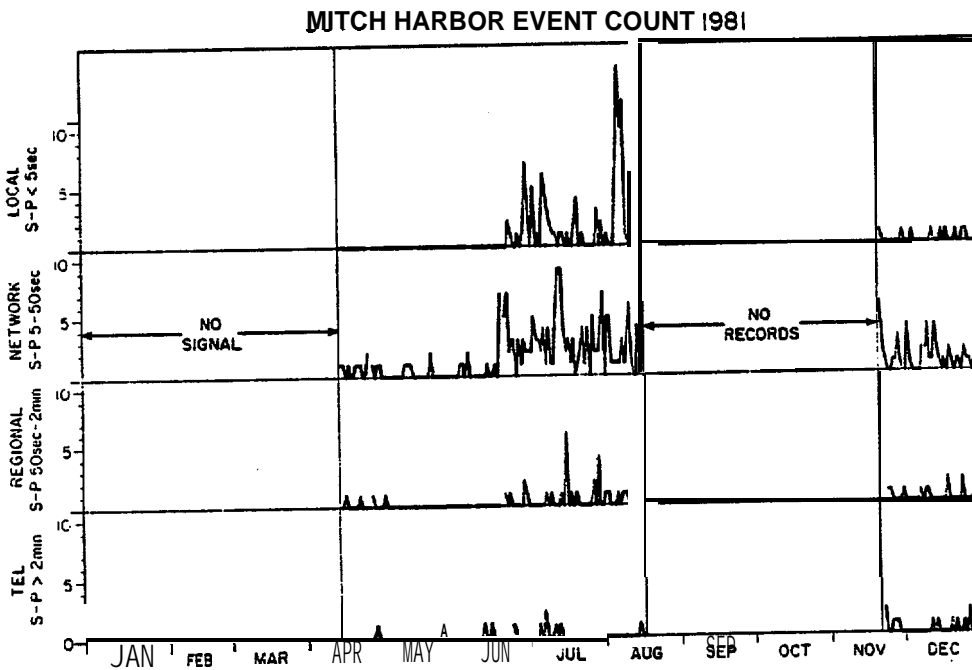
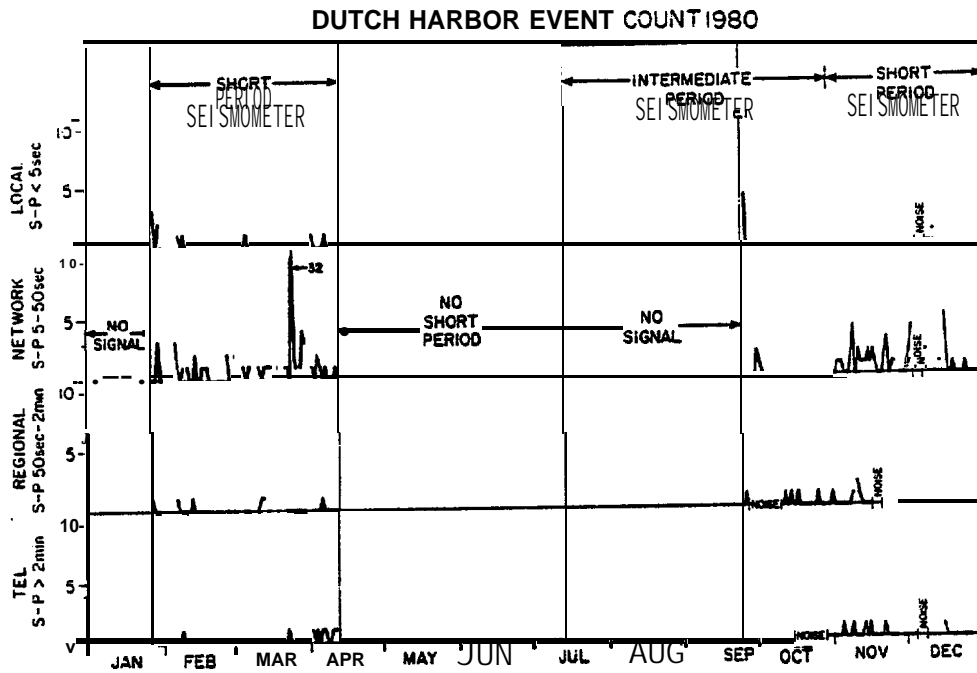


Figure 3.7.2. Number of earthquakes recorded per day by the Dutch Harbor Array in 1980 and 1981. The data are grouped according to S-P travel time.

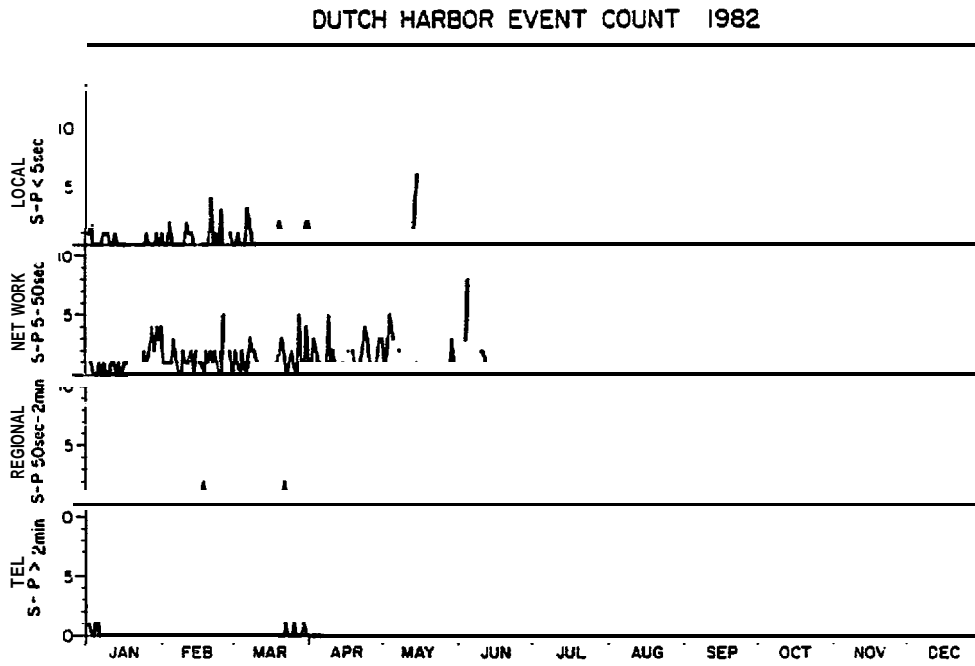


Figure 7.3. Number of earthquakes recorded per day by the Dutch Harbor Array in 1982.

3.8. Tsunami Data

Since Cox and Pararas-Carayannis (1976) compiled tsunami data for Alaska, some revisions and additions to this data set (mostly for the historic period prior to 1898) have been **made** by Davies et al. (1981), Sykes et al. (1980, 1981), McCann et al. (1980), and by House et al. (1981) specifically for the great 1957 event ($M_w = 9.0$).

A thorough analysis of all tsunami data for Alaska is still outstanding. The present report does not alleviate this problem. We merely reproduce here a figure (Figure 3.8.1) taken from Davies et al. (1981) that **is** based on an assessment of the **Sanak-Kodiak** tsunami(s) of 1788 by **Soloviev** (1968). That interpretation may be representative for the kind of tsunami run-up heights that could be expected from a great earthquake rupturing the **Shumagin** Gap, and perhaps portions of the 1938-rupture zone. Figure 3.8.1 shows that tsunami-run up heights may have been as high as 30 m on particularly exposed, southeasterly-facing shorelines and inlets of the islands on the outer shelf platform, while the **inlying** SE-facing shorelines of the Alaska Peninsula may have received run up heights of only about 5 meters, although data for the latter are poorly documented. In specific cases tsunami heights on **inlying**, south-facing shorelines may be much higher as has been dramatically shown by the 1946-tsunami that completely destroyed the Scotch-Cap lighthouse on **Unimak** Island. The base of the lighthouse was about 10 meters above sealevel, yet tsunami run-up heights may have exceeded 30 meters for this **unusually tsunamigenic** event ($M_T = 9.3$, Abe (1979)).

Generally tsunami heights on north-facing shorelines and inlets of the Alaska Peninsula and of major islands of the Aleutian chain are substantially smaller for Aleutian subduction-zone events, and rarely seem to exceed 1 m in height. The effects of seiches, however, (standing wave patterns in contained bodies of waters, narrow bays and inlets) should not be neglected since they can produce locally higher waves, particularly **as a** secondary effect from landslides or volcanic eruptions. In such cases debris may reach bodies of water and partially displace them as transient waves.

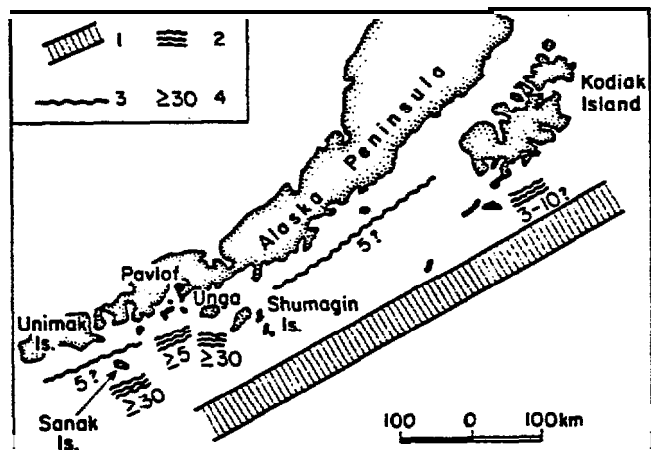


Figure 3.8.1. Diagram (after Davies et al. , 1981) showing tsunami run-up heights (in meters) and inferred earthquake source region of the 1788 event(s) as determined by Soloviev (1968). The symbols in the legend **imply:** 1) hypothetical location of rupture zone, 2) positive known places of appearance of tsunami, 3) probable places of appearance of tsunami , and 4) approximate height of tsunami in meters.

One particular event affecting the Bering Sea side of **Unalaska** Island is of special interest. We do not have a detailed description of the tsunami of 1878 that apparently destroyed the **Aleut** settlement in Makushin Bay on **Unalaska** Island. We assume, however, that run up heights must have exceeded here 5 m, or more, despite the fact that portions of **Unalaska** shelter the **Makushin** Bay from a direct southerly exposure. The Bay is located on a northwesterly promontory on the Bering Sea side of **Unalaska** Island; the bay itself faces, *however*, west to southwest. It is conceivable that the causative earthquake for this tsunami was located on the Bering-Sea side of the arc rather than on the Pacific side, and may have been induced volcanically. Therefore it is of special interest. It suggests that occasionally the Bering *Sea* side may be also exposed to **tsunamigenic** events. This example shows that minimum heights above sealevel exceeding 10 m or more should be required for the base of all critical installations on shores facing the Bering Sea, and probably 30 m or more on shores facing the Pacific ocean. Higher elevations should be sought if technically feasible.

4.1 Seismic Hazards

Finite seismic hazards do clearly exist for any future offshore, nearshore, and onshore structures that would be associated with successful exploration and development of oil or gas resources in the three lease-sale planning areas presently known as the "St. George Basin", the "North Aleutian Basin", both located on the Bering Sea side, and the "**Shumagin** Basin" located on the Pacific side of the Aleutian arc.

We have undertaken a preliminary quantification of the hazard contribution in the St. George Basin that originates from the moderately active local seismic sources on the Bering Sea Shelf itself that lie directly within the region of the **St.** George Basin (Appendix **7.6**). We find from considering the local earthquake sources alone, i.e., excluding contributions from great subduction zone earthquakes near the Aleutian trench, that the probabilities for peak accelerations to exceed 0.2 and 0.5 g (**1g** = earth's gravitational acceleration) measure about 10 and 2 1/2 percent, respectively, during any 40-year period of interest. These probability values should be taken as only preliminary since the acceleration-vs.-distance curves (attenuation laws) that were used are only poorly constrained and the seismic record is very short and probably incomplete. Moreover, these probabilities do not reflect contributions from great Aleutian thrust zone earthquakes to be discussed next.

At this time, and because of absence of sufficient strong motion data in subduction zones in general and from great earthquakes in particular, we cannot determine with sufficient certainty the probabilities of exceedence of certain levels of **groundmotion** that will be associated with great earthquakes that occur on the main thrust zone of the Aleutian arc.

Therefore we have limited ourselves to calculating the conditional probabilities for great earthquakes ($M_w > 7.8$) that can be expected to occur in the various segments of the Aleutian arc (including several Aleutian seismic gaps). These probabilities are

shown in Figure 4. 1.1 for periods of the next one and two decades. The most important **result** of this calculation is that probabilities in the Shumagin seismic gap could be as high as **≈90%** for the 10-year period 1983-1993, and **≈99%** for the 10-year period 1983-2003. If a 40-year period is envisioned as the likely time of interest for oil exploration in the St. George, North Aleutian, and **Shumagin Basin lease** planning areas, it **should** be considered virtually **a certainty** that in their vicinity a great earthquake will occur either individually **in the Shumagin Gap (near 160°W)**, the **Unalaska Gap (≈164°W)**, the 1983-rupture zone (**≈156°W**), or at all of them.

We point out that the probabilities quoted above are those for normally distributed recurrence times and if log-normal distribution of recurrence times applies (see chapter 3.4), than the lower values (shown in solid shading of Figure 4.1.1) would apply.

Which levels and durations of groundmotions would be caused in the three lease-sale planning regions by **great** earthquakes is at present highly uncertain since strong motion data from any great subduction zone earthquake ($M_w > 7.8$) have never been recorded (see chapter 3.3); moreover, the few strong motion data points for the Alaska subduction-zone environment that have been collected for moderate-sized events (chapter 3.3) have been mostly analyzed only with regard to uncorrected (for instrument response) peak acceleration. Since many tall off-shore platform structures and near-shore oil storage and tanker facilities have their natural modes of response at longer periods (1-10 see) than those (**≈0.1 see**) that determine peak accelerations, the most important (i.e., dangerous) aspects of **groundmotions** from great earthquakes to tall structures at or near subduction-zone environments remains poorly researched and therefore cannot be adequately accounted for in the designs. Until this gap in knowledge (and ground motion data) is filled, no accurate, or at least economic, risk assessment to Alaska-Aleutian offshore structures can be made. The consequence is either costly overdesign of engineering structures or, alternatively, a high risk of loss.

In short, a quantitative seismic hazards assessment in the Alaska-Aleutian setting at or near the subduction zone has progressed to date only to the state of a rather complete and quantitative

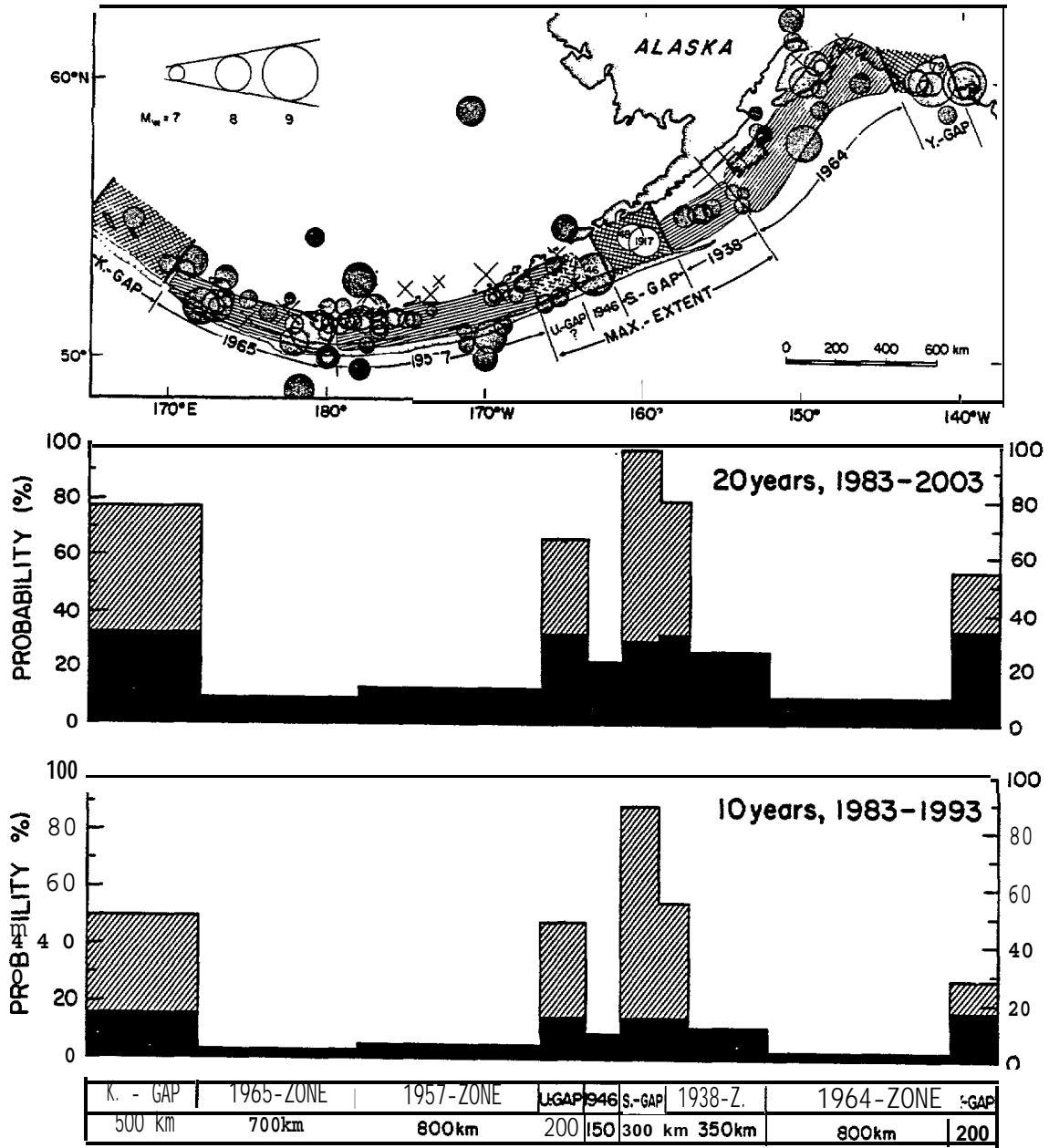


Figure 4.1.1. **Top:** Map view of arc with instrumental seismicity ($M_w > 7.0$) since 1898, **Center:** Conditional probabilities for the occurrence of a great earthquake to occur in each arc segment during the 20-year period 1983 to 2003. Probabilities computed for normal distribution of recurrence times are in diagonal hatching, and for log-normal distribution in solid shading. **Bottom:** Same as center but for 10-year period 1983-1993. Box segments on bottom label the arc-segments and their approximate lengths in km.

seismic source definition. Until actual groundmotion measurements become available the hazards assessment cannot be carried beyond this initial stage except by using very tenuous extrapolations of **groundmotion** attenuation and scaling laws (see chapter 3.3) mostly from other tectonic settings which are unproven for the Aleutian tectonic setting and therefore may or may not apply. The future collection of strong motion data in Alaska from large and great Alaska-Aleutian subduction zone earthquakes emerges as the single most important conclusion from this (negative) assessment.

The early termination of the seismologic components of the NOAA-OCSEAP program severely jeopardizes two such existing efforts to collect the necessary strong motion data (i.e., by Lament-Doherty in the Shumagin seismic gap, and by the **U.S.G.S.** in the Yakataga seismic gap). No fully funded substitute programs have yet emerged to date.

Besides the direct seismic hazards associated with groundshaking, indirect seismic effects from soil liquefaction, ice-, rock- and mud-slides, **crustal** deformation (coastal changes), faulting and tsunamis can be severe and must be accounted for. Effects from changes of coastlines due to **crustal** deformation and of tsunami can be minimized if coastal structures on the Pacific-facing shorelines have their foundations at elevations not below 30 meters above **sealevel** (high tide), and on the Bering Sea facing shorelines not below 10 meters above **sealevel**.

If protective bays, inlets and other narrow bodies of waters at steep coastlines are considered for engineering facilities, site specific studies should be carried out to assess their potential for seiches or surges related to earthquake-induced rock-falls, or to sudden discharges of large volumes of mud, ice, volcanic debris or lakes into such constrained inlets or bodies of water (e.g., surge in Lituya Bay SE-Alaska during 1958 earthquake).

SEABEAM, SEAMARK, bathymetric precision profiler, and single- or multichannel reflection surveys are either still required, or existing ones need to be specifically analyzed for near-surface faulting of the ocean floor, if pipeline routes on the ocean floor will be contemplated at a later stage of development. The near-surface **seismicity patterns** obtained from the **local** and regional seismic

network data and reported for the Shumagin segment in chapters 3.1 and 3.2 (e.g., Figure 3.1.8) can be an important guide where such faulting may be expected to be presently active.

4.2 Volcanic Hazards

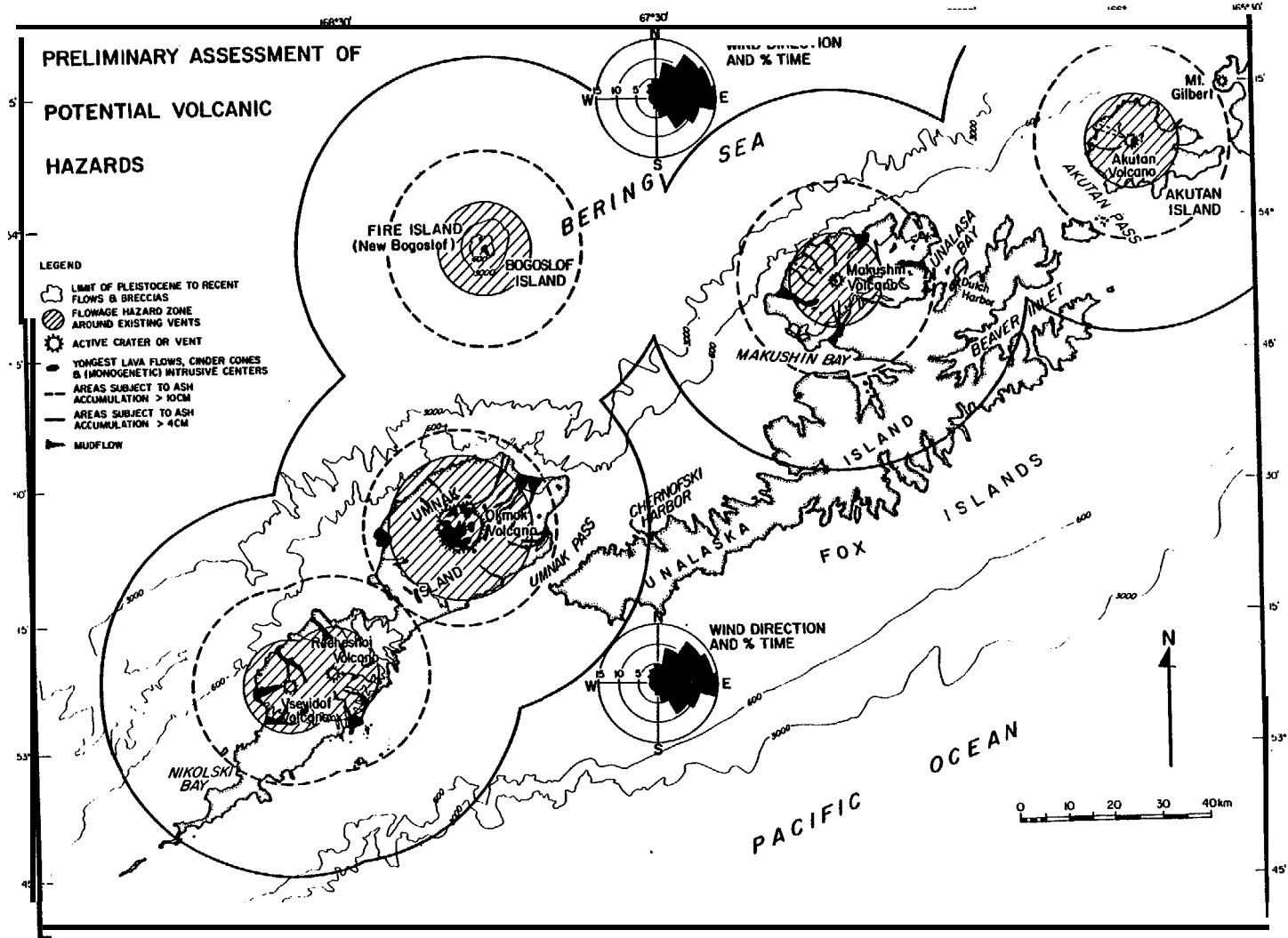
Introduction

Over 74 active volcanoes are located **in** the Aleutian Islands/Alaska Peninsula region (**Simkin** et al., 1981). Of these, ten or more are located in the immediate study areas, including **Pavlof**, **Pavlof** Sister, Akutan, and Makushin volcanoes. Their locations are shown **in** Figures 4.2.1 and 4.2.2. All of these volcanoes are typical andesitic island arc volcanoes.

We have assessed volcanic hazards **in** two ways: 1) temporally, that is the rate of occurrence of eruptions; and 2) spatially, by delineating the areas of greatest hazard near each volcano. For temporal estimates of eruption rate, we have examined: 1) long-term rates of recurrence as recorded by deep sea ash layers (0-2.8 million **years** B.P.); 2) intermediate-term eruption rates as recorded by ash layers found in marine terrace deposits (0-10,000 **years** B.P.); 3) literature search of historic records of eruptions (1760-1982); and 4) documentation of eruptions of **Pavlof** Volcano from 1973 to the present time based on results of studies of **seismicity** associated with recent eruptive activity (**McNutt** and **Beavan**, 1981; **McNutt**, 1981a,b; **McNutt**, 1982a,b; **McNutt** and **Mori**, 1982). (Items (3) and (4) above are described in detail earlier in this report.) Spatial zones of greatest hazards are shown in maps (Figures 4.2.1-4.2.2). Delineation of hazard zones is based on study of mapped deposits and eruptions of volcanoes in Alaska **and** elsewhere. Of special interest is the identification of possible volcanic hazards zones in the **Kupreanof** area, based largely on results of the seismic monitoring efforts in addition to field observations.

Temporal Hazards Assessment

Long-term eruptions rates. Volcanic ash layers from cores recovered south of the Aleutians and the seaward extent of these ashes **are** shown in Figure 4.2.3. At least 20 large andesitic eruptions have occurred since 1.8 million years **B.P.** (**Hays** and **Ninkovich**, 1970).



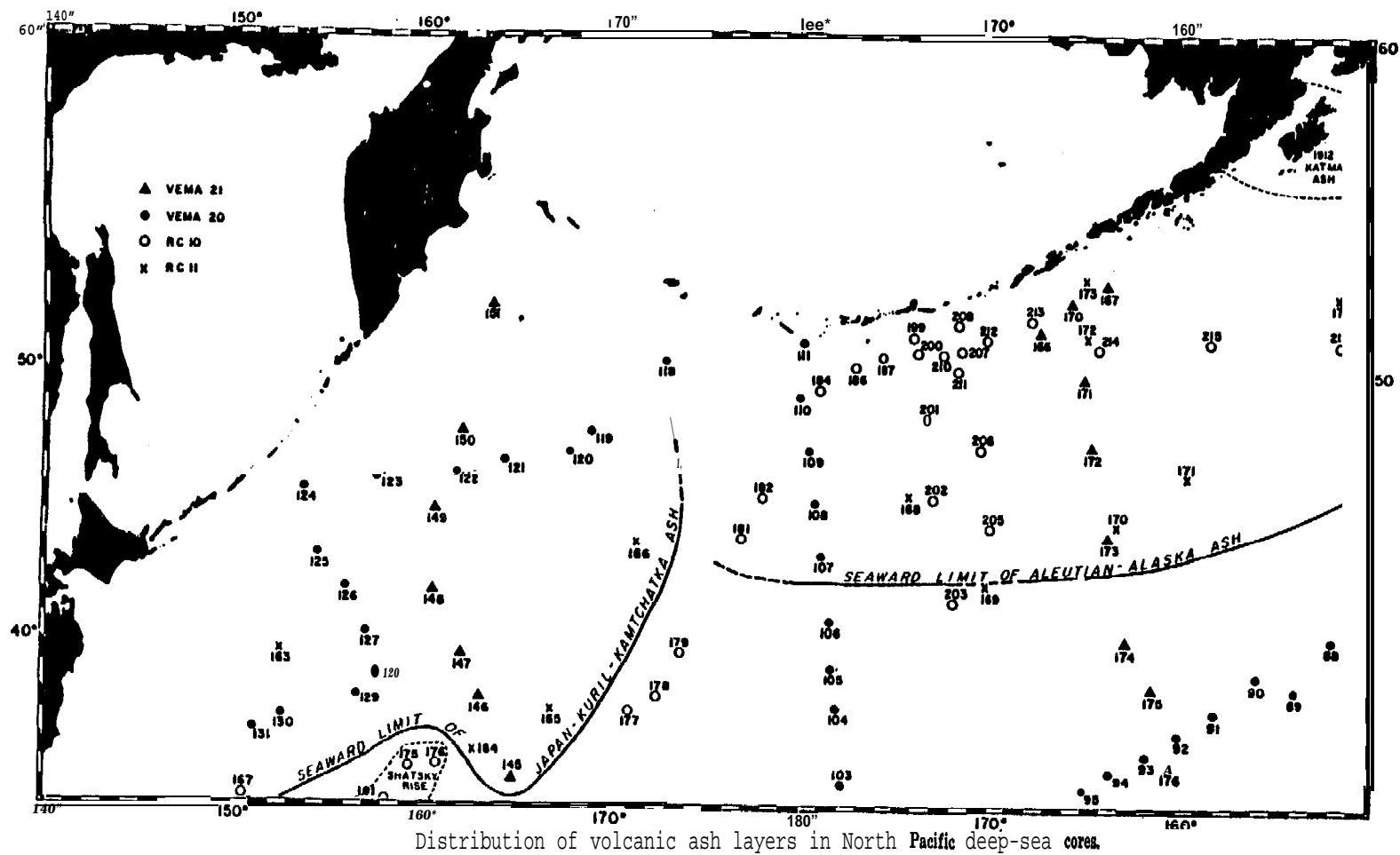


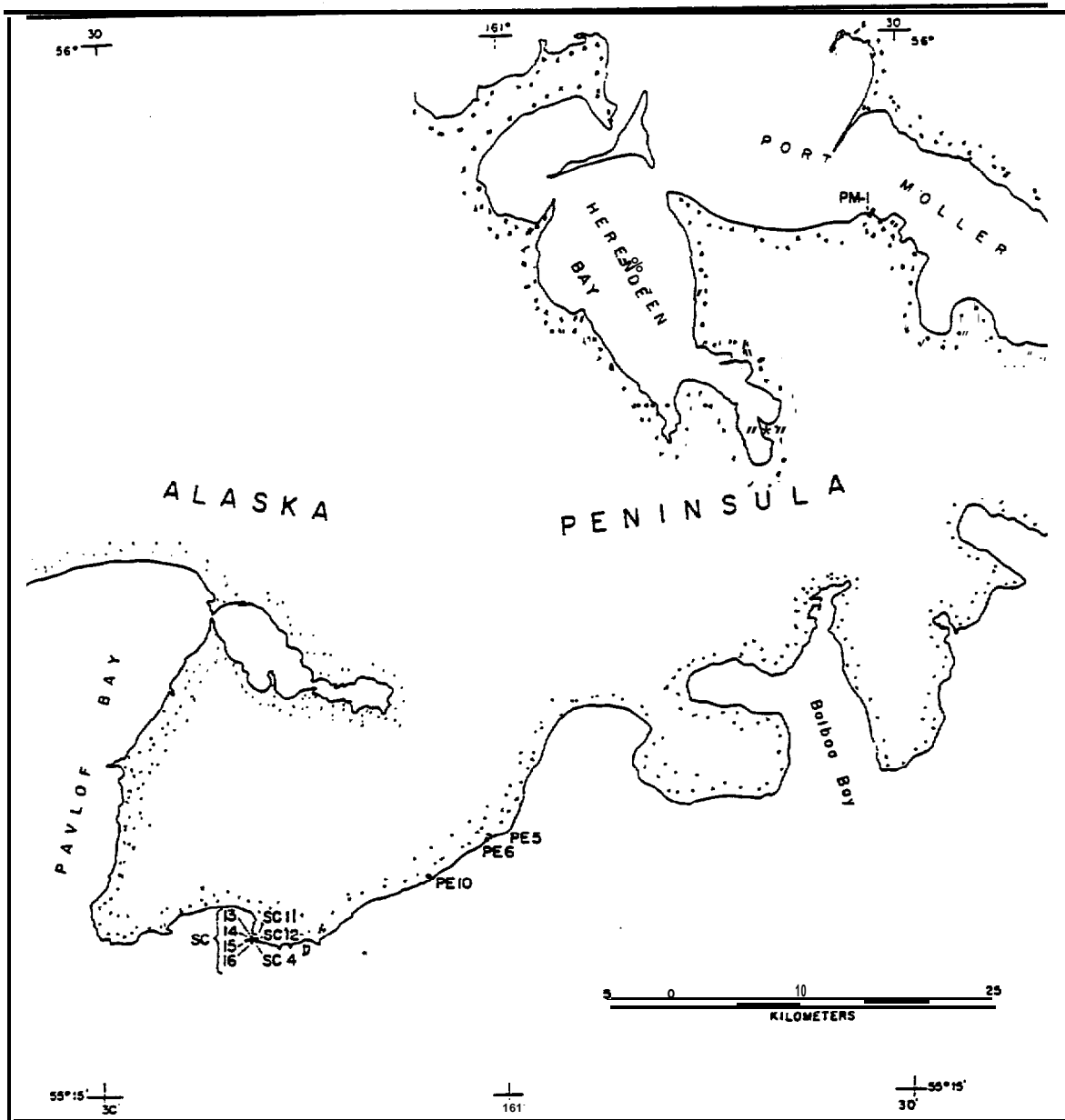
Figure 4.2.3. (Source - Hays and Ninkovich, 1970).

However, cores dating from 1.8 to 2.8 million years **B.P.** in this area contain no ashes, suggesting that the lower Pleistocene (1.8 my. B.P.) was the beginning of the present cycle of volcanism. Dorm and Ninkovich (1980) report rates of explosive Cenozoic volcanism in the North Atlantic varying between 3 and 65 eruptions per million years. Based on the northern Pacific data, we estimate that for the entire Aleutian arc an explosive eruption large enough to produce sufficient ash to form a deep-sea ash layer will occur on the average every 90,000 years during the present cycle of activity. Unfortunately the eruptions which deposited the ash layers cannot be attributed to any specific volcano.

Intermediate term eruption rates. Cores were taken in marine terraces in the Shumagin Islands region during the summer of 1980 by M. Winslow, T. Ray, and C. Heusser (personal communication, 1982). Figures **4.2.4a,b** are maps showing locations of cores. Peat **layers** contained in the cores were dated by the Carbon 14 method, and yield a maximum **age** of 9540 ± 260 years for the oldest and deepest dated layer.

Preliminary study of ash distribution in the cores shows some spatial and/or temporal variation; 2 typical cores are shown in Figures **4.2.5a,b**. Based on study of these cores (Table 4.2.1) we **estimate** the likelihood of an eruption large enough to deposit 1 cm of compacted ash or more in the **Shumagin** Islands region to be approximately once every 1,900 years. Again, these eruptions cannot be ascribed to any specific volcano in the study area.

Temporal hazards summary. The information from deep sea cores, marine terrace cores, and records of historic eruptive activity have been compiled and plotted on a magnitude vs. frequency of occurrence plot (Figure 4.2.6). The plot shows the \log_{10} of the number of eruptions of a given size per 100 years per volcano versus the \log_{10} of the volume of erupted material. In preparing this plot, we made several assumptions. First, we assumed that each of the 74 active volcanic centers could have been, a source for the 20 large eruptions producing deep sea ash cores. We then normalized the result to the



(a)

Figures 4.2.4 a,b. Sample locality maps in Shumagin Islands and adjacent peninsula. Inner Shumagins include Unga, Popof, Korovin, Andronica, Karpa and Henderson Islands. Outer Shumagins include Nagai, Big and Little Koniuji and the islands between them. Simeonof, Chernabura, and Bird Islands are considered to be separate from the Outer Shumagins in this paper. (Source - M. Winslow, written communication, 1982 (used with permission)).

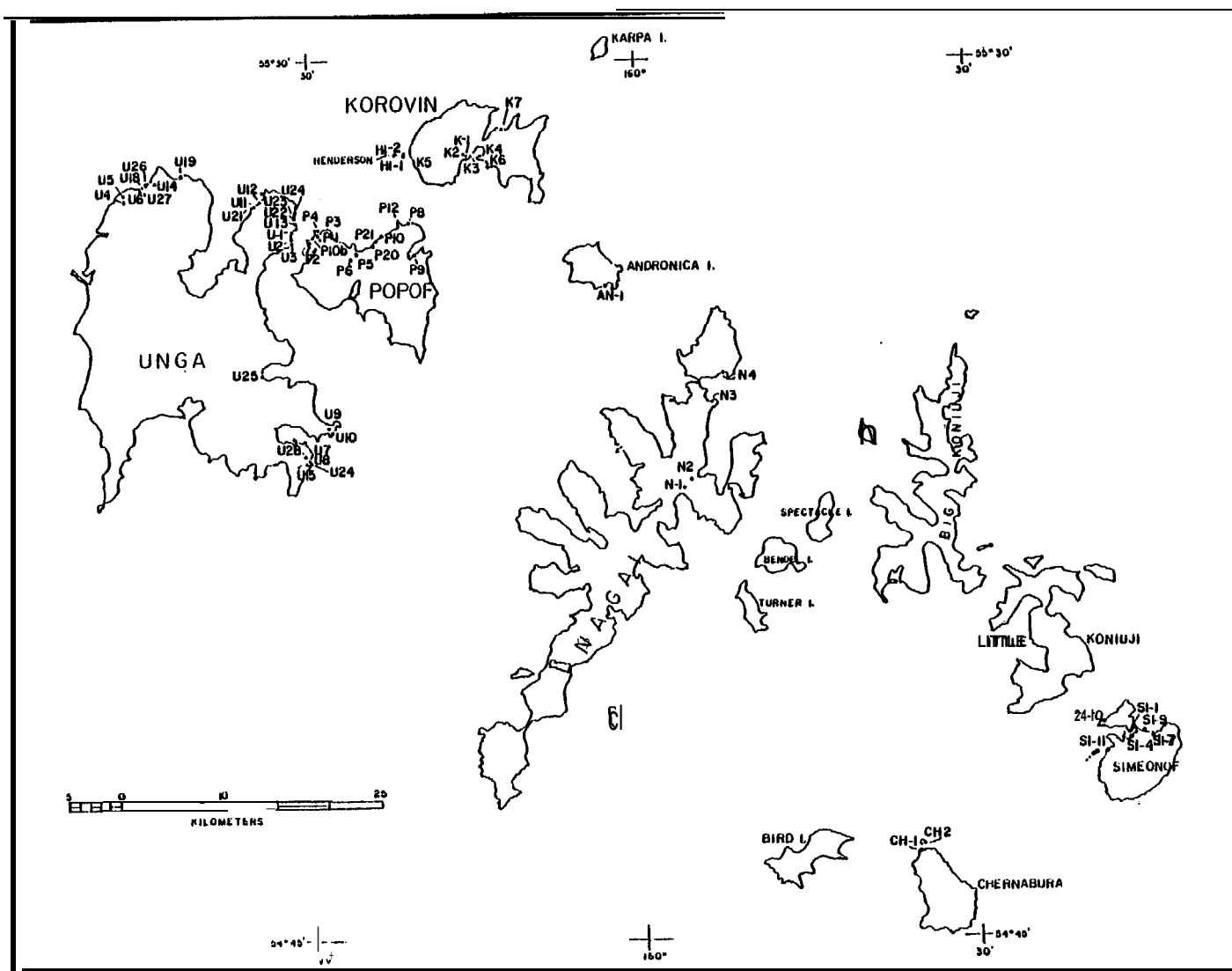
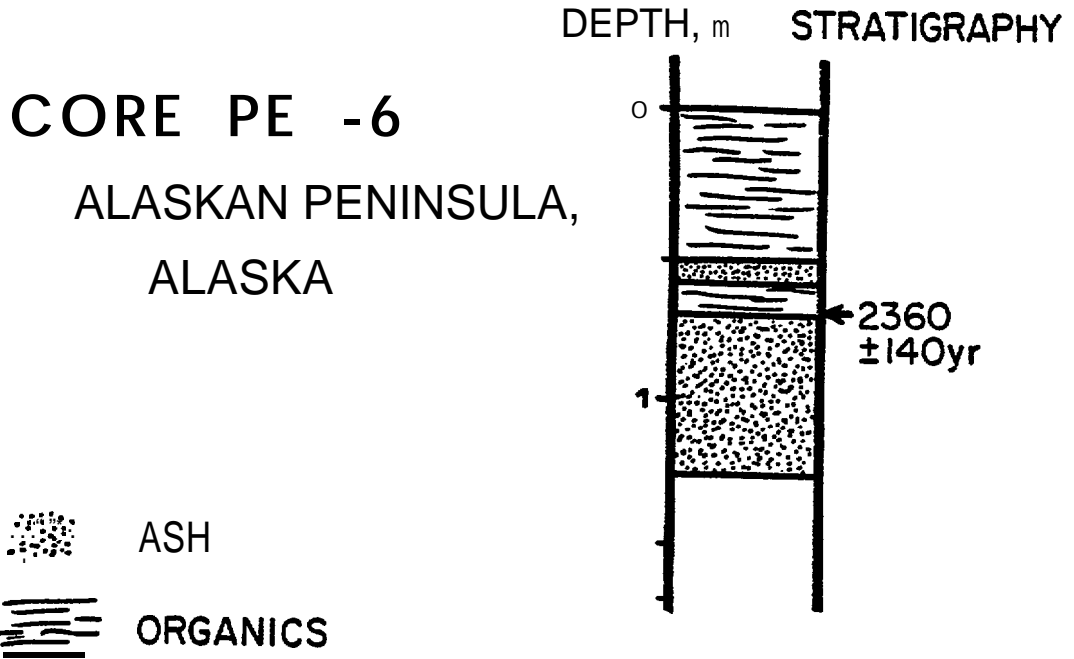


Figure 4.2.4(b). (Source - M. Winslow, written communication, 1982 (used with permission)).



Figures 4.2.5 **a,b**. Examples of volcanic ash layers in cores taken on marine terraces by M. Winslow, C. Heusser, and T. Ray, summer 1979. The oldest dated peat layer gives a Carbon 14 age of 9540 ± 260 years. The maximum number of ash layers in **a** core is four (core U-13) .

TABLE 4.2.1. Carbon 14 Dates and Number of Volcanic Ash Layers for Marine Terrace **Cores.**

<u>1979</u>	<u>Samples</u>	<u>Years B.P.</u>	<u># Ash Layers</u>
Andronica Island	AN-IA	460	1
Korovin Island	K-1	7580 \pm 220	1
Nagai Island	N-3	6050 \pm 230	1
Popof Island	P-2	9180 \pm 340	1
Peninsula	PE-5	2970 \pm 170	1
Peninsula	PE-6	2360 \pm 140	3
Peninsula	PE-10	6320 \pm 260	1
Simeonof Island	S1-1	4160 \pm 160	0
Simeonof Island	S1-4	4460 \pm 150	0
Unga Island	u-7	7500 \pm 180	1
Unga Island	U-8	2030 \pm 130	3
Unga Island	U-13	9130 \pm 250	4
Unga Island	U-14	9540 \pm 260	3

(Source - M. Winslow, written communication, 1982)

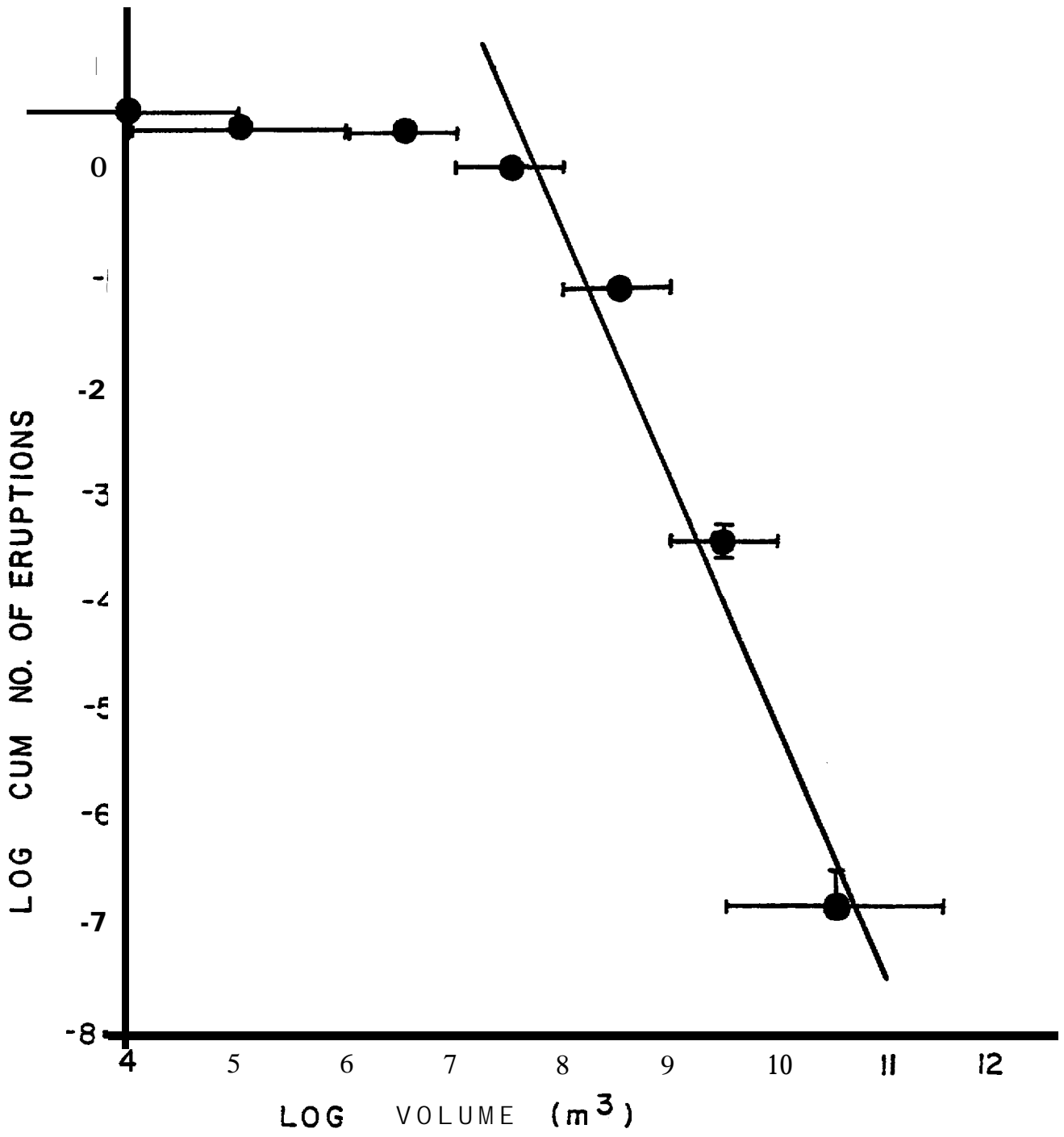


Figure 4.2.6. \log_{10} of the cumulative number of eruptions of a given size per hundred years per volcano vs. the \log_{10} of the volume of eruptive products. The volume is a crude measure of the energy of an eruption. The line is a least squares fit to the 4 data points to the right and has a slope of -2.3. Detection is probably not complete for events smaller than a volume of $3 \times 10^6 \text{ m}^3$. An eruption of volume $7 \times 10^7 \text{ m}^3$ is likely to occur at each volcano once per 100 years.

number of such eruptions per 100 years per volcano. If, however, only half the volcanic **centers are capable of producing** such large eruptions ($10^{9.5} - 10^{11.5} \text{ m}^3$ of ejects) then the rate of **occurrence** would be greater by a factor of 2 ($\log_{10} = 0.3$) as shown by the vertical error bar on the plot. The plotted point thus represents a minimum rate of occurrence. The horizontal error bars, one order of magnitude **in** each direction from a value of $10^{10.5} \text{ m}^3$, indicate that a" smaller close-by eruption and a larger but more distant eruption could have the same ash accumulation at a given location. Similarly, we assumed that the eruptions producing the ash **layers** in marine terrace cores could have originated from any one of 15 ± 5 volcanic centers, with volumes of $10^9 - 10^{10} \text{ m}^3$.

Lastly, we assumed that the recent **catalogue** of **Simkin** et al. (1981) (plus 1982 supplement) is complete for Alaska for eruptions > volcano **explosivity** index 2 (corresponding to volumes > 10^7 m^3) for the period 1942-1982. Military flights took place almost daily during World War II, and commercial or military flights have occurred almost daily ever since. Thus, we think it unlikely that an eruption with VEI > 2 would have been missed. Further, 3 great earthquakes have occurred **in** 1957, 1964, and 1965, rupturing a large portion of the Aleutian arc. Since some authors have argued that volcanic activity may be increased both before large earthquakes (**Kimura**, 1978) and after them (**Carr**, 1977), we note that the time period since **WWII** contains nearly as many years prior to a great earthquake as years after a great earthquake, and hence should be free of possible bias. From the **plot**, we estimate that the largest eruption likely to occur at any volcano in a one-hundred year time interval would have a volume of $7.0 \times 10^7 \text{ m}^3$ of ejects (\pm a factor of 2). The 1976 eruption of Mt. Augustine roughly corresponds to this volume. The volume estimate then forms part of the basis for our delineation of spatial hazards, as outlined in the next section of this report.

Spatial hazards assessment. Volcanic hazards which can affect life and property **in** the vicinity of a volcano include: **1) pyroclastic** surges, flows and **nuees** ardentes; 2) lava flows; 3) debris and mud flows and floods; 4) wind blown ash; 5) noxious fumes,

poisonous gases and acid rains; and 6) volcanic earthquakes. The first four of these hazards are displayed on hazards maps of the western Alaska Peninsula, and **Unalaska** and **Umnak** Islands (Figures 4.2.1 and 4.2.2). The rationale for each of the mapped hazard zones, as well as the unmapped hazards, are given below.

Pyroclastic surges, flows and nuees ardentes represent the most catastrophic potential hazards. These features generally originate from presently active vents or adjacent vents, hence **the** positions of all known Quaternary active vents, cinder cones, etc., are also shown on the hazards maps. The main driving force for the **pyroclastic** surges, flows and nuees ardentes (as well as lava flows) is gravity; generally the material is erupted to some height above the volcano, and the resulting gravitational collapse of the cooling eruption column feeds the flow. Lateral blasts, such as Mt. St. Helens, are not very common. Most known surges and flows **are** limited to distances of about 10-20 km from the volcanoes, and flows usually die out at the topographic base of the volcanoes (D. Miller, personal communication, 1982; Miller et al., 1982). Hence the smaller volcanoes **are** assigned a 10 **km** flowage hazard zone, Okmok Volcano is assigned a **15 km** zone, and the largest volcano in the study area, Mt. Veniaminoff, which is substantially larger than the others, is assigned a **20 km** flowage hazard zone. The extent of known Pleistocene to Recent lava flows and **pyroclastic** surge and flow deposits as mapped by Burke (1965), **Detterman** et al. (1981a,b), Drewes et al. (1961), **Waldron** (1961), and Byers (1959), are included on the hazards maps, and show good general agreement with the assigned 10 to 20 km flowage hazard zones.

Mudflows, debris flows, and floods represent an important hazard for the Alaskan/Aleutian volcanoes. Most of the volcanoes are covered by glaciers, hence a large amount of water is available to form landslides of mud and debris. Mud and debris flows are generally restricted to valleys except for the uppermost portion of the volcanoes, and the flows can travel great distances--several tens of kilometers--from the volcano. Thus we have identified all major valleys and rivers draining each volcano **as** likely sites of future mud and debris flows and floods. Mapped **holocene** mudflows from Mt. Veniaminoff (**Detterman** et al., 1981) demonstrate the areal extent of this hazard.

Wind blown ash is probably the most common and pervasive volcanic hazard. Some ash is emitted during almost every eruption, but except for large eruptions, most of the ash is deposited quite close to the source. The azimuth of greatest ash thickness is strongly controlled by prevailing wind direction which is highly variable in the Aleutians. Figure 4.2.7 shows the maximum ash thickness vs. distance for a number of large eruptions, including several eruptions of size comparable to our estimated one-per-hundred year eruption, with a volume of $7.0 \times 10^7 \text{ m}^3$ (\pm a factor of 2). As shown in that figure, typically 10 cm of ash can be deposited at a distance of 21 km, and a thickness of 4 cm of ash can be expected at a distance of 40 km. These two ash thicknesses are plotted on the hazards maps. The prevailing wind directions are shown in rose *diagrams on* the maps. We note that most of the time the wind blows towards the east; however, we have chosen to draw the ash fall hazard zones as circles centered on the volcanoes to emphasize the fact that significant ash accumulation can occur in any direction **if** the wind happens to be blowing that way during an eruption.

Distribution of noxious fumes, poisonous gasses, and acid rains also depends strongly on wind speed and direction. In general, their distribution will resemble that of the ash fall hazard zones. Again we emphasize that the often strong (up to 100 knots) and highly variable winds typical of the Aleutians make accurate spatial assessment of these hazards very difficult.

Volcanic earthquakes generally occur in high numbers around the times of eruptions. **For** purposes of this report, there are 3 basic types of volcanic earthquakes (other authors have used many different classification schemes): 1) shallow, low-frequency, tremor-like signals of small magnitude such as the events observed at **Pavlof**; 2) larger (up to about magnitude 5) **events** accompanying **or** preceding large explosive eruptions, for example Mt. St. Helens; and 3) large events probably related to subsurface movements of magma but not **necessarily** related to eruptions, such as recent earthquakes in Iceland and Hawaii, (e.g., Einarsson and Brandsdottir, 1980; Wyss et al., 1981). Most volcanic earthquakes originate under or in the immediate vicinity of a volcano. Because of their smaller size the

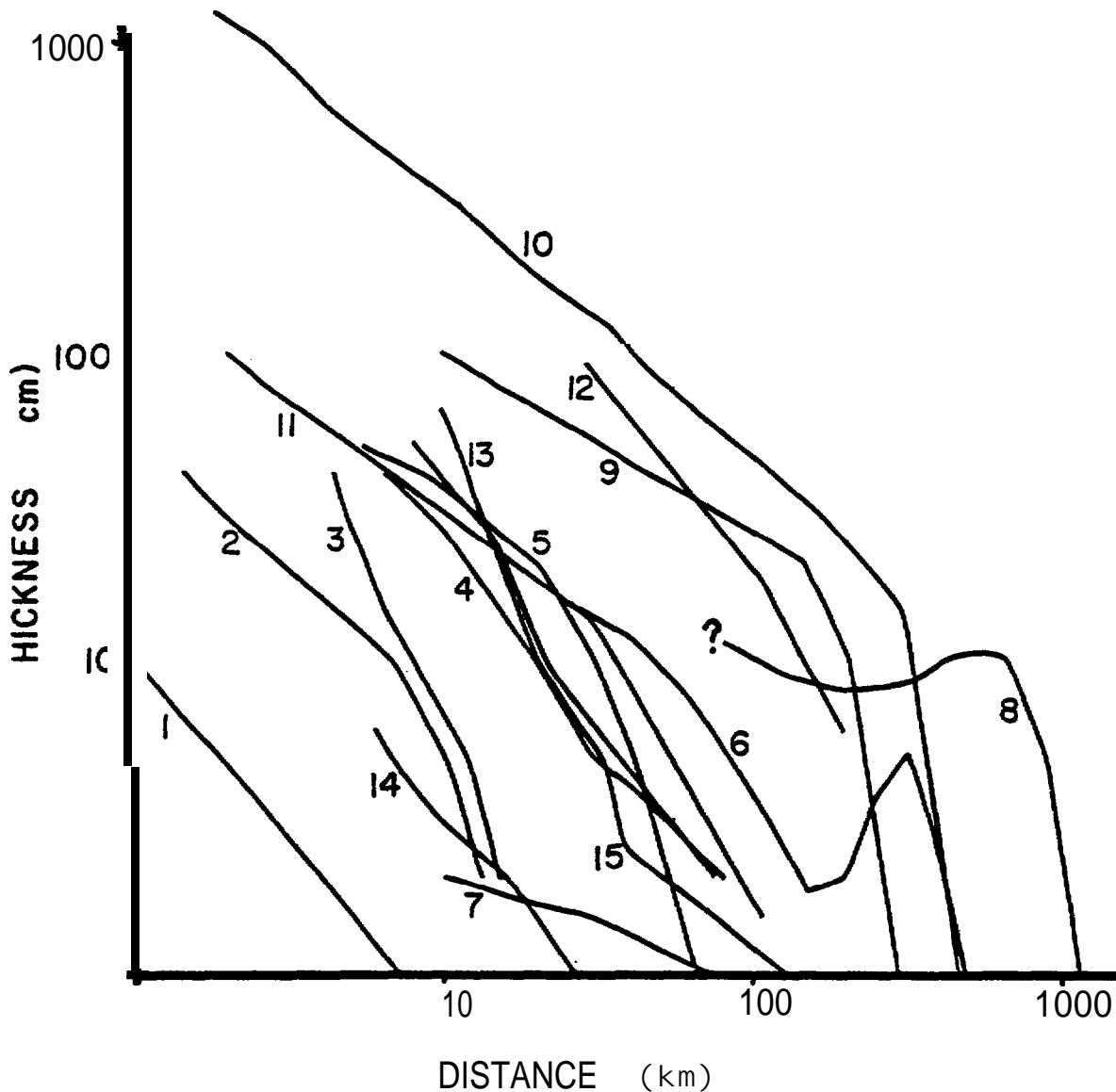


Figure 4.2.7, Maximum ash thickness in cm vs. distance from the vent. Sources of data are given below.

Maximum Ash Thickness vs. Distance

<u>#on Plot</u>	<u>Volcano Name and Year of Eruption</u>	<u>Volume</u>	<u>References</u>
1	Pari cut in	7.0×10^7	Wilcox, 1959
2	Cerro Negro, 1968	1.7×10^7	Taylor & Stoiber, 1973
3	Cerro Negro, 1971	7×10^7	Rose et al., 1973
4	Fuego, 1971	10^7	Rose et al., 1973
5	Hekla, 1947	1.7×10^8	Wilcox, 1959
6	Mt. St. Helens, 1980, May 18	1.5×10^7	Sarna-Wojcicki et al. , 1982
7	Mt. St. Helens, 1842	107	Crandell & Mullineaux, 1978
8	Quizapu, 1932	3×10^9	Wilcox, 1959
9	Santa Maria, 1902	5×10^9	Rosa, 1972
10	Katmai, 1912	3×10^{10}	Sapper, 1905
11	Mt. St. Helens, layer T	10^8	Wilcox, 1959
12	Mt. St. Helens, layer Yn	$1-3 \times 10^9$	Crandell & Mullineaux, 1978
13	Mt. Shasta, (layer R. B.)	10^8	Crandell & Mullineaux, 1978
14	Mt. St. Helens, 1980, May 25	1.4×10^7	Miller, 1980
15	Fuego, 1974 (October)	2.1×10^8	Sarna-Wojcicki et al., 1982
			Rose et al., 1978

seismic hazard due to volcanic earthquakes is quite small compared to the seismic hazard from large subduction zone events.

Shallow seismicity along volcanic axis. Shallow seismicity (at depth less than 30 km) recorded by the **Shumagin** Islands network from 1973-1982 is plotted in Figure 3.1.2. Along the volcanic axis the seismicity is generally low, with the exception of two prominent clusters. One of these is located ≈ 20 km southwest of **Kupreanof** volcano (lat. **56N**, long. **159W**). The site is the same location as several sightings of steam emission, **fumarolic** activity and snow discoloration near the summit of an unnamed mountain at the head of **Stepovac** Bay.

The second cluster is located at lat. 56N, long. **160W**, near Port **Moller**. This area contains several hot springs, one of whose temperatures was measured at about **140°F** during the summer of 1979 (T. Ray, personal communication, 1979). It is interesting to note that the average volcano spacing for this section of the Aleutian arc is about 40 km. However, a gap appears in the Port **Moller** area. It is possible, but unlikely that a new volcano is being formed here.

While the identification of clusters of **seismicity** does not alone unambiguously delineate the possible locations of volcanoes, continued geophysical monitoring and more detailed studies may help to establish the extent to which these two areas may be likely sites of future volcanic activity. Further, we note that **Pavlof** volcano, which has erupted frequently during the last 9 years, has not had such clusters of seismicity located beneath it. **Pavlof's** seismicity instead includes volcanic tremor, B-type events, and explosions, as outlined elsewhere in this report. Thus, it is likely that any future volcanic activity associated with the two clusters of seismicity may have a different character than the activity observed at **Pavlof**.

5. CONCLUSIONS

The prime purpose of this study is to attempt a rather complete and up-to-date instrumental and historic data base of the seismic and volcanic activity associated with the Aleutian arc. We include those adjacent regions in the Pacific and Bering Sea Shelves that fall within or affect the Lease Sale Planning regions known as the "St. George Basin", the "North Aleutian Basin" and the "Shumagin Basin". As part of this effort we have operated a telemetered seismic network in the Shumagin Islands segment of the arc (and Alaska Peninsula), and for short periods of time, at Unalaska Island and the Pribilof Islands. The seismic study has led to a remarkably good spatial seismic source definition and a consistent tectonic model which is important for developing probabilistic predictions of the future space-time behavior of seismicity, especially of great Aleutian subduction-zone earthquakes.

The study has had little opportunity to contribute to solving the open question of severe **groundmotions** associated with major subduction zone earthquakes. The study clearly points to the fact that this open problem of **groundmotions** need to be resolved before attempting any further statistical exposure calculations. The merits of such calculations remains doubtful as long as they are not based on solid data of **groundmotions** of moderate to great subduction zone earthquakes.

Notwithstanding this severe deficiency we conclude that, based only on potential source distributions and on probabilities of occurrences of moderate to great earthquakes in the arc, the seismic hazard near the **Shumagin, Unalaska** and (to a lesser degree) near the **1938** rupture zone is severe for a forthcoming period of interest, and may decrease to more moderate levels (see Appendix 7.6) in the northern portions of the St. George Basin, where local sources may be an important contributing hazards factor.

Volcanic hazards clearly exist and should be accounted for especially when planning for an operational stage of resource extraction. But, except for local and near-shore conditions, they appear to be a less restrictive regional hazards factor in most offshore regions when compared with the seismic hazards.

Crustal deformation and tsunami effects are expected to be severe on the Pacific side of the Aleutian Arc (including the Alaska Peninsula and outlying islands with pacific exposure). The historically observed tsunami run-up heights of up to 30 m, and coastal vertical level changes approaching 10 m or more should set a guideline for preventive measures.

We have established a comprehensive database for future quantitative exposure mapping in the subject region. The actual quantitative probabilistic mapping is not within the scope of this project and remains to be carried out by taking into account the data presented here.

6. UNRESOLVED PROBLEMS

We have discussed throughout this report a variety of unresolved problems that need to be addressed in future efforts if hazards assessment shall progress from producing qualitative to yielding quantitative results. In order of perceived importance we repeat and list the following items:

1) Collection of strong motion data from moderate to great earthquakes within the Aleutian arc.

2) Thorough, digital analysis of these Aleutian **groundmotion** data to derive parameterizations of groundmotions (duration, attenuation, etc.) both in the time and spectral domains that are of direct use to engineering design methods. The importance of data from great earthquakes is stressed.

3) Improve the understanding of statistics of recurrence times of great events in the arc to reduce uncertainties in conditional probabilities (i.e., resolve the question whether recurrence time data conform to normal or long-normal distributions?; is the Markov-process a useful model or not?)

4) Develop a quantitative method to characterize volcanic activity (by volume of ejects, energy, etc.) and of volcanic effects on engineering structures.

5) Continue monitoring seismic, geodetic, sea level and other, tectonic-volcanic data that have a potential to improve medium-to-short term forecasting methods of hazardous events. This phase of data collection has to precede resource production stages by many years in order to establish false-alarm rates. False-alarm rates need to be known in order to not overestimate levels of risk during a 'precursory' phase of observation, preceding a suspected or imminent event. Medium-to-short term forecasting may be useful only to affect operational modes of hazards mitigation. They do not affect the basic long-term hazards assessment important for lease-sale planning and engineering design decisions. Given, however, certain post-lease sale developments and design implementations, such shorter-term measures may considerably reduce damage from an event if preparedness is properly implemented (temporary reduction of storage or production, removal of tanker or service fleets, etc.).

7.1 Earthquake Data Processing Methods

Since 1973 the Shumagin network data have been recorded by several types of instruments. Initially, from July 1973 to August 1975 slow-speed, direct, analog tape recorders that recorded continuously were in use. The develocorder that records the data continuously on film, served as the main recorder from September 1975 until the end of April 1981. Since April 1980 analog, four channel, Teat tape recorders that are event triggered and record FM-modulated signals, have provided data that can be digitized at L-DGO. Such data can be analyzed using the PDP 11/70-UNIX system as any other digital data. Currently, the Teat tape recorders record data only as a back-up to the digital system.

The event triggered, digital data acquisition system (DDAS) that today is the main recording system for the network was installed in December 1980. During most of 1981 we had severe problems with operating the DDAS and the data recovery was less than 30%. In late December it became quite clear that the room temperature at the central station should be kept below 74°F so that the DDAS would function properly. During 1982 we have had almost 100% data recovery from the DDAS. The DDAS was connected to a separate digital event detector in October 1981. The new digital event detector can be accessed (by phone modems) from the L-DGO PDP 11/70-UNIX computer and relevant parameters can be reset. For visual recording the Shumagin network had from the beginning one or two helicorders. During the last three years the number of helicorders was increased from two to five and to eight in October 1981.

Develocorder data processing. Usually, the develocorder data that consisted of continuous seismogram traces from up to 14 stations and two time code channels, were processed in batches. The purpose was to determine hypocenter and magnitude of every locatable earthquake that occurred within 400 km distance and was recorded by the Shumagin network. Initially, the films are scanned for recorded earthquakes and the date and time to the nearest minute of locatable earthquakes are written on a summary sheet (see also Figure 7.1.1). The next step consisted of using a ruler to measure the arrival time

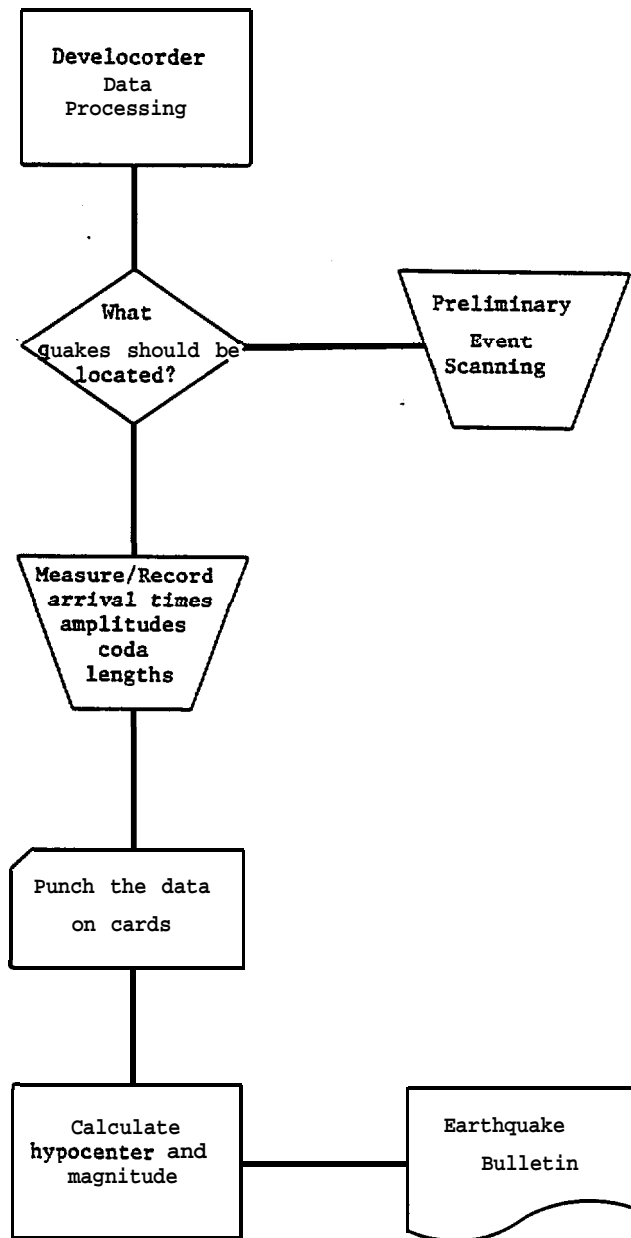


Figure 7.1.1.A block diagram showing how the routine developer data processing was carried out for the Shumagin seismic network, eastern Aleutians, Alaska.

of P- and S-waves and amplitude information on a **develocorder-**viewscreen. A batch of arrival times from 40 to 50 earthquakes was punched on computer cards, or later tapes into a computer file from a terminal, for calculating earthquake **hypocenter** and magnitude. If the calculated hypocenter was found to be of low quality, the arrival times were checked for possible typographical errors or possible erroneous picking of P- or S-wave arrival times. Although this procedure was repeated normally at least three times, often a few "difficult" earthquakes still had **low** quality hypocenter solutions.

Digital data processing. The purpose of the routine digital data processing also is to determine **hypocenter** and magnitude of every locatable earthquake. The following description of the data processing **is** based on the block diagram shown **in** Figure 7.1.2.

First, the arrival time to the nearest minute and the peak amplitude of all the earthquakes that show up on the **helicorder** records are recorded in a logbook. **The DDAS writes 25 to 30 events on the source tape at Sand Point. The table of content **is** generated both on site and at L-DGO using a program called **trdla**. The table of content is compared with the logbook to determine **what files on the digital tape are** earthquakes and which ones are false triggers or bursts of noise. To facilitate further processing hard copies or seismograms are made of each earthquake. Once the hard copies are available the events **are** classified as local (within 400 km distance), regional (400-1200 km), teleseismic (greater than 1200 km), volcanic events or calibration pulses.**

The local events are demultiplexed and stored temporarily on an **rll** disk. The interactive program ping is run from a Tectronix 4014 graphics terminal and a data analyst picks arrival times, amplitudes and periods using cursor controls as is shown in Figures 7.1.3 and 7.1.4. The program addchdv adds instrument codes and attenuation settings to the **pickfile**. The program trgndmn changes amplitude values from digital counts to nanometers of ground motion. The computer program **HYPOINVERSE** (Klein, 1978) is used to calculate **hypocenter** and magnitude using the data stored in the pick file. **HYPOINVERSE** stores the results in four different files as demonstrated in Figure 7.1.5. In Figure 7.1.5 it **is** shown also how each event is

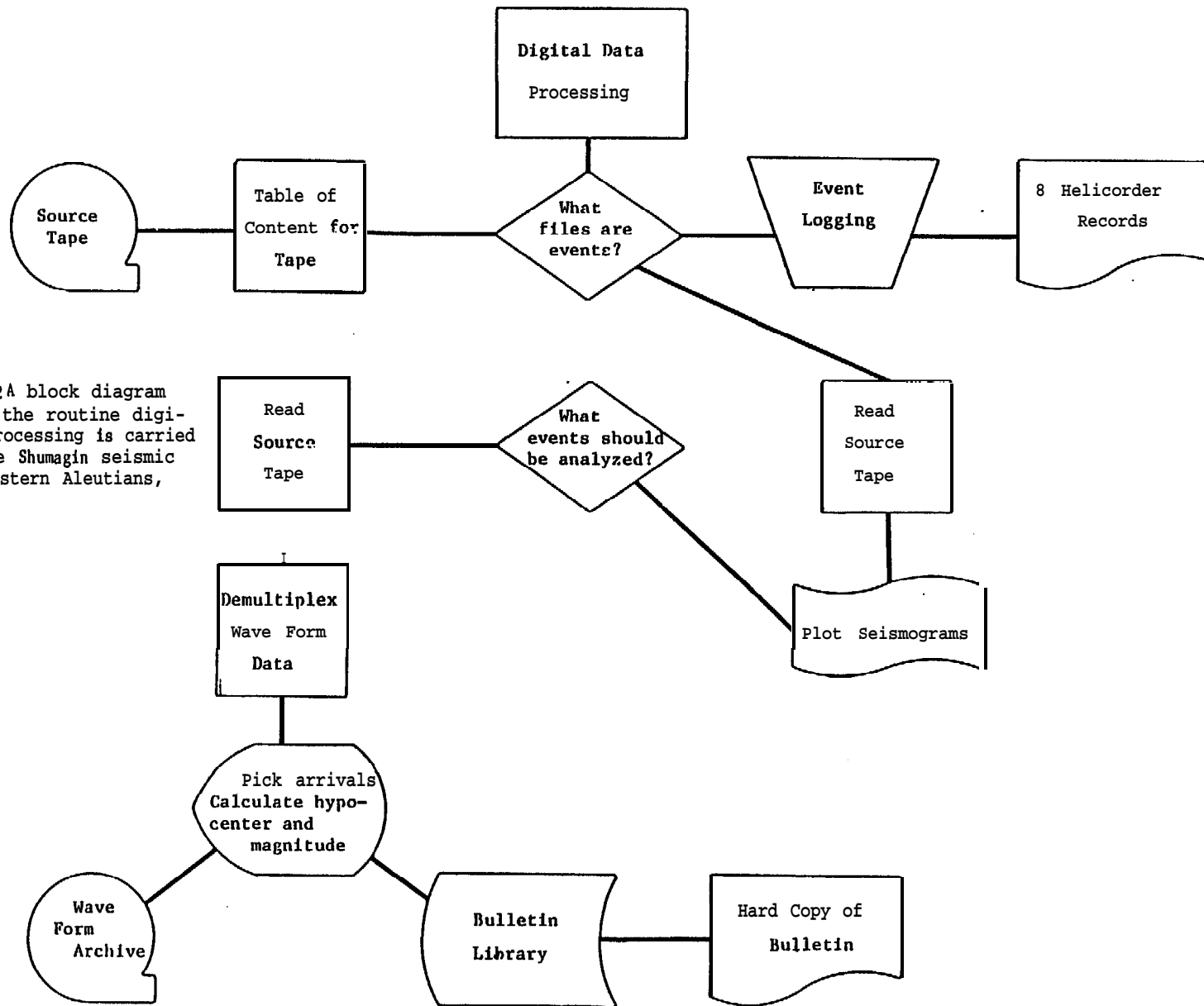


Figure 7.1.2A block diagram showing how the routine digital data processing is carried out for the Shumagin seismic network, eastern Aleutians, Alaska.

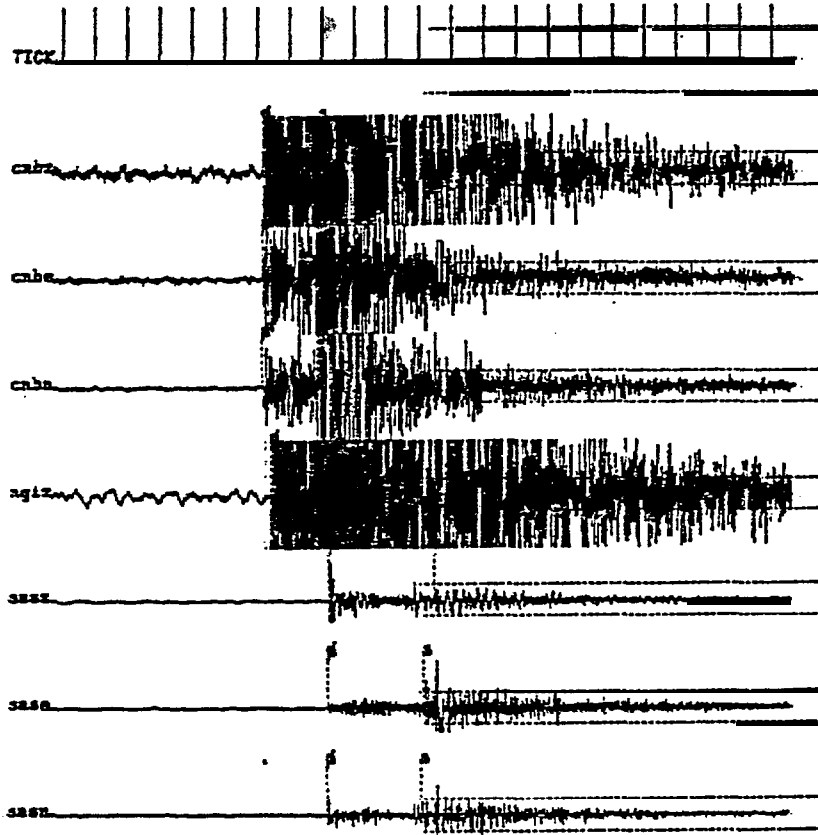


Figure 7.1.3A summary display of seismic traces from the program ping. The analyst can choose which trace he wants to amplify (see Figure 7.1.4). The data analyst can also compare his P- and S-wave picks at the different stations, " and pick coda lengths. Note in this mode the data are shown strongly decimated.

Station: cnbz 33.33 - 57.33 - - - - 1981/12/23 11:14:17.00 14

Pick 2 pic with polarity

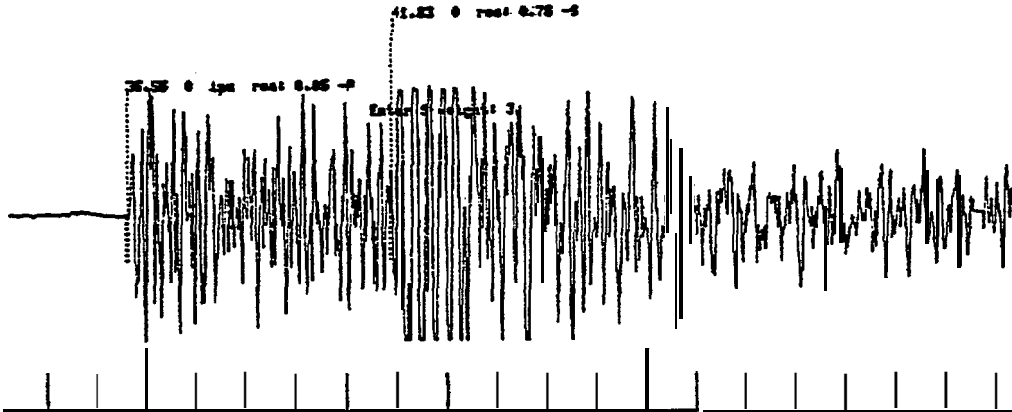
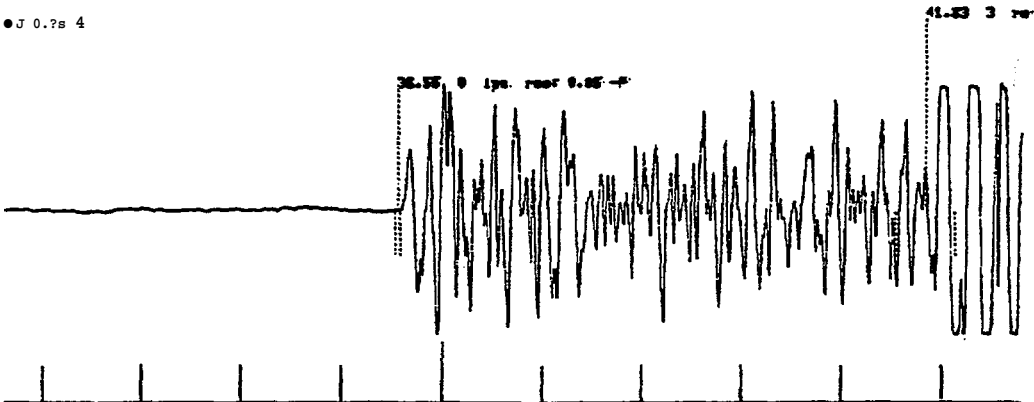


Figure 7.1.4.A sample seismogram from station CNBZ. The distance between tickmarks is 1 second. in this mode the data analyst picks, P-, S-arrivals, amplitude and period, Note that the lower trace is an amplification of the upper trace.

Station: cnbz 32.57 - 42.57 - - - - 1981/12/23 11:14:17.00 14

Pick p-amplitude: (upper/lower)
p-amp -4024
Pick p period (begin/end):
p-per 0.140 7.1 Hz

● J 0.7s 4



the 811223.111417e file is:

1 23 dec 81, 11:14 event no. 1

yr	mo	da	origin	lat	lon	depth	rms	srh	erz	gap	xmag	mag				
81	12	23	1114	38.33	54 42.31	159 54.88	31.29	.39	1.50	3.14	205	2.3				
result dminitr nfr rms rank q sqd																
.39 24.5 3 9 35 15 CD d c d																
sta	dist	azm	sn	p/s	w	sect	ccor	(tobs	-tcal	-dly	res)	ut	xmg	mag	r	info
cabz	24.5	83	138	epu	3	36.58	.00	6.25	6.29	.00	.05	2.03	2.3			.282
cabz	24.5	83	138	epu	3	41.82	.00	11.40	10.73	.00	.78	.51				.073
cabz	24.5	83	138	epu	3	36.59	.00	6.26	6.29	.00	.06	2.03				.282
cabz	24.5	83	138	epu	3	41.54	.00	11.31	10.73	.00	.58	.51				.073
cabz	24.5	83	138	epu	3	36.61	.00	6.28	6.29	.00	.08	2.03				.282
cabz	24.5	83	138	epu	3	41.73	.00	11.40	10.73	.00	.67	.51				.073
ngix	38.4	346	119	epd	3	37.51	.00	7.18	7.65	.00	-.47	2.03				.239
ngix	38.4	346	119	epd	3	43.59	.00	13.26	13.23	.00	.02	.51				.160
ngix	38.4	346	119	epd	3	42.98	.00	12.65	12.80	.00	-.15	2.03	3.3			.120
ngix	38.4	346	119	epd	3	52.83	.00	22.50	22.14	.00	.35	.51				.063
susa	78.7	333	100	ep	3	42.99	.00	12.65	12.80	.00	-.14	2.03				.120
susa	78.7	333	100	ep	3	51.91	.00	21.58	22.14	.00	-.57	.51				.063
susa	78.7	333	100	ep	3	43.01	.00	12.68	12.80	.00	-.12	2.03				.120
susa	78.7	333	100	ep	3	51.77	.00	21.44	22.14	.00	-.71	.51				.063
sgbe	99.5	34e	97	ep	3	45.76	.00	15.43	15.37	.00	.06	2.03				.212
sgbe	99.5	34e	97	ep	3	57.38	.00	27.05	26.59	.00	.46	.51				.056
sgbe	99.5	34e	97	ep	3	45.70	.00	15.37	15.37	.00	.00	2.03				.212
sgbe	99.5	34e	97	ep	3	56.63	.00	26.30	26.59	.00	-.29	.51				.056
dlgz	131.9838	98	ap	1	49.21	.00	18.78	19.60	.00	-.72	1.52					.216
dlgz	131.9838	98	ap	1	66.85	.00	36.52	33.91	.00	2.61	.00					.000
ivfz	134.6	10	94	ep	2	50.88	.00	20.55	19.95	.00	-.60	1.01	2.8			.227
ivfz	134.6	10	94	ep	2	67.48	.00	37.15	34.51	.00	2.63	.00				.000
pvwz	140.7302	94	epd	3	51.06	.00	20.73	20.75	.00	-.02	.51	3.1				.015
pvwz	140.7302	94	epd	3	67.21	.00	36.88	35.90	.00	.98	.51					.057
pvwz	140.7302	94	epd	3	51.66	.00	21.33	21.07	.00	.26	2.03					.232
pvwz	140.7302	94	epd	3	69.84	.00	39.51	36.45	.00	3.06	.51					.056
ps3z	143.2	303	94	ep	3	51.54	.00	21.21	21.07	.00	.14	.51	3.2			.014
ps3z	143.2	303	94	ep	3	71.38	.00	41.05	36.45	.00	4.60	.00				.000
ps4z	143.s	301	94	ep	3	51.50	.00	21.17	21.17	.00	.00	.51	3.1			.015
ps4z	143.s	301	94	ep	3	67.84	.00	37.51	36.62	.00	.88	.51				.058
ps6z	188.4304	94	ep	4	53.53	.00	23.20	22.23	.00	.97	.00					.000
ps6z	188.4304	94	ep	4	73.68	.00	43.35	38.46	.00	4.89	.00					.000
ps7z	133.1	303	84	ep	4	53.67	.00	23.34	22.38	.00	.96	.00	3.4			.000
ps7z	133.1	303	84	ep	4	74.98	.00	43.75	38.72	.00	5.03	.00				.000
drz	153.7	280	94	ep	4	51.72	.00	21.39	22.45	.00	-1.06	.00	2.1			.000
drz	153.7	280	94	ep	4	69.59	.00	39.26	38.84	.00	.42	.51				.092
ps8z	157.2	302	94	ep	3	53.82	.00	23.49	22.91	.00	.58	.51	3.0			.015
ps8z	157.2	302	94	ep	3	70.86	.00	39.72	39.63	.00	.08	.51				.054
ps4z	159.4	303	93	ep	3	54.35	.00	24.82	23.20	.00	.82	.51	3.2			.014
ps4z	159.4	303	93	ep	3	75.31	.00	44.38	40.14	.00	4.84	.00				.000
blhz	173.8	310	83	ep	3	56.32	.00	25.39	25.35	.00	.64	.51	2.3			.011
blhz	173.8	310	83	ep	3	77.30	.00	44.97	43.86	.00	1.11	.51				.044
snkz	186.0	263	93	ep	3	51.01	.00	20.47	20.69	.00	-.22	1.01				.277
snkz	186.0	263	93	ep	3	67.91	.00	36.58	40.17	.00	4.40	.00				.000
balz	191.2	887	33	ep	3	51.99	.00	22.66	27.38	.00	1.28	.51				.030
balz	191.2	887	33	ep	3	68.37	.00	38.04	47.37	.00	4.67	.00				.000

the trial solution was:
 811223.1114302754 4224159 345S 388388 34206 24 4110066 333 9 e 154 0cd 74831s 155 388 811.73

811223.111417e - the original pickoffs file
 811223.111417c - condensed output pickoffs with converted amplitudes
 811223.111417e - the legible version of 811223.111417c
 811223.111417f - the solution in human format
 811223.111417g - the solution in hypoinverse format
 SIDCHAN0ct31 is the channel file used

cnbz	1114231114	3659	5282	41s2	03	76495	58	0	0	245138	0	0	5a	823	292	73	8.131n	0	-36	
cnbz	1114231114	3659	5282	41s2	03	58	58	0	0	245135	0	0	58	0	282	73	8.141gb	0	-42	
cnbz	1114231114	3661	8282	4173	53	67	n	58	0	245135	0	0	58	0	282	73	8.151gb	0	-42	
ngiz	1114231114	3751	-47202	4359	53	2	n	58	0	384119	0	0	246	a	239	150	8.151n	0	-3/6	
sazepd	1114231114	4298	-15202	5283	03	35134	58	1	0	797105	0	0	333	033	120	63	8.291b	1	-22	
sazepd	1114231114	4299	-14252	5191	03	-87	0	58	0	797108	0	0	333	0	120	63	8.311b	0	-22	
sazepd	1114231114	4381	-12502	5177	03	-71	0	58	0	797198	0	0	333	0	a	120	63	8.311b	0	-22
sgoep	1114231114	4576	5282	5730	03	46	0	58	0	995	97	0	348	0	212	56	8.241gb	0	-42	
sgoep	1114231114	4577	5282	5663	03	-29	0	58	0	998	97	0	340	0	a	212	56	8.251gb	0	-42
dlz	1114231114	4921	-721s2	5665	04	261	u	0	0	21349	95	0	292	s	216	0	8.221na	0	-24	
ivfz	1114231114	5088	68101	6748	34	283190	0	0	0	1346	94	0	a	10	c20	227	0	8.221n	0	-30
pvz	1114231114	5106	-2	50	6721	03	98424	58	0	1407	94	0	332	031	15	67	8.311n	0	-42	
ps2	1114231114	5166	26232	6984	03	306	0	58	0	51431	94	0	333	0	3	232	56	8.161gb	0	-36
ps3	1114231114	5154	1450	7135	04	46437	0	0	0	1432	94	0	333	032	14	0	9.111gb	0	-42	
ps4	1114231114	5158	0	50	6784	03	98422	58	0	1439	94	0	331	031	15	5a	6.121gb	0	-3s	
ps5	1114231114	5353	97	0	7365	04	489	a	0	1528	94	0	304	0	0	a	8.201gc	0	-42	
ps6	1114231114	5367	96	0	7498	04	553765	a	0	1531	a4	0	303	034	15	9a	6.211ga	0	-42	
ps7	1114231114	5372	-106	0	6959	03	42	31	0	1537	94	0	298	1721	0	0	6.251n	0	-3a	
ps8	1114231114	5382	58	50	7035	03	8291	58	s	1572	94	0	282	033	15	5a	6.221ga	0	-30	
ps9	1114231114	5435	82	50	7531	04	484458	a	0	1594	93	0	283	032	14	B	7.191ga	0	-48	
blhz	1114231114	5632	54	50	7530	03	111	44	0	1752	93	0	310	023	11	4413	1.81n	0	-42	
snkz	1114231114	5633	-12101	3691	54	440	0	0	0	1860	93	0	263	0	277	J	8.271n	0	-36	
balz	1114231114	5899	223	50	8237	04	467	0	0	192	93	0	267	a	38	0	8.841n	a	-48	
811223.111423254	4231159	5488	312529	35205	2S	3918266	342	12	0	149	0cd	0	65215	150	314	911.73				

Figure 7.1.5. A sample output from HYPONVERSE. Above, the -o file is shown; below the -c file is shown.

given a name that is the date and time, when the digital or analog event detector declared the onset of **an** event. Currently, **all** five files, -p, -c, -o, -7, -h, are stored in an event directory (with a suffix -L) within the bulletin library. The seismograms or the **demultiplexed** waveform data are stored in two files on archive tapes with suffixes -d and -D where -d contains the data and -D contains header information. The pickfile **or** the -p files are stored also on the archive tape.

Figure 7.1.6 contains a simple but very useful graphical representation of the arrival time data. The programs that create this output from the -c file are described by Nicholson and Simpson (1983). The **Wadati** and **Riznichenko** diagrams give an independent estimate of the origin time and of the depth of the **hypocenter**. Further, they also provide an easy **way to** check for data inconsistencies.

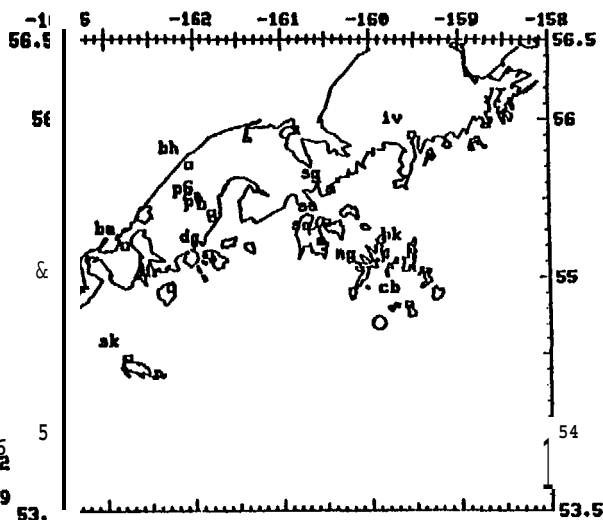
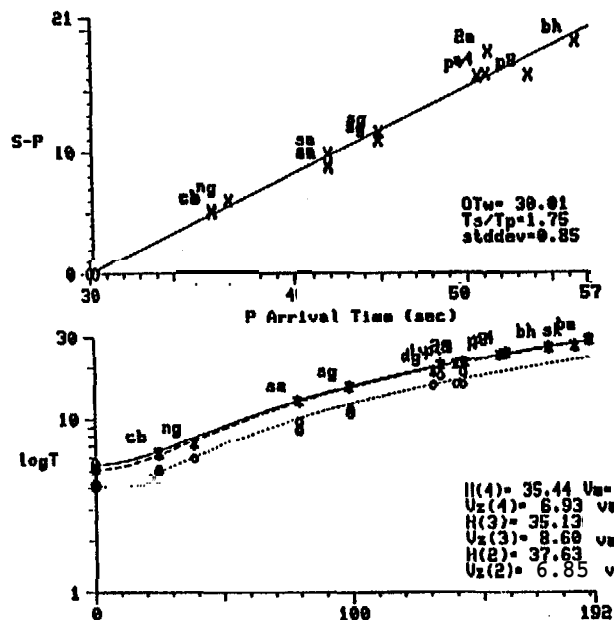
In conclusion, the major advantages of digital data processing can be summarized as follows:

- 1) No measurements done by hand using a ruler are required. The data analyst never needs to copy down by hand such information as, for example, station code, wave type or arrival time. Thus a large source **of** potential error is eliminated.

- 2) Using the program **ping** the seismograms can be band-pass filtered and often signals can be restored that without filtering are just white noise. The **Tectronix** graphics terminal allows the data analyst to amplify or attenuate the data such that the whole dynamic range of **72dB** can be exploited. A **develocorder** record had a typical dynamic range of only 20dB.

- 3) The digital data are processed as single events, and no event is archived until a satisfactory **hypocentral** solution has been found. The develocorder data were usually batch processed and although 3-5% of the events were not properly located the data processing **was** terminated, since chasing a few "difficult" earthquakes was **not** considered worthwhile.

Yr Mo Dy Origin Lat N Lon U Depth Mag RMS Err Err Nsta Gap Dmin Nur Nns Up/Us No.
 81-12-23 1114 30.33 54 42.31 159 54.88 31.89 8.9 0.39 1.50 3.14 20 205 25 35 15 1.73 1



Sta	Diat	Az	i	Ain	Prmk	Psec	Tobs	Pres	Put	Srpk	Ssec	Tobs	Sres	Swt	Up	Us	Up/Us
cb	24.5	58	135	1pu0	36.58	6.25	0.05	2.02	s 3	41.82	11.49	0.76	0.50	6.36	3.46	1.84	
cb	24.5	58	135	epu0	36.59	6.26	0.06	2.02	s 3	41.64	11.31	0.58	0.50	6.35	3.51	1.81	
cb	24.5	58	135	epu0	36.61	6.28	0.08	2.02	s 3	41.73	11.40	0.67	0.50	6.33	3.49	1.82	
ng	38.4	346	119	1pd0	37.51	7.18	-0.47	2.02	s 3	43.59	13.26	0.02	0.50	6.90	3.74	1.85	
sa	79.7	333	100	epd0	42.98	12.65	-0.15	2.02	s 3	52.83	22.50	0.35	0.50	6.77	3.81	1.78	
sa	79.7	333	lee	ep.0	42.99	12.66	-0.14	2.02	s 3	51.91	21.58	-0.57	0.50	6.76	3.97	1.70	
sa	79.7	333	100	epd0	43.01	12.68	-0.12	2.02	s 3	51.77	21.44	-0.71	0.50	6.75	3.99	1.69	
ag	99.5	340	97	ep. e	45.76	15.43	0.06	2.02	s 3	57.38	27.05	0.46	0.50	6.76	3.86	1.75	
ag	99.5	340	97	epd0	45.70	15.37	0.	2.02	s 3	56.63	26.30	-0.29	0.50	6.79	3.97	1.71	
dg	131.9	29a	95	ep. 1	49.21	18.00	-0.72	1.52	s 4	66.05	0.	2.61	0.	7.18	0.	0.	
iv	134.6	10	94	ep.2	50.08	20.55	0.60	1.01	s 4	67.40	0.	2.63	0.	6.72	0.	0.	
pv	140.7	302	94	epd3	51.06	20.73	-0.02	0.50	s 3	67.21	36.88	0.90	0.50	6.95	3.91	1.78	
sa	143.1	303	94	epu0	51.66	21.33	0.26	2.02	s 3	69.114	39.51	3.05	0.50	6.87	3.71	1.85	
s3	143.2	303	94	ep. 3	51.54	21.21	0.14	0.50	s 4	71.38	0.	4.60	0.	6.91	0.	0.	
s4	143.9	301	94	ep.3	51.60	21.17	0.	0.50	s 3	67.84	37.51	0.88	0.50	6.96	3.93	1.77	

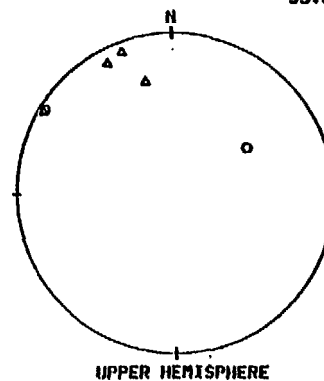


Figure 7.16. A sample output from the program dplt2 written by C. Nicholson. Upper-left is the Wadati diagram; lower-left is the Ruzhichenko diagram. The epicenter is plotted on the map as an open circle close to the station cb. Lower-right an upper hemisphere focal mechanism; A - dilatations; o - compressions; x - are nodal arrivals.

7.2 Magnitude Determinations

Objectives. One of the purposes of operating the **Shumagin** seismic network is to determine the magnitude of local earthquakes. Either the body wave magnitude or the coda length magnitude for local events can be determined. A body wave magnitude is a more useful measure of the size of a local earthquake since it represents the measured ground motion at the respective seismic station. The coda length magnitude can be more *easily* determined since no calibrations of the instruments are needed **as** long as they remain unchanged. The coda length magnitude, however, is not a known function of ground motion and is sometimes dependent on the S-P-arrival time of the local earthquake. Prior to 1980 we determined coda length magnitudes for earthquakes that occurred within our network. Since much of our instrumentation was upgraded in 1980 and **1981** ~~we~~ we were faced with the "task of redetermining our coda length magnitude scale or to calibrate our instrumentation to facilitate the calculation of body wave magnitudes. We decided to calibrate our instrumentation since that permitted us to use **the** network to achieve other scientific goals (for example, attenuation studies, calculation of source parameters) in addition to enabling us to determine body wave magnitudes.

The calibration of the seismic network was carried out in two different ways. First, all individual components were calibrated in the laboratory or specifications on instrument characteristics were obtained from the respective manufacturer. This information (see Figure 7.2.1) was combined into a total system response as described below to determine ground motion in nanometers (rim, 10^{-9} m). Second, the seismic stations were calibrated in the field during the October 1981 field trip. A constant-current-square-wave signal of 10 second period was applied to the calibration coil of the seismometer. These calibration pulses can be used to confirm the results obtained using the first method. Further, at 10 seismic stations in the network a calibration signal is generated automatically every 24 hours to check if the station's calibration changes with time.

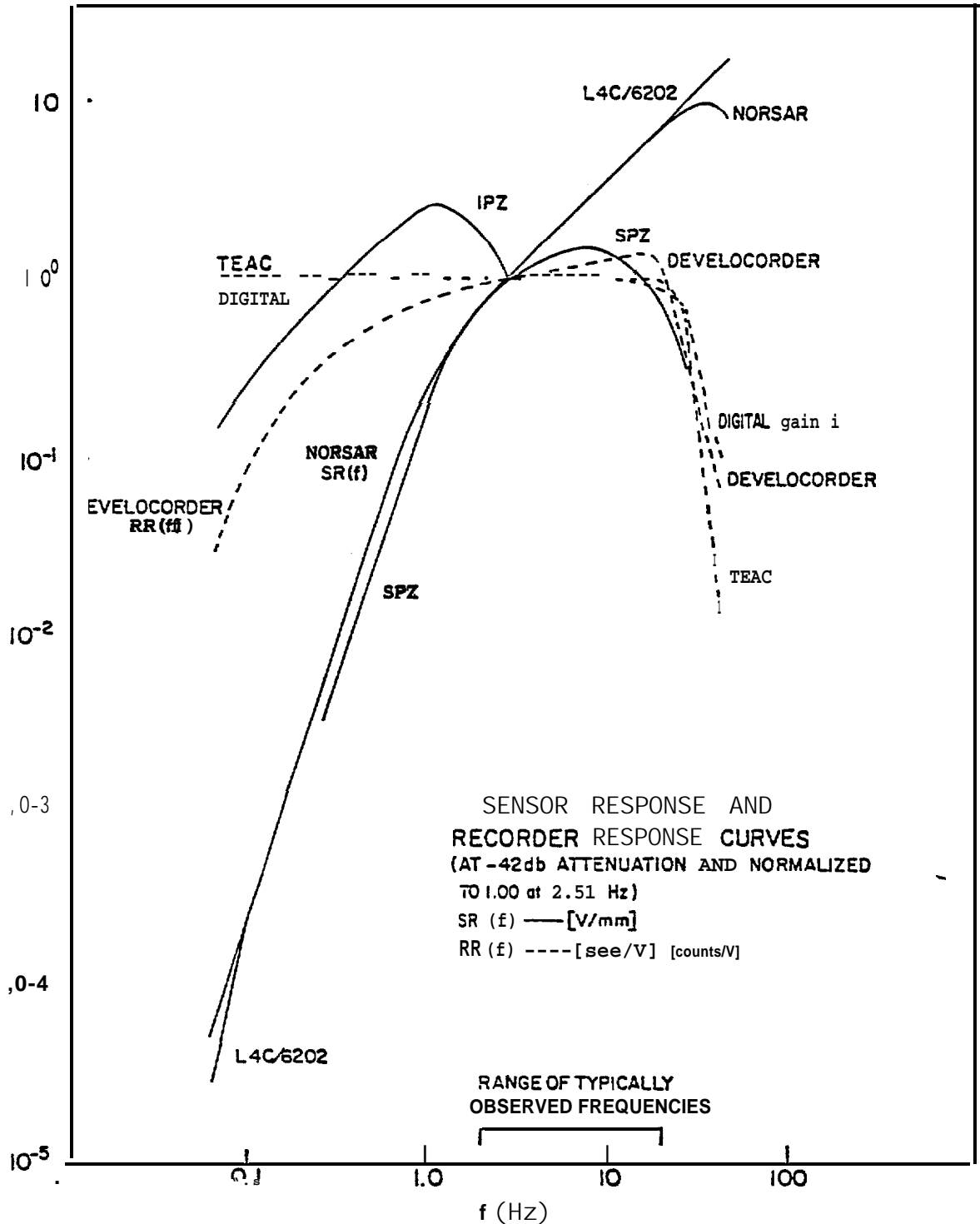


Figure 721. Sensor responses and recorder responses shown as a function of frequency for seismic stations in the Shumagin Network. The sensors are short period vertical (SPZ) and intermediate period vertical (IPZ). The SPZ sensors are either NORSAR HS-10 or Mark L4-C/6202, 1B seismometers. The IPZ sensors are broad band (Baby Benioff) seismometers. The recorders are continuous recording on a film (DEVELOCORDER), an event triggered analog tape recorder (TEAC) and an event triggered digital tape recorder (DIGITAL). Above the horizontal axis the range of typically observed frequencies is shown. The sensor and the recorder responses are combined to get the total, system response as described in the text.

Calibration of the total system response. The total seismograph system **reponse**, TSS(f) at frequency, f, is the product of the sensor response **SR(f)** and recorder response RR(f) (see Figure 7.2.1).

$$\mathbf{TSS(f) = SR(f) \times RR(f)}$$

The sensor response, SR(f), is the product of the seismometer response, S(f), and the amplifier response, A(f), or

$$SR(f) = S(f) \times A(f)$$

The seismometer response as a function of frequency was calculated with the following formula:

$$s(f) = \frac{2\pi f^3 G_E}{[(F_0^2 - f^2)^2 + 4B_t^2 F_0^2 f^2]^{1/2}} \quad [\text{v/mm}]$$

where G_E is the effective motor constant [V/mm/see]

F_0 is the natural frequency [Hz]

B_t is the damping ratio (parallel or series)

The amplifier response vs. frequency (A(f)) was measured during a calibration sequence in the laboratory. This is a relative function that is normalized to 1.0 on the flat portion of its response curve. The sensor response is normalized to a 42 db attenuation of the station amplifier VCO [i.e., total gain is 90 db, (**EMTEL** 6242), or 120 db (**DEVELCO** 6202), hence attenuation 42 db is equivalent to gain 48 db or 78 db, respectively) *since* that is a commonly used value in our network. Since July 1982 the total gain is 72 db for the **EMTEL** 6242.

Further, the sensor response is normalized to 1.0 at 2.51 Hz for numerical convenience. The actual value of SR (2.51) constitutes the sensor gain G^s , or

$$\mathbf{SR(2.51) = G^s}$$

The recorder response function, $RR(f)$ is the product of telemetry gain, $T(f)$ and recording device sensitivity, $R(f)$.

$$RR(f) = T(f) * R(f)$$

The telemetry gain is always set equal to **one**. The recorder sensitivity is determined by the particular input filters that were calibrated in the **laboratory**. The recorder response is normalized at 2.51 Hz and the actual value of **RR(2.51)** constitutes the recorder gain, G^R .

Therefore, the normalized seismogram system response is determined by the **SR(f)** and $RR(f)$ as shown in Figure 7.2.1. To obtain the total system response these curves have to be multiplied by the sensor gain, G^S and recorder gain G^R . If the VCO attenuation setting differs from **-42dB** it is taken into account when calculating G^S .

Typical magnification curves for data recorded by the digital data acquisition system are shown in Figure 7.2.2. The purpose of operating the low gain and the ultra-low gain instruments **is** to enable us to determine magnitudes for larger earthquakes.

Conversion of recorded amplitudes to true ground motion. A program was developed to convert the measured amplitudes to ground motion in nanometers. The appropriate TSS functions are stored for the seismometer, **VCO**, recorder combinations that are listed below. Also stored are the total gain factors for each TSS and an attenuation look-up file for handling the VCO attenuation setting variability, and extra damping pads.

Geophones

Mark **L4-C, 1B**

Geospace HS-10 (3 main coil resistances, 3 external clampings)

Norsar HS-10

Broad Band (Baby **Benioff**) SP, 1P

Amplifiers-VCO's

Entel 6242 (90 db)

Develco 6202 (120 db)

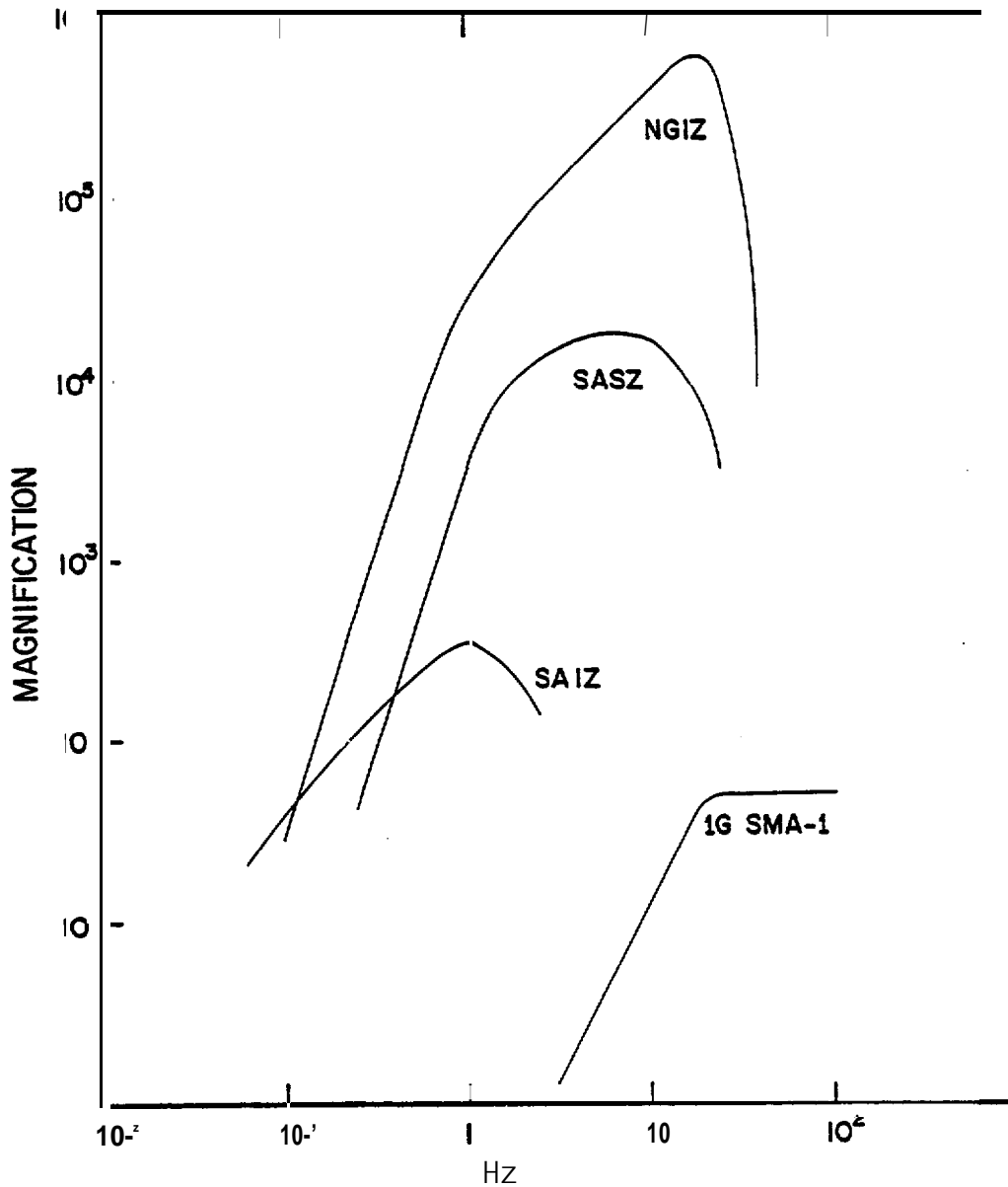


Figure 7.22. Magnification curves for a typical high gain short-period station (NGI at 48 db Amp/VCO gain); the low gain short-period seismometers at Sand Point (SASZ) and the ultra-low gain intermediate period seismometers at Sand Point (SAIZ). The magnification curve for a strong motion accelerograph (1G SMA-1) is shown for comparison.

Recorders

Develocorder

TEAC analog to digital

Digital system (ADC gain 1, 2)

Helicorder

Crown analog tape

Sangamo analog tape

True ground motion **is** simply the recorded amplitude divided by **the** product of the total seismograph system response, total gain and attenuation factors.

Calculation of earthquake magnitude. To determine the local magnitude scale such that **it is** calibrated with respect to the body wave magnitude, m_b published **in** monthly PDE bulletins, the following approach is taken:

From Richter (1958) we have for a Wood-Anderson instrument

$$M_L = \log A - \log A_0$$

where A is **the** zero to peak of the largest phase on the record in mm and A_0 **is** a distance correction. When correcting for the gain **of** the W-A we obtain

$$M_L = \log (A/2800) - \log A. + \log 2800$$

$$M_L = \log (A_q) - 6 + \log 2800 - \log A_0$$

where A_q now is measured ground **motion in** nanometers (rim). Instead of measuring the largest phase on the record which **in** our case is **most** often a surface wave or an S-wave, **we** measure the largest amplitude in the P-wave train. This permits us to determine a local body wave magnitude as

$$m_b = \log A_{pq} - 2.55 - \log A_0.$$

We prefer to use the largest P-wave amplitude (A_{pg}) since it is less often saturated or clipped than the **S-** or surface wave amplitudes.

To compare the values of magnitudes determined by the **Shumagin** network with values published by the National Earthquake Information Service (**NEIS**) in monthly or weekly PDE bulletins, we have plotted in Figure 7.2.3 magnitudes from PDE against magnitudes from the **Shumagin** network. The data are tabulated also in Table 7.2.1. We note that nearly all the PDE or **PMR** magnitudes are greater than 4.0. Unfortunately, this is the range where the **Shumagin** network starts saturating and amplitudes of earthquakes larger than magnitude 4.0 may be clipped. Nonetheless, the data plotted in Figure 7.2.3 indicate that the **Shumagin** magnitudes in the range from 3.0 to 5.0 are underestimated by 0.3-0.5 magnitude units. (These Shumagin magnitudes are shown in columns 73-75 in data files submitted to NOAA).

Coda length magnitude. In rare cases we still report coda length magnitudes when a body wave magnitude cannot be determined. The surface wave magnitude, i.e., coda length magnitude, reported (as shown in **cols.** 61-63 in data files submitted to NOAA) are determined using the FMAG formulation of **J.C.** Lahr (1980) and his empirical constants derived for Alaska.

$$FMAG = C_1 + C_2 \log (F_\gamma) + C_3 \Delta + C_4 Z + C_5 (\log (F_\gamma))^2$$

$$\begin{array}{lll} C_1 = -1.15 & C_3 = 0.0035 & C_5 = 0.0 \\ C_2 = 2.0 & C_4 = 0.007 & \end{array}$$

C_5 may be determined in the future with a larger data set "to compensate for the nonlinear relationship of \log (coda) and magnitude."

F = F-P time; measured from P onset to 1 cm p-p amplitude cut-off

Δ = epicentral distance (km)

Z = hypocentral depth (km)

γ = station correction (1 used here)

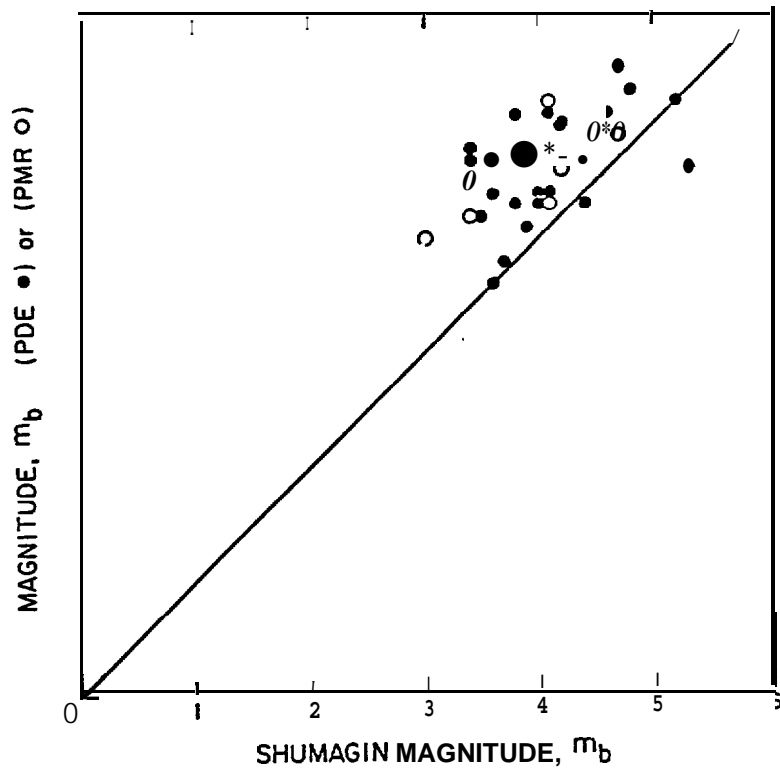


Figure 7.2.3. Comparison between magnitude values determined by the Shumagin network and values published by NEIS in monthly and weekly PDE-bulletins. The straight line has a slope of one. Open circles are PMR magnitudes.

TABLE 7.2.1. Earthquakes Located by Both the Shumagin Network and PDE

The respective magnitudes are plotted in Figure 7.2.3.

<u>Date.Time</u>	<u>Shumagin</u>		<u>Depth</u> (km)	<u>Xmag.</u>	<u>PMR</u>	<u>MB</u>	<u>Avg.</u>	<u>Msz</u>
	<u>Latitude</u>	<u>Longitude</u>						
810107.165917	55N50	154W4 1	6*	3.4	4.5m	4.8m	4.8	
810417.232919	57N59	154W06	94*	5.3		4.5w/4.6m	4.6	
810510.225302	56N22	161W21	200	4.0		4.3w/m	4.3	
810524.102339	55N58	159W24	118	3.2				
810605.070951	52N24	164W52	11*	4.7	4.9w/m	5.5w/m	5.5	4.6w
810607.175257	53N24	164W51	17*	4.3	4.6w/m	5.0w/m	5.0	
810613.132129	53N25	163W13	3	4.3		4.9w/5.0m	5.0	4.4w/m
810625.013632	54N50	159W45	31	4.1	5.2w/m	4.8w/m	4.8	
810801.014319	59N21	150W54	160*	5.2		5.1w/5.2m	5.2	
810815.103113	56N06	156W46	77	4.1		5.1w	5.1	
810818.225548	55N39	158W43	39	3.6		4.4w/m	4.4	
810906.132045	56N32	156W09	45*	3.8		4.3w/m	4.3	
810913.201210	54N16	163W43	66	3.0	4.0m			
810927.121347	57N09	153W25	154*	3.6				
811114.004324	53N44	164W30	81	4.6		5.1w/m	5.1	
811118.193511	53N22	163W58	30	3.6		4.7m	4.7	
811209.122.304	52N50	154W37	33*	4.5	4.9	4.9w/m	4.9	
811228.102821	54N44	160W37	30	3.7	3.8w		3.8	
820102.202712	55N35	157W13	13*	4.1	4.3m	4.4m	4.4	
820122.090046	55N49	159W00	84	4.0		4.4w/m	4.4	
820129.140307	53N31	163W55	3	3.4	4.2w/m	4.7w/m	4.7	
820131.112437	58N52	153W31	68*	4.4		4.3w/m	4.3	
820216.180231		156W21	8	4.0		4.7w/m	4.7	
820219.025102	53N36	164W35	10	4.4		4.7w/4.6m	4.7	
820315.145325	52N42	162W00	4	3.8		5.1w/5.0m	5.1	4.3w/m
820404.234113	52N45	167W15	1*	3.9		4.3w/m	4.3	
820415.162109	54N01	161W28	23*	4.8		5.3w/m	5.3	
820416.084700	53N21	163W09	11*	3.5		4.2w/m	4.2	
820416.084946	53N2 3	163W06	6	3.6		3.6w/m	3.6	

*Assigned depth of hypocenter; w-weekly, m-monthly PDE Bulletin, Aug. - PDE magnitude plotted in Fig. 7.2.3.

7.3 Annual Plots of Shumagin Network Seismicity 1973-1982

As a necessary step in preparing this report we put a large effort into reorganizing, refining and recompiling all the **arrival** time data recorded by the Shumagin network and the computed hypocenters since 1973 to the middle of 1982.

First the arrival time data was organized into monthly **pickfiles** (e.g., files containing all the arrival times of all the events recorded during that month) in a standard **HYPOINVERSE** format. Then the whole data set was relocated using **HYPOINVERSE** (Klein, 1978). To choose a reasonable trial depth each month of data was passed through a filter that simulates a Reyners and **Coles** (1982) cross section. **If** a **hypocenter** happened to be located outside of the filter boundaries, several different possible values of trial depth were tried until a consistent solution was found.

The results of this effort are shown below in Figures 7.3.1 through 7.3.11. Table 7.3.1 contains the total number of located earthquakes each year. In Figure 7.3.11 we have plotted all the earthquakes that were located by the **Shumagin** network from 1973 to 1981. Each year of data, which contains all locatable earthquakes observed during that year, **is** shown also separately in Figures 7.3.1 through 7.3.10. Although the continuity of data recording varies considerably through time, the annual **seismicity** maps and cross sections indicate how the seismic activity changes in space from one **year** to another. Both variations **in** the scattered background **seismicity** and temporal occurrence of seismicity clusters **can** be seen in the annual **plots**. Each cross section is taken along the line shown on the respective map striking north 30° west. The different symbols indicate within which depth range the earthquake is located, (triangles: **0-40 km**; x: **40-120 km**; diamonds: **120-250 km**; and rectangles: depth greater than 250 km). No magnitude information is included **in** Figures 7.3.1 through 7.3.11.

We have used the flat-layered earth **model that is** shown in Table 7.3.2 to locate earthquakes beneath the Shumagin Islands network. Some of the features **in** the cross sections show linear clusters of **hypocenters** at constant depths which coincide with the layer

boundaries in this model. This artifact is caused by poor depth control which mainly results from incomplete network coverage in offshore regions.

As an aid for studying Figures 7.3.1 through 7.3.11 we summarize the most important characteristics of each data set below:

1973 (Figure 7.3.1). Generally scattered **seismicity**, similar to the patterns observed in 1975 and **1981**. A cluster of seismicity is located below **Kupreanof** Volcano on the Alaska Peninsula.

1974 (Figure 7.3.2). The large cluster located at the southern end of the Nagai Island included two moderate size earthquakes ($m_b = 5.8, 6.0$).

1975 (Figure 7.3.3). Generally" scattered **seismicity** similar to the pattern observed **in** 1981. The Cold Bay link was installed and hence, event detection was improved west and south of Cold Bay and **Sanak** Island.

1976 (**Figure 7.3.4**). Scattered seismicity and some small **clusters** near the **Nagai** Island.

1977 (Figure 7.3.5). The seismicity is evenly scattered throughout the **Shumagin** Islands region.

1978 (Figure 7.3.6). Concentrated activity located **west** of the **Shumagin** Islands. A cluster of activity near the Korovin Island continues in 1979.

1979 (Figure 7.3.7). Several earthquakes deeper than 200 km were observed. High level of activity along and above the lower edge of the main thrust zone accounts for the doubling of number of earthquakes located in 1979. A main shock of magnitude (**M_s**) 6.5 was located at **55.1°N** and **157.0°W**.

- 1980 (Figure 7.3.8). The seismicity is less scattered than during 1981. A wide band of seismicity **subparallel** to the Sanak Basin and concentrated clusters in the Port **Moller** region and near Nagai Island are prominent features during 1980.
- 1981 (Figure 7.3.9). The **seismicity** is evenly scattered throughout most of the Shumagin region. A cluster of **seismicity** appears east of Sanak Island.
- 1982 (Figure 7.3.10). Prominent cluster of shallow activity located west of Deer Island. The lower plane of the Benioff zone is unusually quiescent. High level of activity south and west of **Sanak** Island.
- 1973-1981 (Figure 7.3.11). Note the high **level** of **activity** along the lower edge of the main thrust zone and **within** the upper plate along the southeastern part of **the** Shelf. This activity may indicate the existence of possible **imbricate** thrust faults. The main thrust zone is a region of low level of activity. Horizontal bands of seismicity (seen in the cross section) are caused by the lack of depth control. The upper plane of the Benioff zone has a higher level of seismic activity than the lower plane.

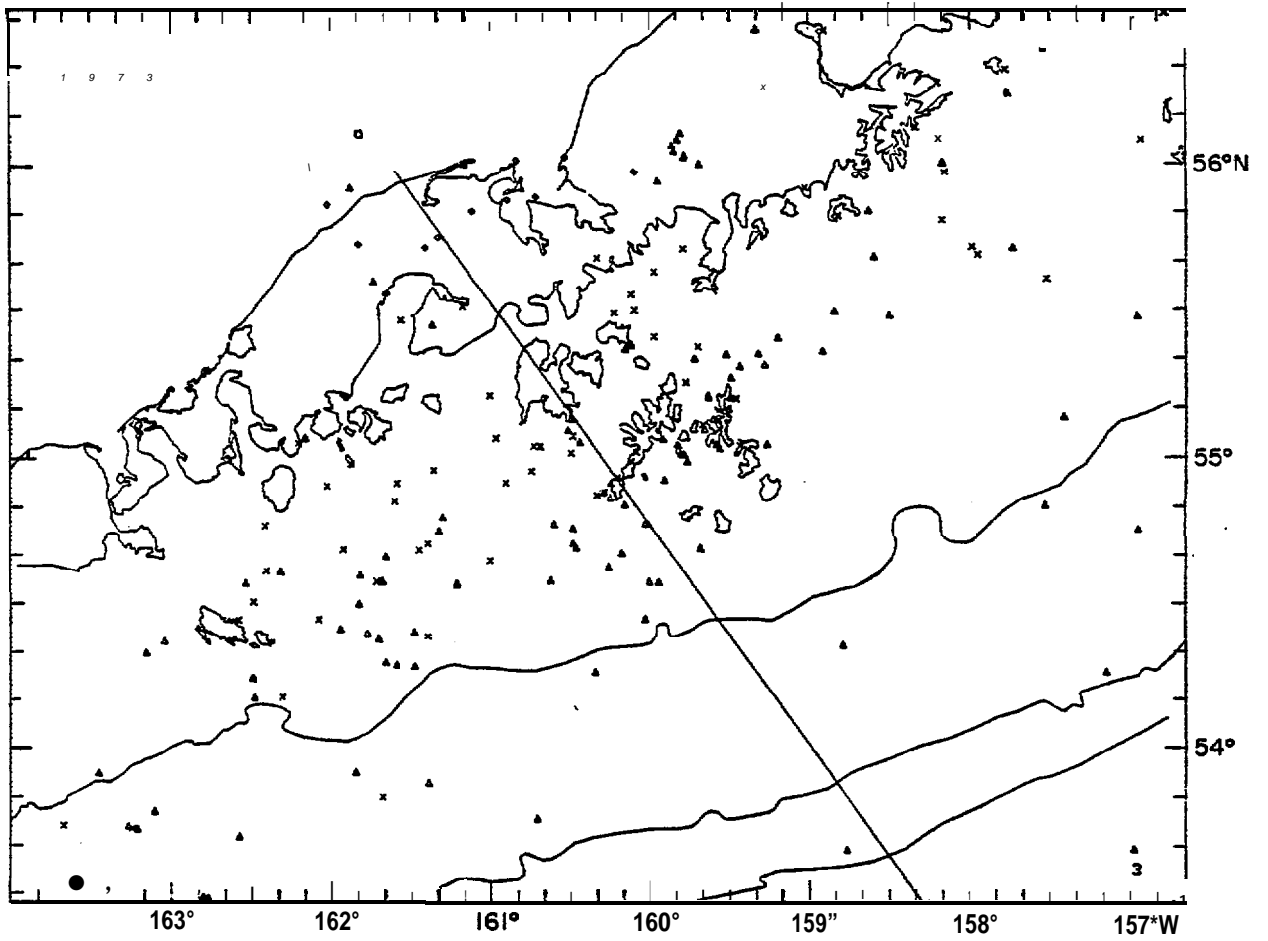
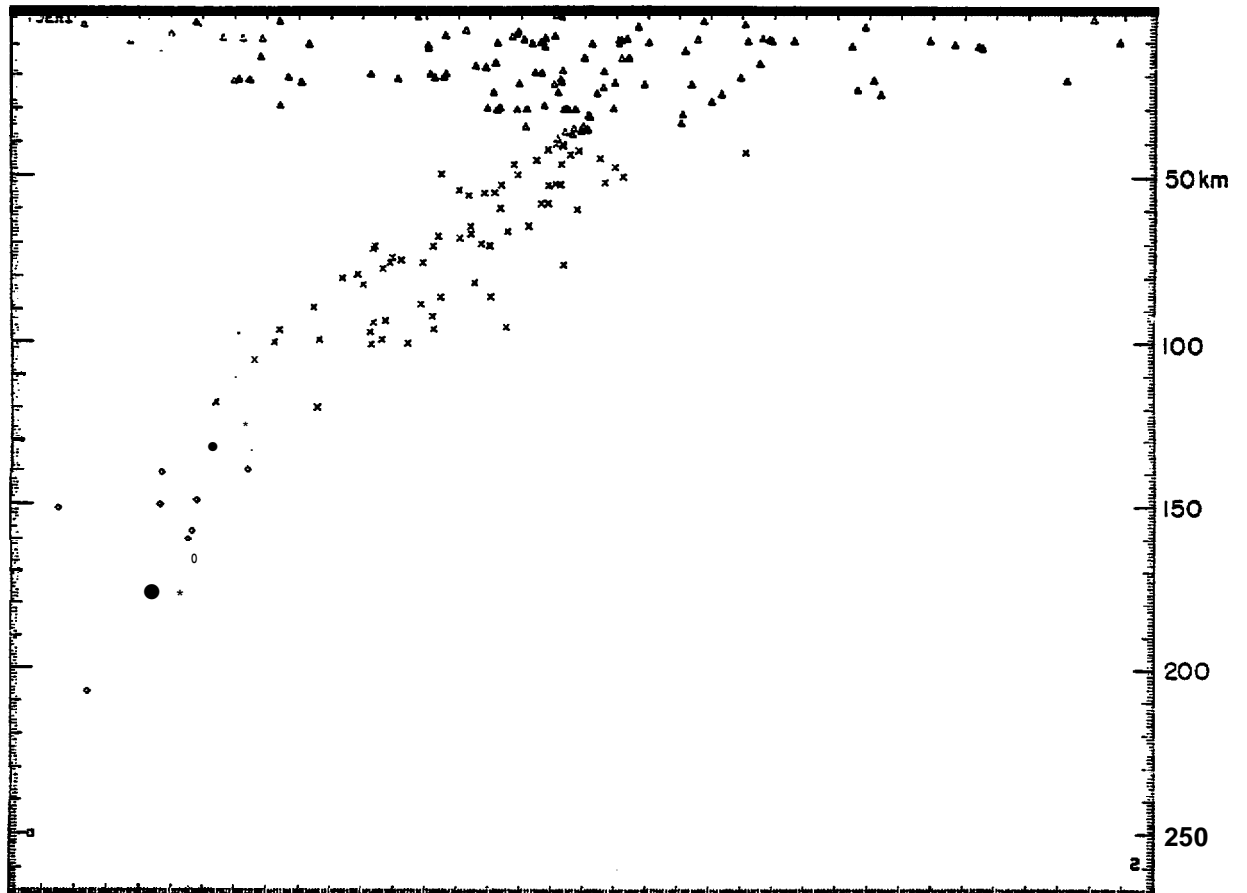


Figure 7.3.1. Seismicity located by the Shumagin network during 1973.



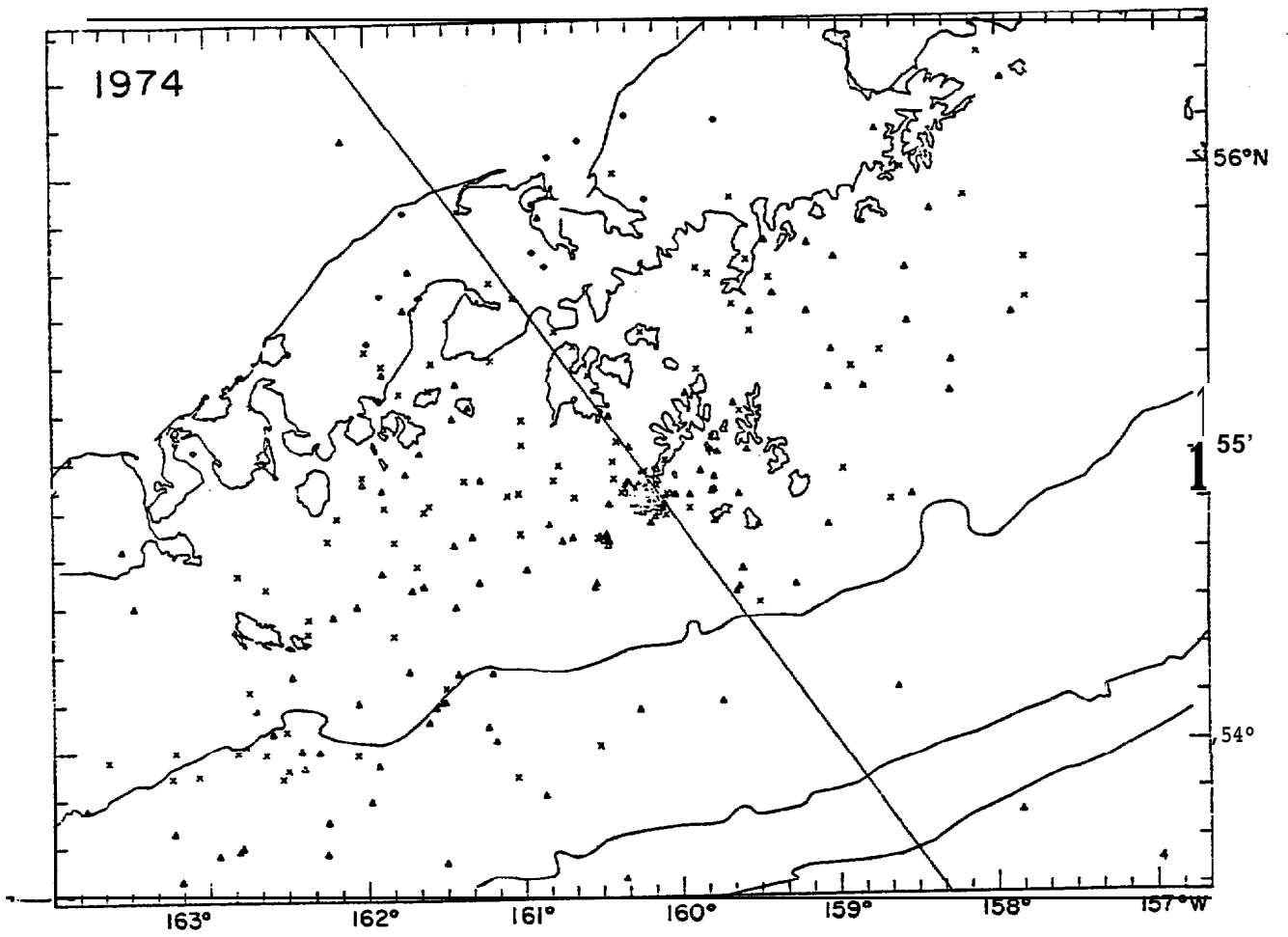
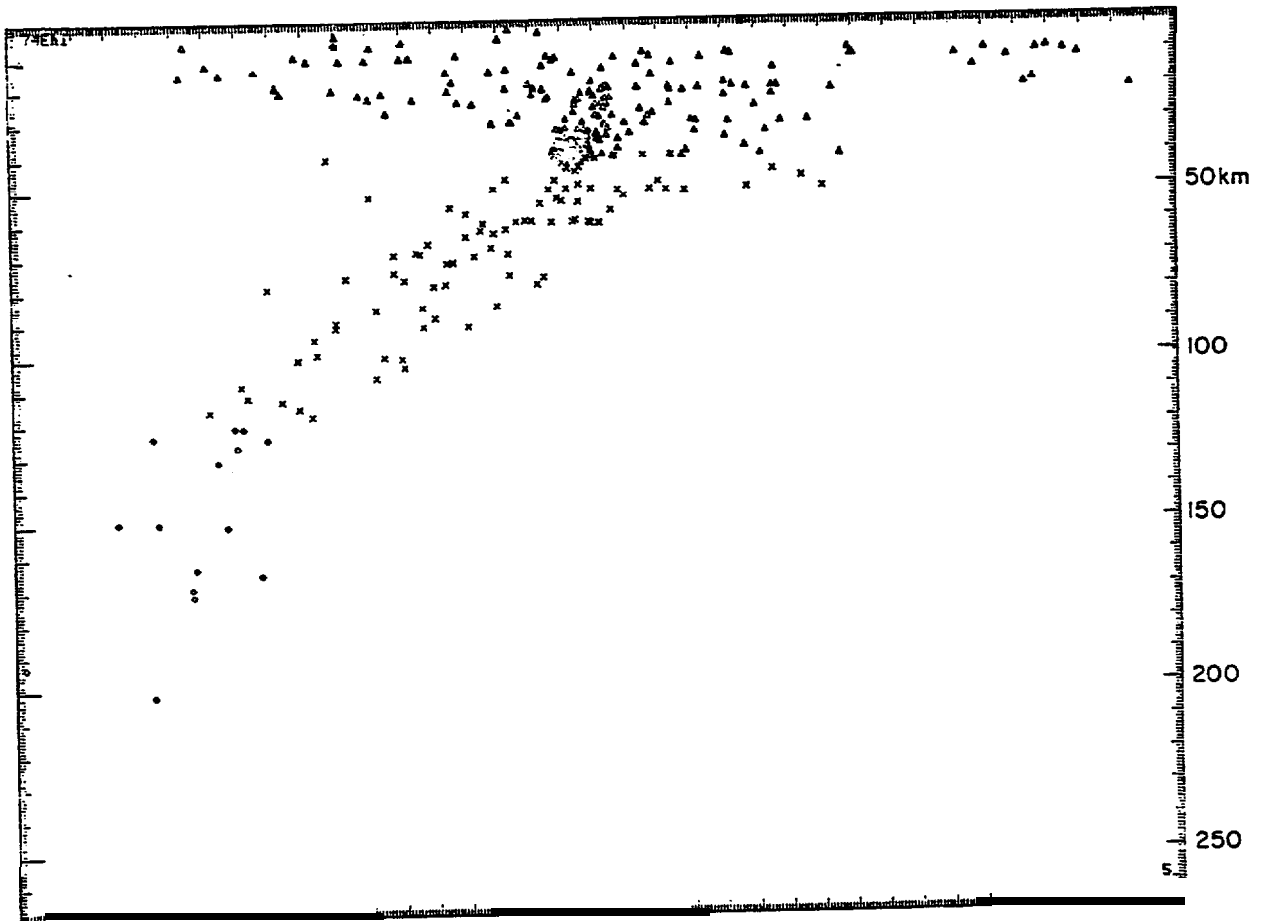


Figure 7.3.2. Seismicity located by the Shumagin network during 1974.



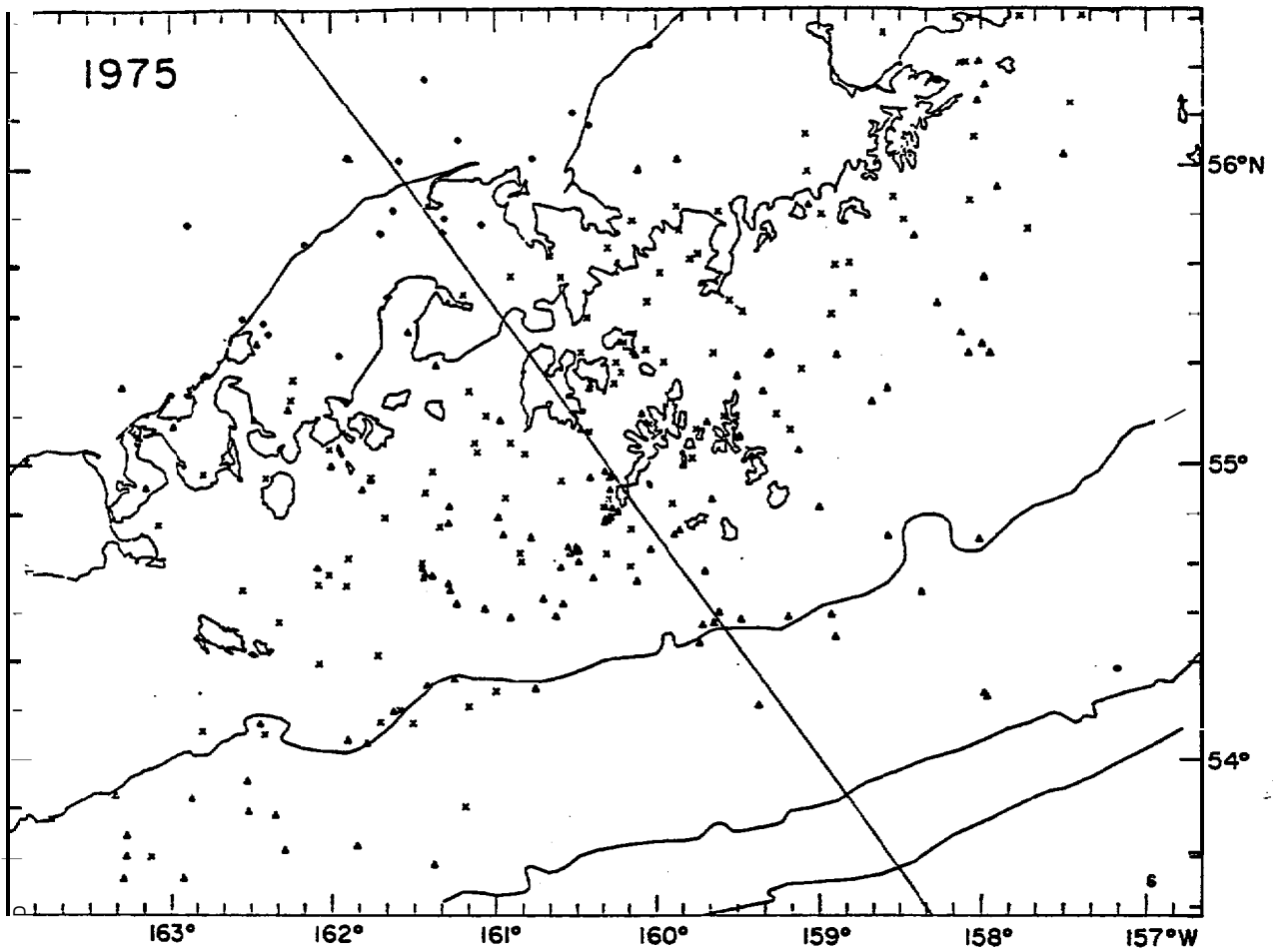
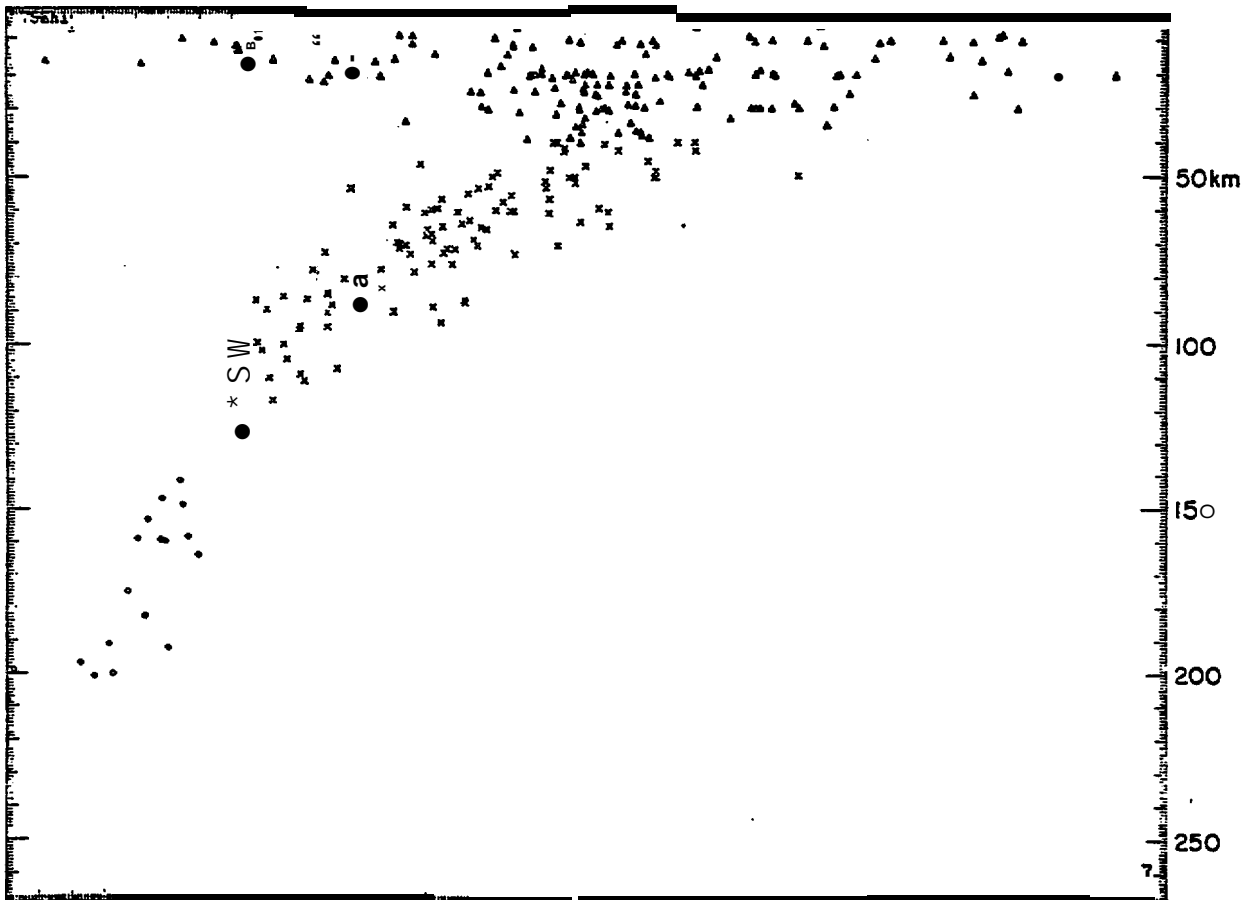


Figure 7.3.3. Seismicity located by the Shumagin network during 1975.



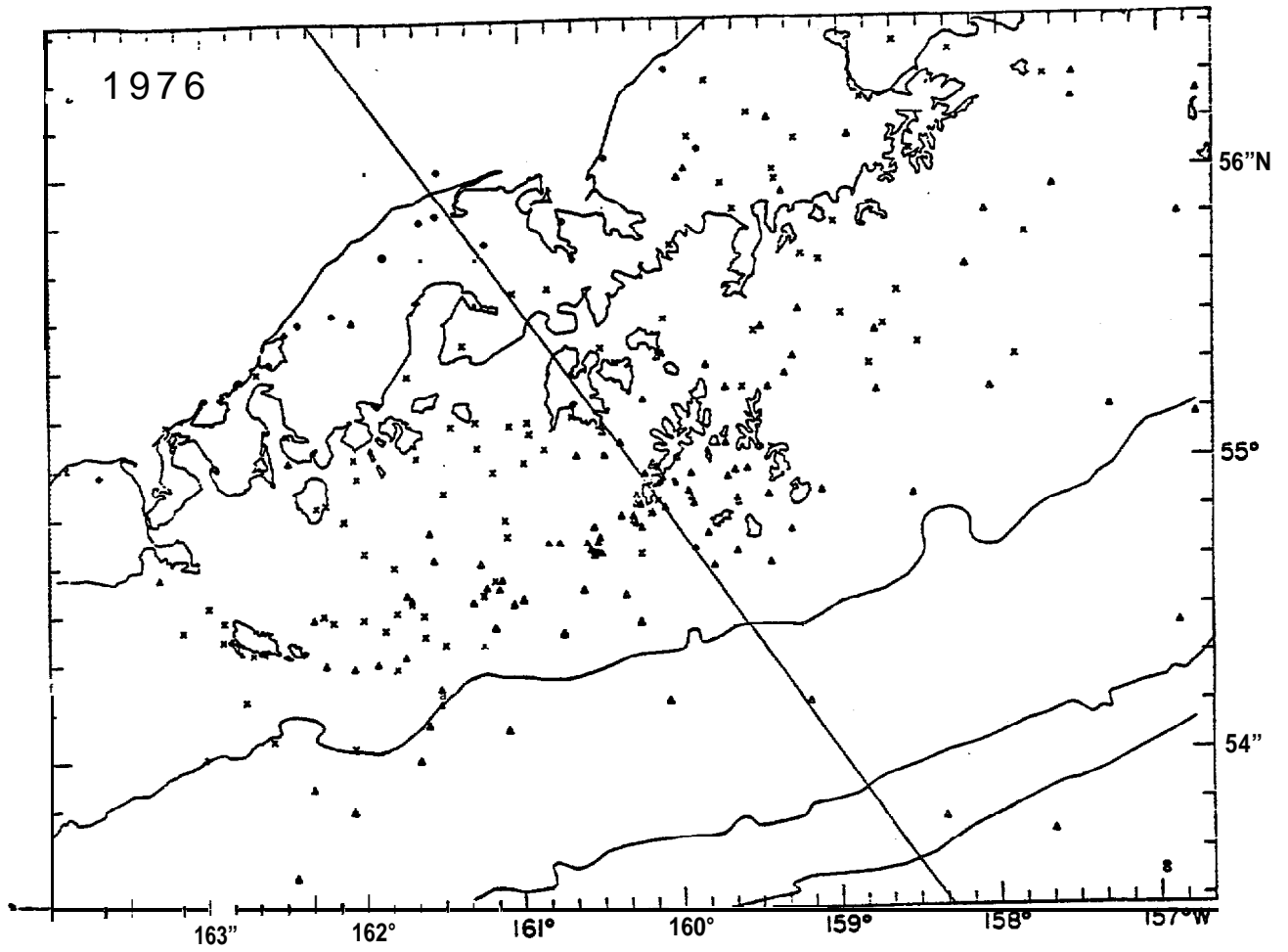
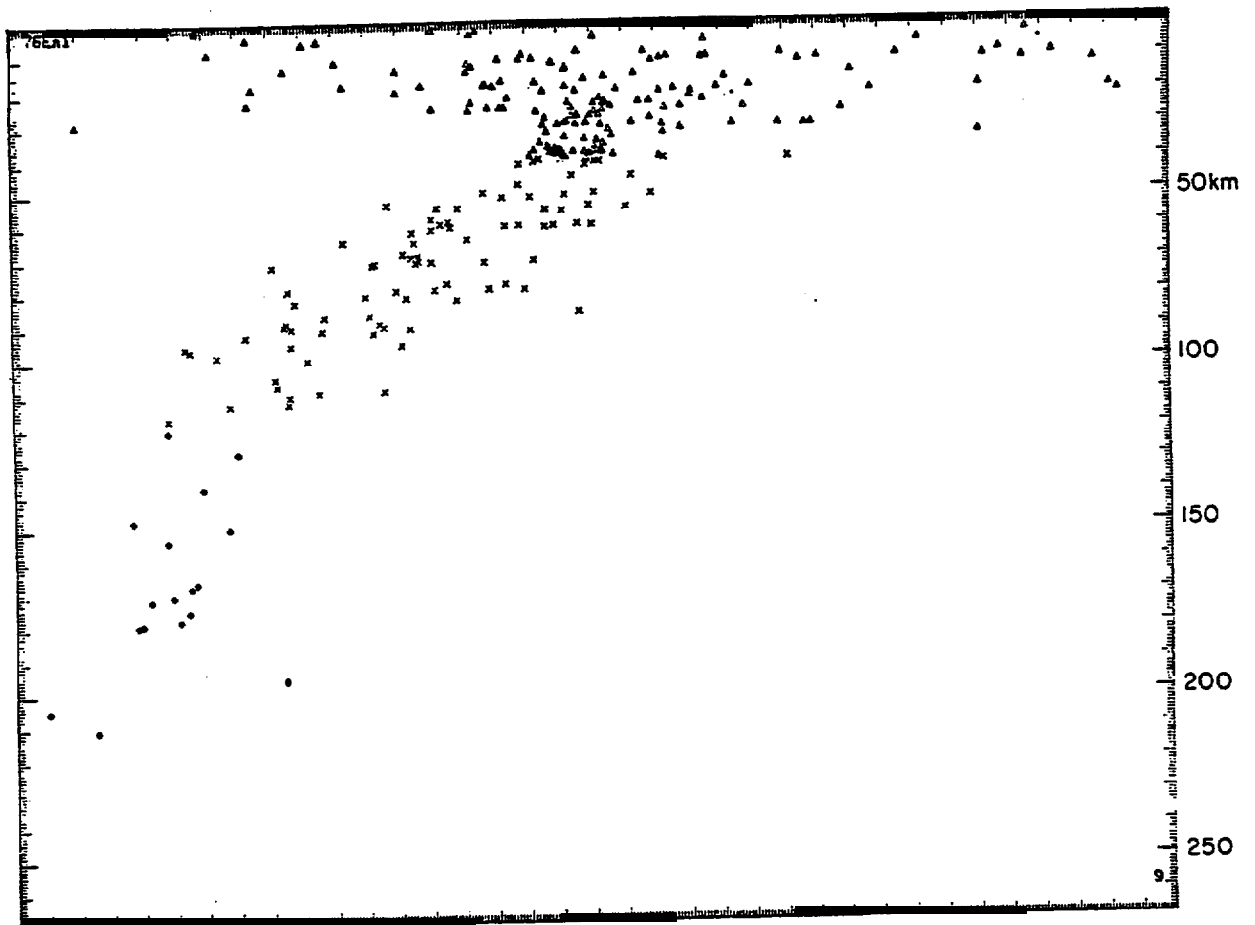


Figure 7.3.4. Seismicity located by the Shumagin network during 1976.



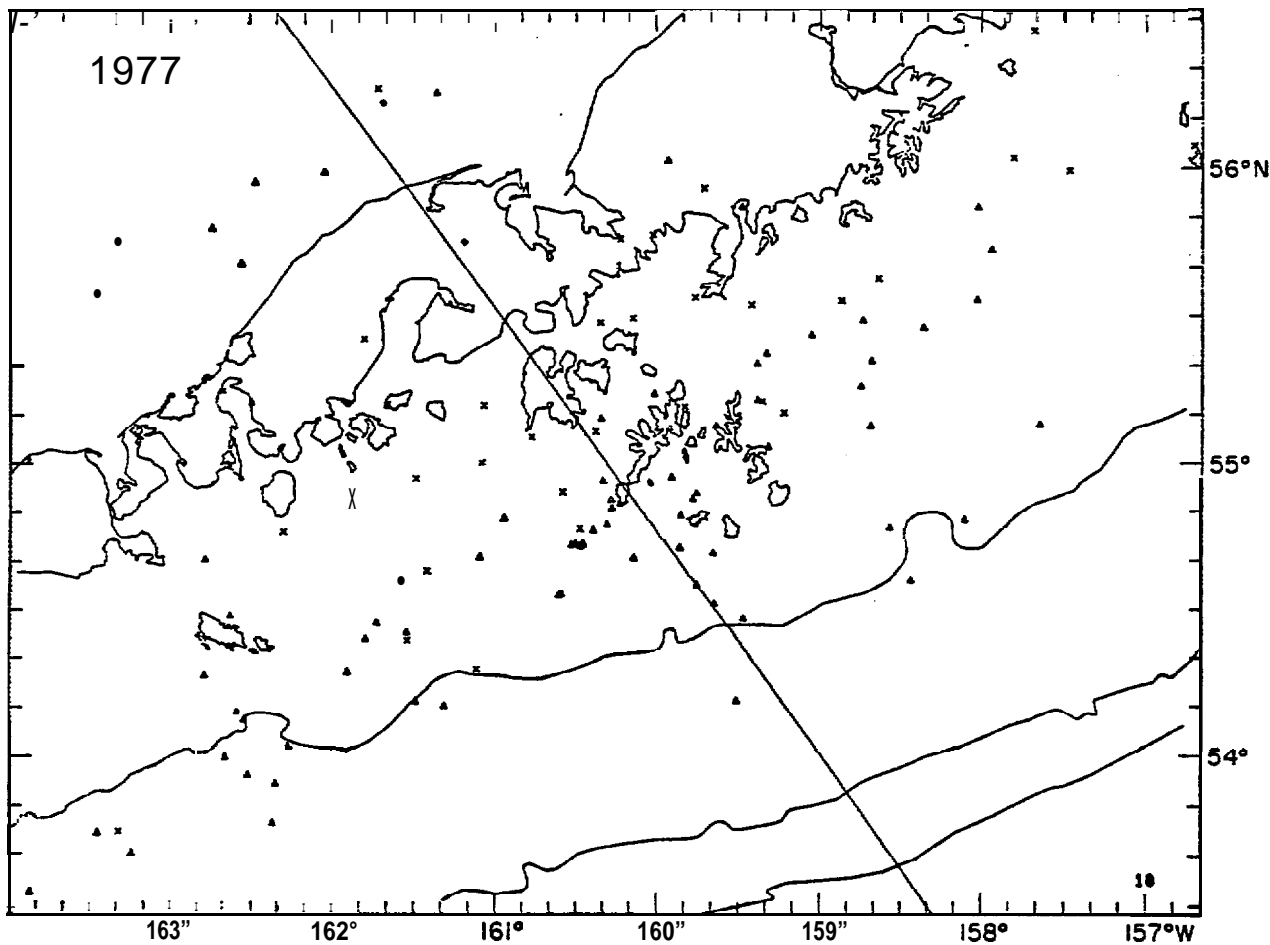
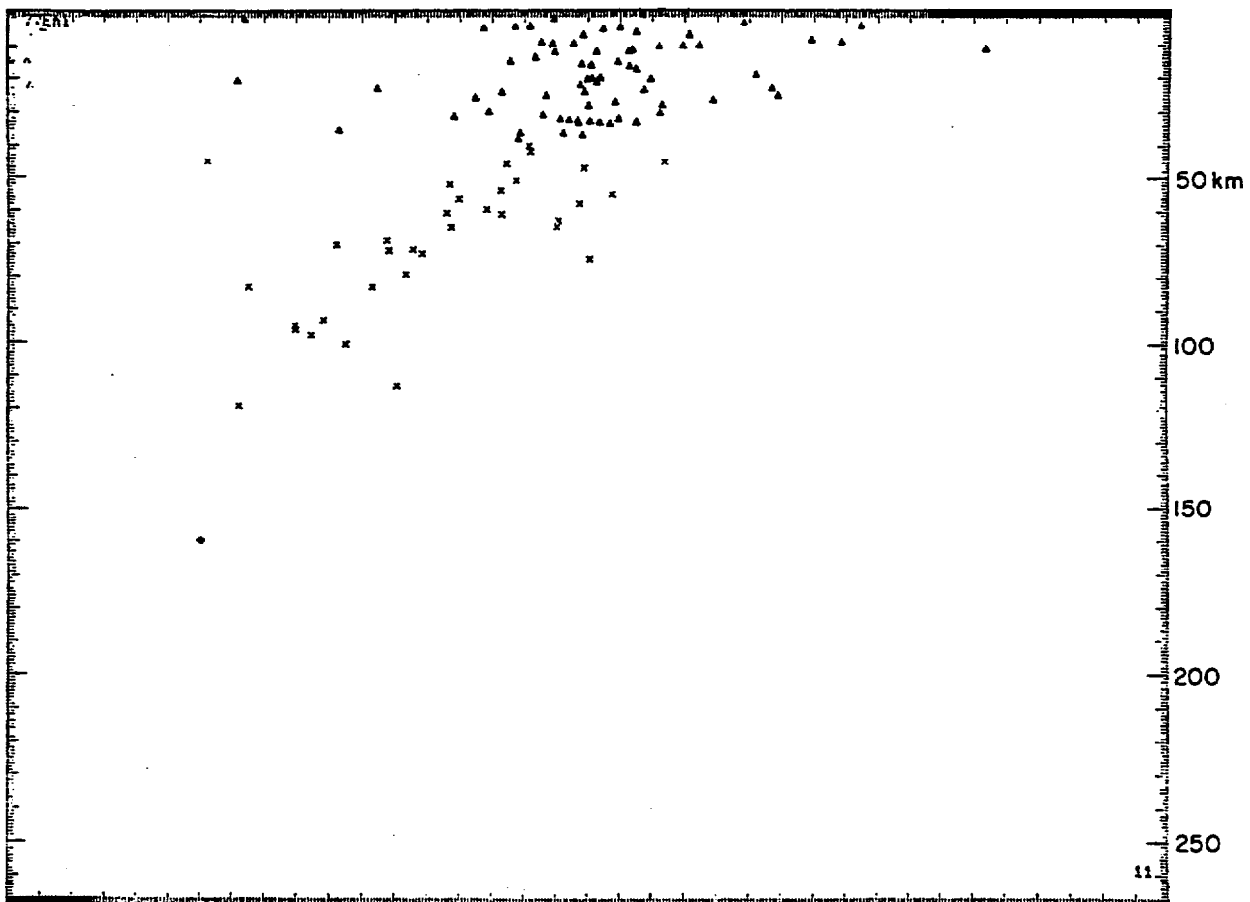


Figure 7.3.5. Seismicity located by the Shumagin' network during 1977.



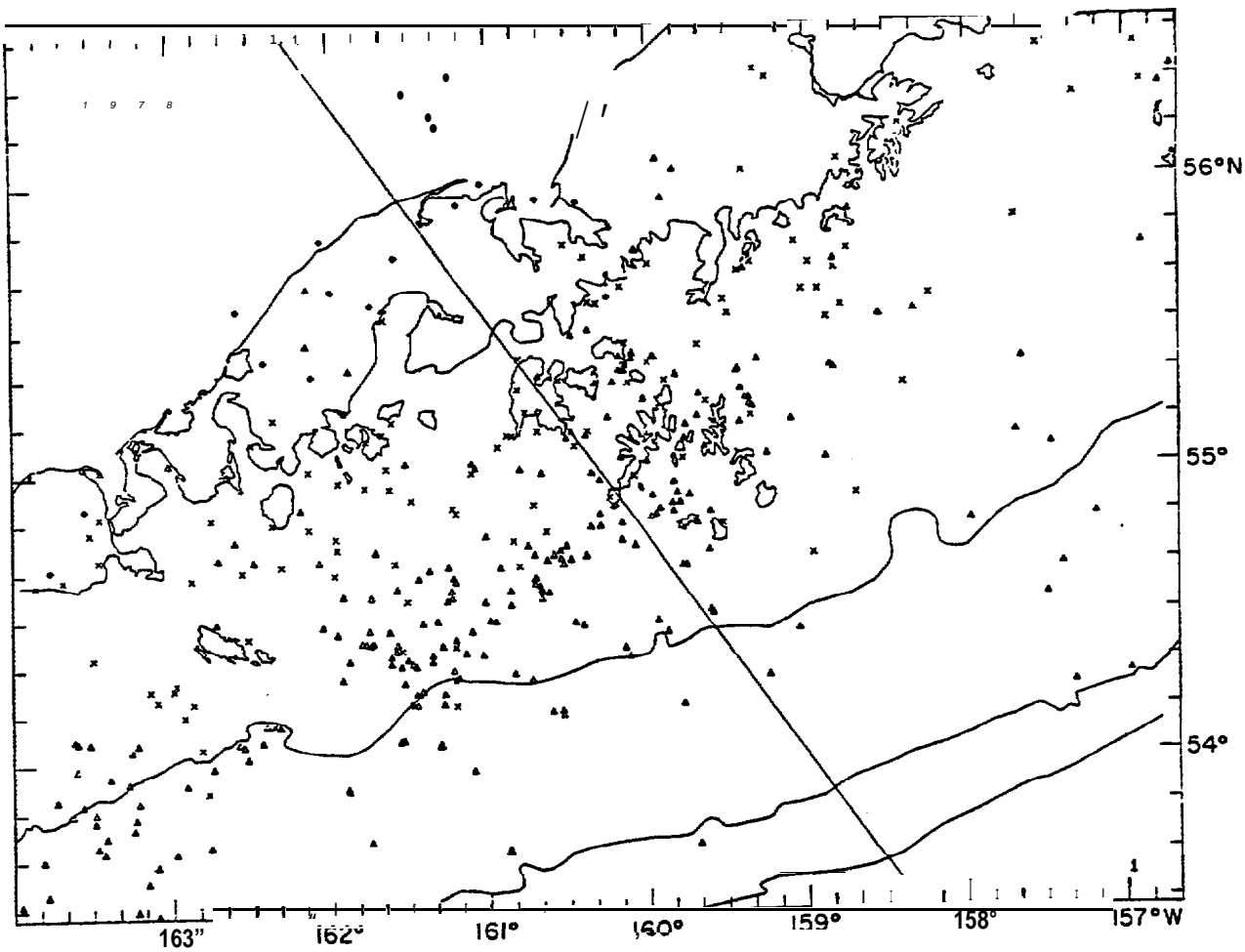
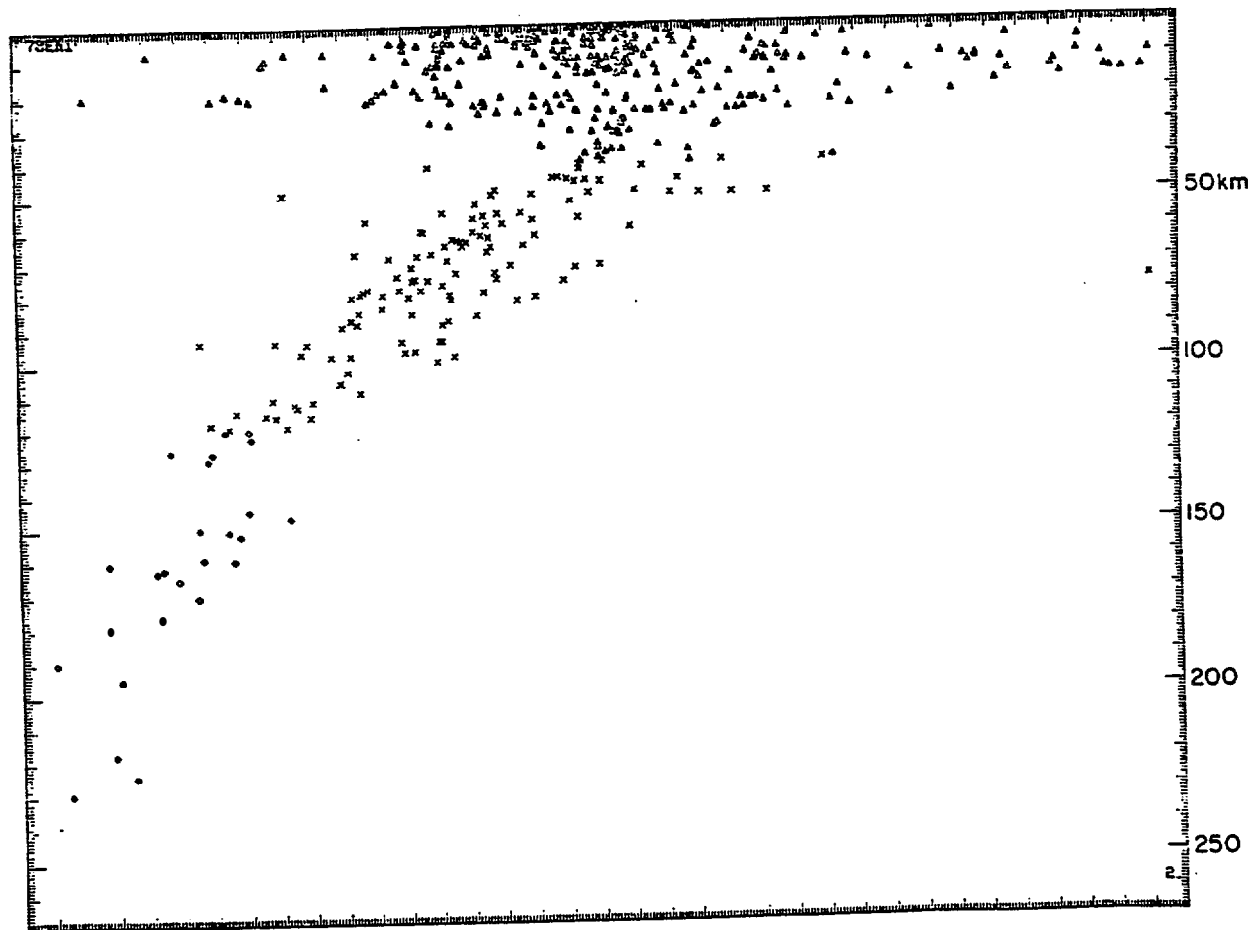


Figure 7.3.6. Seismicity located by the Shumagin Network during 1978.



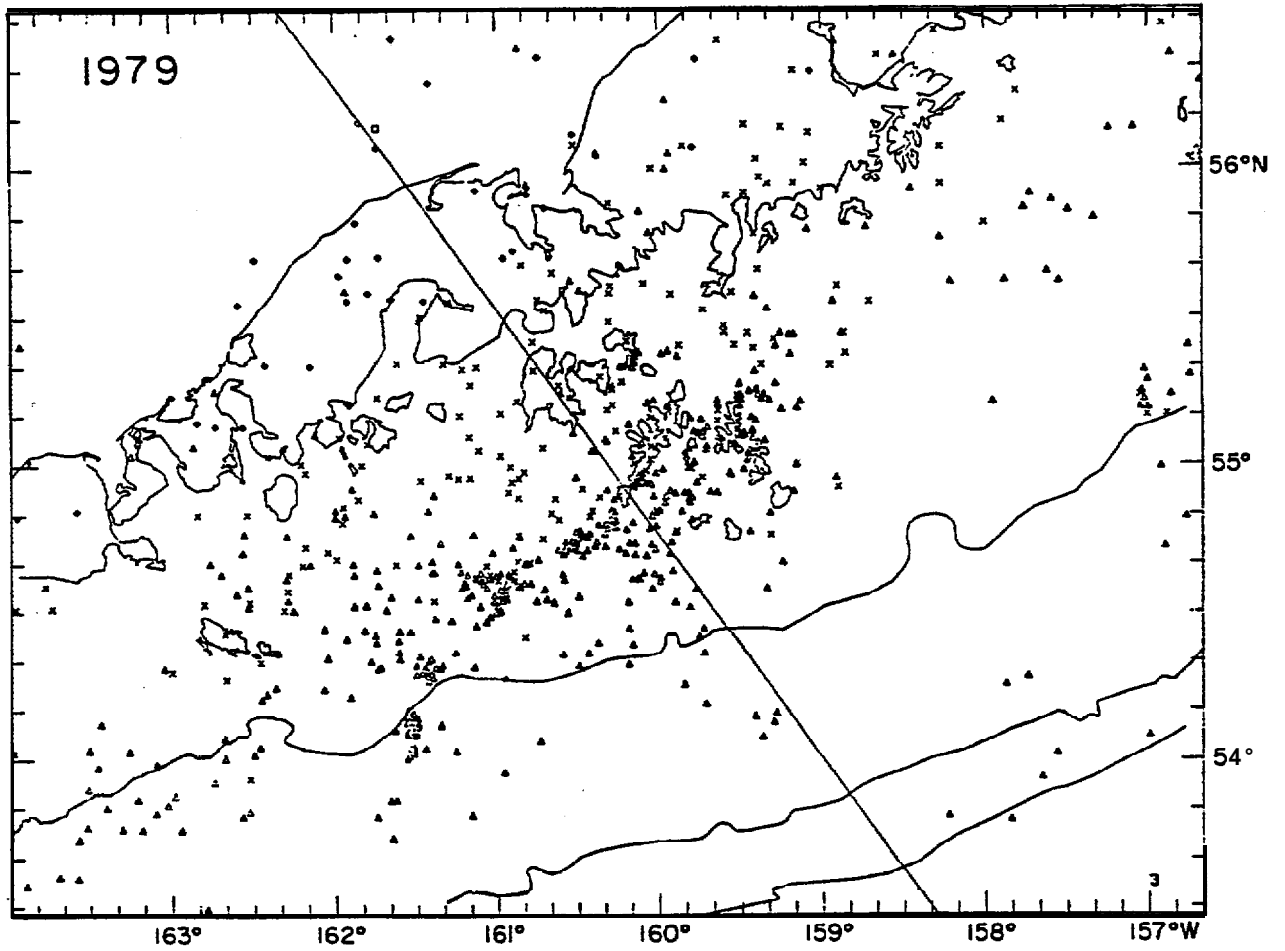
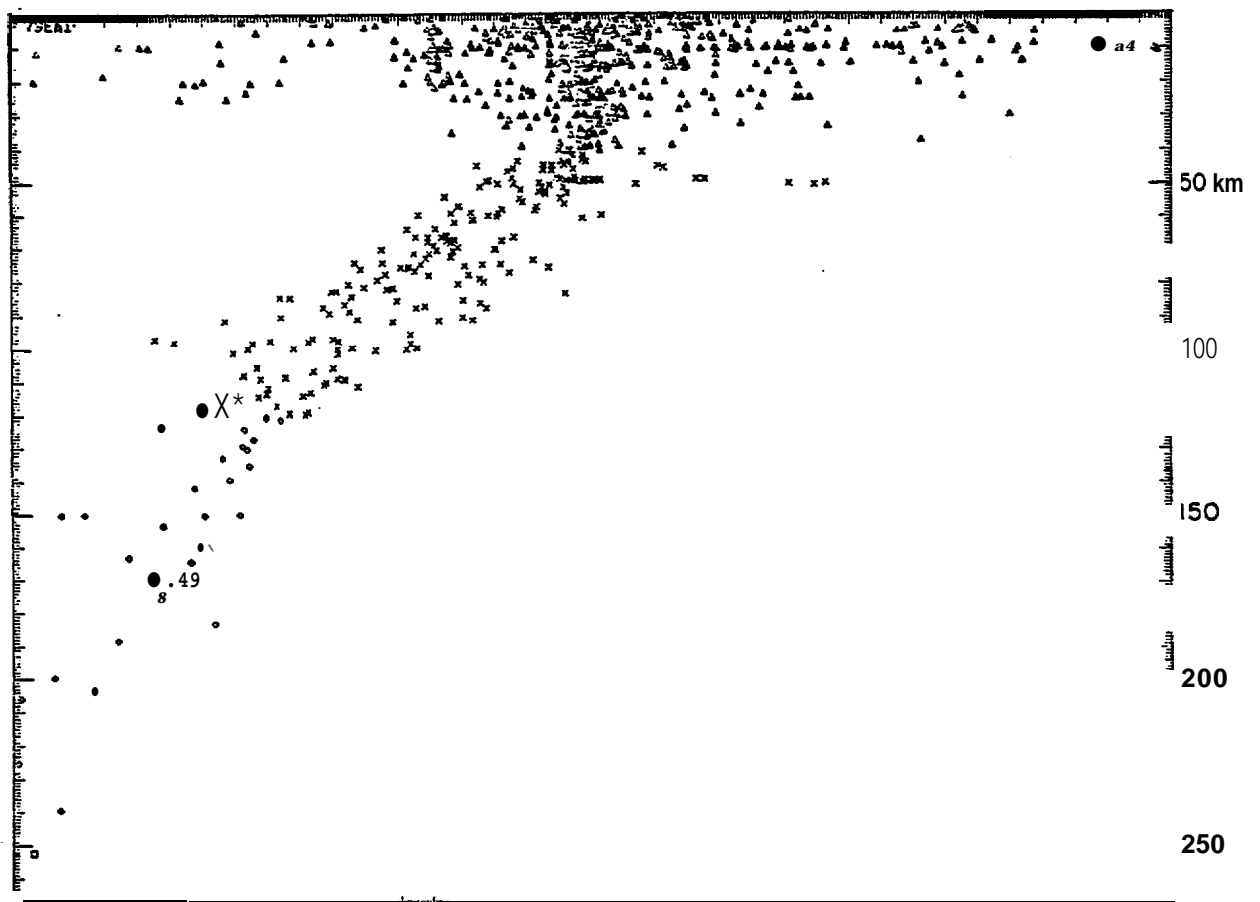


Figure 7.3.7. Seismicity located by the Shumagin network during 1979.



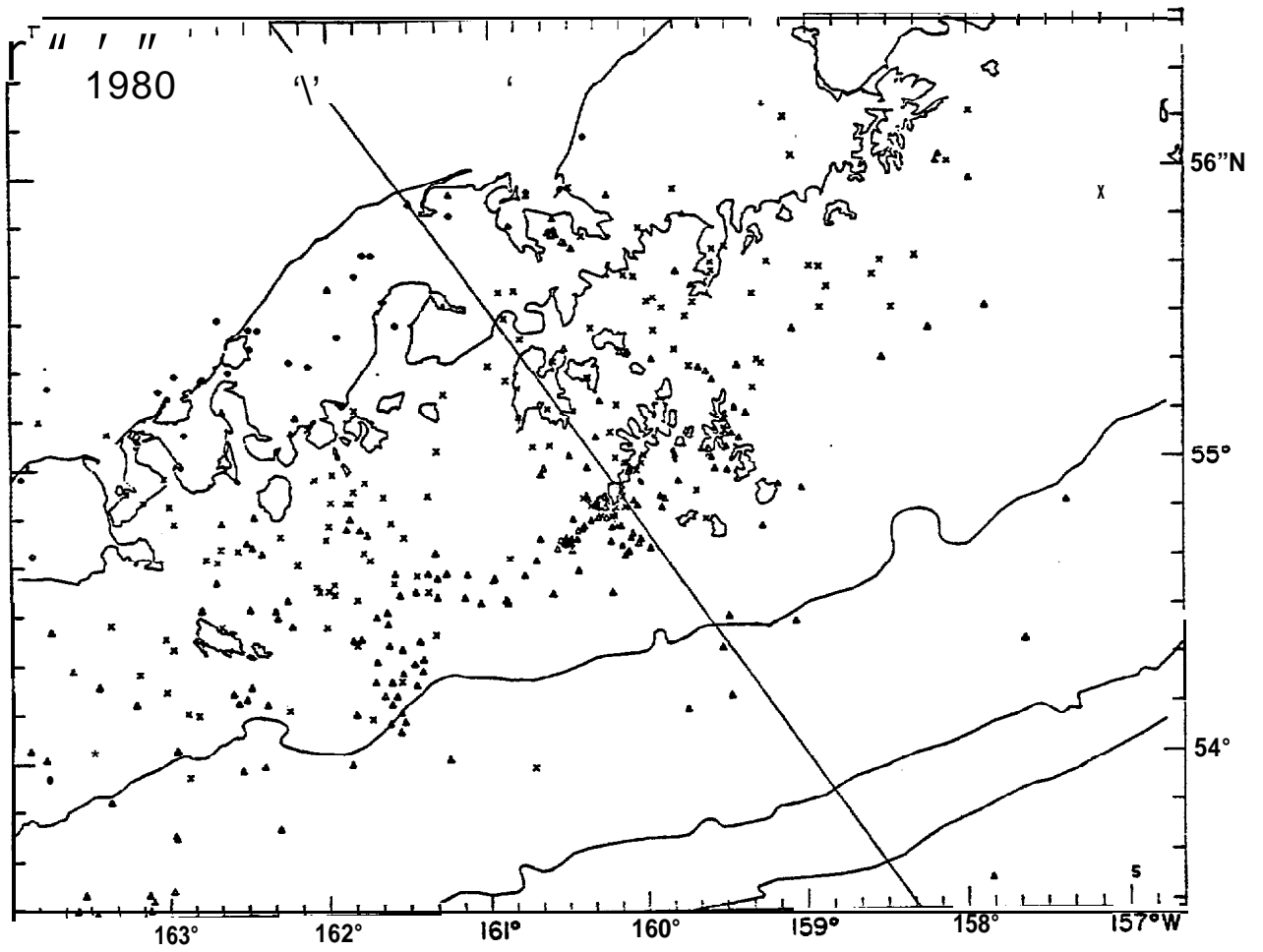
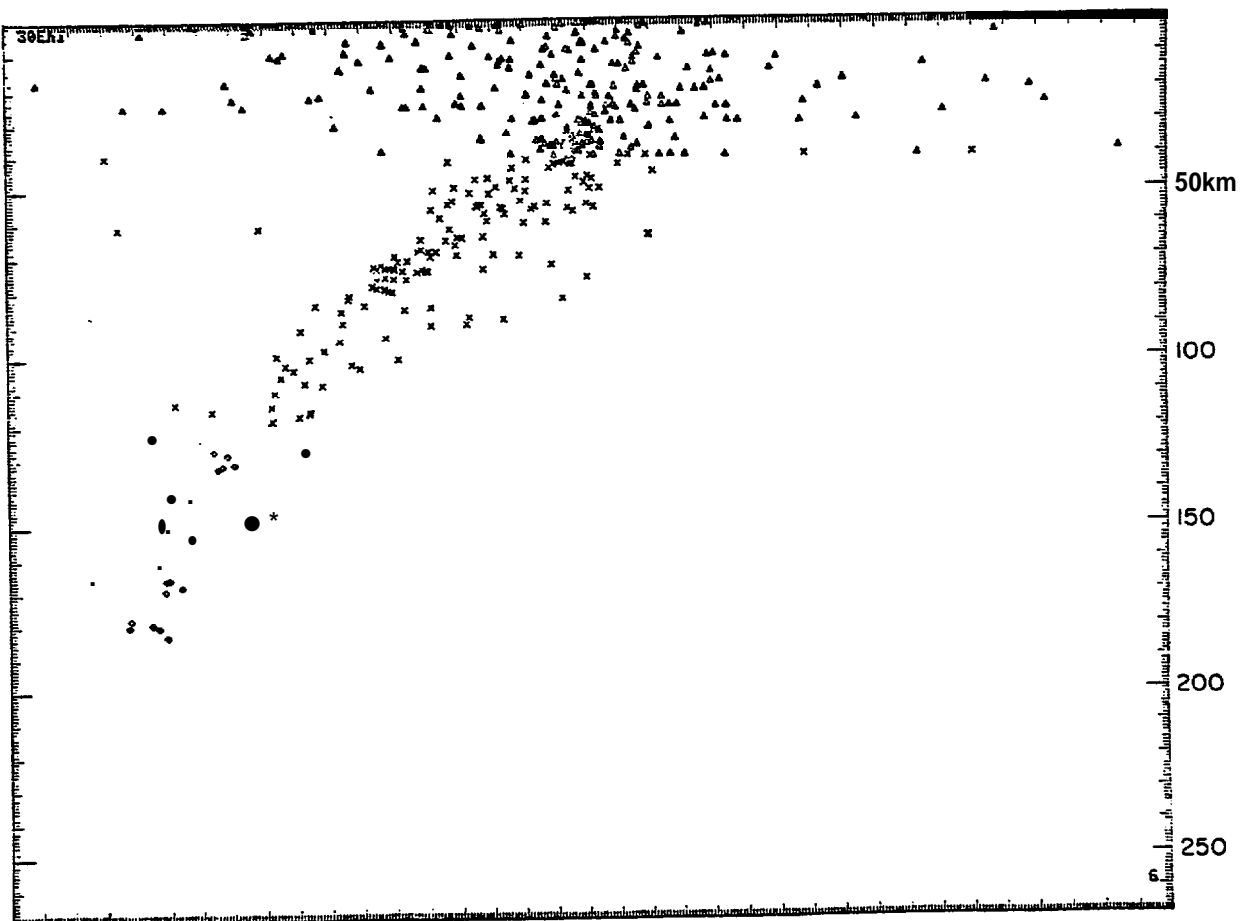


Figure 7.3.8. Seismicity located by the Shumagin Network during 1980.



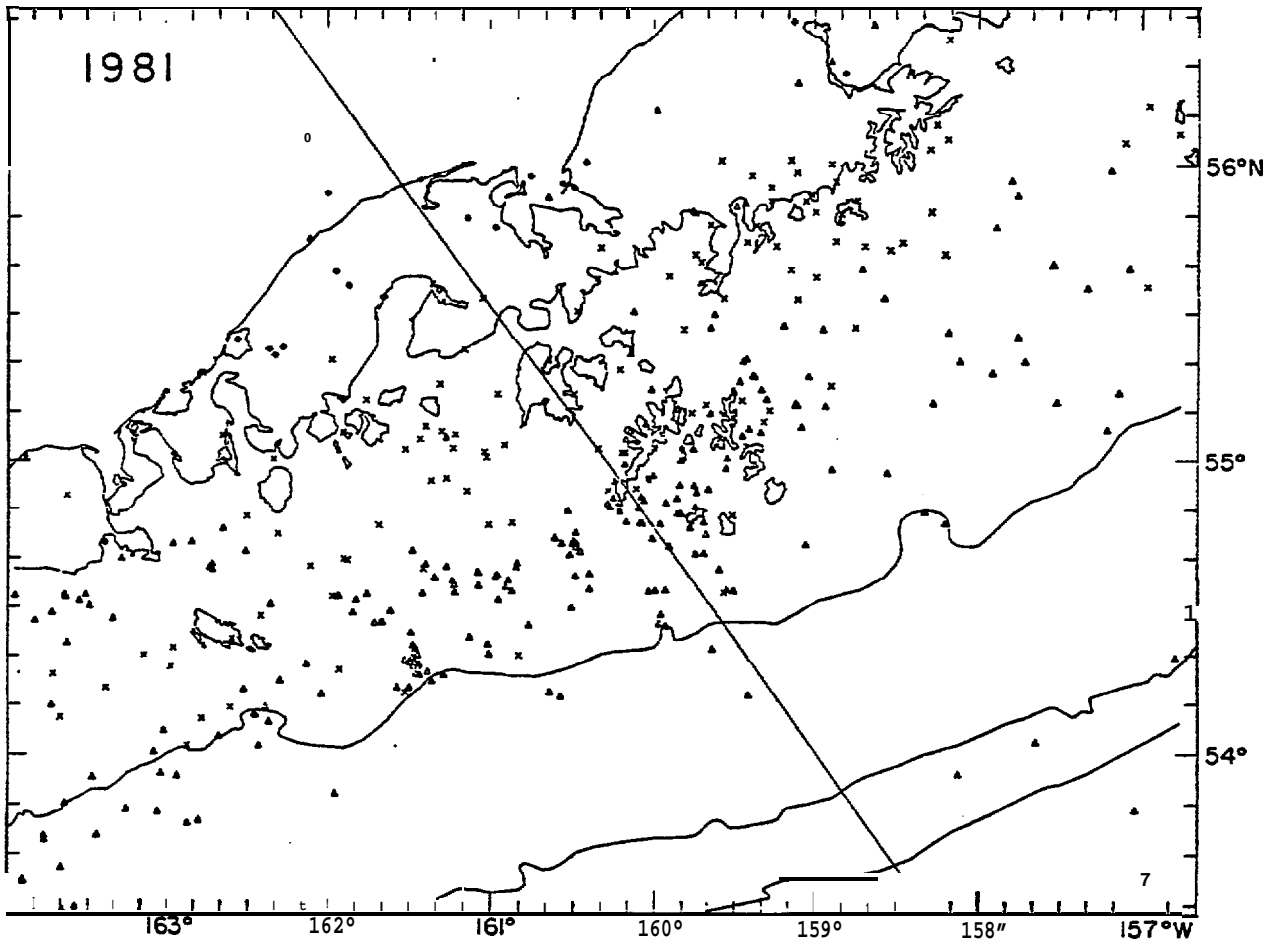
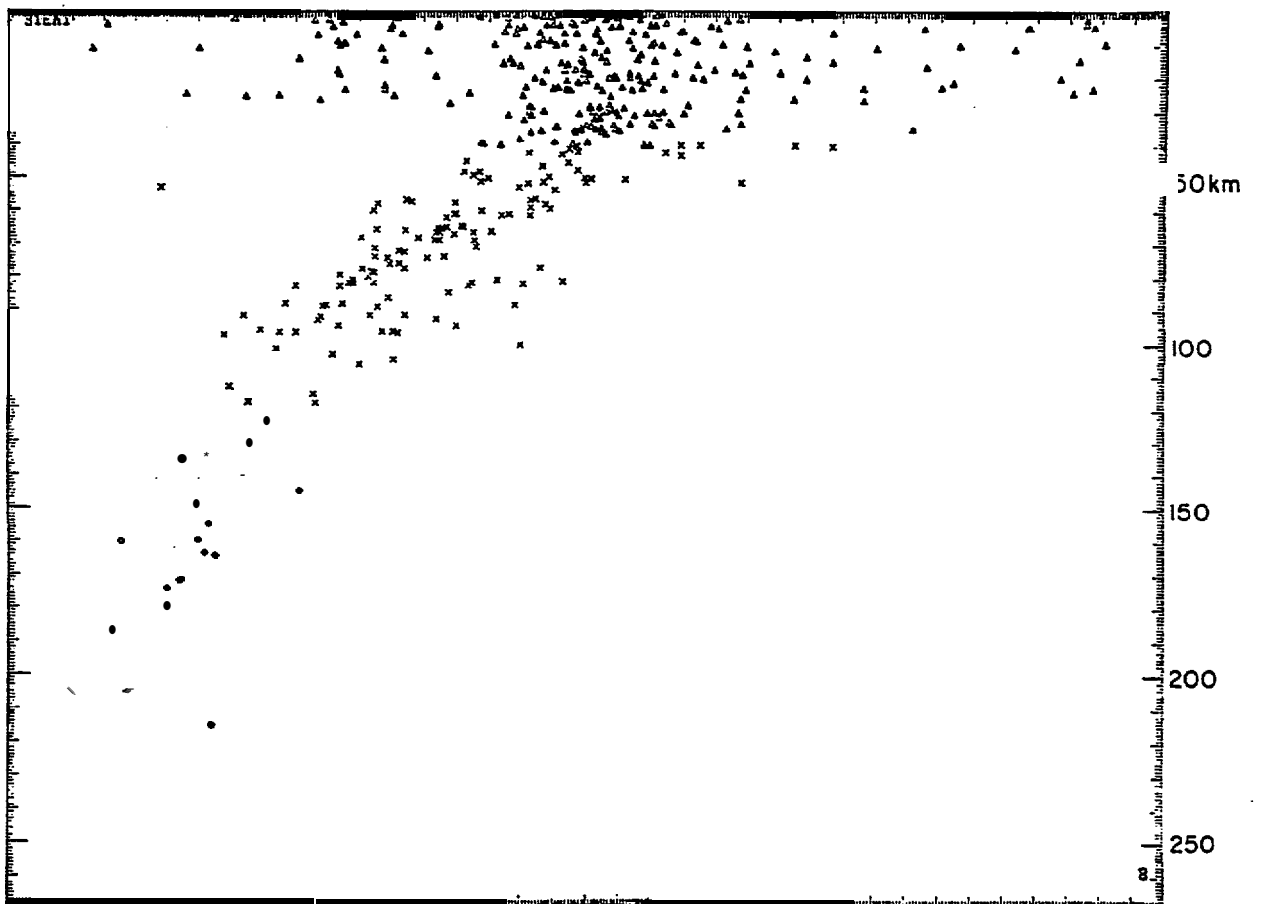


Figure 7.3.9. Seismicity located by the Shumagin Network during 1981.



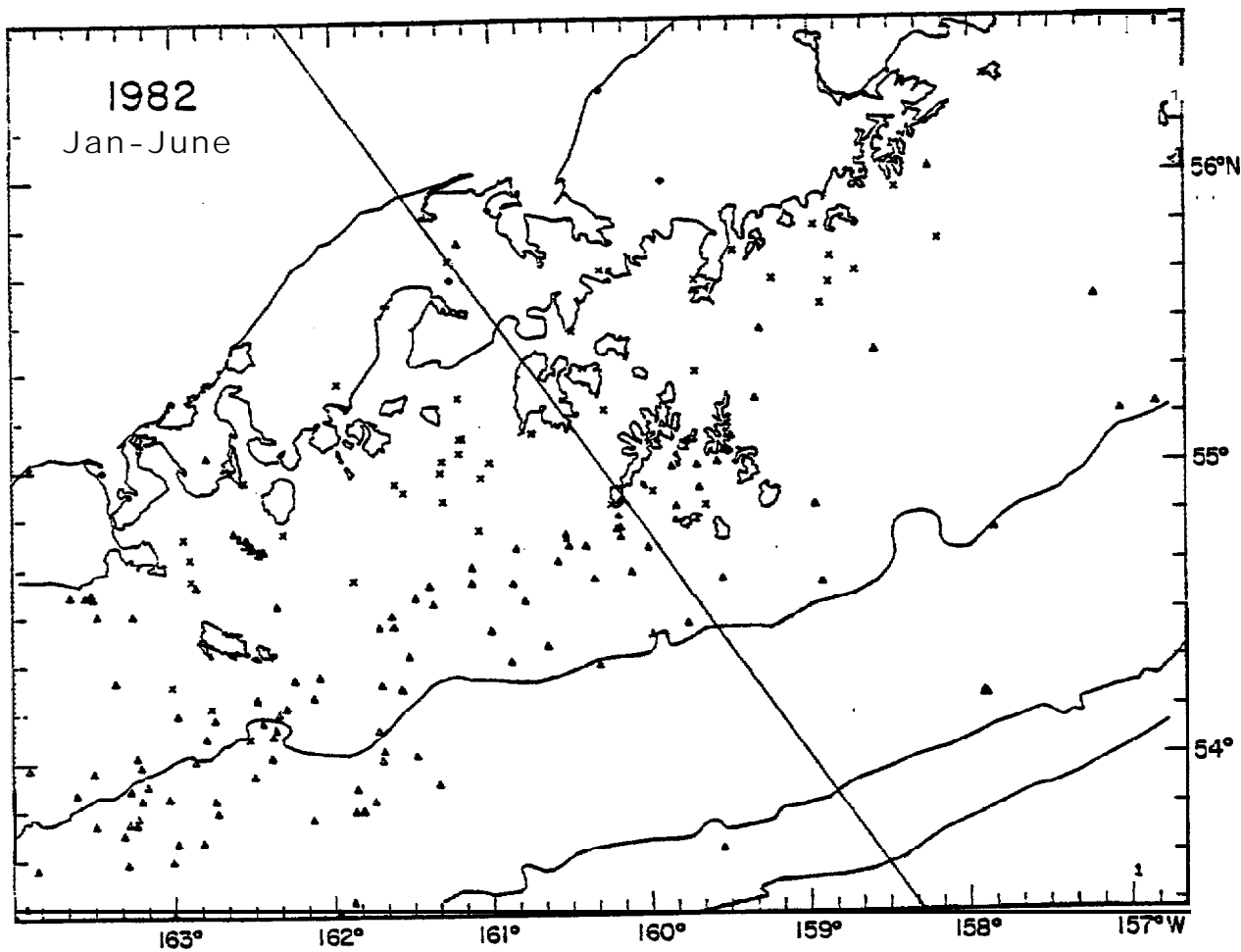
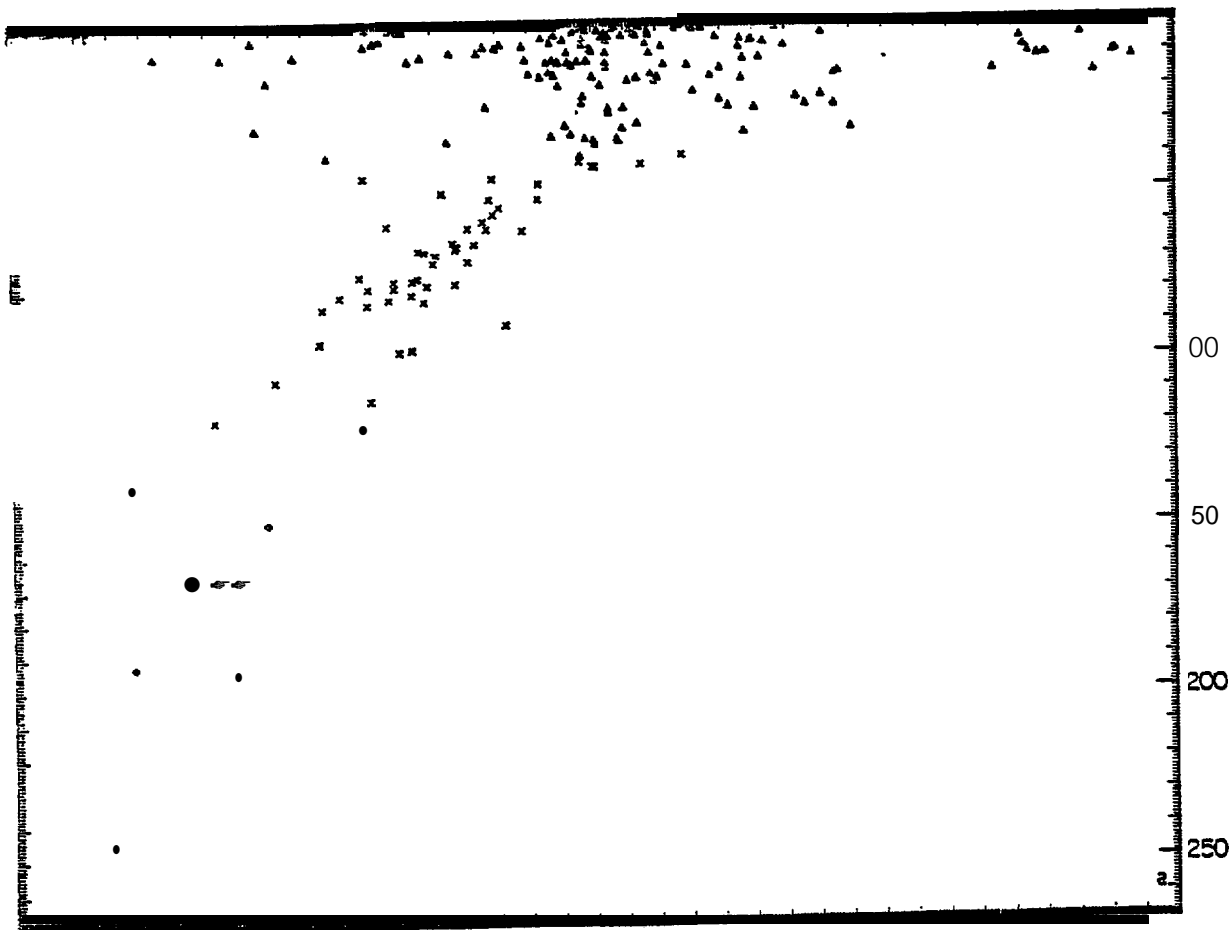


Figure 7.3.10. Seismicity located by the Shumagin network from January-June, 1982.



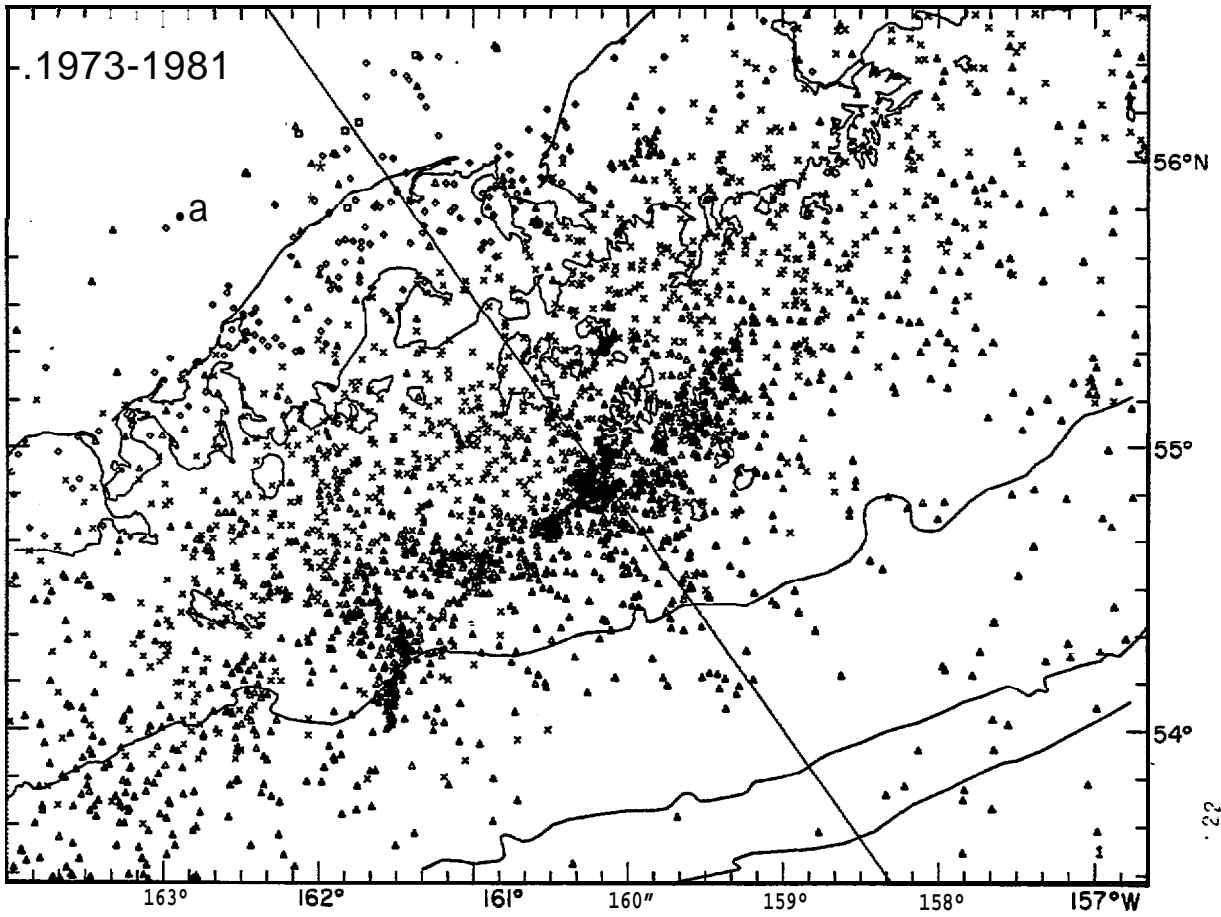


Figure 7.3.11. Seismicity located by the **Shumagin** network from 1973-1981.

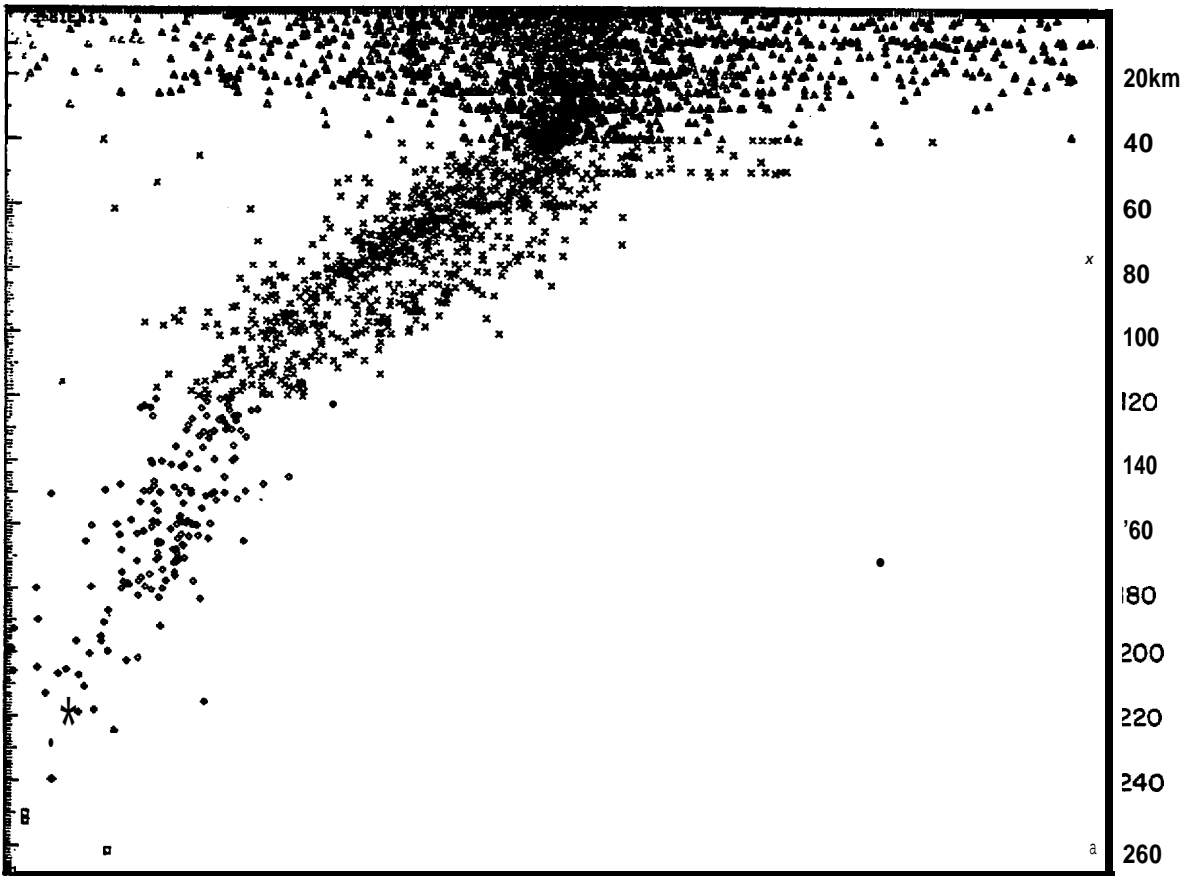


TABLE 7.3.1. Number of Earthquakes Located by the **Shumagin** Network and **NEIS/PDE** Bulletin per year in the Region **52°-57°N** and **156°-165°W**

<u>Year</u>	<u>Shumagin Network</u>	<u>PDE Bulletin</u>
1973	211	22
1974	328	25
1975	302	20
1976	279	10
1977	118	15
1978	475	19
1979	808	42
1980	448	25
1981	438	17

TABLE 7.3.2

Flat-Layered P-Velocity Model for the **Shumagin** Islands Array Region

P-Wave Velocity of Layer (km s ⁻¹)	Depth to Top of Layer (km)
3.44	0.00
5.56	" 1.79
6.06	3.65
6.72	10.18
7.61	22.63
7.90	38.51
8.26	90.19

A ratio of P-wave velocity to S-wave velocity of 1.73 was adopted for all layers.

7.4 Shumagin Network Status 1973-1982

One of the goals of operating a seismic network is to collect a data set that is continuous both in time and space. Such a complete data set is needed to facilitate studies of possible temporal and/or spatial patterns in the seismicity.

Maintaining a seismic network in continuous operation in the hostile environment of the eastern Aleutians, however, has proven to be a challenging undertaking. Both failures of antiquated recording equipment and individual seismic stations have contributed to substantial gaps in the data.

In Figure 7.4.1 we show the 1982 station configuration of the **Shumagin** network and in Table 7.4.1 we list station names and geographical coordinates. The three station network on St. Paul Island in the **Pribilofs** was removed in August-1981. Furthermore, in 1982 we closed down the **Unalaska** network and under a temporary agreement we made the central station equipment in Dutch Harbor available to Dr. John Davies who is now the state seismologist for the State of Alaska.

The continuity of data recording varies considerably through time as is shown in Figures 7.4.2 to 7.4.6. In Figures 7.4.2 to 7.4.6 we use the following notation: 1) a solid bar means the station operated continuously and data were being recorded; 2) a hatched bar means that the station operated intermittently and data were being recorded; 3) an open bar means that the station was not operating although data were being recorded; 4) a gap in the histograms showing no station status indicates that no data was recorded during that time period by the main recording device. One or two **helicorders**, however, have operated fairly continuously since 1973.

During the early years, 1973-1977, significant gaps in the data were caused by the frequent failures of obsolete equipment such as an aging tape recorder or **develocorder**, which in some instances lasted for extended periods of time before repairs could be carried out. The number of stations in the **Shumagin** network has increased through time. Initially, in 1973 seven remote stations were installed. In 1975 the number of stations had increased to 14. In 1976 the

12-station **Pavlof** subarray was installed. Today, the **Shumagin** network is trimmed back and consists of 13 stations where five stations are three-component stations and the **Pavlof subarray consist** of **four** stations. The data coverage since 1978 has been fairly continuous both in terms of recording, and in terms of station survival rate through the winter. Both quality and continuity of the retrieved data are presently excellent.

TABLE 7.4.1

EASTERN ALEUTIAN REGIONAL NETWORKS OPERATED BY LAMONT-DOHERTY GEOLOGICAL OBSERVATORY, 1973-1982

<u>Network</u>	<u>Station</u>	<u>Code</u>	<u>Components</u>	<u>N. Lat</u>	<u>W. Long</u>	<u>Error(m)*</u>	<u>Elev.(m/f)</u>	
Shumagin	Chernabura Island	CNB	SPZ,E,N	54°49.22'	159°35.30'	50(2)	90 295	
	Nagai Island	NGI	SPZ	55°02.36'	160°04.15'	27(2)	240 787	
	Squaw Harbor	SQH	SPZ,E,N	55°13.20'	160°33.74'	30?(2)	360 1181	
	Ivanof Bay	IVF	SPZ	55°73.75'	159°31.80'	22(2)	275 902	
	Big Koniuji Island	BKJ	SPZ	55°09.40'	159°33.53'	30(0)	146 480	
	San Diego Bay	SGB	SPZ,E,N	55°32.75'	160°27.23'	31(2)	275 902	
	West Unga	NUN	SPZ	55°19.87'	160°44.40'		150 492	
	Port Moller	PMA	SPZ	55°58.72'	160°29.83'		320 1050	
	Sand Point	SAN	SPZ,E,N	55°20.40'	160°29.83'	22(2)	23 75	
				IPZ,E,N				
	False Pass	FSP	SPZ	54°57.2'	163°27.4'	30(1)	200 660	
	Baldy Mountain	BAL	SPZ	55°11.593'	162°47.208'	1(6)	360 1180	
	Sanak Island	NK	SPZ	54°25.44'	162°46.52'	70(6)	159 522	
	Deer Island	DRR	SPZ	54°55.41'	162°16.99'	2s(2)	380 1246	
	Dolgoi Island	DLG	SPZ	55°08.46'	161°50.15'	32(2)	367 1204	
	Coal Harbor	CUR	R	55°19.9'	160°44.4'	500(3)	150 492	
	Pavlof Volcano	PVV	SPZ,E,N	55°22.451'	161°47.399'	1o(5)	164 538	
	Black Hill	BLH	SPZ,E,N	55°42.15'	162°03.95'	40(6)	390 1279	
	Beaver Bay	BVB	R	55°31.9'	160°59.2'	1000(1)	518 1700	
	Pavlof	Pavlof North-4	PN4	SPZ	55°25.819'	162°01.369'	1o(5)	434 1424
Pavlof North-6		PN6	SPZ	55°27.118'	161°54.888'	1o(5)	814 2670	
Pavlof North-7		PN7	S P Z	55°26.591'	161°56.781'	1o(5)	780 2258	
Pavlof North-8		PN8	SPZ	55°26.623'	162°01.246'	1o(5)	605 1984	
Black Hill		BLH	R	55°42.15'	162°03.95'	40(6)	390 1279	
Pavlof South-1		Ps1	SPZ	55°25.339'	161°44.173'	1o(5)	300 983	
Pavlof South-2A		P S2A	SPZ	55°24.205'	161°48.189'	20(6)	455 1465	
Pavlof South-3		PS3	SPZ	55°23.517'	161°49.014'	1o(5)	450 1476	
Pavlof South-4		PS4	SPZ	55°21.238'	161°52.091'	1o(5)	520 1707	
Zachery Bay		ZRR	R	55°18.66'	160°44.43'	10(6)	183 600	

TASLE 7.4.1 (con't.)

<u>Network</u>	<u>Station</u>	<u>Code</u>	<u>Components</u>	<u>N. Lat</u>	<u>W. Long</u>	<u>Error(m)*</u>	<u>Elev.(m/f)</u>
Dutch Harbor	Dutch Harbor	DUT	SPZ,E,N IPZ,E,N	53°53.9'	166°32.2'	1000(3)	60 197
	Ballyhoo	BHR	R	53°54.8'	166°31.9'	2000(8)	427 1400
	Akutan Volcano	AKI	S P Z	54°06.7'	166°03.1'	1000(8)	457 1500
	Makushin Volcano	MAK	SPZ	53°54.9'	166°47.9'	1000(8)	366 1200
	Upper Shaishnikof River	USR	SPZ	53°46.0'	166°41.75'	1000(9)	610 2000
	Sedanka Island	SDK	SPZ	53°40'	166°08'	2000(9)	366 1200

Legend:

R = repeater only, high gain
 SPZ,E,N = short period, high gain vertical,
 horizontal east and north
 IPZ,E,N = intermediate period, low gain vertical,
 horizontal east and north

*Source Codes:

- (0) theodolite survey, Surveyor crew 13 June 1978
- (1) picked from C and GS chart 8802, September 1978
- (2) picked from 1:63K maps, May 1978
- (3) picked from 1:250K maps, May 1978
- (4) taken from October 1975 list of station coordinates
- (5) geodimeter/theodolite survey made June-August 1977
- (6) measured from nearby benchmark, June-August 1977, August 1978
- (7) proposed from C and GS charts 8994,8995
- (8) ' proposed from 1:250K USGS maps
- (9) proposed from 1:1M Aeronautical Chart CE-13

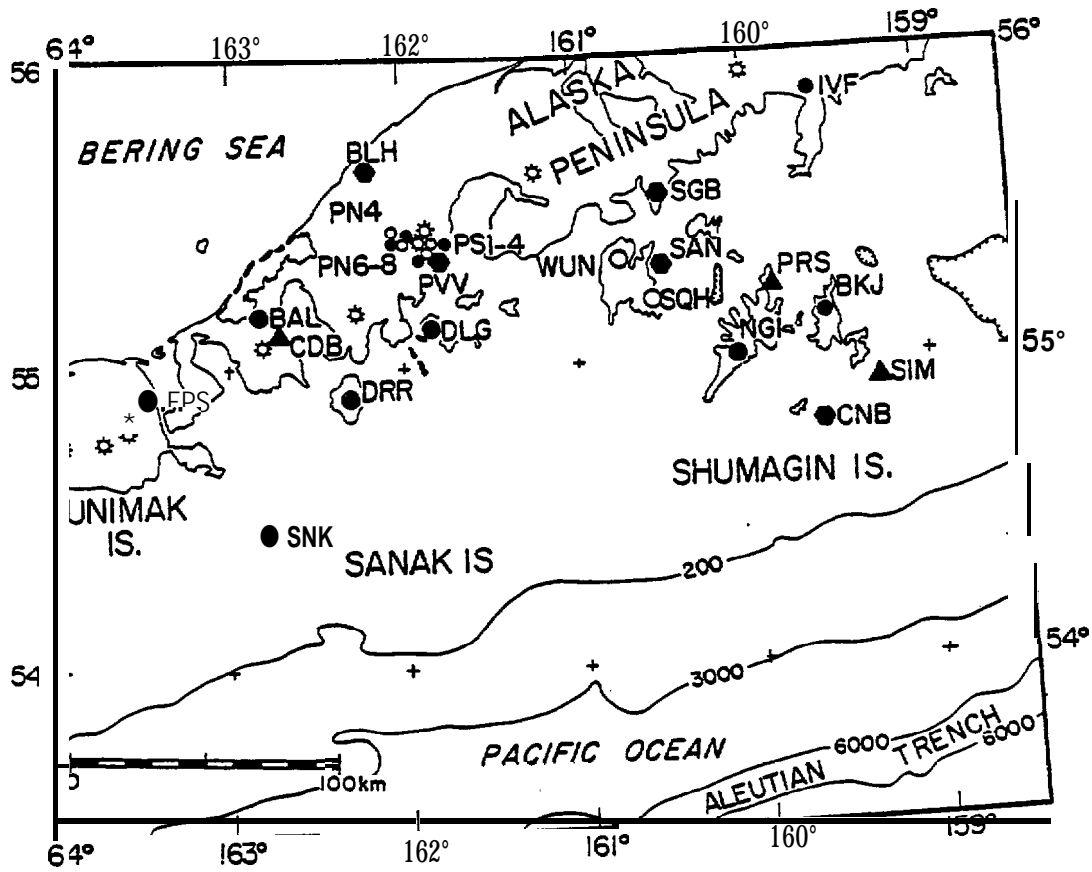


Figure 7.4.1. The Shumagin seismic network, Alaska. Filled circles are short period, single (vertical) component seismic stations. The hexagons are short period, three component seismic stations. Open circles are seismic stations that have been removed. Strong motion accelerographs (SMA-1) are located at the seismic stations SNK, DRR, DLG, SGB, SAN, NGI, BKJ, IVF, and CNB and 3 SMA-1's are located separately at CDB, SIM, and SIM (shown as triangles).

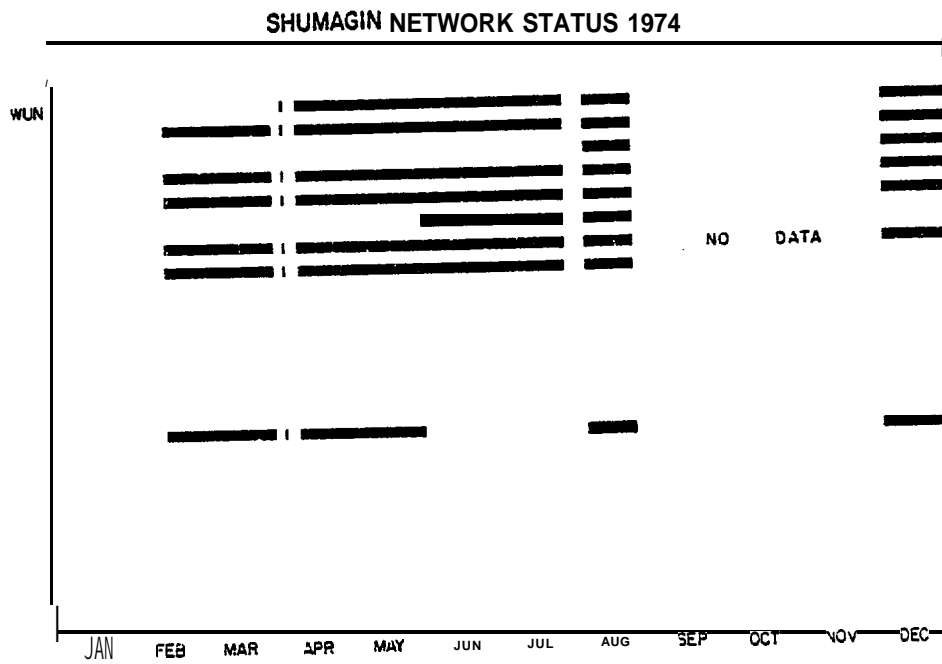
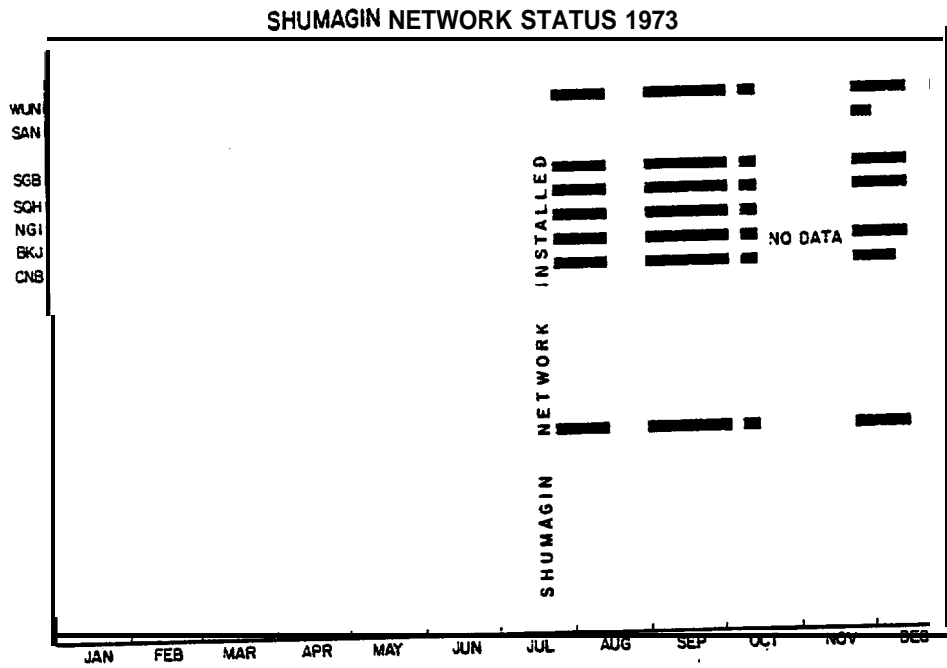
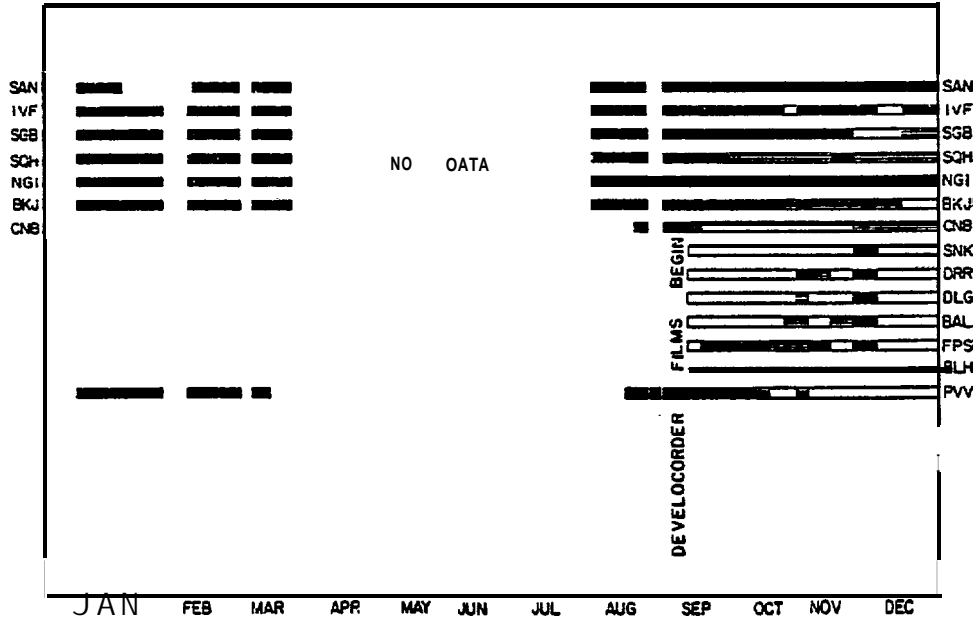


Figure 7.4.2. Operational status of the Shumagin network in 1973 and 1974.

SHUMAGIN NETWORK STATUS 1975



SHUMAGIN NETWORK STATUS 1976

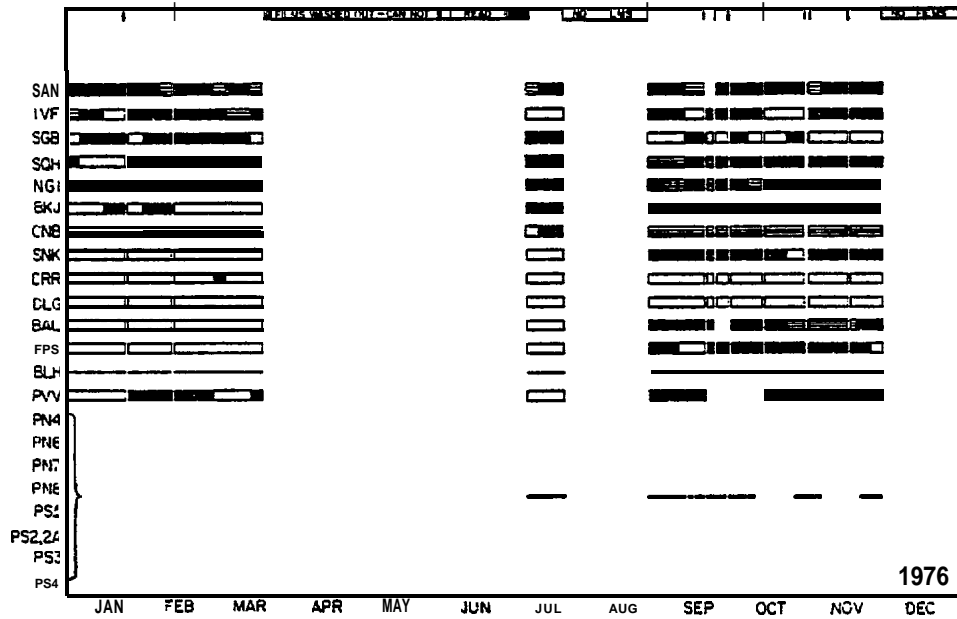
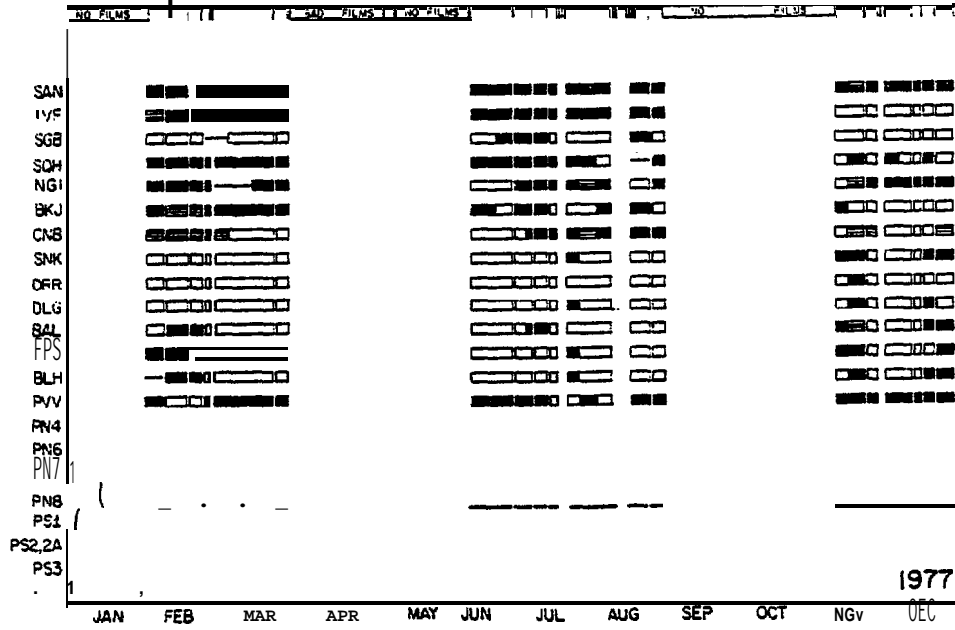


Figure 7.4.3. Operational status of the Shumagin network in 1975 and 1976.

SHUMAGIN NETWORK STATUS 1977



SHUMAGIN NETWORK STATUS 1978

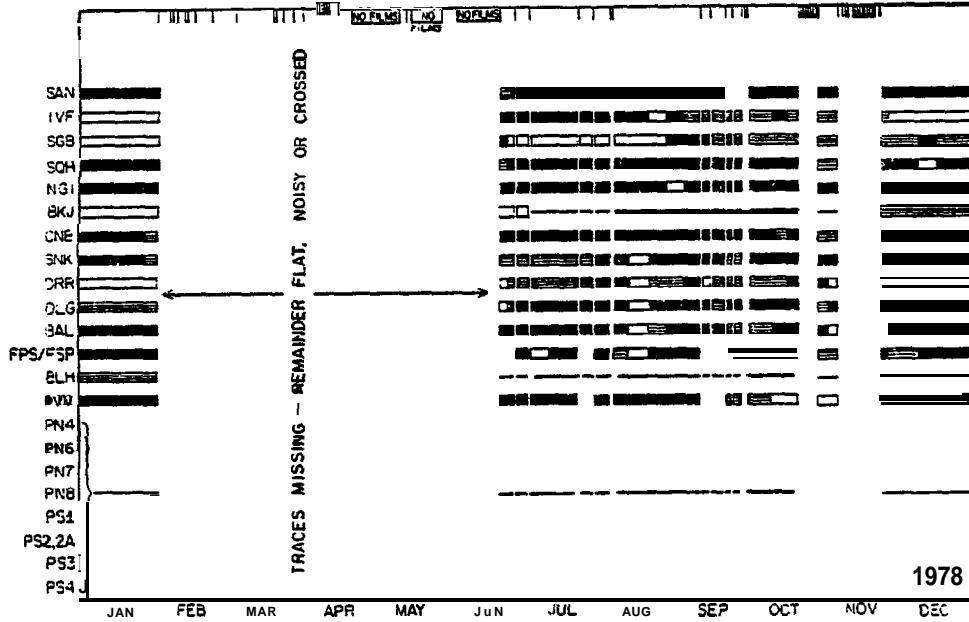
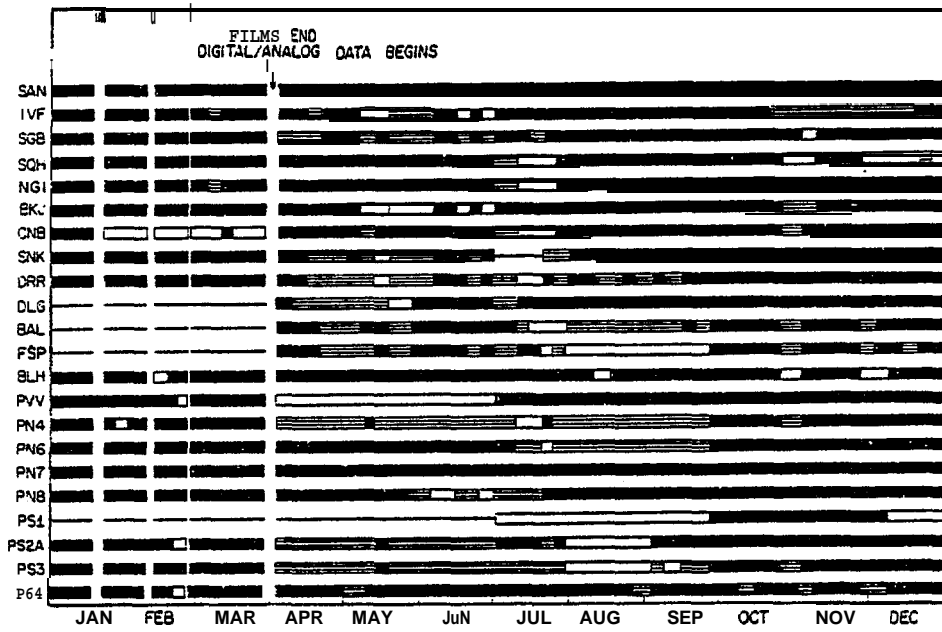


Figure 7.4.4. Operational statue of the Shumagin network in 1977 and 1978.

SHUMAGIN NETWORK STATUS 1981



SHUMAGIN NETWORK STATUS 1982

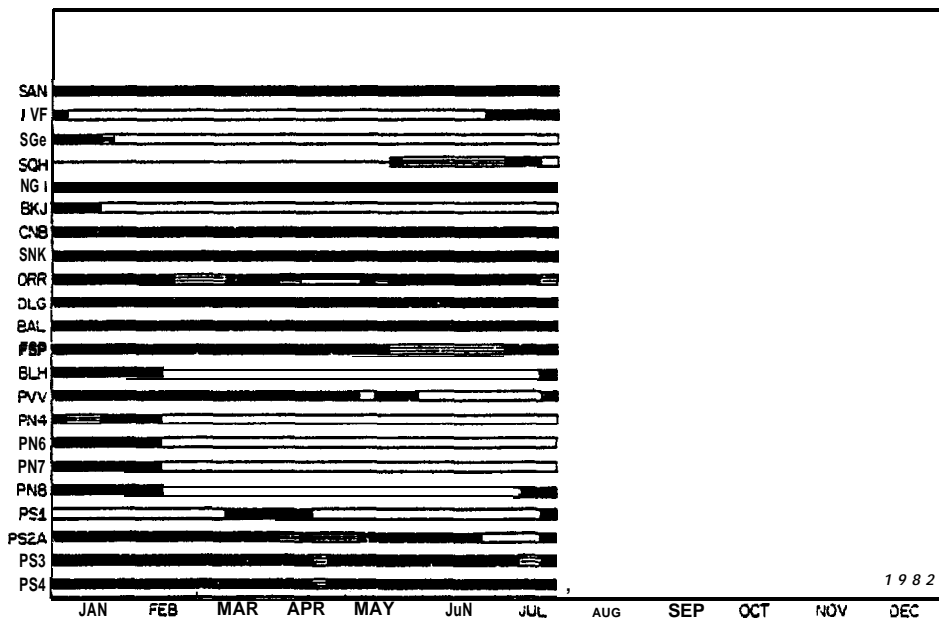


Figure 7.4.6. Operational status of the Shumagin network in 1981 and 1982.

7.5 Seismic and Eruptive Activity of Pavlof volcano, 1973-1982

Pavlof Volcano has had 5 major eruptions and several episodes of minor explosions since seismic monitoring began in fall 1973. The major eruptions occurred in 1973, 1975, 1976, 1980, and 1981 (Table 7.5.1). Station PW, 7.5 km to the SE of the volcano's summit (Figure 7.5.1), has been used as the seismic **monitoring** station. Data have been continuously displayed on **helicorder** records since fall 1973, except during short periods of time when the station malfunctioned. The station consisted of a single short-period (1 Hz) seismometer from 1973 until 1982; in summer 1982 the station was upgraded to 3 components. (The vertical **component** is still displayed on the **helicorder**). An equipment change in 1979 resulted in a gain reduction of about a factor of three. When feasible, other stations of the local network installed in 1976 were displayed on the **helicorder** if station **PVV** malfunctioned.

Four types of seismic events of probable volcanic origin have been observed on **Pavlof** seismograms and are shown in Figure 7.5.2: high-frequency tremors, B-type earthquakes (shallow events with emergent arrivals and no clear S-phase), explosion earthquakes, and volcanic tremor. Magnitudes of B-type events range from -0.2 to 1.0. B-type events have b-values (negative slope of magnitude-frequency relation) ranging between 1.9 and 2.6 (**McNutt, 1981a,b; McNutt and Beavan, 1981; McNutt, 1982a,b; McNutt and Mori, 1983**). Figures 7.5.3-7.5.7 show the numbers of B-type earthquakes and explosions per day for all data from 1973, 1974, most of 1975, and all of 1981 and 1982. Data for the remainder of 1975, 1976-1980, and 1983 are still being analyzed, however, all records have been scanned. Table 7.5.1 was prepared based on detailed study of reduced data as well as scanning of remaining records. Also, there were virtually no volcanic events recorded from spring of 1977 until fall of 1980, so the data set presented here is actually more complete than it may appear.

During major eruptions with strong lava fountaining the **seismicity** increases from a background level of several 10's of events

per day to several thousand events per day and/or continuous high amplitude volcanic tremor. This **can be seen** in Figures 7.5.3, 7.5.5, and 7.5.6. The increase in **seismicity** and onset of eruption occur quite abruptly, that is on a scale of a few hours. The smaller eruption episodes consisting of numerous explosions are accompanied by increases in seismicity to a level of several hundred events per day (Figures 7.5.4 and 7.5.6) . The increase takes place on a scale of 3-4 days, during which time **seismicity** has been observed to correlate with the solid earth tides (**McNutt and Beavan, 1981**).

To date, only the two eruption styles and accompanying **seismicity** described above have been observed. The historic record, however, contains some descriptions of other perhaps more vigorous activity (Table 3.5 .2-see years 1845 and 1906-1911). We can **only** speculate about the seismicity accompanying these eruptions. However, several "descriptions of felt earthquakes (which remain to be verified) suggest that perhaps larger shocks than those which have been recorded to date (up to about magnitude 1.0) have occurred at the **volcano in the past**. We further note **that no** locatable events have occurred at shallow depths beneath the volcano, and only four located events have occurred within 15 km of the volcano from 1973 to 1982. We speculate that the volcano has erupted so frequently that the conduit has remained open and has not permitted large **enough** stresses to build up to cause larger earthquakes.

Lastly, the volcano sits roughly in the middle of the **Shumagin** seismic gap. The historic record gives an indication that some eruptions may have occurred at the time of large nearby earthquakes (Tables 3.5.1 and 3.5.2, see years 1786 and **1917**) . Thus, we have some reason to anticipate possible eruptive activity accompanying the expected large or great earthquake. We feel we are in an excellent position to compare the seismic and eruptive activity of **Pavlof** Volcano during the pre-seismic, co-seismic and post-seismic periods of seismicity at the adjacent Pacific-North American Plate boundary.

TABLE 7.5.1. Preliminary list of Pavlof Volcano eruptions, 1973-1983, deduced from seismicity.

<u>Date</u>	<u>Description of Activity</u>	<u>Seismogram Characteristics*</u>	<u>Confirmation</u>
Nov. 13-14, 1973	major magmatic	volcanic tremor	photograph-lava fountaining & ash column
Mar. 12-14, 1974	explosive	explosion quakes	
before Sep. 1-21, 1974	explosive	explosion quakes	
Oct. 29 - Nov. 17, 1974	explosive	explosion quakes	
Nov. 25 - Dec. 16, 1974	explosive	explosion quakes	
Dec. 25 - Jan. 06, 1975	explosive	explosion quakes	
Sep. 13-15, 1975	magmatic	volcanic tremor	
before Sep. 18-21, 1975	explosions	explosion quakes	
Sep. 23-24, 1975	magmatic	volcanic tremor	photograph-lava fountaining & ash column
Sep. 25 - Oct. 06, 1975	explosions	explosion quakes	
Ott". 06-12, 1976	magmatic(?) & explosive	volcanic tremor & explosion quakes	
Nov. 02-04, 1976	explosive	explosion quakes	
Nov. 10-22, 1976	magmatic	volcanic tremor (note-long duration but low amplitude)	
Nov. 11-12, 1980	major magmatic	volcanic tremor	photograph-lava fountaining & ash column
before? Mar. 30 - May 28, 1981	explosive	explosion quakes	
Sep. 26-27, 1981	major magmatic	volcanic tremor	field party-witnessed lava flow

*b-type earthquakes always occur, but in higher numbers during eruptions.

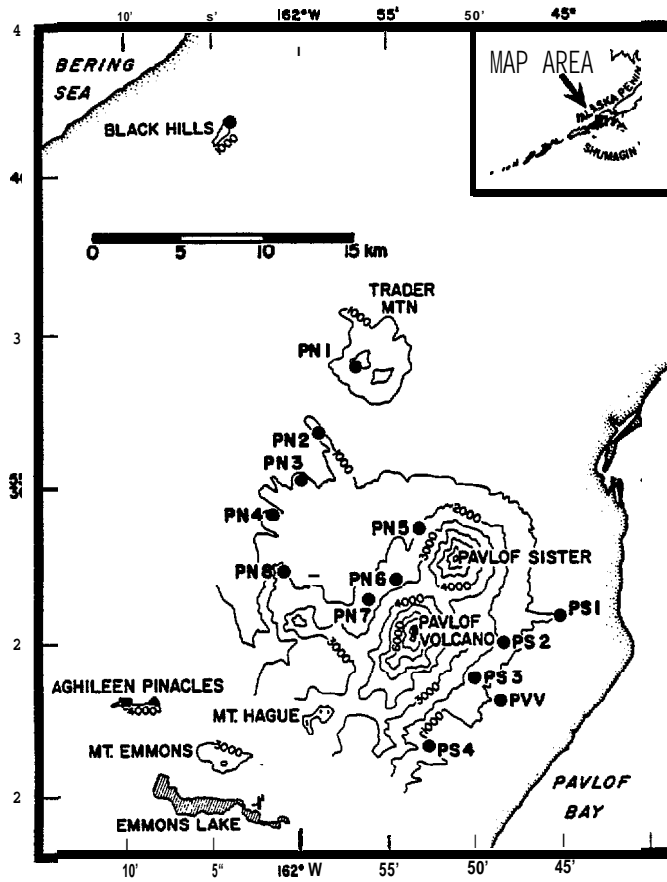


Figure 7.5.1. Map showing stations of the Pavlof seismic array. Station PVV, 7.5 km SE of the volcano's summit, is the monitoring station and was installed in 1973. The remaining stations were installed in 1976; some have been re-wired in 1981 and 1982.

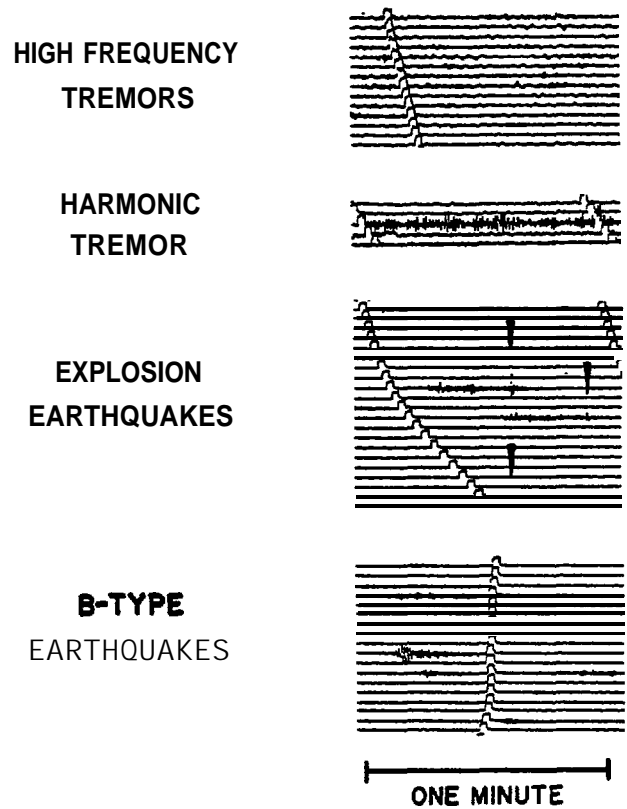


Figure 7.5.2. Types of seismic signals recorded on helicorder from station PVV. Arrows point to air shock phase of explosion earthquakes. Note the similar frequency content (~ 1.4 Hz) of B-type earthquakes, harmonic tremor, and ground waves from the explosion earthquakes.

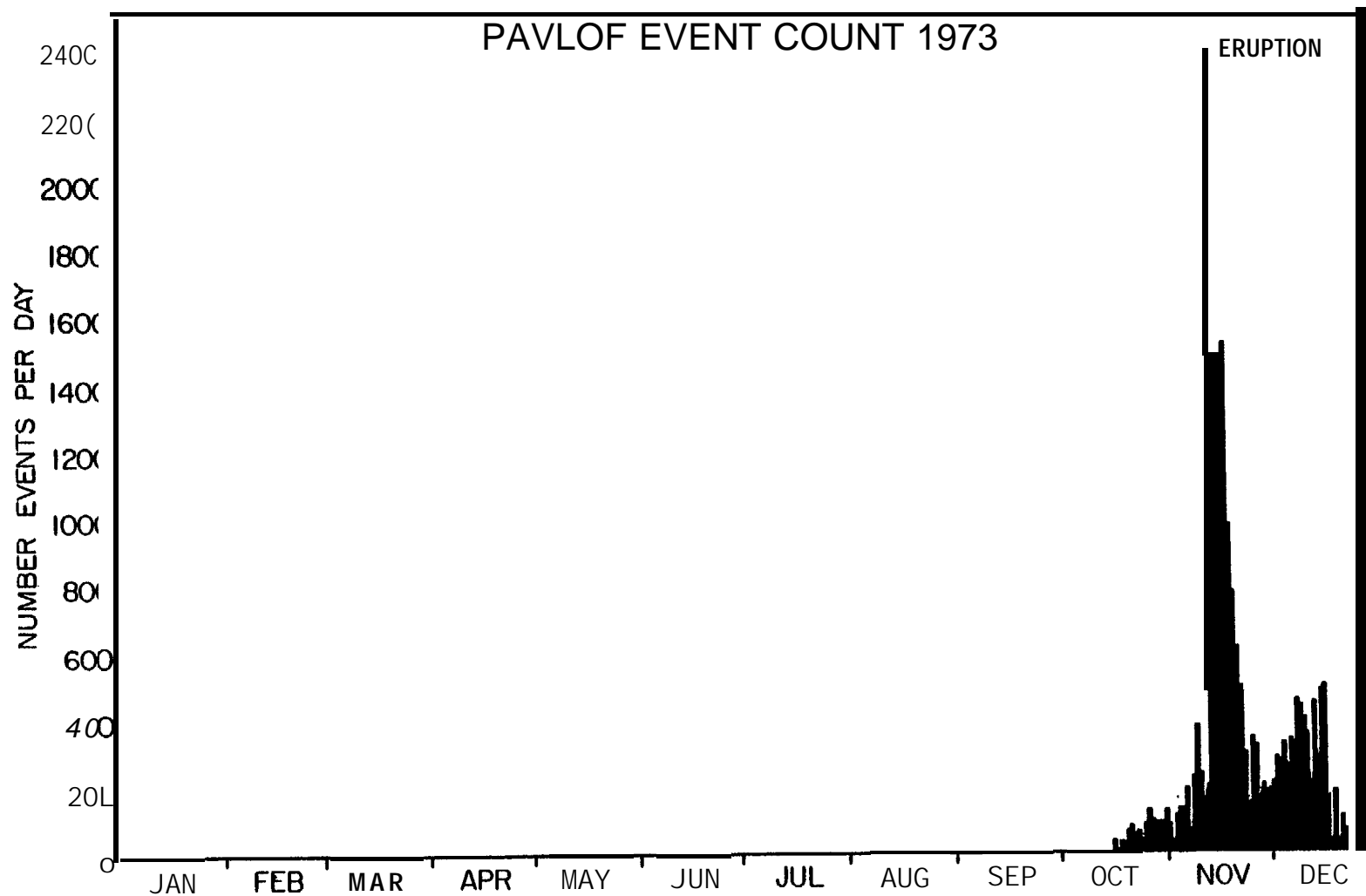


Figure 7.5.3. Number of B-type earthquakes and explosions per day.

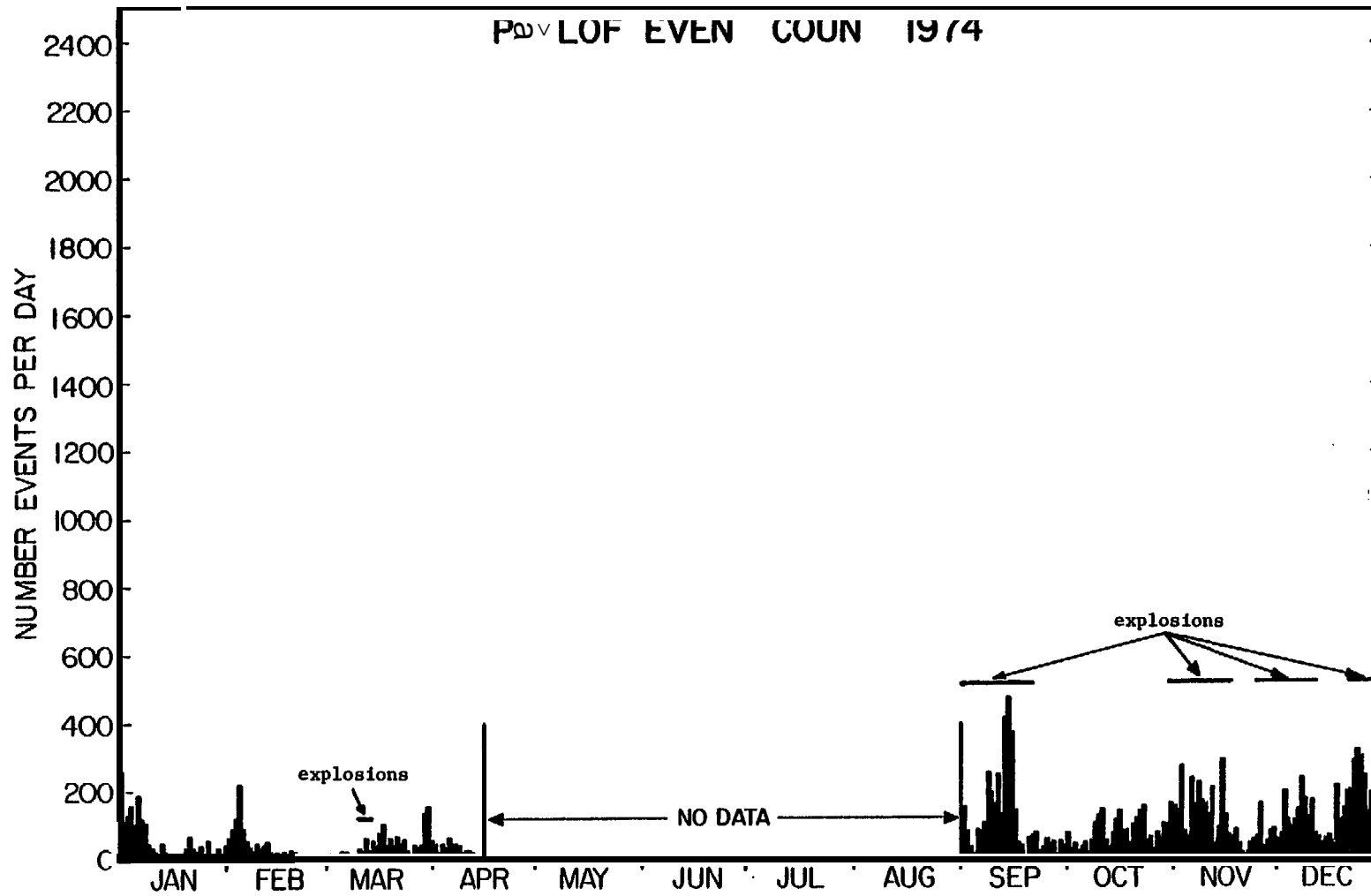


Figure 7.5.4. Number of B-type earthquakes and explosions per day.

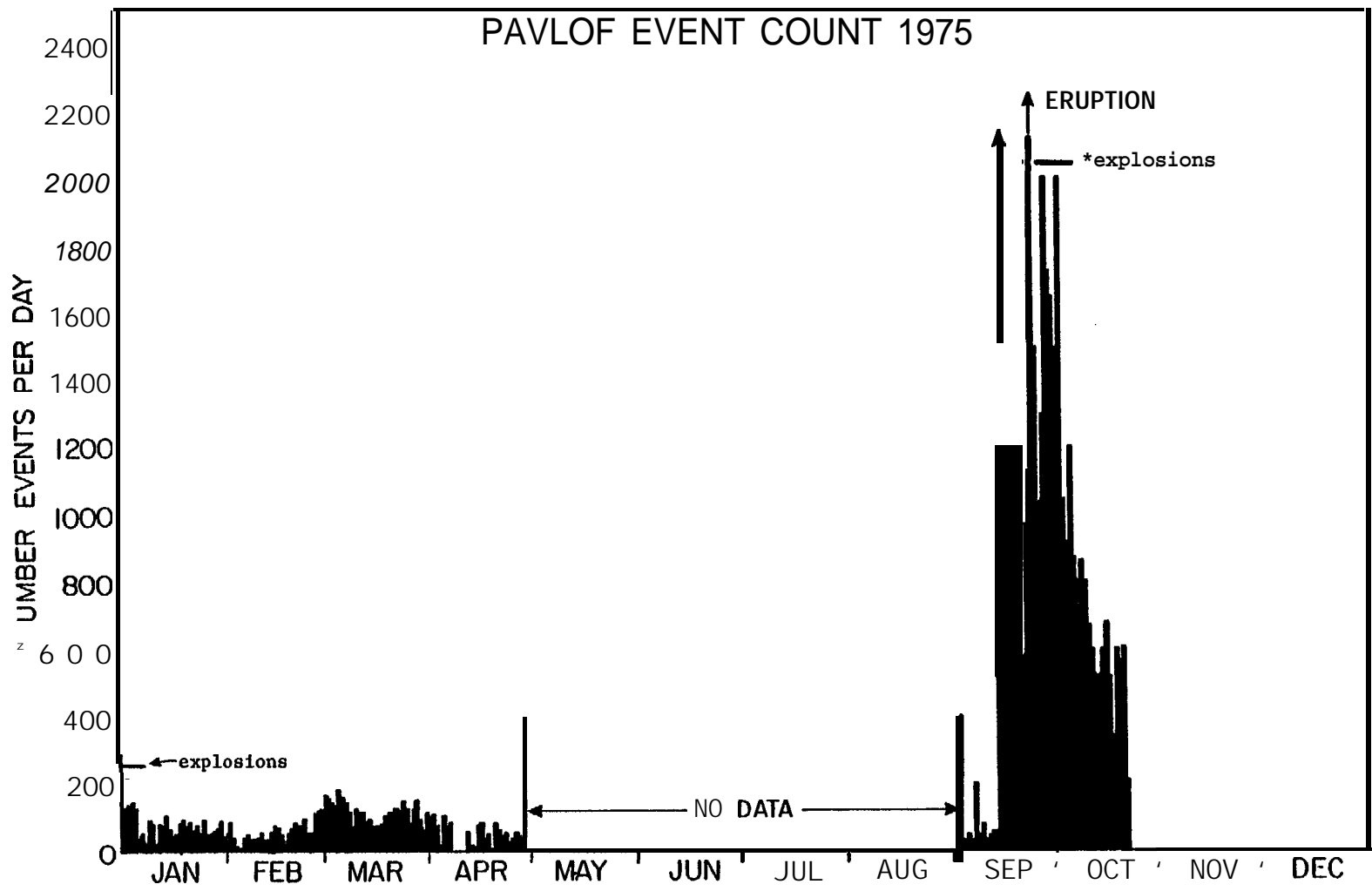


Figure 7.5.5. Number of B-type earthquakes and explosiona per day,

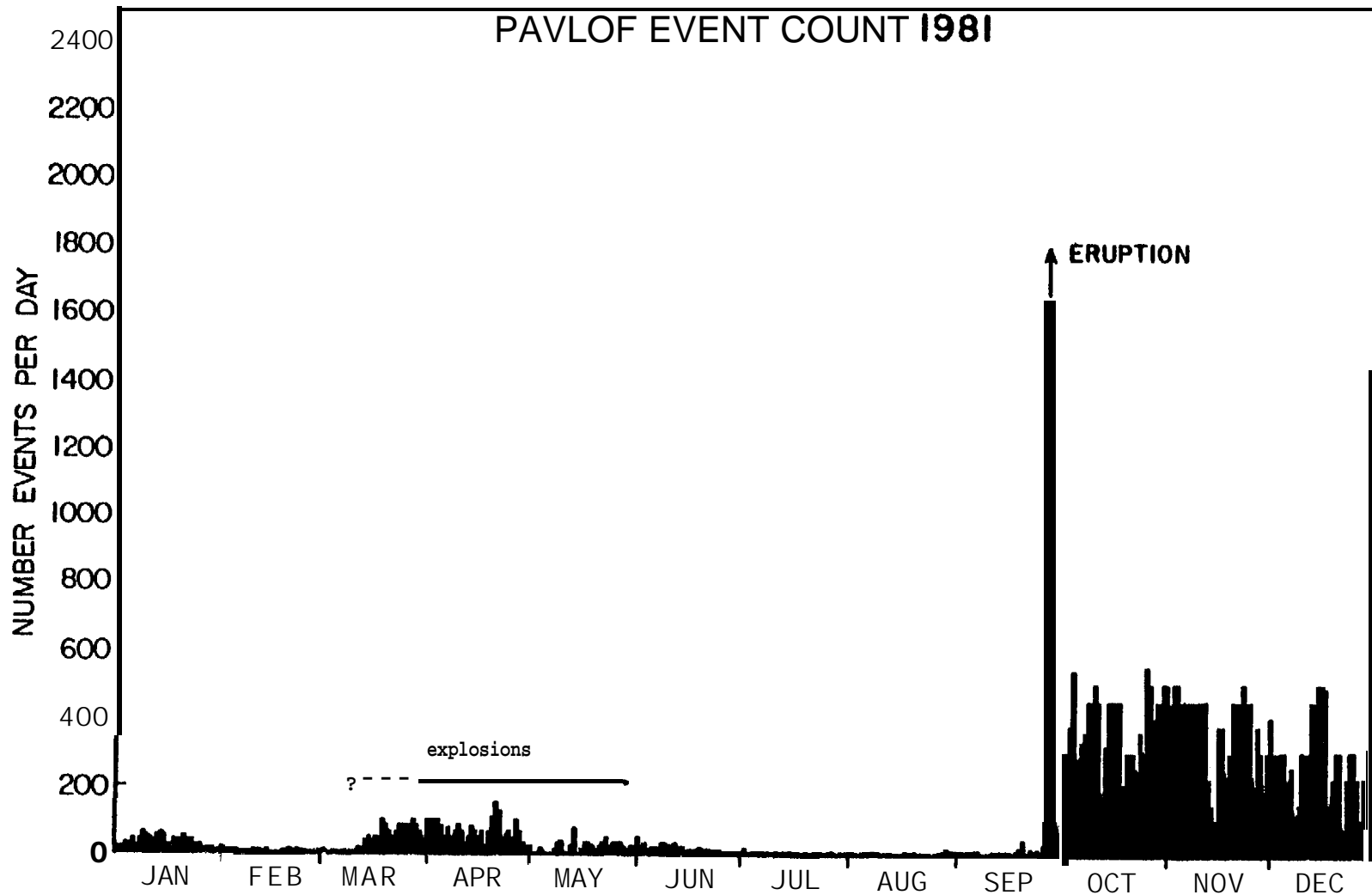


Figure 7.5.6. Number of B-type earthquakes and explosions per day.

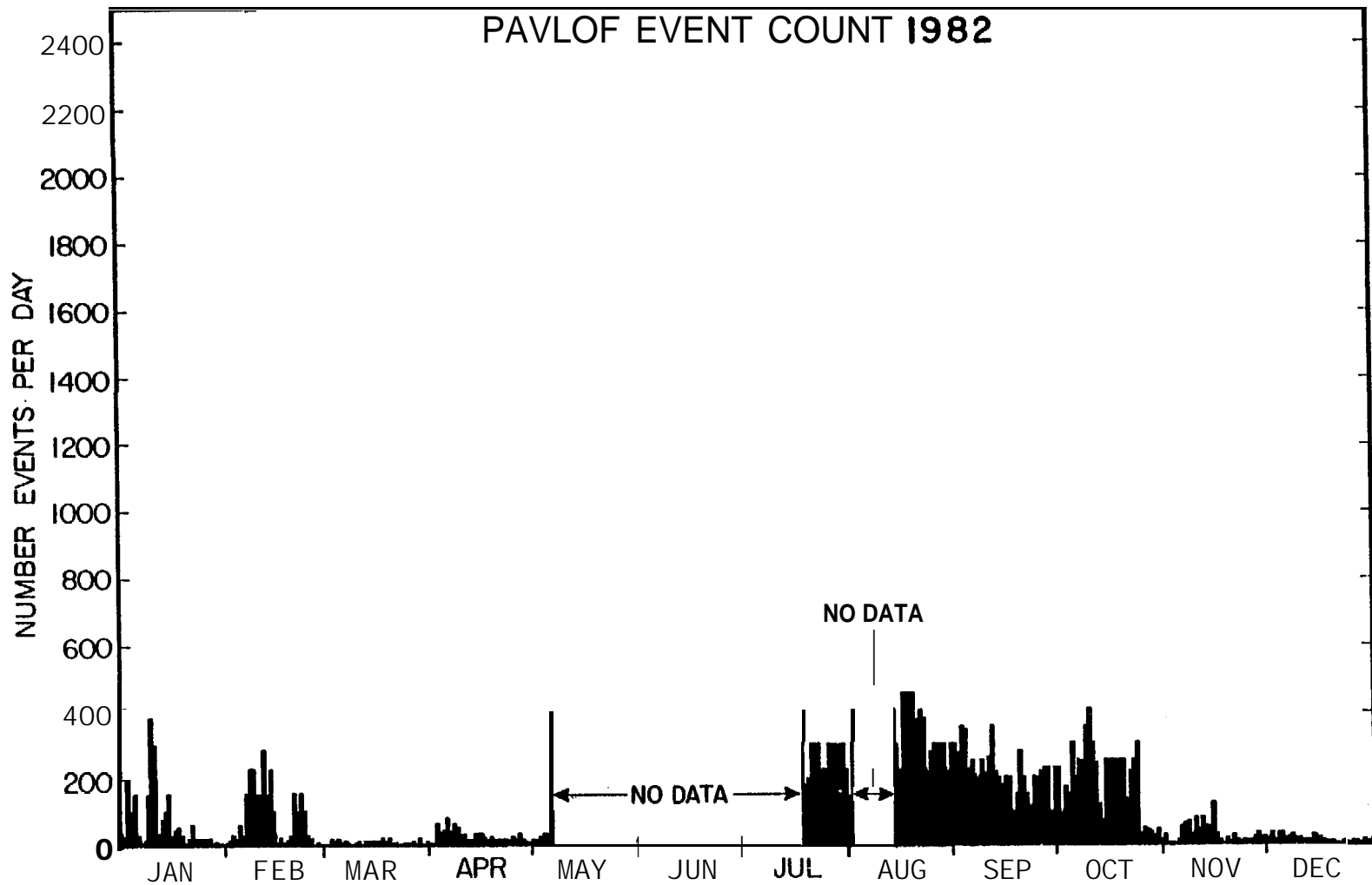


Figure 7.5.7. Number of B-type earthquakes and explosions per day.

7.6. Preliminary Risk Assessment in the St. George Basin

SEISMICITY

Historic Record

Data. The earthquake record prior to the development of sensitive seismographs in the late 1890's and early 1900's relies on observations of the effects of earthquakes on people and objects. For southern Alaska, the Aleutians **in** particular, these observations are most complete during the period of the Russian occupancy, generally from about 1740 to 1870. Earthquakes for this period have been cataloged by Davis and **Echols** (1962), **Coffman** and vonHake (1973), and Kissinger et al. (manuscript **in** preparation); these references will be abbreviated 1, 2, and 3, respectively.

Pribilof Islands. The historic record of earthquakes in the **Pribilof** Islands region is summarized in Tab. **7.6.1**. Because the epicenters and maximum intensities of these events are so poorly known it is not possible to compare the occurrence rate for this period, 1815-1861, to that computed below from the **teleseismic** record for the period 1957-1978. Significant, is the observation that the 1836 earthquake caused damage rated at **Modified-Mercalli** Intensity X on the **Pribilof** Islands themselves. This event, those of **1847** and 1954, which were felt with intensity (**M.M.**) V-VI, and those of 1925, 1942, 1958, and 1959 with magnitudes of 7.2, 6.75, 6.38, and 6.50, respectively (Tab. 7.6.2) demonstrate that large earthquakes have occurred in the St. George region, the **Pribilof** Islands in particular, and must be expected in the **future**. This expectation is quantified in the section below on the **teleseismic** record.

TABLE 7.6.1

All Events in the Greater St. George Basin Region for the Period 1925 through 1978

Date	HrMn	Sec	Lat	Long	Depth	Mag	Date	HrMn	Sec	Lat	Long	Depth	Mag	
250819	1207	27.30	5S	14.40	167 41.40	.00	670806	1854	15.00	55	.66	168 .00	.00	4.10
250905	1638	17.50	54	48.80	170 37.80	.00	67/39\$9	315	28.00	54	12.00	168 42.00	142.00	3.90
330427	1156	6.80	55	.00	166 .00	.00	671130	937	12.00	66	.00	163 .90	.00	4.30
370718	1011	12.00	5 5	.00	165 .00	.00	671213	1756	45.00	54	18.00	170 24.00	33.00	4.00
410501	707	48.00	57	36.00	166 36.00	.00	680114	1331	35.00	55	.00	164 .00	.00	4.00
410806	615	4.00	55	30.00	163 .00	128.00	680305	530	27.00	55	12.00	163 42.06	.00	4.05
410806	615	6.00	55	45.00	163 .00	150.00	680323	0	34.10	56	25.00	162 18.00	188.00	4.80
410806	615	12.00	55	42.00	162 24.00	200.00	680530	1622	21.00	54	12.00	168 54.00	.00	4.50
410928	533	18.00	56	.00	164 .00	.00	690729	539	47.00	54	48.00	165 6.00	.00	3.50
420610	1478	.00	57	30.00	163 .043	.00	690801	326	9.00	54	48.00	165 6.00	.00	3.50
440929	1908	14.00	57	30.00	169 .00	.00	690802	438	29.00	54	48.00	165 6.00	.00	3.40
470S25	1554	48.00	57	30.00	169 .00	.00	690828	502	21.00	54	48.00	165 6.00	.00	3.40
511001	1011	40.00	55	.00	166 .00	.00	691105	459	54.00	54	18.00	167 36.00	.60	3.50
550717	2158	23.00	54	24.00	168 18.00	.00	691123	1015	20.00	55	42.00	166 .00	33.00	.00
570310	2034	.00	55	.00	166 .00	.00	691127	711	37.00	55	46.20	164 .00	33.00	.00
570312	449	30.00	55	.00	164 .00	.00	691129	1652	.00	54	18.00	167 36.00	.00	3.80
570323	1029	10.00	54	30.00	165 30.00	.00	691130	421	2.00	56	24.00	166 48.00	.00	3.60
570328	1251	45.00	55	.00	166 15.00	.00	691207	13	13.00	54	38.00	171 .00	33.00	.09
570521	1501	53.00	55	.00	164 .00	.00	691212	351	1.06	55	10.00	164 54.00	154.00	4.20
570531	1619	39.00	55	.00	169 .00	.00	700126	833	49.00	57	18.00	163 .00	33.60	.00
570609	2051	33.00	55	.00	167 30.00	.00	700427	552	6.00	54	18.00	167 36.00	.00	3.45
580303	1618	23.00	55	37.20	166 20.40	45.00	700703	437	.00	57	6.00	164 .00	35.00	.08
590421	1242	50.00	56	.00	162 30.00	.00	791128	228	57.00	54	12.00	168 18.00	.00	3.50
590512	0457	39.20	55	9.00	168 14.40	17.00	701202	1814	50.50	55	54.60	163 58.20	221.00	4.70
600109	1749	7.00	55	30.00	165 .00	.00	701203	646	15.50	54	18.00	167 36.00	.00	3.39
601030	2156	20.60	56	36.00	167 12.00	70.00	701212	345	2.00	54	18.00	167 36.00	.00	3.50
610114	1639	9.00	55	30.00	165 .00	.00	701212	1517	21.00	64	18.00	167 36.00	.00	3.50
610326	2010	31.70	55	42.60	164 .60	50.00	710805	1351	9.30	55	43.08	164 55.20	33.00	5.10
610326	2010	44.40	55	36.60	163 48.00	176.00	711231	844	47.20	54	51.06	164 23.22	33.00	4.50
620408	2209	31.40	54	48.60	165 .60	25.00	720513	1309	26.10	54	54.86	166 36.66	.00	.00
630508	850	54.00	55	30.00	163 48.00	.90	730630	507	1.39	54	7.32	168 38.82	.00	.00
640311	459	45.60	54	42.00	169 54.00	33.00	730820	2226	28.60	55	47.16	166 51.78	.00	4.40
640330	1921	51.00	55	30.00	168 6.00	30.00	740609	606	40.70	54	7.80	17H 48.54	.00	.00
640501	1557	28.90	56	4.80	167 36.00	33.00	740724	1916	56.30	55	48.00	162 15.05	113.00	4.19
640504	226	33.70	55	57.60	162 48.00	200.00	741019	54	44.60	54	37.62	165 10.00	.00	4.30
640827	310	19.40	54	6.00	167 24.00	33.00	750129	1854	51.36	55	50.64	175 29.04	.00	.60
640912	432	34.00	54	48.00	170 .00	33.00	759210	220	58.49	54	59.94	169 36.78	.00	4.00
650215	943	4.30	55	48.00	166 42.00	35.00	750311	1849	46.11	54	34.68	169 9.66	.66	4.56
650325	2000	19.00	S	25.20	155 6.00	33.00	751110	1303	47.16	57	30.66	170 25.08	33.00	.00
650406	1737	35.50	55	30.00	166 48.00	33.00	760930	143	27.30	56	28.08	162 32.94	75.00	.00
651022	1626	48.40	56	37.20	169 40.20	7.00	761023	825	31.00	55	2.64	165 55.32	188.40	4.70
666717	153	4.00	56	29.40	167 2.40	4.0.00	761025	1124	7.76	57	8.02	165 56.58	33.00	4.65
661130	56	25.00	55	.00	167 .00	.00	770327	1841	57.90	57	34.00	169 57.00	33.00	4.20
670502	1756	33.00	57	.00	164 .08	.00	780626	252	56.60	57	37.20	169 55.80	33.00	4.20
670703	922	35.30	54	37.20	166 .00	120.00	781207	16	49.247	54	40.20	165 36.00	127.00	4.60

336

*NR: '58 and '59 events added after analysis; both depths for '1 event inadvertently included in analysis.

TABLE 7.6.2

Shallow Events in the Limited St. George Basin Region
for the Period 1957 through 1978

<u>Date</u>	<u>HrMn</u>	<u>Sec</u>	<u>Lat</u>	<u>Long</u>	<u>Depth</u>	<u>Mag</u>
570310	2034	.00	55 .00	165 .00	.00	. 00
570312	449	30.00	55 .00	164 .%0	. 0 0	.00
570323	1029	10.00	54 30.00	165 30.00	. 00	.00
570328	1251	45.00	55 .00	166 15. 00	.00	.00
570521	1501	53.00	55 .00	164 .00	.00	.00
570609	2051	33.00	55 .00	167 30.00	.00	.00
600109	1749	7.00	55 30.00	16S .00	.00	.00
601030	2156	20.60	56 36.00	167 12.00	70.00	.00
610114	1639	9.00	55 30.00	165 .00	2.22	5.75
610326	2010	31.70	55 42.60	164 .60	50.00	.00
620408	2209	31.40	54 48.60	165 .60	25.00	.00
630508	850	54.00	55 30.00	163 48.00	.00	5.50
640330	1921	51.00	55 30.00	168 6.00	30.00	4.30
640501	1557	28.90	56 4.80	167 36.00	33.00	4.30
650215	943	4.3 0	55 48.00	166 42.00	35.00	4.50
650325	2000	19.80	55 25.20	165 6.00	33.00	4.20
650406	1737	35.50	55 30.00	166 48.00	33.00	4.20
651022	1626	48.40	56 37.20	169 40.20	7.00	4.70
660717	103	4.00	56 29.40	167 2.40	40.00	4.80
661130	56	25.00	55 .00	167 .00	1.11	4.20
671130	937	12.00	56 .00	163 .00	2.22	4.30
6S0114	1331	35.00	55 .00	164 .00	.00	4000
680305	530	27.00	55 12.00	163 42.00	.00	4.00
690729	539	47.00	54 48.00	165 6.00	.00	3.50
690801	326	9.00	54 48.00	165 6.00	2.22	3.50
690802	438	29.00	54 48.00	165 6.00	2.22	3.40
690828	502	21.00	54 48.00	165 6.00	.00	3*4B
691123	1815	20.00	55 42.00	166 .00	33.00	.00
691127	711	37.00	55 46.20	164 .00	33.00	.00
691130	421	2.00	56 24.00	166 48.00	1.11	3.60
710805	1351	9.30	55 43.08	164 55.20	33.00	5.10
711231	844	47.20	54 51.06	164 23.22	33.00	4.50
720513	1309	26.10	54 54.06	166 36.66	.00	.00
730820	2226	28.60	55 47.16	166 51.78	1.11	4.40
741019	54	44.60	54 37.62	165 10.80	.00	4.30
751118	1303	47.16	57 30.66	170 25.08	33.00	.00
770327	1841	57.90	57 34.80	169 57.00	33.00	4.2 0
780626	252	56.60	57 37.20	169 55.80	33.00	4.2 0

Teleseismic Record

Data. The teleseismically located earthquakes compiled in Tab. 7.6.2 are derived from four sources: (1) ISC (International Seismological Center), (2) PDE (Preliminary Determination of Epicenters, published by the USGS and archived by NOAA), (3) relocations by Tobin and Sykes (1966), and (4) relocations by Sykes (1971). These events are mapped in Fig 7.6.1. We restrict this analysis to events in the crustal material containing the St. George Basin; therefore, deep events (depth greater than 110 km, shown by dashed circles in Fig. 7.6.1) are excluded. From their locations (Fig 7.6.1) it can be seen that these deep events occur within the northernmost limb of the downgoing slab of Pacific lithosphere.

Interspersed with the epicenters of the deep events are those of about 30 events, the depths of which are unknown. Since we would like to account for these events in our analysis we observe that in the same area there are 7 shallow events and 13 deep events. We will assume that the same ratio of shallow-to-deep events holds for 30 events mentioned above.

To the northwest of this band of interspersed epicenters of deep and shallow events there are 19 additional events with unknown depths. We assume from their locations that these are shallow and, for purposes of identification assign them the depth 1.11 km (Tables 7.6.2 and 7.6.3).

In Fig 7.6.1 epicenters appear to be concentrated in the immediate region of the St. George Basin. A second concentration is centered in the southwest corner of the search area; these events are in the vicinity of the Umnak Plateau and the Bering Canyon. Lastly, a few outliers occur in the northeast part of the area. We further restrict the analysis by reducing the geographic area to the immediate St. George Basin region as shown in Fig 7.6.2 and the time interval to the 22 year period 1957-1978 as shown in Figure 3B. The resultant data set (Table 7,6.3) is the basis for the analysis that follows.

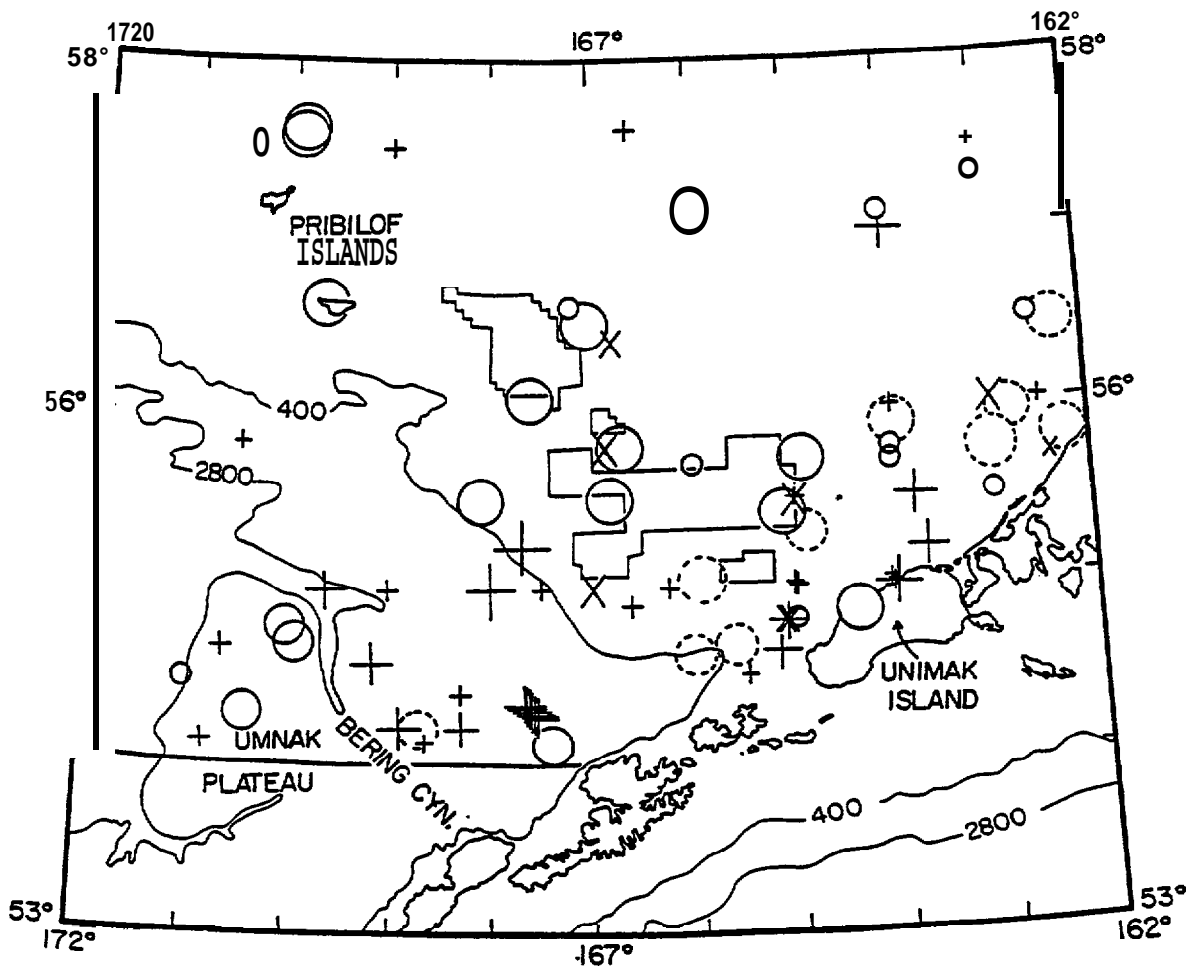


Fig. 7.6.1 Earthquake epicenters, greater St. George Basin area, 1925 through 1978. Epicenter symbols are scaled by magnitude according to height (minutes = $6.5 + 1.66 M$); crosses represent events with unknown depth; x's those with depths inferred to be shallow; solid circles, those known to be shallow ($Z \leq 75$ km); dashed circles, those known to be deep ($Z \geq 113$ km). The greater St. George Basin area is bounded on the north, east, and west by the edges of the region shown; the southern boundary is the heavy line along 54-N to its intersection with the Aleutian arc and then along the northern edge of the arc. The potential lease areas are encompassed by the light rectangular boxes. Isobaths are in meters.

TABLE 7.6.3

Frequency of Occurrence by Magnitude

<u>j</u>	<u>M</u>	<u>n</u>	nr	<u>N</u>	<u>log N</u>
1	5.75	1	1.606	1.606	0.206
2	5.1	1	1.606	3.212	0.507
3	4.8	1	1.606	4.818	0.683
4	4.7	1	1.606	6.424	0.808
5	4.5	2	3.212	9.636	0.984
6	4.4	1	1.606	11.242	1.051
7	4.3	3	4.818	16.060	1.206
8	4.2	5	8.030	24.090	1.382
9	3.6	1	1.606	25.696	1.410
10	3.5	1	1.606	27.302	1.436
11	3.4	<u>1</u>	<u>1.606</u>	28.908	1.461
TOTALS		18	28.908		

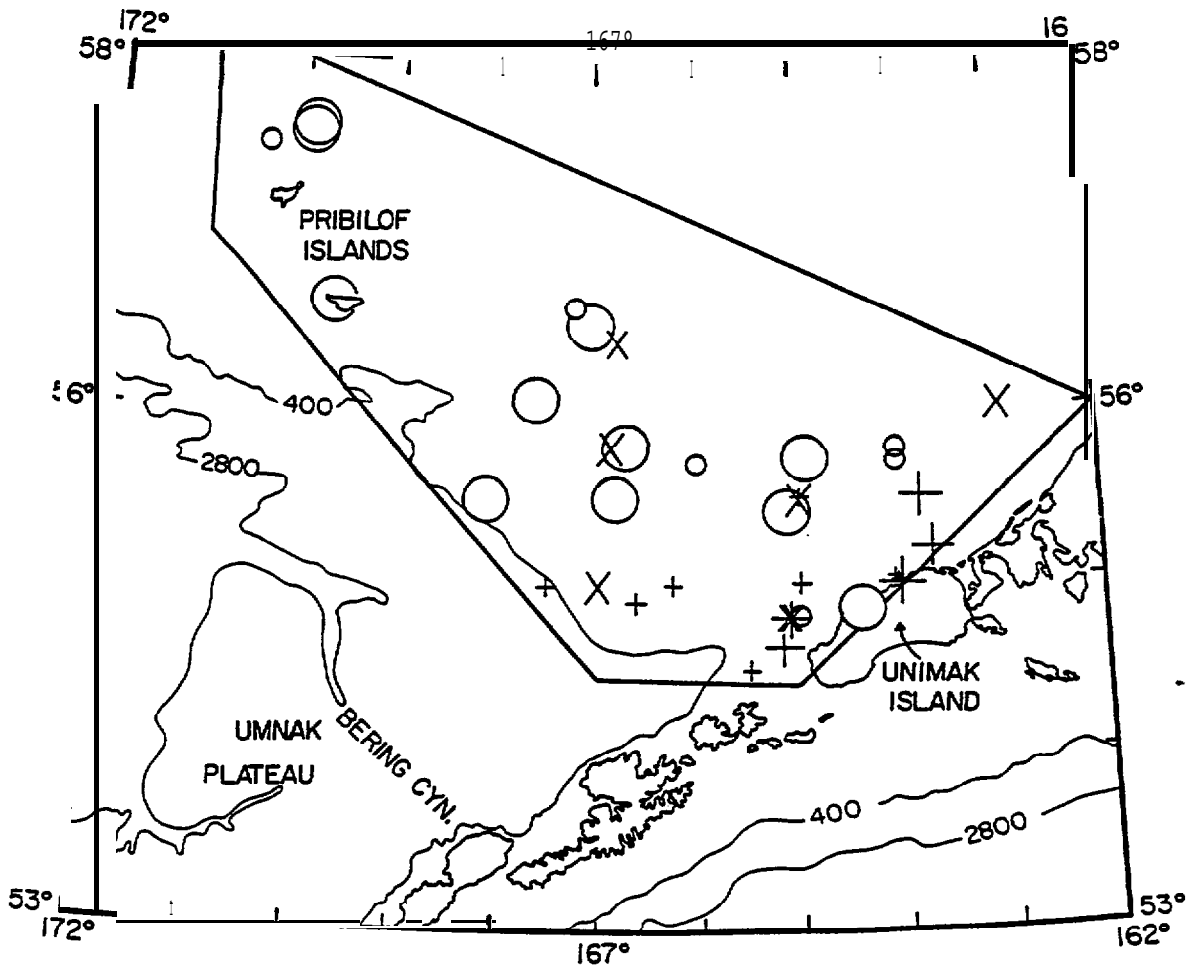


Fig 7.6.2 Epicenters of shallow ($Z < 70$ km) earthquakes, limited St. George Basin area, 1957 through 1978. Symbols are as in Fig 7.6.1. The limited St. George Basin area is bounded approximately by the heavy line.

Frequency of Occurrence for Events in Various Magnitude Ranges

This calculation is summarized in Tab 7.6.4. From Tab 7.6.3 we have 14 events for which both the magnitude and depth are known or inferred. Also, there are 10 events of unknown depth whose magnitudes are known. We assume that every third one of these (in order of decreasing magnitude) is shallow and for identification assign them a depth of 2.22. This results in a total of 18 events with known magnitudes that are known or inferred to be shallow. The magnitudes of these events and the number at each magnitude are listed in columns 2 and 3, respectively. In addition to these 18 events there are 6 for which only the depth is known (or inferred) and 14 for which the depth is unknown. The epicenters of the latter 14 are above the northern limb of the downgoing slab, so some of them are probably deep. We assume that the same ratio of shallow-to-deep events holds for these 14 as held for the 20 (7 shallow, 13 deep) enumerated above from the data set in Tab 7.6.2. Therefore, we infer that 4.9 of these 14 were shallow. Adding these 4.9 to the 6 known to be shallow we obtain an additional 10.9 shallow events for which to account that have unknown magnitudes. Thus, the total number of shallow events that occurred in the limited St. George basin region during the years 1957 through 1978 is 28.9. We assume that these additional 10.9 events are distributed by magnitude the same as the 18 for which magnitudes are known; therefore, since 28.9 is 1.606 times 18 we multiply the n in column 3 of Tab 7.6.4 by $r = 1.606$ to obtain the nr listed in column 4. Thus, nr is the estimated number of events at each magnitude for the specified region and time interval. We next obtain the cumulative number at successively smaller magnitudes, N, by summing the nr down column and listing the partial sums in column 5. That is:

$$N_j = \sum_{i=1}^j (nr)_i$$

Thus N_j is the number of events larger than or equal to M_j where j is the row number. The last column is simply the logarithm (base 10) of the corresponding entry in the previous one. This is computed for the b-value plot shown in Figure 7.6.4.

TABLE 7.6.4

Reports of Volcanic Activity in the Eastern Aleutian Arc from Okmok Volcano,
Umnak Island to Pavlof Volcano, Alaska Peninsula

Volcano	Report of Activity		Eruption ¹ Potential	Number of Reports ²				Remarks	
	<u>Earliest</u>	<u>Latest</u>		<u>A</u>	<u>E</u>	<u>Q</u>	<u>I</u>		
Okmok	1805	- 1958	5	1	9	4	3	2	1878, Makushin Village destroyed
Bogoslof	1796	- 1926	5	14	12	1	27		1796,1883,1926: island-forming events
Makushin	1768	- 1980	5	22	7	2	31		two volcanoes active in 1768, Bishop Pt. mudflow 30m high at shore
Akutan	1790	- 1980	5	35	16	2	53		mud flow 1929, 1 km lava flow 1978
Akun	1828	- 1880	1	3	0	0	3		no historic eruptions, deeply dissected
Pogromni	1795	- 1965	4	9	7	1	17		
Westdahl	1826	- 1979	4	4	4	0	8		1m of ash fell on Scotch Cap forcing evacuation, damaging light, floods washed our road, 1978
Fisher	1826	- 1826	1	1	0	0	1		questionable report of eruption, 1826
Shishaldin	1775	- 1979	5	47	230	70			1978 Sept. 28, caused radio interference
Isanotski	1690	- 1845	3	6	4	1	1	1	1825: mudslides, ash to Pavlof Bay
Roundtop	none		0	0	0	0	0		no reports
Frosty	1768	- 1951	1	4	0	0	4		reports for Walrus 6 Morshova assigned to Frosty (3)
Amak	1700	- 1715	1	1	0	0	1		no activity since 1804 at latest
Emmona	1768	- 1953	1	4	0	0	4		reports for Medvednikof assigned to Emmons (4)
Pavlof	1790	- 1980	5	49	30	180			1914 eruption: 5 cm of sand on Unga
Pavlof's Sister	1762	- 1786	2	--	--	--	--		not active since major eruption in 1786

Footnotes for Table 7.6.4

(1) Eruption Potential: scale 0-5

- 0 - no historic activity
- 1 - no historic eruptions, but smoke or steam reported
- 2 - last eruption in 1700's
- 3 - last eruption in **1800's**
- 4 - last eruption in 1900's
- 5 - last eruption in 1900's and $I > 25$

(2) A = reports of activity
E = reports of activity including eruptions
Q = reports of eruptions with earthquakes
I = **A + E + Q**

Note that A includes E and E includes Q so that reports of earthquakes are added 3 times into the index, I, -and reports of eruptions 2 times, whereas reports of activity (smoke, steam, etc.) are **only** counted once.

(3) **Morzhovoi** = Walrus (**Orth**, 1967) but Walrus Peak is nonvolcanic. **Waldron** (1961) thinks Morshova and Frosty are the same. We tentatively agree.

(4) Medvied = Bear; Medvednikova **Zaliv** = Bear Bay on Alaska Peninsula at **162°W** (**Orth**, 1967). Since **Emmons** Volcano is at **162°W** it seems possible that the old (≤ 1850) reports for Medviednikof refer to **Emmons**. Note that **Emmons** **received** its present name \sim 1940.

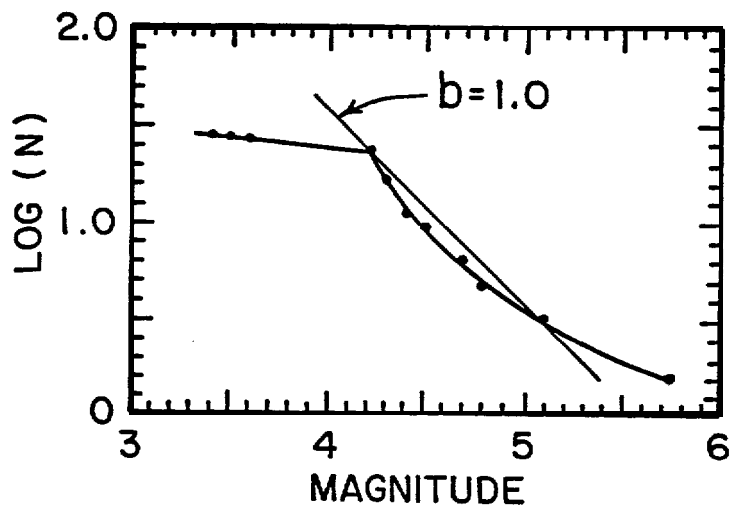


Fig. 7.6.4 Logarithm cumulative number of earthquakes vs. magnitude for the limited St. George Basin region during the period 1957 through 1978. Light line labeled $b = 1.0$ is a plot of the relation $\log N = a - bM$ with $a = 5.58184$ and $b = 1.0$. The shallow slope of the heavy curve below $M = 4.2$ indicates that the data set is incomplete below this magnitude; i.e., $M = 4.2$ is the detection threshold for this region and period. The increasing slope near $M = 5.0$ suggests that more events of $M \geq 5$ were observed than would usually be the case for this time interval.

The b-value is the absolute value of the slope of the well-known relation

$$\log N_j = a - bM_j. \quad (1)$$

We expect a b-value of about 1.0 which is the slope of the reference line plotted in Fig 7.6.4. The shape of the curve in this plot **is** controlled by the numbers of events **actually** observed at each magnitude listed in Tab 7.6.4, column 3. The shallow slope above magnitude 4.2 indicates that $M \approx 4.2$ is about the detection threshold for this data set. The increase in slope toward higher magnitude implies that more events with $M > 5.0$ were observed than would usually be the case for this region and interval. We note that the slope **in** the magnitude range $4.2 \leq M \leq 5.0$ **is** very close to 1.0. To determine the value of "a" **in** (1) it is best to use the values of M_j and N_j corresponding to the lowest magnitude above the detection threshold; viz., $M = 4.2$ and $N = 24.09$. This maximizes the number of observations used and hence minimizes the importance of observing or not observing any given event. Using the above values we obtain

$$a = \log (24.09) + 4.2 = 5.58184 \quad (2)$$

where we have assumed $b = 1.0$.

Using (1) and (2) we can compute the number of events expected within any magnitude range from

$$N(M_i, M_j) = N_i - N_j; \quad M_i < M_j. \quad (3)$$

We next assume that $N(M_i, M_j)$ is the expected value for the St. George basin region for any 22 year interval and that the number of events per unit time is distributed according to the Poisson function. We can then write (Hald, 1952, p. 732) the probability for the occurrence of one or more events in a given range $M_i \leq M \leq M_j$ and time interval $\tau = t$ years $\div 22$ is given by

$$P_{ij}(\text{one or more}) = 1 - P_{ij}(\text{none}) = 1 - e^{-N(M_i, M_j)\tau} \quad (4)$$

Using (1) through (4) and $t = 40$. years we find:

j	M_j	N_j	$N(M_{j-1}, M_j)$	$P_{j-1, j}$ (one or more)
1	4	38.18	-----	-----
2	5	3.818	34.36	1.0000
3	6	.3818	3.436	0.9981
4	7	.03818	.3436	0.4646
5	8	.003818	.03436	0.0606

The probability for the occurrence of an event of a certain size is not directly of interest: what is of more interest is the joint probability that the event will occur and that it will cause damage. We will reduce the problem to the exceedence of two specific accelerations; viz., 0.2 and $0.5g$. The conditional probability that given an event of a certain size it will cause accelerations greater than or equal to α is

$$P(ij|\alpha) = \frac{\pi r_{ij}^2(\alpha)}{A} \quad (5)$$

where $r_{ij}(\alpha)$ is the radius from the site of interest within which the event must occur if the acceleration is to reach α , and $A = 80,770 \text{ km}^2$ is the total area of the limited St. George Basin region as outlined in Fig 7.63. Therefore, the joint probability that an event of a certain size will occur and it will be close enough to exceed an acceleration of α is given by

$$P(ij \text{ and } \alpha) = P_{1j} \text{ (one or more)} P(ij|\alpha). \quad (6)$$

Finally, the total (or marginal) probability that α will be exceeded is the sum of the probabilities of each of the possible cases, neglecting terms of order $(P(ij \text{ and } \alpha))^2$ and higher: i.e.,

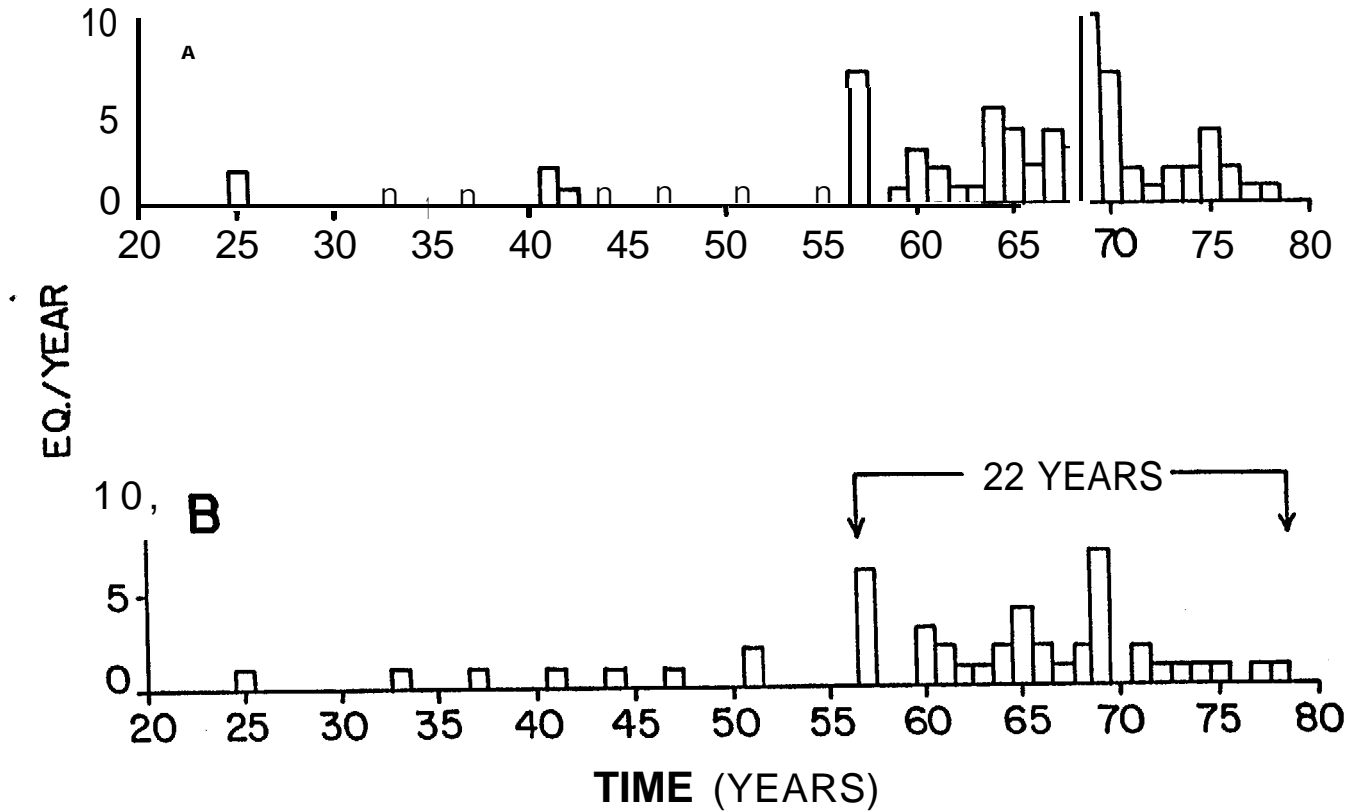


Fig. 7.6.3. Earthquakes per year for (A) the greater and (B) the limited St. George Basin region. Origin time for this histogram is the year 1900. The 22 year time span indicated for 1957 through 1978 is the period used in the computation of the probabilities that accelerations of 0.2 and 0.5 g would be exceeded at a specific site. It is clear from this figure that the detection threshold was higher in previous years, hence the restriction to the last 22 years for the analysis.

$$P(a) = \sum_{j=2}^5 P_{j-1, j}(\text{one or more}) P(j-1, j | a) \quad (7)$$

where, **as** above, $j=1$ corresponds to $M = 4.0$, 2 to 5.0, *etc.*

The radii, $r_{ij}(a)$ are scaled from the plot of acceleration-vs.-distance given in Fig 7.6.5. **Most** of the data in this figure were compiled by Page et al. (1972) for the western U.S. The larger symbols represent data collected at Sand Point, in the Shumagin Islands. The Aleutian data show systematically higher accelerations at a given distance than do those of the western U.S. Therefore these data are used to determine the intercepts of the lines labeled 4.5, 5.5, *etc.*, in Fig 7.6.5, **while** the western U.S. data are used to determine the slopes. The line labeled 4.5 is used to specify the acceleration-vs.-distance relation for earthquakes **in** the magnitude range $4.0 \leq M \leq 5.0$, that labeled 5.5 for the range $5.0 \leq M \leq 6.0$, *etc.* Thus, for example, the radius from a given site **within** which an earthquake in the range $6.0 \leq M \leq 7.0$ must occur **if** the acceleration is to exceed 0.5g is 30 km. From (5) the conditional probability that should such an earthquake occur in the St. George Basin region **it** will be close enough to a given site to cause an acceleration greater than 0.5g is

$$P(3,4|0.5) = \frac{\pi 30^2}{80,770} = 0.035 \quad (8)$$

Calculation of the probabilities for the ground acceleration to exceed 0.2 or 0.5 in 40 years for a site within the St. George Basin region is summarized in Tab 7.6.5. The values in this table are determined using (1) through (7) and the relations plotted in **Figure** 7.6.5. These calculations indicate for the limited **St. George** Basin region in a 40 year period the probability to exceed 0.2g is about 11% and that to exceed 0.5g **is** about 3%.

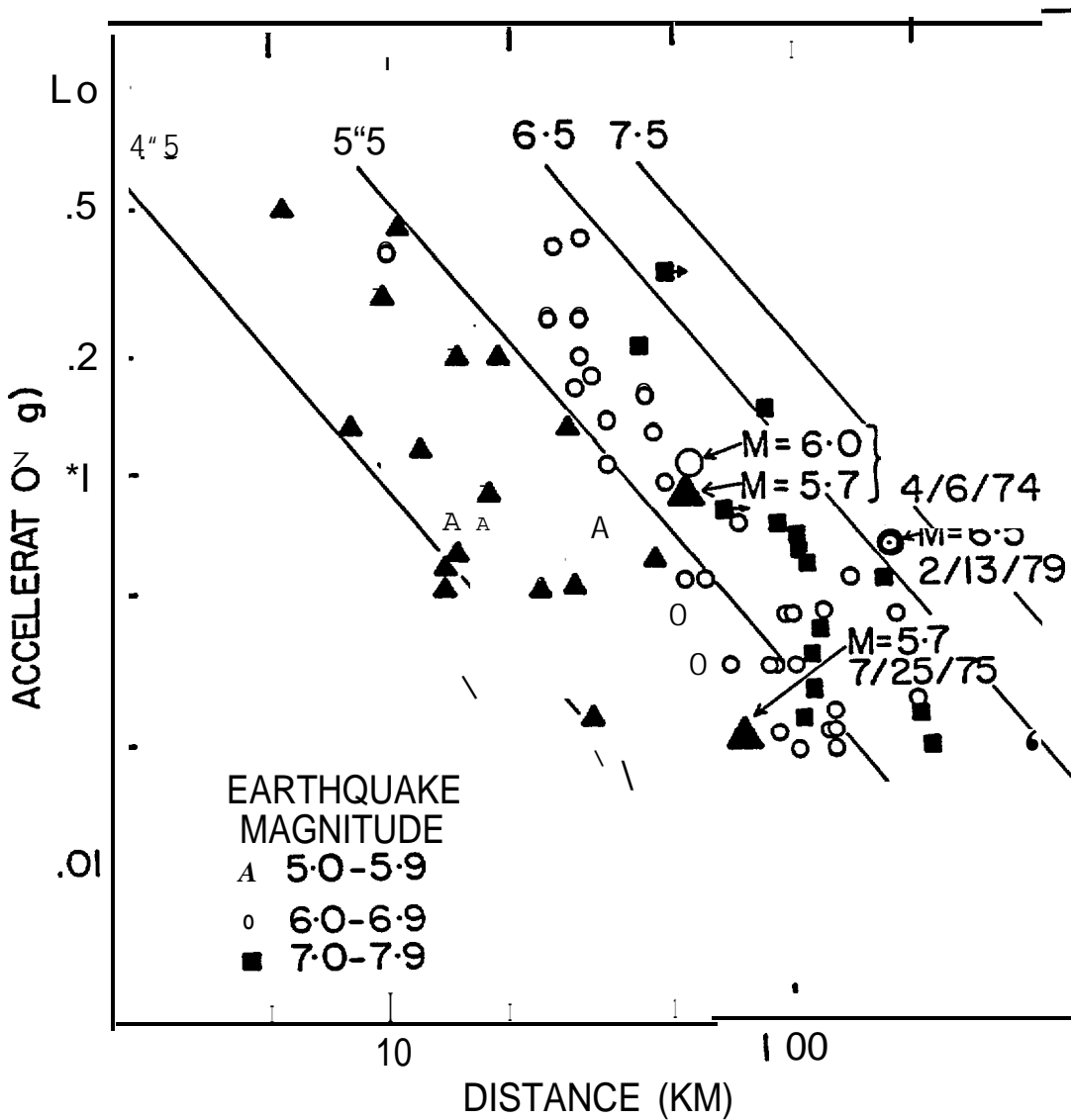


Fig. 7.6.5 Peak acceleration vs. distance for some western U.S. earthquakes (small symbols, page et al., 1972) and eastern Aleutian earthquakes (large symbols, Davies et al., 1979 and 1976; House and Boatwright, 1980). The lines labeled 4.5, 5.5, 6.5, and 7.5 are used to define the relationship between acceleration and distance for events in the magnitude ranges 4-5, 5-6, 6-7, and 7-8, respectively. The slopes of these lines are determined by the western U.S. data and the intercepts by the Aleutian data.

Local Record

Data. A **Geospace HS-10/1B** seismometer was installed in the Seismic Cottage (near the National Weather Service Observatory) on St. Paul Island during October 1975. This instrument is recorded on a Helicorder with a magnification at 5 Hz of about 17,500. The magnification of the St. Paul seismograph is limited by the surf noise propagated by the **alluvium** on which the Seismic Cottage **is** located.

In an attempt to determine the azimuth of the events recorded by this station, two **remote stations** were installed on St. Paul Island in July 1980. None of the local events recorded since then have been impulsive enough so that arrival times could be read with any confidence. Therefore, all of the data discussed in this section were recorded by the local, **short** period, vertical seismograph at St. Paul Island.

Table 7.6.6 gives arrival **times**, distances (**from** S-P times), and magnitudes for events detected at St. Paul (**SNP**) which might have occurred in the St. George Basin; without azimuths, only the distance can be specified. Magnitudes were calculated using Richter's (1958, p. 342) local scale and a correction determined by comparing the SNP magnitudes for the larger events to those listed in the PDE. Some larger ($M \approx 5$) events in the Aleutian arc between the Fox Islands and the Alaska Peninsula were included for this analysis.

Comparison of Seismic Rate

Figure 7.6.6 is a plot of magnitude vs. distance which shows that the magnitude threshold at about 450 km. is approximately 4.0. In other words, an earthquake in the southern St. George Basin must have a magnitude greater than or equal to 4.0 to be detected at SNP. Therefore, in comparing seismicity rates, the analysis must be restricted to events of 4.0 and larger.

There are only 3 such events listed in Table 7.6.6., all between $M = 4$ and $M = 5$. Thus, in the nomenclature of the previous section, $N(M_4, M_5) = 3$ which can be extrapolated (assuming a b-value of 1.0) to: $N(M_5, M_6) = 0.3$, $N(M_6, M_7) = 0.03$, and $N(M_7, M_8) = 0.003$. Using (4) from that section and the above $N(M_{j-1}, j)$, the $P_{j-1, j}$ (one or more) for $j=2$ through 5 are 1.00, **0.98**, 0.32, and 0.04, respectively. These are

TABLE 7.6.5

Probability for Acceleration to Exceed 0.2 or 0.5g in
40 Years for a Site Within the St. George Basin Region

j	M_j	$r_{j-1,j}(a)$ (km)	$P_{j-1,j}$ {one or more}	$P\{j-1,j a\}$	$P\{j-1,j \text{ and } a\}$
<u>for $a = 0.2g$ and $t = 40$ years:</u>					
1	4.0	—	—	—	—
2	5.0	5	1.0000	0.00097	0.00097
3	6.0	20	0.9981	0.016	0.02597
4	7.0	60	0.4646	0.14	0.06504
5	8.0	100	0.0606	0.39	0.02363
				<u>$P(0.2) =$</u>	<u>0.10561</u>

for $a = 0.5g$ and $t = 40$ years:

1	4.0	—	—	—	—
2	5.0	2.5	1.0000	0.00024	0.00024
3	6.0	10	0.9981	0.0039	0.00389
4	7.0	30	0.4646	0.035	0.01626
5	8.0	50	0.0606	0.097	0.00588
				<u>$P(0.5) =$</u>	<u>0.02627</u>

TABLE 7.6.6

Events Detected at SNIP in Distance Range Such That Origin in
St. George Basin is Possible

Time Interval: May 1977- July 1980

Date	Time	Distance (des.)	Distance (km)	Magnitude
77 05 20	12:50	0.58	.64	2.2
77 07 20	21:19	1.34	149	2.7
77 07 21	12:56	2.17	240	3.8
77 08 11	01:54	2.4s	272	3.8
17 09 23	17:21	0.71	85	2.1
77 11 30	00:15	0.92	102	2.0
78 03 07	02:56	0.77	85	4.1
78 07 13	13:26	2.17	241	4.5
7a 07 24	14:52	0.16	68	3.0
78 08 06	01:51	3.88	431	4.0
78 06 24	09:01	2.27	252	3.6
78 09 24	16:43	0.79	88	3.0
78 11 28	17:42	1.01	112	2.5
79 04 29	14:16	0.3s	42	1.8
60 02 0s	13:38	0.69	77	2.s
60 03 22	10:31	2.08	231	3.s
08 07 23	17:13	0.46	51	1.6

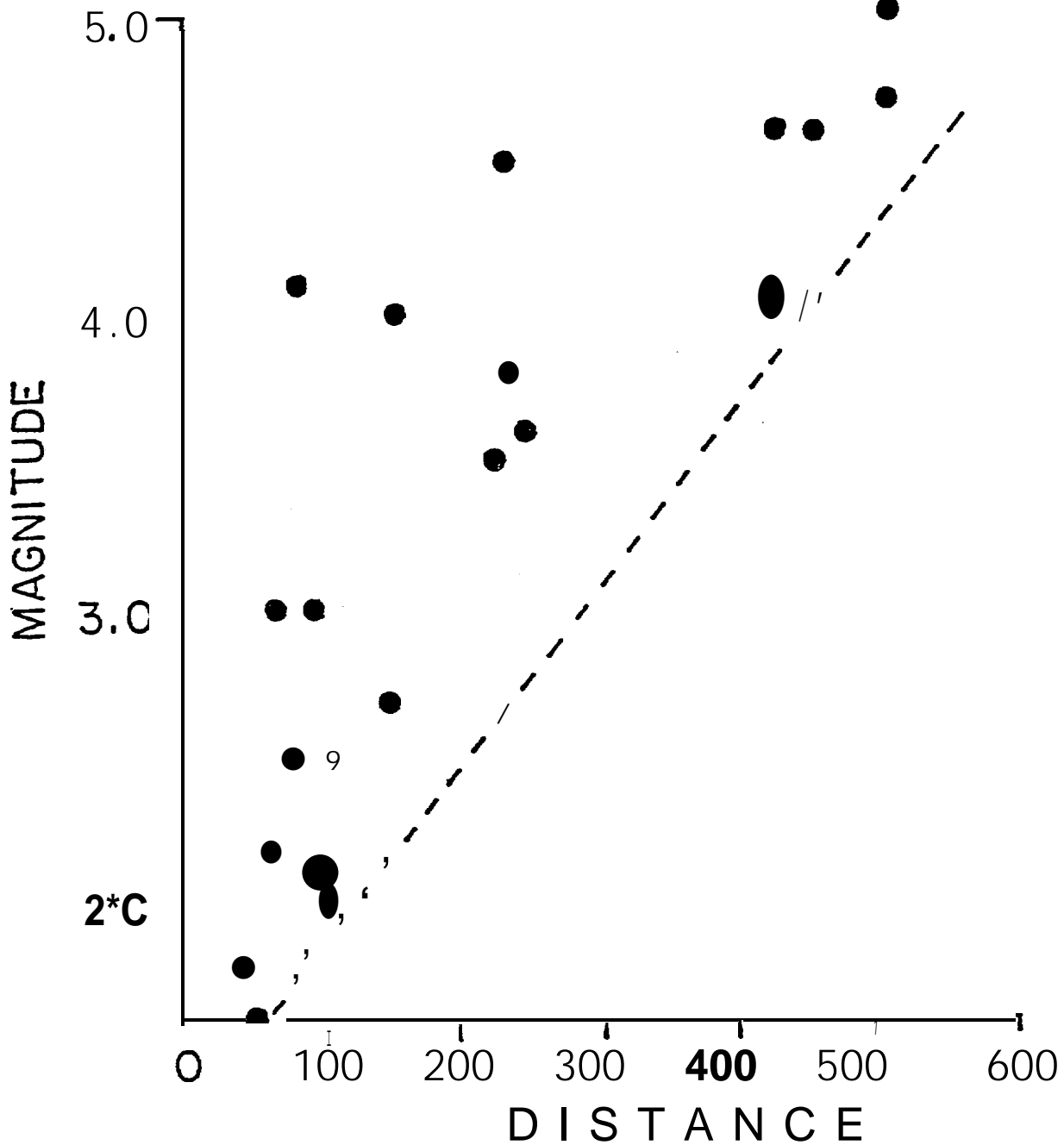


Fig. 7.6.6. Detection threshold for **St. Paul** Seismic station (**SNP**). Plotted is local magnitude (**see text**) vs. distance based on S-P time (the interval between the arrival of the P-wave and the S-wave). Since the southern end of the St. George basin is a **little** over 400 km from St. Paul Is., the smallest earthquake that can be detected over the whole basin by **SNP** is about ML - 4.0.

the probabilities that an earthquake in the respective range of magnitudes will occur within 40 years. The comparable probabilities computed from the teleseismic data are 1.00, 0.998, 0.46, and 0.06. Thus, the local data over a $3 \frac{1}{6}$ year span indicate the same order of activity as do the *teleseismic data over* a 22 year span.

VOLCANIC ACTIVITY

Pribilofs. **Mushketov** and **Orlov** (1893, p. 198) report "a submarine earthquake and eruption" northeast of St. George in 1815. Barth (1956) references Landgrebe (1855) for the statement that "flames have been seen **to rise** from the sea northeast of the **Pribilof Islands**". It is likely that both of these reports are based on a report from Kotzebue around 1821 to 1828 which we have not been able to find. Barth (1956, p. 154) concludes "However, in spite of these assertions any present volcanic activity must be regarded as doubtful". Hopkins (1976) similarly concludes "The volcanic hazard is small on and near St. Paul Island and negligible elsewhere". He also **states** "The numerous isolated shocks **in** the vicinity of the **Pribilof Islands** are probably [emphasis ours] mostly ancient, eroded, volcanic centers. . . appropriate **paleontological** or **radiometric** methods [should be] used to establish their age". We conclude that volcanic activity is unlikely but suggest that Hopkins' advice be followed if any structures are to be built on or near St. Paul and St. George.

Makushin Bay. In 1878 the village of **Makushin** was destroyed by an earthquake (**Mushketov-Orlov**, 1893, p. 468). The earthquake and associated tsunami have been reported as part of a crater-forming event at **Okmok** Volcano (**Hantke**, 1951). Apparently the village was destroyed by the tsunami that swept along the north shore of **Unalaska** Island. Note that **Makushin** Bay is also exposed to **Bogoslof** Volcano at a distance roughly equal to that of **Okmok**.

Scotch Cap. The 1978 eruption of **Westdahl** deposited 1 m of ash on the U.S. Coast Guard light station at Scotch Cap. The ash damaged the light and forced the evacuation of the site, **meltwater** floods washed out the road to Cape Sarichef.

Other Volcanic Activity. Tab 7.6.7 is a summary of reports of volcanic activity (Hickman, unpublished files) in the eastern Aleutian arc from Okmok Volcano on **Umnak** Island to **Pavlof** Volcano on the Alaska Peninsula. Of the 16 volcanoes listed, 8 are rated as having a high potential for eruption (4,5 on a scale of 0-5; see footnote 1, Table 7.6.7) : Okmok, **Bogoslof**, Makushin, Akutan, Pogromni, **Westdahl**, Shishaldin, and **Pavlof**. **Isanotski** is given a moderate potential (3) and the remaining seven are rated at a low to negligible potential (2-0).

For the purpose of siting a pipeline terminal/tanker facility those volcanoes with a high potential for eruption should be regarded as likely to produce the following hazards:

- (1) **lavaflo**ws, **mudslides**, floods , incandescent bombs, and nuee ardent on the flanks and **in** valleys around the volcano.
- (2) ash and sand clouds capable of depositing up to a meter of material several tens of km downwind from the volcano and a few centimeters of material at 100 to 150 km. The fine particles will produce a plume in which planes should not fly 100 to 200 **km** wide and 200 to 500 km **long**. This phase **may persist for hours to days**.
- (3) local tsunamis to distances of 100 **to** 150 km.
- (4) several hours to 10's **of** hours of radio interference during the eruption.

7.7 List of Publications Partially Supported by Contract NOAA 03-5-022-70

Jacob, K.H., K. Nakamura, and J.N. Davies, Trench-volcano gap along the Alaska-Aleutian arc: Facts, and speculations on the role of terrigenous sediments for subduction, Maurice Ewing **Series, 1**, edited by M. Talwani and W. Pitman III, pp. 243-258, AGU, Washington, D.C. 1977.

Nakamura, K., K.H. Jacob, and J.N. Davies, Volcanoes as possible indicators of tectonic stress orientation - Aleutians and Alaska, **PAGEOPH, 115**, 87-112, 1977.

Bilham, R., A sea-level recorder for tectonic studies, **Geophys. J. Roy. astr. Soc., 48**, 307-314, 1977.

Davies, J.N., K.H. Jacob, and L.R. Sykes, A comprehensive study of the seismotectonics of the eastern Aleutian arc and associated volcanic systems, Eight-Year Synopsis 1970-1978, to U.S. Department of Energy, 1978.

Davies, J.N., and L.S. House, Aleutian subduction zone seismicity, volcano-trench separation and their relation to great thrust-type earthquakes, **J. Geophys. Res., 84**, 4583-4591, 1979.

Bilham, R., and J. Beavan, Satellite telemetry of sea-level data to monitor crustal motions in the Shumagin Islands region of the Aleutian arc, in **Proc. Conf. Terrestrial and Space Techniques in Earthquake Prediction Research, 1979**.

House, L., and J. Boatwright, Investigation of two high stress-drop earthquakes in the Shumagin Seismic Gap, Alaska, **J. Geophys. Res., 85**, 7151-7165, 1980.

Davies, J.N., L.R. Sykes, L. House, and K.H. Jacob, Shumagin seismic gap, Alaska Peninsula: History of great earthquakes, tectonic setting, and evidence for high seismic potential, **J. Geophys. Res., 86**, 3821-3856, 1981.

Sykes, L.R., J.B. Kissinger, L. House, J.N. Davies, and K.H. Jacob, Rupture zones of great earthquakes, Alaska-Aleutian arc, 1784-1980, **Science, 210**, 1343-1345, 1980.

McCann, W.R., O.J. Perez, and L.R. Sykes, 1980. Yakataga seismic gap, southern Alaska: Seismic history and earthquake potential, **Science, 207**, 1309-1314.

Perez, O.J., and K.H. Jacob, 1980. Tectonic model and seismic potential of the eastern Gulf of Alaska and Yakataga seismic gap, **J. Geophys. Res., 85**, 7132-7150.

Perez, O.J., and K.H. Jacob, 1980. St. Elias, Alaska earthquake of February 28, 1979: Tectonic setting and precursory seismic pattern, **Bull. Seismol. Soc. Amer., 70**, 1595-1606.

Boatwright, J., 1980. Preliminary body wave analysis of the St. Elias, Alaska earthquake of February 28, 1979, **Bull. Seismol. Soc. Amer., 70**, 419-436.

House, L., **L.R. Sykes**, **J.N. Davies**, and **K.H. Jacob**, Identification of a possible seismic gap near **Unalaska** Island, Eastern Aleutians, Alaska, in Earthquake Prediction, An International Review, Maurice Ewing Series, 4, edited by **D.W. Simpson** and **P.G. Richards**, pp. 81-92, AGU, Washington, D.C. 1981.

Sykes, L.R., **J.B. Kisslinger**, L. House, J. Davies, and K. Jacob, Rupture zones and repeat times of great earthquakes along the Alaska-Aleutian arc, in Earthquake Prediction, An International Review, Maurice Ewing Series, 4, edited by **D.W. Simpson** and **P.G. Richards**, pp. 73-80, AGU, Washington, D.C., 1981.

Nakamura, K., G. **Plafker**, **K.H. Jacob**, and **J.N. Davies**, A tectonic stress trajectory map of Alaska using **information** from volcanoes and faults, Bull. **Earthq. Res. Inst.**, 55, Part **1**, 89-100, University of Tokyo, **1980**.

McNutt, S.R., and **R.J. Beavan**, Volcanic earthquakes at **Pavlof** Volcano, Alaska, correlated with the solid earth tides, Nature, 294, 615-618, 1982.

Reyners, M., and K. **Coles**, Fine structure of the dipping seismic zone and subduction mechanics in the **Shumagin** Islands, Alaska, J. **Geophys. Res.**, 87, 356-366, 1982.

McNutt, S.R., and **R.J. Beavan**, Correlation of the solid earth tide with volcanic earthquakes at **Pavlof** Volcano, Alaska, Proceedings of the 9th International Symposium on Earth Tides, New York, **1981**.

House, L., and **K.H. Jacob**, Thermal stress in descending **lithospheric** slabs and implications for double seismic zones and downdip stress polarities, Nature, 295, 587-589, 1982.

McNutt, S., Seismic monitoring of volcanoes in the Aleutians, Volcano News, 11, page 7, 1982.

House, L.S., and **K.H. Jacob**, Earthquakes, plate subduction, and stress reversals in the eastern Aleutian arc, J. **Geophys. Res.**, in press, 1983.

Mori, J., Dynamic stress drops of moderate earthquakes of the eastern Aleutians and their relation to a great earthquake, Bull. **Seism. Soc. Am.**, 73, 1077-1097, 1983.

Mori, J., Short- and long-period subevents of the February 4, 1965, Rat Islands earthquake, Bull. **Seism. Soc. Am.**, in press, 1983.

Mori, J., Duration of **P-** and **S-wave** pulses for small earthquakes in the **Shumagin** Islands, Alaska, submitted to Bull. **Seism. Soc. Am.**, 1982.

Beavan, J., E. **Hauksson**, **S.R. McNutt**, R. **Bilham**, and **K.H. Jacob**, Tilt and **seismicity** changes in the **Shumagin** seismic gap, submitted to Science, 1983.

Beavan, R., R. **Bilham**, and K. Hurst, Coherent tilt signals observed in the **Shumagin** seismic gap: Detection of time-dependent subduction at depth, submitted to J. **Geophys. Res.**, 1983.

8. REFERENCES

- Abe, K., 1979. Size of great earthquakes of 1837-1974 inferred from tsunami data, J. Geophys. Res., 84, 1561-1568.
- Abe, K., 1981. Magnitudes of large shallow earthquakes from 1904 to 1980, Phys. Earth Planet. Int., 27, 72-92.
- Aki, K., 1981. A probabilistic synthesis of precursory phenomena, in Earthquake Prediction, An International Review, Maurice Ewing Series, 4, edited by D.W. Simpson and P.G. Richards, pp. 566-574, AGU, Washington, D.C.
- Barth, T.F., 1956. Geology and petrology of the **Pribilof** Islands, Alaska, U.S. Geol. Surv. Bull. 1028-F, 101-160.
- Beavan, R., R. Bilham,** and K. Hurst, 1983. Coherent tilt signals observed in the **Shumagin** seismic gap: Detection of time-dependent subduction at depth, submitted to J. Geophys. Res.
- Bendat, J.S., and **A.G. Pierson**, 1981. Random Data: Analysis and Measurement Procedures, **Wiley-Interscience** Publ., New York.
- Burke, C.A., 1965. **Geologic** map of the Alaska Peninsula, Geol. Soc. Am. Memoir 99, part 2, sheets 1 and 2.
- Byers, J.M., Jr., 1959. Geology of **Umnak** and **Bogoslof** Islands, Aleutian Islands, Alaska, U.S. Geol. Surv. Bull. 1028-L, 267-369.
- Carr, M.J., 1977. Volcanic activity and great earthquakes at convergent plate margins, Science, 197, 655-657.
- Coffman, J.L.,** and **C.A. von Hake**, 1973. Earthquake history of the Us., Revised Edition (through 1970), Publication 41-1, NOAA Environ. Data Service, Boulder, Colorado.
- Cox, D., and G. Pararas-Carayanis, 1976. Catalog of Tsunamis in Alaska, U.S., 78 pp., Dept. of Commerce, **NOAA/EDS**, Asheville, North Carolina.
- Crandell, D.R.,** and **D.R. Mullineaux**, 1978. Potential hazards from future eruptions of Mount St. Helens Volcano, Washington, U.S. Geol. Surv. Bull. 1383-c, C1-C26.
- Davies, J.N., and L. House, 1979. Aleutian subduction zone seismicity, volcano-trench separation, and their relation to great thrust-type earthquakes, J. Geophys. Res., 84, 4583-4591.

- Davies, J., L. Sykes, L. House, and K. Jacob, 1981. Shumagin seismic gap, Alaska Peninsula: History of great earthquakes, tectonic setting, and evidence for high seismic potential, J. Geophys. Res., 86, 3821-3856.
- Davis, T.N., and C. EchoIs, 1962. A table of Alaska earthquakes, 1788-1961, **Geophys. Inst.**, Univ. of Alaska, Fairbanks, **Alaska**, Geophys. Rep. No. 8.
- Detterman, **R.L.**, **T.P. Miller**, **M.E. Yount**, and **F.H. Wilson**, 1981a. Geologic map of the Chignik and Sutwik Island Quadrangles, Alaska, U.S. Geol. Surv. Map 1-1229, 1:250,000.
- Detterman, R.L., T.P. Miller, M.E. Yount, and F.H. Wilson, 1981b. Quaternary geologic map of the **Chignik** and **Sutwik Island** Quadrangles, Alaska, U.S. Geol. Surv. Map 1-1292, 1:250,000.
- Dorm, W.L., and D. **Ninkovich**, 1980. Rate of Cenozoic explosive volcanism in the North Atlantic Ocean inferred from deep sea cores, J. Geophys. Res., 85, 5455-5460.
- Drewes**, H., **G.D. Fraser**, **G.L. Snyder**, and **H.F. Barnett**, Jr., 1961. Geology of **Unalaska** Island and adjacent insular shelf, Aleutian Islands, Alaska, U.S. Geol. Surv. Bull. 1028-S, 583-676.
- Duda, S.J., 1965. Secular seismic energy release in the **circum-Pacific** belt, Tectonophysics, 2, 409-452.
- Einarsson, P., and B. Brandsdottir, 1980. Seismological evidence for lateral magma intrusion during the July 1978 deflation of the **Krafla** Volcano in NE-Iceland, J. Geophys., 47, 160-165.
- Glover**, D.P., 1980. Historical Seismogram Filming Project, Second Progress Report, Rpt. SE-24, August 1983, 63 pp., **NOAA/EDS**, Boulder, Colorado.
- Glover**, D.P., and H. Meyers, 1981. Historical Seismogram Filming Project, Third Progress Report, Rpt. SE-28, World Data Center A, Solid Earth Geophysics, NOAA/OCS, Boulder, Colorado.
- Glover**, D.P., and H. Meyers, 1982. Historical Seismogram Filming Project, Fourth Progress Report, Rpt. SE-33, World Data Center A, Solid Earth Geophysics, NOAA-National Geophys. Data Center, Boulder, Colorado.
- Gutenberg, B., and **C.F. Richter**, 1949. Seismicity of the Earth, First Edition, Princeton Univ. Press, 273 pp., Princeton, New Jersey.

- Gutenberg, B., 1956. Great earthquakes 1896-1903, Trans. Amer. Geophys. Union, 37, 608-614.
- Habermann, R.E., 1983. Teleseismic detection in the Aleutian Island arc, J. Geophys. Res., 88, 5056-5064.
- HaId, E., 1952. Statistical Theory with Engineering Applications, Wiley Publishers, New York, 97 pp.
- Hantke, G., 1951. Review of volcanic activity 1941-47 (in German), Bull. Volcan., 11.
- Hauksson, E.**, 1982. Some source parameters of small earthquakes in the Shumagin seismic gap, Alaska, (abstract), Earthq. Notes, 53, 40.
- Hays, J.D., D. **Ninkovich**, 1970. North Pacific deep-sea ash chronology and **age** of present Aleutian underthrusting, in Geological Investigations of the North Pacific, edited by J.D. Hays, GSA Memoir 126.
- Hopkins, D.M., 1976. Fault history of the **Pribilof** Islands and its relevance to bottom stability in the St. George Basin, in Environmental Assessment of the Alaska Continental Shelf, Principal Investigators Annual Reports, April 1975-March 1976, **NOAA/BLM** OCSEAP, Geology Volume, 13, 41-68.
- House, L., and J. Boatwright, 1980. Investigation of two high stress-drop earthquakes in the **Shumagin** seismic gap, Alaska, J. Geophys. Res., 85, 7151-7165.
- House, L., and **K.H. Jacob**, 1983. Earthquakes, plate subduction and stress reversals in the eastern Aleutian arc, J. Geophys. Res., in press.
- House, L., **L.R. Sykes**, **J.N. Davies**, and **K.H. Jacob**, 1981. Identification of a possible seismic gap near **Unalaska** Island, Eastern Aleutians, Alaska, in Earthquake Prediction, An International Review, Maurice Ewing Series, 4, edited by **D.W. Simpson** and **P.G. Richards**, pp. 81-92, AGU, Washington, D.C.
- Jacob, et al., 1983. Probabilities for future great earthquakes in the Alaska-Aleutian arc based on past moment release, in preparation.
- Joyner, W.B.**, and **D.M. Boore**, 1981. Peak horizontal acceleration and velocity from strong-motion records including records from the

- 1979 Imperial Valley, California, earthquake, Bull. Seism. Soc. Am*, 71, 2011-2038.
- Kanamori, H., 1977a. The energy release in great earthquakes, J. Geophys. Res., 82, 2931-2988.
- Kanamori, H., 1977b. Seismic and aseismic slip along subduction zones and their tectonic implications, in Island Arcs, Deep Sea Trenches and Back-Arc Basins, Maurice Ewing Series, 1, edited by M. Talwani and W.C. Pitmann, pp. 1963-174, AGU, Washington, D.C.
- Kanamori, H., and K. Abe, 1979. **Re-evaluation** of the turn-of-the-century seismicity peak, J. Geophys. Res., 84, 6131-6139.
- Kelleher**, J.A., 1970. Space-time seismicity of the Alaska-Aleutian seismic zone, J. Geophys. Res., 75, 5745-5756.
- Kimura, M., 1978. Significant eruptive activities related to large interplate earthquakes in the northwestern Pacific margin, J. Phys. Earth, 26, S557-S570.
- Kisslinger, J., J. Davies, L. Sykes, L. House, and K. Jacob, 1983. Historical earthquakes of Alaska and the Aleutian Islands: A compilation of original references, some newly translated, in preparation.
- Klein, 1978. Hypocenter location program HYPOINVERSE, part 1: Users guide to versions 1, 2, 3, and 4; part 2: source listings and notes, U.S. Geol. Surv. Open-File Rpt. 78-694, 114 pp.
- Lahr, J.C., 1980. **Hypoellipse/Multics**: A computer program for determining local earthquake hypocentral parameters, magnitude, and first motion pattern, U.S. Geol. Surv. Open-File Rpt. 80-59.
- Lahr**, J.C., C.D. Stephens, H.S. Hasegawa, and J. Boatwright, 1980. Alaskan seismic gap only partially filled by 28 February 1979 earthquake, Science, 207, 1351-1353.
- Landgrebe, G., 1855. Naturgeschichte der Vulkane, Gotha.
- McCann, W.R., O.J. Perez, and L.R. Sykes, 1980. **Yakataga** seismic gap, southern Alaska: seismic history and earthquake potential, Science, 107, 1309-1314.
- McCann, W.R., S.P. Nishenko, L.R. Sykes, and J. Krause, 1980. Seismic gaps and plate tectonics: seismic potential for major plate boundaries, Pure Appl. Geophys., 117, 1082-1147. "

- McNutt, S., 1981a. **Pavlof** volcano "eruption report, EOS, Trans. AGU, 62, 13-14.
- McNutt, S., 1981b. **Pavlof** volcano eruption report, EOS, Trans. AGU, 62, 717-718.
- McNutt, S.R., and R.J. Beavan, 1981. **Volcanic** earthquakes at **Pavlof** Volcano, Alaska, correlated with the solid earth tide, submitted to Nature.
- McNutt, S., 1982a. Seismic monitoring of volcanoes in the Aleutians, Volcano News, 11, 7.
- McNutt, S., 1982b. Analysis of volcanic tremor from **Pavlof**, Fuego, **Pacaya**, San **Cristobal**, and Mas aya volcanoes, Bol. de Volcanologic, Heredia, Costa Rica, in press.
- McNutt, S., and J. Mori, 1982. Analysis of B-type earthquakes and explosions at **Pavlof** Volcano, Alaska, abstract, EOS, Trans. AGU, 64, 45.
- Meyers, H., 1976. A historical summary of earthquake epicenters in and near Alaska, NOAA Technical Mere. EDS-NSGDC-1, National **Geophys.** and Solar Terrestrial Data Center, Boulder, Colorado.
- Meyers, H., and C.A. von Hake, 1976. Earthquake data file summary, key to geophysical records documentation no. 5, National Oceanic and Atmospheric Administration, Environmental Data Service, 32 pp "
- Meyers, H., R.J. Brazee, J.L. Coffman, and S.R. Lessig, 1976. An analysis of earthquake intensities and recurrence rates in and near Alaska, NOAA Technical Report EDS-NGSDC-3, National **Geophys.** and Solar Terrestrial Data Center, Boulder, Colorado.
- Miller, C.D., 1980. Potential hazards from future eruptions in the vicinity of Mount Shasta Volcano, northern California, U.S. Geol. Surv. Bull. 1503, 43 pp.
- Miller, C.D., D.R. Mullineaux, D.R. Crandell, and R.A. Bailey, 1982. Potential hazards from future eruptions in the Long Valley-Mono Lake area, east-central California and southwest Nevada - a preliminary assessment, U.S. Geol. Surv. Circular 877, 10 pp.
- Minster, J.B., and T.H. Jordan, 1978. Present-day plate motions, J. Geophys. Res., 83, 5331-5354.

- Mushketov, I.**, and **A. Orlov**, 1893. Catalog of earthquakes of the Russian Empire, Contr. Russian Geog. Sot., in general geography, 26, 582 pp.
- Nicholson, C., and **D.W. Simpson**, 1983. Routine processing for **crustal** earthquake locations and velocity models, in preparation.
- Orth, D.J., 1967. Dictionary of Alaska place names, U.S. Geol. Surv. Prof. Paper 567, 1084 pp.
- Page, R.A., 1968a. Aftershocks and microaftershocks of the great Alaska earthquake of 1964, Bull. Seism. Sot. Am., 58, 1131-1168.
- Page, R.A., 1968b. Focal depths of aftershocks, J. Geophys. Res., 73, 3897-3903.
- Page, R.A., **D.M. Boore**, **W.B. Joyner**, and **H.W. Coultner**, 1972. Ground motion values for use in the seismic design of the **Trans-Alaska** Pipeline System, U.S. Geol. Surv. Circ. 672.
- Pérez**, O.J., and **K.H. Jacob**, 1980. Tectonic model and seismic potential of the eastern Gulf of Alaska and **Yakataga** seismic gap, J. Geophys. Res., 84, 7132-7150.
- Pérez**, O.J., and **K.H. Jacob**, 1980. St. **Elias**, Alaska earthquake of February 28, 1979: tectonic setting and precursory seismic pattern, Bull. Seism. Sot. Am., 70, 1595-1606.
- Purcaru**, G., and H. Berckhemer, 1978. A magnitude scale for very large earthquakes, Tectonophysics, 49, 189-198.
- Purcaru**, G., and H. Berckhemer, 1982. Quantitative relations of seismic source parameters and a classification of earthquakes, Tectonophysics, 84, 57-128.
- Reyners, M., and K. **Coles**, 1982. Fine structure of the dipping seismic zone and subduction mechanics in the **Shumagin** Islands, Alaska, J. Geophys. Res., 87, 356-366.
- Richter, C.F., 1958. Elementary Seismology, **W.H. Freeman and Co.**, San Francisco, **Calif.**, 768 pp. .
- Rose, W.I., Jr., 1972. Notes on the 1902 eruption of Santa Maria Volcano, Guatemala, Bull. VolcanoI. , 36, 29-45.
- Rose, W.I., Jr., **A.T. Anderson, Jr.**, **L.G. Woodruff**, and **S.B. Bonis**, 1978. The October 1974 basaltic tephra from **Fuego** Volcano: description and history of the magma body, J. **Volcanol. Geotherm. Res.**, 4, 3-53.

- Rose, W. I., Jr. , S. Bonis, **R.E.** Stoiber, M. Keller, and T. Bickford, **1973.** Studies of volcanic ash from two recent Central American eruptions, Bull. Volcanol. , 37, 338-364.
- Rothé, J.P.**, 1969. The seismicity of the earth, 1953-1965, UNESCO, Paris.
- sapper, K., 1905. In den Vulkanbieten Mittleamerika und Westindieu, Stuttgart, 334 pp.
- Sarna-Wojcicki, A.M.**, S. Shipley, **R.B.** Waite, Jr., D. Dzurisin, and **S.H.** Wood, 1982. Areal distribution, thickness, mass, volume, and grain size of air-fall ash from the six major eruptions of 1980, in The 1980 Eruptions of Mt. St. Helens, Washington, edited by **P.W. Lipman**, and **D.R. Mullineaux**, U.S. Geol. Surv. Prof. Paper 1250.
- Shimazaki, K.**, and T. Nakata, 1980. Time predictable recurrence model for large earthquakes, Geophys. Res. Lett., 7, 279-282.
- Simkin, T.**, L. Siebert, L. McClelland, D. Bridge, C. **Newhall**, and **J.H.** Latter, 1981. Volcanoes of the World, **Hutchinson Ross Publ. Co.**, Stroudsburg, Penn., 232 pp.
- Solov'iev, S.L.**, **1968.** Sanak-Kodiak tsunami 1788, Problems Tsunami, Nauka, Moscow, 232-237.
- Sykes, L.R., 1971. Aftershock zones of great earthquakes, seismicity gaps, earthquake prediction for Alaska and the Aleutians, J. Geophys. Res., 76, 8021-8041.
- Sykes, L.R., **J.B.** Kisslinger, L. House, J. Davies, and **K.H.** Jacob, **1980.** Rupture zones of great earthquakes, Alaska-Aleutian arc, 1784-1980, Science, 210, 1343-1345.
- Sykes, L.R., and **R.C.** Quittmeyer, 1981. Repeat times of great earthquakes along simple plate boundaries, in Earthquake Prediction, An International Review, Maurice Ewing Series, **4**, edited by **D.W. Simpson** and **P.G. Richards**, pp. 217-247, **AGU**, Washington, D.C.
- Sykes, L.R., **J.B.** Kisslinger, L. House, J. Davies, and **K.H.** Jacob, 1981. Rupture zones and repeat times of great earthquakes along the Alaska-Aleutian arc, 1784-1980, in Earthquake Prediction, An International Review, Maurice Ewing Series, **4**, edited by **D.W. Simpson** and **P.G. Richards**, pp. 73-80, **AGU**, Washington, D.C.
- Sykes, L.R., and S. Nishenko, 1983. Probabilities of occurrence of large **plate** rupturing earthquakes for the **San** Andreas, **San**

- Jacinto** and Imperial faults, California, 1983-2003, submitted to J. Geophys. Res.
- Tarr, R.S., and L. Martin, 1912. The earthquake at **Yakutat** Bay, Alaska, in September 1899, U.S. Geol. Surv. Prof. Paper 69.
- Taylor, P.S., and **R.E. Stoiber**, 1973. Soluble material on ash from **active** Central American volcanoes, Bull. Geol. Soc. Am., 84, 1031-1042.
- Thatcher, W., and G. **Plafker**, 1977. The 1899 **Yakutat** Bay, Alaska earthquakes, Intern. Union. Geod. Geophys., IASPEI/IAVCEI Assembly, abstract, pp. 54, Durham, England.
- Tobin, D.G., and **L.R. Sykes**, 1966. Relationship of **hypocenters** of earthquakes to the geology of Alaska, J. Geophys. Res., 71, 1659-1667.
- Utsu**, T., 1962. On the nature of three Alaskan aftershock sequences of 1957 and **1958**, Bull. Seism. Soc. Am., 52, 279-297.
- Waldron**, H.H., 1961. Geologic reconnaissance of Frosty Peak Volcano and vicinity, Alaska, U.S. Geol. Surv. Bull. 1028T, 677-708.
- Wesnousky**, S.G., **C.H. Scholz**, and K. **Shimazaki**, 1982. Deformation of an island arc: rates of moment release and **crustal** shortening in **intraplate** Japan determined from seismicity and quaternary fault data, J. Geophys. Res., 87, 6829-6852.
- Wilcox, R.E., **1959**. Some effects of recent volcanic ash falls with **especial reference to** Alaska, U.S. Geol. Surv. Bull. 1028-N, 409-476.
- Wildenstein-Mori, A., and **C.B. Crouse**, 1981. Strong motion data from Japanese earthquakes compiled by Exxon Production Reserach **Comp., Report SE-29, NOAA-NEIS,** Boulder, Colorado.
- Winslow, M.A., 1982. Uplift and tilting in the **Shumagin** gap, southwestern Alaska, part I, Geologic studies, Final Report for Contract EAR 79-10608, prepared for the Geophysics Section, National Science Foundation, Washington, D.C.
- Woodward-Clyde** Consultants, 1978. Offshore Alaska seismic exposure study, prepared for Alaska Subarctic Operators Committee (**ASOC**), March, 6 volumes.
- Woodward-Clyde, 1982. Development and initial application of software for seismic exposure evaluation, vol. II, Seismic Exposure

Software Application, Final Report, prepared for NOAA, contract **NA-80-RAC-000-91**, San Francisco.

- Wyss, M., and **J.N. Brune**, 1968. Seismic moment, stress and source dimensions for earthquakes in the California-Nevada region, J. Geophys. Res., **73**, 4681-4694.
- Wyss, M., 1979. Estimating maximum expectable magnitude of earthquakes from fault dimensions, Geology, **7**, 336-340.
- Wyss, M., F.W. Klein, and A.C. Johnston**, 1981. Precursors to the **Kalapana** $M = 7.2$ earthquake, J. Geophys. Res., **86**, 3881-3900.
- Wyss, M., and R.E. Habermann**, 1982. Conversion of m_b to M_s for estimating the recurrence time of large earthquakes, Bull. Seism. Soc. Am., **72**, 1651-1662.
- Yoshii, T., 1975. Proposal of the 'aseismic front', Zishin, **28**, 365-367.
-